Charged Dendrimers as Antimicrobial Coatings for Biomaterials

Dissertation
zur Erlangung des Doktorgrades
der Naturwissenschaften (Dr. rer. nat.)
der Fakultät IV
Chemie und Pharmazie
der Universität Regensburg

vorgelegt von
Diplom-Chemikerin Verena Katzur
aus Geretsried (geboren Evander, Südafrika)
2015

Die Daten zur Anfertigung der Dissertation wurden in der Zeit vom 10/2007 - 7/2010 an der Universität Regensburg akquiriert und im Zeitraum 8/2010 - 7/2015 innerhalb der Elternzeit zusammengefasst und ausgewertet

Promotionsgesuch eingereicht am:	07. Juli 2015
Kolloquiumstermin:	15. September 2015
Die Arbeit wurde angeleitet von:	Priv. Doz. Dr. Rainer Müller
Prüfungsausschuß:	Priv. Doz. Dr. Rainer Müller
	Prof. Dr. Dipl.-Ing. Jürgen Geis-Gerstorfer
	Prof. Dr. Werner Kunz
Vorsitzender:	Prof. Dr. David Díaz-Díaz

Beauty is the first test:
there is no permanent place
in this world
for ugly mathematics
(Godfrey Harold Hardy)

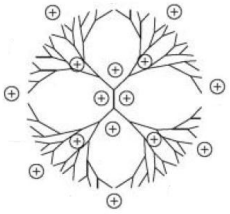

Might this also apply to biochemistry?

Abstract

According to a survey conducted in October 2012 a third of all dental implants is affected by peri-implantitis ten years after insertion. Unfortunately, the impact of surface properties, such as charge, wettability and coating agility on protein adsorption and subsequent biological events, like bacterial adhesion and biofilm formation, is still not fully unravelled. To date there are no bi-functional coatings that suppress the adhesion and growth of pathogenic organisms while simultaneously stimulating the integration of the implant into the surrounding tissue. A coating combining both properties is believed to reduce the incidence of peri-implantitis at the trans-gingival passage. Therefore, this thesis focuses on the preparation and characterization of covalent surface modifications terminated by functional groups, capable of generating charge in aqueous solution. The following functionalities were chosen for this purpose: the ammonium (-NH_3^+), the pyridinium (-$N^+C_5H_5$), the sulfonate (-SO_3^-), and the carboxylate (-COO^-) functionality. They were inserted in two diverse basic coatings. On the one hand as a terminal group in the well known "self-assembled monolayer" (SAM) system based on linear alkyl silanes on silicon dioxide surfaces and on the other hand at the periphery of immobilised polyamidoamine (PAMAM) dendrimers. Non-ionizable methyl terminated coatings, poly(ethylene glycol) functionalized surfaces and highly hydrophilic oxidized SiO_2 surfaces served as references. Dendrimers were chosen since they are an efficient and omnipresent structural element in nature (see e.g. nerves). The functionalities dendritically arranged at a surface are believed to be of higher concentration and possess a higher degree of freedom in comparison to the functionalities anchored within the rigid SAM system. The immobilization of PAMAM onto the substrata was achieved by a thin siloxane coating terminated by carboxylic acid anhydride moieties.

The first part of this thesis focuses on the preparation and physico-chemical characterization of the above mentioned coatings. Diffuse-reflectance infrared Fourier transformed spectroscopy (DRIFT), X-ray photoelectron spectroscopy (XPS) and a chemiluminescence based assay for the detection of terminal amino groups were performed to determine the preparation success of the surface modifications. The impact of the functional groups in their corresponding fixation on the electrokinetic potential was assessed by electrokinetic measurements. Furthermore, the wettability of the surfaces was determined by static water contact angle measurements.
The dendrimer backbone resulted in a higher or comparable wettability of the surface in comparison to the fixation of the identical functionality via linear alkyl chains. At SAM-coatings a mainly pronounced negative electrokinetic potential (-30 mV to -120 mV) was detected in neutral aqueous solution, with the exception of the amino-group terminated SAM at which a value around zero was determined. In contrast, the novel coatings based upon dendrimers

are rather moderately charged (-20 mV to 30 mV) at pH 7. The ζ-potential value in dependence of the pH of the surrounding solution at the SAM-coatings was observed to depend solely on the ionization behaviour of the surface confined functionalities, whereas the "effective" ζ-potential-pH profiles at the PAMAM-coatings could only be explained considering film swelling and structural rearrangements. That the dendrimer maintained its flexibility upon immobilization was also supported by pilot sum frequency spectroscopy (SFG) measurements at the coating/air interface. No unambiguous correlation was recognized between wettability and charge.

The second part of this thesis investigates the influence of the surface modifications on protein adsorption from saliva and serum, as well as bacterial adhesion and viability of *Streptococcus gordonii DL1* and *Staphylococcus aureus* in the presence and absence of a pre-coat from the former mentioned physiological solutions. In addition the impact of the surfaces coatings on human MG-63 osteoblast attachment was inspected.
The PAMAM-coatings showed comparable or lower amounts of protein upon the surfaces after the exposure to human whole saliva in comparison to their linear analogues. Serum exposure resulted in an adverse effect, maintaining or supporting the adsorption of proteins on PAMAM-coatings in comparison to the alkyl chain based films. Both bacteria investigated preferred dendrimer based coatings terminated by cationic functionalities and avoided the settlement on surfaces functionalized by dendrimers with anionic or neutral periphery. PAMAM-COOH is as effective and PAMAM-CH_3 nearly as effective as the gold standard SAM-PEG in prohibiting bacterial attachment. This property was even slightly enforced after serum conditioning, whereas it was slightly reduced after saliva contact. In contrast all SAM coatings were colonized by both bacteria irrespective of the terminal functionality. Regarding the vitality of the adhering bacteria, *S. gordonii*, was only influenced by pyridinium coated samples, whereas the bactericidal effect was stronger on PAMAM-Py than at the SAM-Py coated surfaces. This effect was lost after saliva pre-conditioning. The vitality of *S. aureus* was also reduced on pyridinium terminated coatings, but the most pronounced effect was achieved with PAMAM-CH_3. After serum exposure this bactericidal property was maintained. The antimicrobial property of PAMAM-NH_2, reported in literature, could not be preserved after tethering the molecule to the surface. Cell adhesion studies with human MG-63 osteoblasts showed comparable cell numbers on the dendrimer based coatings in comparison to the alkyl chain based coatings terminated by the same functionality, but after serum exposure higher cell numbers could be detected on the dendrimer based coatings in comparison to their linear analogues bearing the same functionality.

This study demonstrates, that a surface fixation of the terminal groups via a dendrimer possesses a higher potential of modulating the oral biological response, than the supplement

of the same functional groups via linear alkyl chains. Since PAMAM-CH_3 revealed a gentle antimicrobial property towards *S. aureus* and reduced the settlement of bacteria, PAMAM-CH_3 might be promising in reducing peri-implantitis at the trans-gingival passage without minimizing the attachment of bone forming cells.

Keywords: Electrokinetic surface properties, ζ-potential, dendrimers, self-assembled monolayers (SAM), protein adsorption, bacterial adhesion, biomaterials, anti-microbial coatings

Zusammenfassung

Gemäß einer Umfrage vom Oktober 2012 sind ein Drittel aller dentalen Zahnimplantate zehn Jahre nach ihrem Einsatz von Periimplantitis betroffen. Leider ist der Einfluss von Oberflächeneigenschaften, wie Ladung, Benetzbarkeit und Beweglichkeit auf Proteinadsorption und den darauf folgenden biologischen Ereignissen immer noch nicht vollständig geklärt. Bis heute gibt es keine bifunktionalen Beschichtungen, welche die bakterielle Adhäsion und deren Wachstum unterbinden, während sie die Integration des Implantats in das umgebende Gewebe unterstützen. Eine Beschichtung, welche beide Eigenschaften vereint, ist vermutlich geeignet, das Auftreten einer Periimplantintis an der transgingivalen Durchtrittstelle zu vermindern. Deshalb konzentriert sich diese Arbeit auf die Präparation und Charakterisierung von kovalenten Oberflächenmodifikationen, terminiert durch funktionelle Gruppen, welche in der Lage sind in wässriger Lösung Ladungen auszubilden. Hierfür wurden folgende Funktionalitäten ausgewählt: die Ammonium- (-NH_3^+), die Pyridinium- (-$N^+C_5H_5$), die Sulfonat- (-SO_3^-) und die Carboxylatgruppe (-COO^-). Sie wurden in zwei unterschiedliche Basisbeschichtungen eingebracht. Zum einen als endständige Gruppen in das wohl bekannte „self-assembled monolayer“ (SAM) System basierend auf linearen Alkylsilanen auf Siliziumdioxid und zum Anderen an die Peripherie immobilisierter Polyamidoamin Dendrimere (PAMAM). Nicht ionizierbare methylterminierte Beschichtungen, Polyethylenglykol funktionalisierte Oberflächen und oxidierte Siliziumoberflächen dienten als Referenzoberflächen. Dendrimere wurden deshalb gewählt, weil sie ein effizientes, häufig in der Natur verwendetes Strukturelement (siehe z.B. Nerven) sind. Zudem wurde bei einer dendritischen Anordnung sowohl eine höhere Oberflächenkonzentration als auch eine bessere Zugänglichkeit der Funktionalitäten erwartet als durch die Verankerung in einem starren SAM-System. Die Immobilisierung von PAMAM wurde mittels einer dünnen Siloxanschicht mit terminalen Anhydriden erreicht.

Der erste Teil dieser Arbeit ist auf die Präparation und physikalisch-chemische Charakterisierung der oben genannten Beschichtungen fokussiert. Infrarotspektroskopie (DRIFT) in diffuser Reflexion, Röntgen-Photoelektronen Spektroskopie (XPS) und ein Aminogruppen detektierender, auf Chemilumineszenz basierender Test wurden angewandt um die erfolgreiche Darstellung der Oberflächenmodifikationen zu ermitteln. Der Einfluss der funktionellen Gruppen in ihrer jeweiligen Fixierung auf die effektive Oberflächenladung wurde mit Hilfe elektrokinetischer Messungen untersucht. Des Weiteren wurde die Benetzbarkeit der Oberflächen durch statische Kontaktwinkelmessung mit Wasser erfasst.
Hinsichtlich Ihrer Benetzbarkeit zeigt sich eine PAMAM-Beschichtung in etwa gleich hydrophil oder hydrophiler als die SAM-Beschichtung mit gleicher Funktionalität. Für alle SAM-Beschichtungen wurde in neutraler wässriger Lösung ein vorwiegend stark negativ aus-

geprägtes elektrokinetisches Potential (-30 mV bis -120 mV) detektiert, mit Ausnahme der mit Aminogruppen terminierten SAM-Beschichtung, deren Wert um Null lag. Im Gegensatz dazu, zeichneten sich die neuen Beschichtungen, basierend auf Dendrimeren, durch eine moderate Oberflächenladung (-20 mV to 30 mV) bei pH 7 aus. Während das ζ-potential in Abhängigkeit vom pH der umgebenden Lösung an den SAM-Beschichtungen ausschließlich von dem Ionisierungsverhalten der gebundenen chemischen Funktionalitäten abhängt, konnten die „effektiven“ ζ-potential-pH Verläufe an den Dendrimerbeschichtungen nur unter der Annahme von Quellvorgängen und strukturellen Umlagerungen erklärt werden. Vorversuche mit Hilfe von Summenfrequenzspektroskopie (SFG) an der Beschichtungs/Luft Grenzfläche unterstützten die Annahme, dass das Dendrimer nach der Anbindung an die Oberfläche eine gewisse Flexibilität behält. Es konnte kein eindeutiger Zusammenhang zwischen Benetzbarkeit und Oberflächenladung hergestellt werden.

Der zweite Teil dieser Arbeit untersucht den Einfluss der Oberflächenmodifikationen auf die Proteinadsorption aus Speichel und Serum, als auch die Bakterienadhäsion und Bakterienvitalität von *Streptococcus gordonii DL1* und *Staphylococcus aureus* in Anwesenheit und Abwesenheit einer Präadsorptionsschicht aus den zuvor genannten physiologischen Lösungen. Zusätzlich wurde die Adhäsion von humanen MG-63 Osteoblasten untersucht.
Die PAMAM-Beschichtungen zeigten vergleichbare oder geringere Mengen an Protein nach Kontakt mit humanem Speichel im Vergleich zu deren linearen Analogen. Gegensätzliches wurde nach dem Kontakt mit Serum beobachtet, wo die Dendrimerbeschichtungen vergleichbare oder höhere Mengen an Protein adsorbierten als ihre auf linearen Alkylketten basierenden Filme. Beide in der Arbeit untersuchten Bakterientypen banden bevorzugt an kationisch terminierte PAMAM-Beschichtungen und vermieden die Besiedelung von Dendrimerbeschichtungen mit anionischer oder neutraler Peripherie. PAMAM-COOH zeigte sich als effektiv und PAMAM-CH_3 ähnlich effektiv wie der Goldstandard SAM-PEG in der Unterbindung von Bakterienadhäsion. Diese Eigenschaft wurde sogar leicht verstärkt nach Vorkonditionierung mit Serum, während sie nach Speichelkontakt leicht reduziert wurde. Im Gegensatz zu den PAMAM-Beschichtungen wurden alle SAM-Beschichtungen von beiden Bakterien unabhängig von der terminalen Gruppe besiedelt. Die Vitalität des adhärierenden Bakteriums *S. gordonii* wurde nur von pyridiniumbeschichteten Oberflächen beeinflusst, während der antibakterielle Effekt auf PAMAM-Py stärker war als auf der SAM-Py Oberfläche. Dieser Effekt wurde durch die Konditionierung mit Speichel aufgehoben. Die Vitalität von *S. aureus* wurde auch von den Pyrdinium-Beschichtungen reduziert, aber der stärkste Effekt wurde an der PAMAM-CH_3 Oberfläche erzielt. Nach Konditionierung mit Serum wurde diese Eigenschaft beibehalten. Die antibakterielle Eigenschaft von PAMAM-NH_2, gemäß Literaturangaben, konnte nach der Anbindung des Moleküls nicht beibehalten werden. Zellstudien mit humanen MG-63 Osteoblasten zeigten vergleichbare Zellzahlen auf den PAMAM

sowie den SAM-Beschichtungen bei gleicher terminaler Funktionalität. Nach Konditionierung mit Serum konnten auf den PAMAM- Beschichtungen höhere Zellzahlen ermittelt werden als auf den analogen SAMs.

Diese Arbeit zeigt, dass die Fixierung der funktionalen Gruppen durch das Dendrimer ein höheres Potential besitzt, die orale biologische Antwort zu modellieren, als eine Bereitstellung der gleichen funktionellen Gruppe mittels einer linearen Alkylkette. Da PAMAM-CH_3 einen leichten antibakteriellen Charakter bezüglich *S. aureus* aufweist und antiadhäsiv wirkt, scheint diese Beschichtung primär in der Lage zu sein, die Periimplantitis zu reduzieren, ohne die Anheftung von knochenbildenden Zellen entschieden zu vermindern.

Schlüsselwörter: Elektrokinetische Oberflächeneigenschaften, ζ-Potential, Dendrimere, Selbstorganisierende Monoschichten (SAM), Proteinadsorption, Bakterielle Adhäsion, Biomaterialien, Antibakterielle Beschichtung

Preface

This PhD thesis is based on scientific research that was carried out at the department of Physical and Theoretical Chemistry at the University of Regensburg and is part of a comprehensive study on novel biomaterial coatings based on dendrimers. Cooperating partners contributing to the investigation of this new coating type are the Department of Operative Dentistry and Periodontology at the University Hospital of Regensburg, the Section of Medical Materials and Technology at the Centre of Dentistry in Tübingen, and the Department of Oral Biology at the State University of New York Buffalo (NY, USA). It was due to the financial support of the Deutsche Forschungsgemeinschaft (DFG) that this project could be realized.

This work would not have been possible without the help and guidance of the following people:

First of all, I would like to thank Priv. Doz. Dr. Rainer Müller for encouraging and supervising this thesis. Furthermore, for introducing me to the fascinating, comprehensive science of biomaterials. For constantly encouraging me during the progress of this work and benefiting from his expert knowledge in this field. And especially, for his patience!

Likewise, I would like to thank Prof. Dr. Werner Kunz for providing premises and instrumentation requisite for accomplishing this work. Short conversations were always path-breaking, entertaining and impressive.

Furthermore, my special thanks goes to the group of Prof. Dr. Motschmann and his staff, Dr. Christiane Stage und Dr. Peter Karageorgiev. They are an outstanding team!

I owe my gratitude to Prof. Dr. Geis-Gerstorfer and Dr. F. Rupp for their pleasant collaboration and memorable meetings in Regensburg and Tübingen. I thank Prof. Dr. Dr. Helmut Schweikl and Prof. Dr. Gottfried Schmalz for the cordial openness and introduction into dental science. Furthermore, I would like to thank Dr. Karl-Anton Hiller for the data management of the biological investigations.

In particular, I would like to thank Andreas Eidt and Dipl. Chem. Erika Deigele, for the pleasant teamwork. I owe the accomplishing of this work in particular to Mrs E. Deigele. Her relentless request about the progress of this work and the unbroken connection to Regensburg helped me to never lay this work aside.

I owe the staff of the company Anton Paar (Austria), especially Dr. Alexandra Ewers,

Dr. Christiane Onitsch, Dr. Thomas Luxbacher my deepest gratitude for inviting me and providing me with the necessary knowledge to perform a few measurements on the Electro Kinetic Analyser (EKA - SurPASS) and even lending this instrument to me for a short while. That was a very valuable contribution in the accomplishment of this thesis.

My sincere thanks goes to all students that supported me in my laboratory work, especially in the time of pregnancy. Alexandra Mattschas, Eva Maria Schöll, Tatjana Leibßle, Alexander Spengler, Matthias Knorn, Ulrike Vogl all distinguished by exemplary dedication.

There are no words which can adequately express my thanks to my husband, Michael Moschberger, and our kids, Konstantin und Cosima. If it was not for my husband, I could not have spent all those hours in front of the computer and above literature.

Unimaginable would have been the managing of this thesis, if I would not have been so lucky to have such dedicating parents and parents in law. Both performed outstanding in day caring for our children! Thank you so, so much! Furthermore, it is dear to my heart to express the sincere appreciation and gratitude to my parents, who supported and guided me in all aspects of my life.

Last but not least, I would like to thank my sister, Dipl.-Ing. Eva-Maria Katzur and my dearest friend, Dr. Eva-Maria Wagner, for their thorough proof-reading.

Publications

Surface-immobilized PAMAM-dendrimers modified with cationic or anionic terminal functions: physicochemical surface properties and conformational changes after application of liquid interface stress
Verena Katzur, Mirjam Eichler, Erika Deigele, Christiane Stage, Peter Karageorgiev, Jürgen Geis-Gerstorfer, Gottfried Schmalz, Stefan Ruhl, Frank Rupp, Rainer Müller
Journal of Colloid and Interface Science, Volume 366, Issue 1, Pages 179-190, 2012

The impact of dendrimer-grafted modifications to model silicon surfaces on protein adsorption and bacterial adhesion
Mirjam Eichler, Verena Katzur, Lutz Scheideler, Michael Haupt, Jürgen Geis-Gerstorfer, Gottfried Schmalz, Stefan Ruhl, Rainer Müller und Frank Rupp
Biomaterials 32 (2011) 9168-9179

Influences of protein films on antibacterial or bacteria-repellent surface coatings in a model system using silicon wafers
Rainer Müller, Andreas Eidt, Karl-Anton Hiller, Verena Katzur, Michael Subat, Helmut Schweikl, Satoshi Imazato, Stefan Ruhl und Gottfried Schmalz
Biomaterials 30 (28):4921-9 (2009)

Conference Contributions

Surface-immobilized charged dendrimers - a new type of antiadhesive or antimicrobial surface modification?
Rainer Müller, Verena Katzur, Mirjam Eichler, Helmut Schweikl, Karl-Anton Hiller, Gottfried Schmalz, Stefan Ruhl, Lutz Scheideler, Jürgen Geis-Gerstorfer, Frank Rupp
Jahrestagung der Deutschen Gesellschaft für Biomaterialien,
Gießen, Germany, 10.-12. November 2011

Human salivary protein adsorption onto chemically modified silica beads
Gregory White, Verena Katzur, Molakala Reddy, Rainer Müller, Robert Baier, Stefan Ruhl
General Session of the International Association of Dental Research,
San Diego, USA, 16.-19. March 2011

Adhesion and Viability of Oral Bacteria on Charged Self-Assembled Monolayers
Helmut Schweikl, Andreas Eidt, Karl-Anton Hiller, Gottfried Schmalz, Verena Katzur, Rainer Müller, Mirjam Eichler, Frank Rupp, Jürgen Geis-Gerstorfer, Stefan Ruhl

23rd European Conference on Biomaterials,
Tampere, Finnland, 11.-15. September 2010

Conditioning layer formation on charged dendrimers
Mirjam Eichler, Ingrid Stephan, Verena Katzur, Rainer Müller, Lutz Scheideler, Jürgen Geis-Gerstorfer, Frank Rupp
Jahrestagung der Deutschen Gesellschaft für Biomaterialien,
Tübingen, Germany, 8.-10. October 2009; BIOmaterialien 2009, 10, 105

Surface-functional groups of model substrates as determinant for protein adsorption
Verena Katzur, Rainer Müller, Mirjam Eichler, Jürgen Geis-Gerstorfer, Frank Rupp, Karl-Anton Hiller, Helmut Schweikl, Gottfried Schmalz, Stefan Ruhl
International Association for Dental Research - Continental European Division,
Munich, Germany, 9.-12. September 2009

Adhesion of Streptococcus Gordonii to positively and negatively charged self-assembled monolayers
Verena Katzur, Andreas Eidt, Mirjam Eichler, Karl-Anton Hiller, Gottfried Schmalz, Stefan Ruhl und Rainer Müller
3rd International Symposium of Interface Biology of Implants,
Warnemünde, Germany 13.-15. May 2009; BIOmaterialien 2009, 10(S1), 76

A systematic investigation of physico-chemical surface parameters influencing the adsorption of saliva proteins and the adherence of oral bacteria
Verena Katzur, Mirjam Eichler, Frank Rupp, Jürgen Geis-Gerstorfer, Karl-Anton Hiller, Helmut Schweikl, Gottfried Schmalz, Stefan Ruhl und Rainer Müller
Jahrestagung der Deutschen Gesellschaft für Biomaterialien,
Hamburg, Germany 20.-22. November 2008; BIOmaterialien 2008, 9, 203-204

Contents

Part I

Introduction

Bacterial attachment to surfaces is an ubiquitous phenomenon [1]. In the field of medicine, microbial adhesion of pathogenic germs on implants leads to biomaterial-associated infections (BAI). A BAI is a dreaded incidence after implantation because a biofilm formed by colonising bacteria is difficult to eradicate by antibiotics, antimicrobials or the hosts immune system [1][2]. This is due to the dense structure [2], a small accessible surface area, and a reduced metabolic activity of the biofilm [3]. Has this inauspicious case occurred, a removal of the biomaterial is often inevitable and a secondary surgery indispensable [1][2][4]. According to a recent survey at least a third of all dental implants are affected by peri-implantitis (see Fig.: 0.1) 10 years after implantation (Dr. R. J. Meissen [updated: 31.10.2012, accessed: 17.03.2013] www.zp-aktuell.de).

Figure 0.1: Peri-implantitis at the gingival sulcus
©PD Dr. Sönke Harder, Praxisklinik für Zahnmedizin und Implantologie, Munich

At present biomaterial research is endeavoured to create surfaces that suppress the adhesion and growth of pathogenic organisms and simultaneously stimulate the integration of implants into the surrounding tissue, especially for those that are intended to remain in the body for long durations, as in the case of dental implants. Up to now, numerous systems have been invented and investigated for the application on implants, such as coatings with non-adhesive character, coatings with the ability to release antibiotics, coatings impregnated with silver, surface modifications bearing bactericidal components to kill bacteria on contact, and surfaces facilitated by protein sequences to promote host cell adhesion [3]. Unfortunately, none of the mentioned strategies combines antimicrobial and cell integration properties.

Many antimicrobial substances possess cationic structural elements as for example the well known cetylpyridinium chloride (CPC), a cationic quaternary ammonium compound present in plenty products for dental hygiene. Positive charges are known to destabilize and disrupt the in netto negatively charged cell surface of bacteria. Regarding cell adhesion, it was found that charged surfaces promote the adhesion of bone-forming cells in comparison to uncharged

surfaces [5]. Besides electrostatic interactions, multivalent interactions, a key concept in biorecognition [6], play a significant role in biological processes. This PhD-thesis describes the preparation, characterization and evaluation of coatings combining the auspicious concepts of surface charge and multivalency as potential biomaterial coatings.

For this purpose smooth silicon wafers were covalently functionalised with dendrimeric structures terminated by common ionic organic groups (X) of different structure and polarity capable of generating charge in an aqueous medium at the physiological pH of 7.4. Additionally, silicon wafers were functionalised by self-assembled monolayers (SAMs) of unbranched alkyl chain siloxanes comprising the same functional groups as the dendrimer based coatings. The following picture (view Fig.:0.2) illustrates the concept this thesis focuses on.

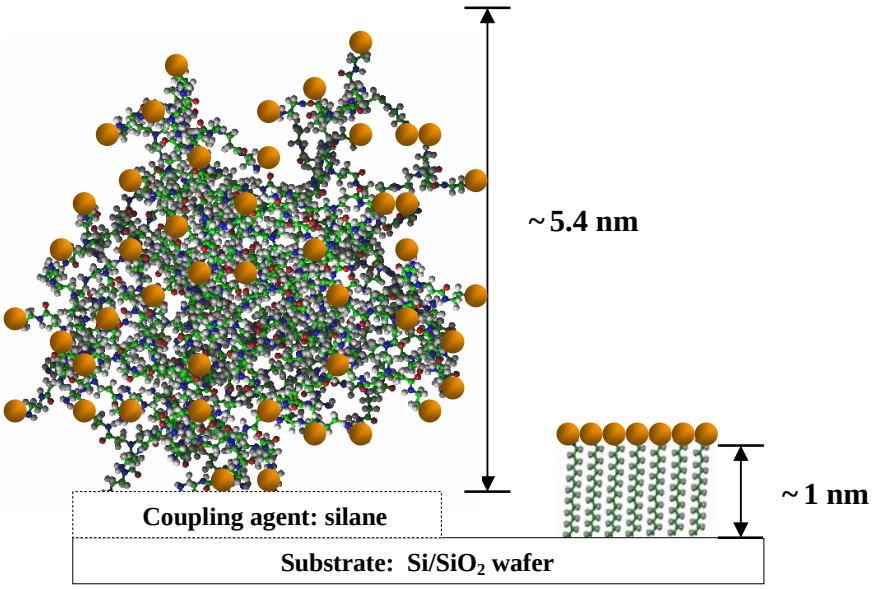

Figure 0.2: Schematic representation of the two types of surface modifications investigated within this thesis. The coating on the right hand side represents the thin, stiff monolayer functionalisation based on self assembled alkyl chains, whereas the coating on the left hand side represents the rather thick, flexible monolayer functionalisation based on dendrimers. The orange spheres symbolise the positions of terminal groups. For a better overview only 46 terminal groups are indicated at the dendrimer, whereas 128 are present.

The coating on the right hand side represents the thin, rigid, highly ordered monolayer functionalisation based on SAMs. From the perspective of an approaching molecule SAMs are a monofunctional flat surface. In contrast, the coating on the left hand side represents the rather thick, flexible monolayer functionalisation based on dendrimers. Dendrimers are globular in shape and thus approaching molecules face a multifunctional, wavy surface. An increase in surface charge was expected by expanding the coating dimensions from a two dimensional distribution of charge carriers to a three dimensional distribution. A dendrimeric

molecule was chosen to provide the centres of charge because the terminal functionalities within a dendrimer are much closer to each other than in linear polymers. Furthermore, dendrimers possess a well-defined structure [7] ideal to study surface structure-reactivity relationships.

The dendrimer chosen for this project is polyamidoamine (PAMAM-NH_2) of the fifth generation (G5). Polyamidoamine contains numerous amide bonds just like a protein and is of comparable size to natural proteins. Moreover polyamidoamine has shown antimicrobial properties in solution, as well as anti-inflammatory activity [8]. The terminal groups symbolised by orange balls in Fig. 0.2 and selected for this study are ammonium (-NH_3^+), and pyridinium (-$N^+C_5H_5$) moieties to generate positive surface charge. Negatively charged surfaces were aimed at by introducing carboxylate (-COO^-) and sulfonate (-SO_3^-) moieties. Plain oxidized unmodified surfaces of silicon dioxide (-$Si-O^-$), methyl terminated coatings (-CH_3) and polyethyleneoxide (-PEG) coatings were chosen as references.

It is only possible to correlate observed biological responses to physico-chemical surface properties if the surface characteristics are analysed as precisely and comprehensively as possible. An IR-spectrometer with a diffuse reflectance accessory recording surface modifications on silica particles, X-ray photoelectron spectroscopy (XPS) and wettability measurements were carried out on functionalised silicon wafers, and a chemiluminescence based assay detecting free amino groups was used to verify the successful preparation of the surface coatings. Introducing IR-Vis sum frequency spectroscopy measurements were performed on some coatings revealing molecular orientations at the solid/air interface. Information on the charge formation processes at the solid/liquid interface was gained by electrokinetic measurements.

In order to evaluate the applicability of these ultra-thin films for biomaterial purposes the impact of the surface modifications on microbial adhesion, microbial vitality and cell attachment were examined considering protein adsorption (determined by a colorimetric assay) readily occurring from surrounding body fluids (serum or saliva) after implantation. The conditioning film, resulting from serum or saliva, mediates between the biomaterial surface and the physiological environment. Its constitution depends on the functionalisation of the substratum, and is thus depended on the surface charge, and influences the adhesion of cells and bacteria as well as their further destiny. Therefore, only a surface coating maintaining antimicrobial and cell integration properties after the exposure to physiological solutions may be regarded as a promising biomaterial coating for implants. *Streptococcus gordonii* DL1 an early colonizer of oral surfaces, and *Staphylococcus aureus* a common pathogenic bacteria very often responsible for infections at metal implants were chosen for the biological investigations.

This PhD thesis was performed at the Institute of Physical and Theoretical Chemistry at the University of Regensburg (Germany) and was part of a cooperation project with the Department of Operative Dentistry and Periodontology at the University Hospital of Regensburg (Germany), the Section of Medical Materials and Technology at the Center of Dentistry in Tübingen (Germany) and the Department of Oral Biology at the State University of New York (Buffalo). It was a further task of this PhD thesis to develop coating strategies for numerous silicon-based substrata of different geometry and stability (quartz crystal resonators, glass slides, silica spheres, silica beads, silicon dioxide particles, double-side polished silicon wafers and single-side polished silicon wafers) and supply all departments with sufficient numbers of model surfaces. The substratum diversity was necessary because of the numerous analytical methods that were applied in this project by the participating departments: Static protein adsorption and bacterial adhesion data acquired by A. Eidt (MTA) under the supervision of Prof. Dr. S. Ruhl (Department of Oral Biology at the State University of New York, Buffalo, USA) at the Department of Operative Dentistry and Periodontology at the University Hospital of Regensburg (Germany) are included in this thesis. Furthermore, cell adhesion experiments performed by C. Waha (MTA) under the supervision of Prof. Dr. Dr. H. Schweikl at the Department of Operative Dentistry and Peridontology at the University Hospital of Regensburg (Germany) are mentioned here to complete the biomaterial testing. Dynamic protein adsorption and bacteria adhesion studies, as well as surface energy calculations were performed at the Section of Medical Materials and Technology at the Center of Dentistry in Tübingen (Germany) by Msc M. Eichler in the course of her PhD thesis under the supervision of Dr. F. Rupp and Prof. Dr. Geis-Gerstorfer utilizing quartz crystal microbalance and dynamic contact angle analysis. Static and dynamic examinations were carried out because biofilm formation may occur supra-gingivally and sub-gingivally in the oral cavity. The former surfaces are exposed to shear forces, whereas the later are not.

Even though various processes and factors that influence adhesion have been unravelled, no generally valid theory exists to explain the complex process of interactions between bacteria, cells, proteins and surfaces. An improved knowledge of the interactions between biomaterial surface, the mediating protein layer and the subsequent adherence of cells and/or bacteria is essential for the development of biomaterial coatings or functionalized surfaces with properties optimized for their field of application.

Part II

Fundamentals

1 Biomaterial Surfaces

1.1 Adsorption and Adhesion Processes at Biomaterials

Within seconds after the insertion of an artificial object into a physiological fluid (e.g. body fluids, such as blood or saliva) protein adsorption will occur. The layer formed by the adsorbed proteins is referred to as a conditioning film (within the oral cavity the conditioning film caused by saliva is termed "pellicle"). Only later, micro-organisms and cells reach the biomaterial. They face a surface covered by proteins upon their arrival instead of the originally implanted surface. The conditioning film mediates between the substratum and the surrounding fluid and controls proceeding reactions, thus making it extremely relevant in the design of biomaterials. [9]

The physico-chemical properties of a substratum surface and the composition of the contacting physiological fluid provoke conditioning films of different protein composition, packing, density and/or configuration [9]. Whereas the composition and properties of the biofluid and the micro-organisms/biomolecules are pre-given, surface characteristics can be altered using surface modification strategies. Surface modifications of varying chemical structure and composition influence the physico-chemical surface characteristics such as hydrophobicity, surface charge, and topography, addressing only a few of them [10]. These factors effect protein adsorption and eventually the pace and composition of the proceeding biofilm or cell-attachment. Therefore, changes in physico-chemical substratum parameters influence biofilm formation and tissue adhesion indirectly.

The complex composition of physiological fluids, containing numerous different proteins and highly adaptive bacteria [4], changing their physico-chemical properties depending on environmental conditions, nutritional status and their state of growth [11], make both, protein adsorption and subsequent cell/bacteria adhesion, a very complex process. Furthermore, biomechanical conditions determined by the location of the process are also of importance, i.e. if the centre of action is exposed to hydrodynamic shear or not.

Initial protein adsorption and bacterial adhesion was attempted to be described by the theories applied in colloid and interface chemistry, neglecting metabolic processes, growth or

conformational rearrangements [12]. Therein, initial adhesion/adsorption is described to be governed by a combination of basic forces. These forces are, besides the always present attractive van der Waals forces, electrostatic interactions, hydrogen bonding, and the Brownian motion. Further forces are direct or indirect consequences of the former mentioned basic forces. Two physico-chemical approaches are mainly mentioned in literature: surface thermodynamics [13] and the extended-Derjaguin-Landau-Verwey-Overbeek (x-DLVO) theory. [1][14][9]

The **thermodynamic approach** describes adsorption as a process of minimizing the Gibbs energy of a system. The surface free energies (SFE) of the substratum and the bacterium are determined by wettability measurements. The energy between the bacterium and the surface is calculated based on the assumption that the interfaces bacterium/water and surface/water are replaced by a surface/bacterium interface. Critical is the use of thermodynamic equilibrium equations in a mainly irreversible process. Furthermore, no conformational changes, appendages at bacteria, or inhomogeneous bacterial envelops are taken into account. Up to now, no universal relationship between interfacial free energies and adhesion/adsorption has been found. [15][9]
The **x-DLVO** theory describes the interaction energy as function of the distance between the colloidal particle (here, the approaching micro-organism or proteins) and the surface [1]. The Gibbs energy is a sum of van der Waals forces, electrostatic forces and short range Lewis acid-base (i.e., hydrogen bridges) interaction energies [15].

The following two subsections will give a small impression on the topics protein adsorption and bacterial adhesion. The section thereafter addresses methods already known for a very long time, and new approaches in current research, to prohibit the formation of biofilms on surfaces.

1.1.1 Protein Adsorption

Commonly proteins accumulate at solid/liquid interfaces. A proteophobic behaviour is observed in only very few cases and will be addressed in section 1.2.

Proteins are biopolymers composed of amino acids with hydrophobic and hydrophilic side chains. Hydrophilic side chains can be of ionisable or non-ionisable chemical moieties. Because ionisable moieties are able to form positive and negative charges, proteins can be referred to as polyampholytes [16]. Proteins are folded in such a way that the hydrophilic side chains interact with water, whereas most of the hydrophobic side chains are hidden within the biomolecule to prevent water contact [17].

Brownian motion (i.e., diffusion) and liquid flow (i.e., convection) transport proteins towards a surface. Long range (attractive van der Waals forces > 50 nm, and repulsive non-specific electrostatic interactions about 10 - 20 nm) and short range forces (specific electrostatic interactions 2 - 10 nm, displacement of water by hydrophobic groups 0.5 nm, specific interactions < 1 nm) govern primary adhesion that is, theoretically, reversible [9]. Subsequent conformational changes, optimizing interactions with the substratum [18], and the attachment to the surfaces via several segments make protein adsorption an almost irreversible process [16]. Protein removal can only be achieved utilizing detergents or by inducing changes in pH and/or ionic strength. Even diluting the adjacent solution does not lead to protein desorption. However, a replacement of proteins with higher mobility, by proteins with limited mobility but higher affinity for the surface may still change the protein composition upon a surface ("Vroman effect" [16]) with time.

W. Norde [16] studies protein adsorption onto surfaces already since the early 1970s and has acquired a comprehensive knowledge in this field. He divides proteins into two classes: structurally labile proteins and structurally stable proteins (meaning their ability to remain in their native state) and refers to them as "soft" (e.g. α-lactalbumin) and "hard" (e.g. lysozyme) proteins. Upon adsorption hard proteins undergo limited structural changes, whereas soft proteins undergo larger structural changes. He published a table with predictions regarding protein adsorption onto charged surfaces of different wettability, that all his experiments were in line with. A transcript of this table is presented below (Table 1.1). He concludes that proteins of any type adsorb onto hydrophobic surfaces, irrespective of

Protein	Surface			
	Hydrophobic		Hydrophilic	
	+	-	+	-
Hard				
+	✔	✔	✘	✔
-	✔	✔	✔	✘
Soft				
+	✔	✔	✔	✔
-	✔	✔	✔	✔

Table 1.1: Scheme proposed by W. Norde to predict whether a protein adsorbs (✔) to a surface or not (✘) [16]; "+" and "-" signs refer to the netto charge of the protein and the surface, respectively.

the surface charge. The reason why all proteins adhere to hydrophobic surfaces (apolar), even if electrostatically unfavourable, maybe the dominant influence of the dehydration of the hydrophobic surface (i.e., liberating water molecules and increasing entropy). In some cases additional support is obtained by hydrophobic interactions between protein and surface

upon unfolding ("denaturation"). At polar (hydrophilic) surfaces hard proteins only attach, if they are electrostatically attracted, whereas soft proteins even adsorb if the surface is electrostatically hostile (i.e., same charge). The driving force for hard proteins to adsorb are the ionic interactions and the liberation of counter-ions. The driving force for soft proteins to accumulate at polar surfaces may originate from the gain of conformational entropy as the protein reorientates on the surface and looses secondary and tertiary structures (i.e., order). This seems to outweigh unfavourable dehydration of hydrophilic surfaces and electrostatic repulsion. [16]

The observations and illustrations made by W. Norde et al. help to develop a slight understanding on the nature of proteins and their behaviour upon surface approach. But, even though this classification is useful to explain the result of many investigations, it is not a generally valid principle. This is attributed to the heterogeneous character of proteins (each protein has its own "personality" [16]) and the multiple additional factors influencing adhesion.

1.1.2 Bacterial Adhesion

As already mentioned in the introduction (I) of this thesis, microbial surface contamination is a dreaded incidence in many fields of life, like food packaging, marine biofouling, surgical instruments, biomaterials, and many others. Great efforts have been undertaken, since many years, to design surface coatings, which prohibit bacterial attachment. Unfortunately, just like in the case of proteins mentioned in the previous subsection (1.1.1), little knowledge has been gained on the relationship between material surface characteristics, such as surface energy expressed by hydrophilicity/hydrophobicity, charge, polarity and topography, and bacterial adhesion. The mechanism of initial bacterial colonization is suggested to be dependent on both, physico-chemical (non-specific; dependent on the overall characteristics of the adhering species) and specific bio-chemical interactions (localized adhesion sites on cell surfaces) [10], just like in the case of proteins. Bacterial adhesion is strongly related to the type and amount of proteins upon the surface, which is dependent on the surface properties of the biomaterial. [19]

The size of a typical bacterial cell is 0.5 - 5.0 micrometers, whereas an average human cell is about 10 micrometers in size. Most common bacteria can be divided into two classes, namely gram-positive (e.g. *Staphylococcus aureus*) and gram-negative (e.g. *Escherichia coli*) bacteria. This classification is based on a staining technique, developed in 1884 by Hans Christian Gram, characterizing bacteria by structural characteristics of their cell wall. Gram-positive bacteria appear purple upon staining with crystal violet, whereas gram-negative bacteria

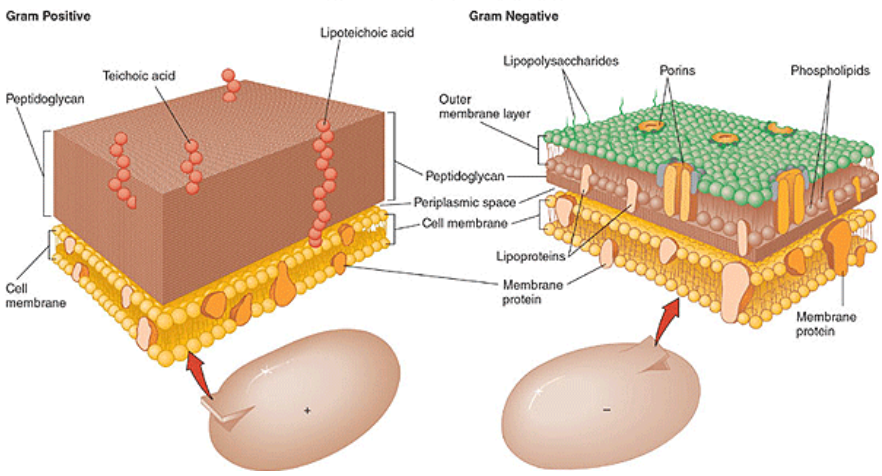

Figure 1.1: A scheme illustrating the arrangement of components at the envelopes of the two main classes of bacteria: gram-negative and gram-positive; ©The McGraw-Hill Companies, Inc. Permission required for reproduction or display

do not retain the stain and are counter stained by safranin or fuchsine appearing red or pink under the microscope. Figure 1.1 illustrates the structural differences among the cell envelops of two main types of bacteria.

Gram-positive bacteria are surrounded by many layers of peptidoglycan (linear polysaccharide with a short peptide sequence) which are penetrated by lipoteichoic acids (glycerol phosphate, ribitol phosphate). Peptidoglycan is found in prokaryotes only. The peptidoglycan is composed of N-acetyl glucosamine and N-acetyl muramic acid as alternating sugars. The glycan chains are cross-linked by peptide chains. It is worth mentioning that most enzymes in mammalian hosts are unable to degrade peptidoglycan with one important exception: lysozyme. The overall charge of gram-positive bacteria is negative due to the phosphoryl groups in the teichoic and teichuronic acid residues. Carboxylic acid moieties along the teichuronic acid intensify the overall negative charge [20].

The cell envelope of gram-negative bacteria is thinner but of higher complexity. Gram-negative bacteria also possess a peptidoglycan layer but much thinner than gram-positive bacteria and not positioned at the outer envelope of the cell. The peptidoglycan sheet is surrounded by an additional layer composed of lipopolysaccharides (LPS), phospholipids (only confined on the inner side of the membrane), and porins. Phosphoryl and 2-keto-3-deoxyoctonate carboxylate groups control the charge of gram-negative bacteria [20]. There are no teichoic or lipoteichoic acids present.

The outer cell wall also possess binding sites for Ca^{2+} and Mg^{2+} ions stabilizing the structure

of the outer membrane. Due to the structural properties mentioned above, the cell surface of bacteria possess an overall negative electrostatic charge [20][21]. In contrast to bacteria, the cell membrane of human erythrocytes (representatives of normal mammalian cells) is mainly composed of zwitterionic phosphatidylcholine, phosphatidylethanolamine and sphingomyelin penetrated by sterols. Phosphatidyl serine is also present carrying a negative charge. The overall charge of mammalian cells is rather neutral to slightly acidic [22]. The higher negative charge on the envelope of bacteria makes them more susceptible to be deteriorated by cationic antimicrobials than mammalian cells.

The net cell surface charge of bacteria can be determined by estimating their electrophoretic mobility in an electric field [20]. In the past, determined electrophoretic mobilities of bacteria were transferred into zeta-potentials using Smoluchowski formalism (for further information view subsection 4.2.1). This is a very questionable method and has been dismissed by many authors, especially by J. Duval. He criticises the implementation of bacterial surface properties into colloidal interaction theory because bacteria are no hard and impermeable particles. They are heterogeneous, permeable and soft, forming rather an interphase to the surrounding fluid than a well-defined interface. As such, the location of the slip plane at a bacterial interphase is ambiguous and he recommends the abundance of concepts like zeta-potential, surface potential and surface charge. He proposes a diffuse soft particle electrokinetic (DSPE) formalism for deriving interphasial properties. The DSPE model is based on a full numerical integration of the governing electrohydrodynamic equations of soft particles and allows the exploration of the effects of chemical heterogeneities and the physically diffuse character of the soft microbial interphase on electrophoretic motion. Interphasial characteristics obtained by using the DSPE formalism on microbial electrophoretic mobilities may shed light into correlations between electro-hydrodynamic characteristics of the microbial interphase and bacterial attachment. [23][16]

1.2 Current Antimicrobial Concepts

There are four main types of antimicrobial coating concepts currently used for biomaterials. One concept is based on the anti-adhesive character of the surface modification, preventing micro-organisms, cells and bio-macromolecules from settling onto the surface. A further concept is based on coatings comprising immobilized antimicrobial substances killing bacteria on contact. Also coatings containing a reservoir of the biocidal molecules, referred to as antibiotic/antimicrobial release systems, are used for biomaterial implants. Surface modifications bearing tissue-integrating factors are also part of antimicrobial concepts because surfaces with adhering cells are not prone to microbial colonization. All four types have their advantages, disadvantages and application fields, which will be addressed shortly in this section. At the end of this section a rather new type of coating will be introduced.

1.2.1 Anti-Adhesive Coatings

The gold standard in anti-adhesive coatings is poly(ethylene glycol) (PEG). Also surfaces coated by oligo(ethylene glycol)$_n$ (n = 3 - 6) (OEG) groups possess anti-adhesive properties. Even though studied for many years the mode of action has not been fully unravelled yet. Organisms and proteins are said to be sterically repelled by the PEG chains, except for *Pseudomonas aeruginosa* strains [15]. PEG chains are of high agility and this is suppressed by the arrival of large molecules. A decrease in conformational freedom reduces entropy and is energetically unfavourable [24]. Upon compression the polymer concentration increases on the surface but water diffuses back into the PEG layer causing hydration and expansion of the chains. Therefore two main parameters counter compression and induce repulsion: the entropic reset force and the osmotic force. Both, the formation and the concentration of the ethylene glycol units and thus their ability in binding interfacial water are most probably decisive for the proteophobic character of a PEG-surface [25]. Chains containing a higher amount of ethylene oxide units were found to be more proteophobic than shorter chains. The strong disadvantage of this surface modification is its susceptibility to auto-oxidation [26][27], thus having no long term stability.

Following the structure of PEG coatings, hydrophilic polymer chains end-grafted at high density onto surfaces seem currently the most promising strategy in resisting adherence [16]. This type of modification is referred to as **polymer brush coatings** because the chains stretch away from the surface into the adjacent medium [2][1][19]. Just like in PEG coatings, compression of the strongly hydrated polymer chains upon macromolecule/micro-organism approach increases the osmotic pressure and decreases the mobility (conformational entropy) of the polymer chains in the brush, causing repulsion of the approaching biomolecule [1].

Hydrophilic polymers like poly(N-vinyl pyrrolidone) (PVP), poly(oxazoline) and poly(N,N-dimethylacrylamide) also show reduced adhesion capacity. This is attributed to the fact that these surface coatings swell strongly in aqueous medium and the hydrogels formed causes unfavourable bacterial attachment conditions as the surface properties are similar to the water phase.

Comprehensive tests to shed light into the mechanism of protein resistant surfaces were conducted by Whitesides et al.. They tried to correlate protein resistance to molecular structure patterns and found the following molecular characteristics to be apparently essential to create protein resistant coatings : polar functional groups with hydrogen bond accepting groups (electronegative atom) but no hydrogen bond donating groups and the presence of no net charge (zwitterionic structures). [26]

Non-adhesive coatings are for example used for contact lenses and catheters [3], but may not be used for areas where tissue integration is desired.

1.2.2 Antimicrobial-Releasing Coatings

Coatings loaded with silver, silver salts and silver composites are already applied in urinary catheters and wound bandages. The bioactive components are solubilised silver ions. In vitro experiments in the oral cavity with silver-based glass-ionomer cement provided no promising results [1]. Silver sulfonamides, particularly silver sulfadiazine, were a classic treatment for wound burns over the years [28], but bacteria were observed to develop Ag sulfadiazine resistance.

Antibiotic-releasing systems (gentamycin) are used in total hip and knee arthroplasties, but the implant can only incorporate a specific weight percent of antibiotics without affecting its physical stability. The shady side of such release systems is the fact that after an initially high release (even at toxic concentration levels) of antibiotics the release continues for a long period of time at concentrations lower than needed to be effective, leading to the development of bacterial resistance. [1]

The general drawback of this concept is the difficulty to provide sustainable concentrations of the biocides for a prolonged period of time after the burst release, especially in areas like the oral cavity where the adjacent solution is continuously replaced. Furthermore, mobile biocidal molecules may diffuse away from the target area causing undesired side effects in other regions. Therefore, the immobilization of biocides was the focus of research in the recent years. [1][29]

1.2.3 Contact-Killing Surface Coatings

Molecules containing one or two cationic moieties (e.g. benzalkonium chloride, cetylpyridinium chloride) are well known antimicrobial agents in aqueous solution. Their mode of action is based on non-specific interactions. Cationic antimicrobials adsorb readily onto the net negatively charged bacterial cell surface [6]. The cationic molecules disrupt the cell membrane and cause the cell to disintegrate [6]. Electrolytes like potassium ions and phosphate leave the cell, followed by nucleic materials [6][21]. Eventually the cell dies. Generally an enhanced adsorption is expected for polycationic molecules, but the increased size may reduce the permeability into the cell [6]. The most common family of cationic biocides are quaternary ammonium compounds (QACs). They have a detergent like structure, that is a hydrophobic hydrocarbon chain with a polar head group, but whereas the head groups in detergents contain a negative charge, these molecules contain a positive charge at their head groups. They are effective, because of ionic and hydrophobic interactions between the antimicrobial and the microbial cell [1]. They are most effective when they posses an alkyl chain with at least eight carbon atoms [30][6][31]. QACs retain their antibacterial properties even after tethering to a surface without being released into the body [1][29][32]. Unfortunately the killing on contact leaves a layer of dead bacteria providing a good platform for the adherence of new bacteria [1]. The application of these coatings is only reasonable where few bacteria need to be killed or where the immune system helps to get rid of the dead micro-organisms [1]. The removal may be achieved by brushing teeth and thus these coatings may be promising for the application in the oral cavity [1].

1.2.4 Tissue-Integrating Surface Coatings

In biomaterial research the phrase: "race for the surface" was coined by A. G. Gristina. He presumes that the fate of the biomaterial is dependent on who wins the competition for the surface, tissue-integrating cells or bacteria. If the tissue cells win the race, they will occupy the surface and make bacterial colonization unlikely [4]. Therefore, tissue integration promoted by films bearing cell adhesion mediators (e.g. fibronectin) or peptide sequences like RGD (RGD: arginine-glycine-aspartic acid), a component of many extra cellular matrix molecules (e.g., fibronectin, fibrinogen, and vitronectin), are a further concept for antimicrobial surface coatings [1].

1.2.5 Auspicious Concept: Multifunctional coatings

Coatings killing bacteria upon contact are more promising than antimicrobial release coatings, especially, for dental applications [1]. Most coatings for biomaterials are mono-functional, i.e. either aiming on inhibiting biofilm formation or in stimulating tissue integration [1]. Multifunctional coatings providing both, anti-adhesive or on contact-killing properties in com-

bination with tissue integrating factors are an auspicious concept for biomaterial coatings [3]. Bifunctional coatings may be especially promising for the prevention of peri-implantitis, since the fate of dental implants also depends on a race for the surface between biofilm formation and tissue integration [1].

2 Surface Coatings based on Polyamidoamine (PAMAM)

Polyamidoamine is a dendrimer. Dendrimers are a remarkable sub-class of hyperbranched polymers. They possess a beautiful radial symmetry, are highly branched, mono-disperse, almost spherical in shape, and emanate from a central core [30]. The following section will briefly introduce dendrimers and in particular the structural features and properties of polyamidoamine. Thereafter, the advantages of applying dendrimers in antimicrobial concepts will be addressed. The terminatory section summarizes immobilization strategies for polyamidoamine already mentioned in literature. Joining both, effective immobilization techniques and antimicrobial enhancement by dendrimers seems to be a very promising approach for bactericidal coatings.

2.1 Dendrimers

Dendritic structures are ubiquitary motifs in nature and have been successfully applied throughout evolution. They enable a particular function to be available at multiple, densely packed positions at the same time. This can sometimes lead to an amplification of this function, exceeding the effectiveness that would be obtainable when summarizing all single functional units involved. This is referred to as a synergistic effect achieved by the dendritic arrangement of a particular function. The high local concentration of functional groups may also be denoted as "multivalency", especially if charged moieties are involved. [17]

Trees, for example, utilize dendritic motifs to enhance photosynthesis by exposing numerous leaves to sunlight (view Figure 2.1). Below the surface a dendritically shaped root system accomplishes peak performance in collecting water from the soil. In our body the network of bronchioles and alveoli within the lungs, the arterial network and the central nervous system are designed in dendritic structures in order to maximize the exchange of mate-

Figure 2.1

"Four trees"
by Egon Schiele (1890-1918)

rial/information with the surroundings. [17]

In 1978 Vögtle and co-workers prepared the first dendritic molecules by organic synthesis. Taking up on this idea, Tomalias group at Dow Chemicals developed larger, amide bond containing, star-like macromolecules and termed this new class "dendrimers". The word "dendrimer" is of Greek origin, where "dendros" means "tree" and "meros" means "part". Tomalia and co-workers invented polyamidoamine (PAMAM) in the 1980s.

2.1.1 Structural Features

Dendrimers are composed of three constitutive parts as depicted by a second generation polyamidoamine in Figure 2.2: a core (here: ethylene diamine), concentric homo-structural layers around the core called "generations" (indicated by dotted circles in 2.2), and terminal groups.

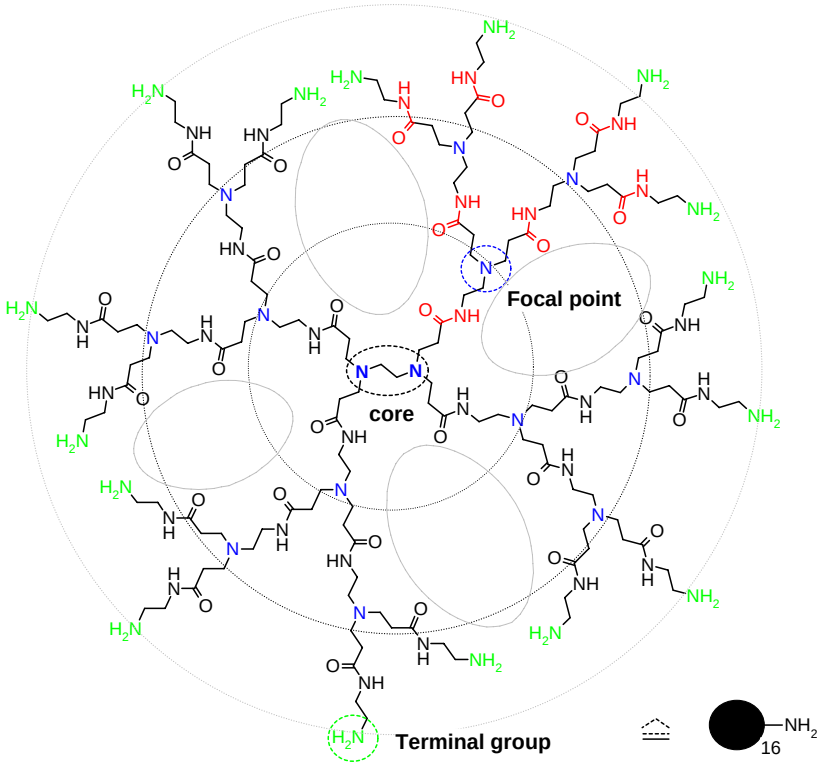

Figure 2.2: Schematic representation of a second generation (G2) polyamidoamine (PAMAM) terminated by amino groups. Circles depict the layers of re-occurring units. Branching points, referred to as focal points, are highlighted in blue. Terminal groups are marked in green and the central core is presented in black. The four ovals in grey accentuate the large voids occurring within dendrimers. Within one dendron all amide bonds are highlighted in red. At the bottom right corner an convenient abbreviation for the voluminous molecule is shown.

Each generation is terminated by focal/branching points (marked in blue) if not situated at the dendrimer periphery. Generations at the rim of the dendrimer are terminated by end

groups. The number of focal points counted along one dendrimer branch from the centre to the periphery represents the generation number of the presented dendrimer. There are discrepancies in literature regarding the counting of generations. Some researchers refer to the inner core as "G0" [17] as originally proposed by Tomalia [7], but the main manufacturer of PAMAM, Dendritech Inc., refers to the first actual dendrimer as "G0" - Tomalia uses this terminology as well, in later publications [33]. The word "Generation" is abbreviated by a capital "G" followed by the respective number of re-occurring layers around the core. The outermost functional groups are termed "end groups" or "terminal groups". Furthermore, dendrimers possess large inner cavities between the dendrons as shown by the grey ovals in Figure 2.2. These are well shielded from the exterior. Because of the large molecular dimensions of dendrimers they may be abbreviated by a "black ball" (presented in Figure 2.2, bottom right corner) only representing the terminal groups by chemical structures. This representation is especially favoured if reactions at the periphery are of interest only [17].

All three structural elements of a dendrimer - the core, the region between core and periphery (dendrons), and the outermost multivalent surface - can be tailored by organic synthesis in such a way that the dendrimer obtains different molecular properties, functions, sizes, molecular weights, and solvent interactions [30]. Voids within the dendrimer serve as endo-receptors and the terminal functional groups as exo-receptors [34]. A skilful design of both, endo- and exo-receptors, has been applied to design dendrimers for gene delivery [8], anti-sense oligonucleotide transfection agent [35], chemical sensing, metal complexing agents [36], nanoreactors for particle synthesis [36], nanoscale catalysts [37], micelle mimics [37], high-performance polymers [37], adhesives [37], and drug transport agents [30][38]. As an example, most drugs are hydrophobic and not very soluble in water [30]. Therefore, dendrimers with an apolar interior and water soluble terminal groups have been designed to transport the hydrophobic drugs in the bloodstream [17][30][8].

2.1.2 Dendrimer Synthesis

Dendrimers are either synthesized by divergent or by convergent approach [30]. Dendrimer preparation by divergent approach starts from a multi-functional core. Successive reaction and purification steps cause radial growth of the dendrimer [30]. Dendrimers synthesized by this method are, e.g. PAMAM from Dendritech Inc. (Midland, MI, USA) and PPI (poly(propylene)imine) from DSM (Geleen, Netherlands). The molecular weight (MW) and the number of terminal groups increase rapidly with each generation, as demonstrated for PAMAM-NH_2 in Table 2.1.

G	MW [g/mol]	∅ [Å]	End groups
0	517	15	4
1	1,430	22	8
3	6,909	36	32
5	28,826	54	128
8	233,383	97	1024
10	934,720	135	4096

Table 2.1: Theoretical properties of PAMAM-NH_2, kindly provided by Dendritech Inc. (Midland, MI, USA). PAMAM$-NH_2$ (G5) is highlighted since all experiments carried out for this thesis are based on this molecule.

In line with the generational growth of PAMAM-NH_2 the number of terminal groups is doubled and the molecular weight (MW) gets approximately twice as high. The increasing molecular weight and the large amount of terminal groups that need to be functionalized within each step causes reduced reaction kinetics and results in low yields of fully converted molecules [17]. Separation from defect dendrimers becomes more and more difficult with increasing generation because of the high molecular similarity [17]. Dendrimer growth is also limited by steric hindrance. At a certain stage a full conversion of all terminal groups becomes impossible due to the intensive crowding at the dendrimer periphery [30]. PAMAM dendrimers, for example, are only commercially available as methanolic solutions up to G10.

As mentioned above, PAMAM-NH_2 is synthesised by the divergent approach. The reaction pathway is depicted in Figure 2.3.

Each generational growth is composed of two successive reaction steps:

- **Step 1:** The core molecule (e.g., ethylene diamine or ammonia; the use of ammonia reduces the multiplicity of the core from 4 to 3) is reacted with acrylic acid methyl ester in methanol by exhaustive **Michael addition** to form tertiary amines.
- **Step 2:** Ester groups are split by exhaustive **Amidation** using ethylene diamine.

Both steps are performed at low temperatures (i.e., 25 - 50°C). Higher temperatures (i.e., above 80°C) cause intramolecular cyclization, retro-Michael reactions and intermolecular transamidation reactions resulting in imperfect dendrimers. A detailed description of the synthesis procedure and possible sources of error are mentioned in reference [7]. The synthesis steps are generally monitored by ^{1}H and ^{13}C NMR, size exclusion chromatography and infrared spectroscopy. Information on the final structural conformation is obtained by light scattering, titrimetry, mass spectroscopy and elemental analysis. [7]

Dendrimers prepared by convergent approach are synthesised from the periphery towards the core. That means that the dendrimer branches (dendrons) are prepared in advance and af-

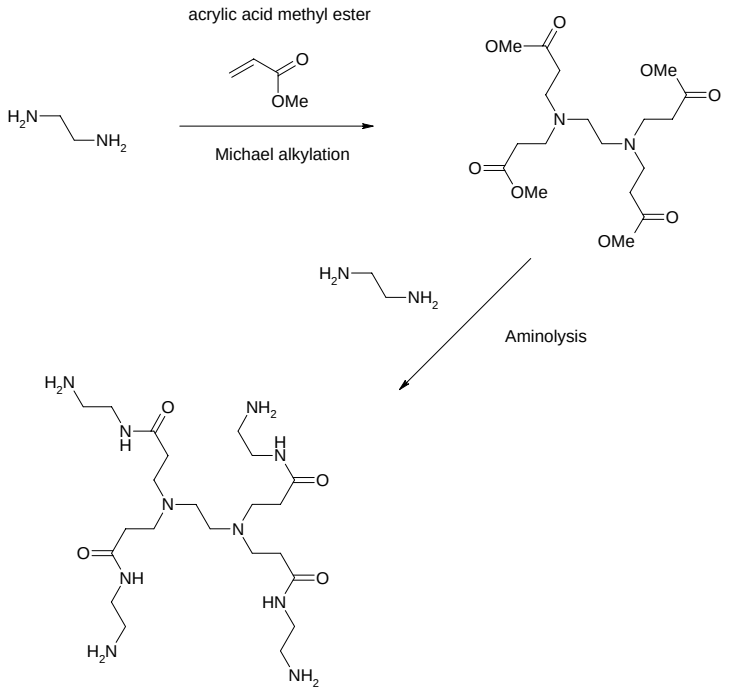

Figure 2.3: PAMAM-NH_2 synthesis by divergent strategy as invented by Tomalia and co-workers [7]. Within this picture the first two steps in PAMAM-NH_2(G0) preparation are illustrated. Dendrimers of higher generation are obtained by sequential Michael addition and Amidation.

terwards connected to a multifunctional core. Reactions proceed much faster because smaller molecules and less end groups are involved in each reaction step. Furthermore, the reactant molecule differs strongly from the product in molecular size making separation easier [17]. The preparation of defect-free dendrimers by this approach is of higher probability and one can even connect dendrimer branches of different chemistry to one central core [30].

In contrast to structurally imperfect and polydisperse polymers, dendrimers are well-defined and monodisperse [17]. However, iterative synthesis steps and associated purification necessary for production result in very high prices for dendrimeric macromolecules [30].

2.1.3 PAMAM Properties

It is because of these extensive and still not completely resolved properties on PAMAM, that this subsection will focus on PAMAM mainly, instead of illustrating dendrimer properties in summary. Just like proteins, each type of dendrimer seems to have its own character. This can be illustrated nicely by the two very different protonation patterns that are predicted for the structurally not too dissimilar dendrimers PAMAM-NH_2 and PPI-NH_2.
Both dendrimers, PAMAM-NH_2 and PPI-NH_2, possess primary amines on the exterior and

tertiary amines throughout the dendrimer interior as presented in Figure 2.4, where both dendrimers of G1 are juxtaposed against one another. Depending on the pH of the solution, amino groups may be protonated or not. Protonation of basic functions results in the formation of positive charges and thus to an overall charge development.

Primary and tertiary amines protonate independently in large PAMAM-NH_2 dendrimers at

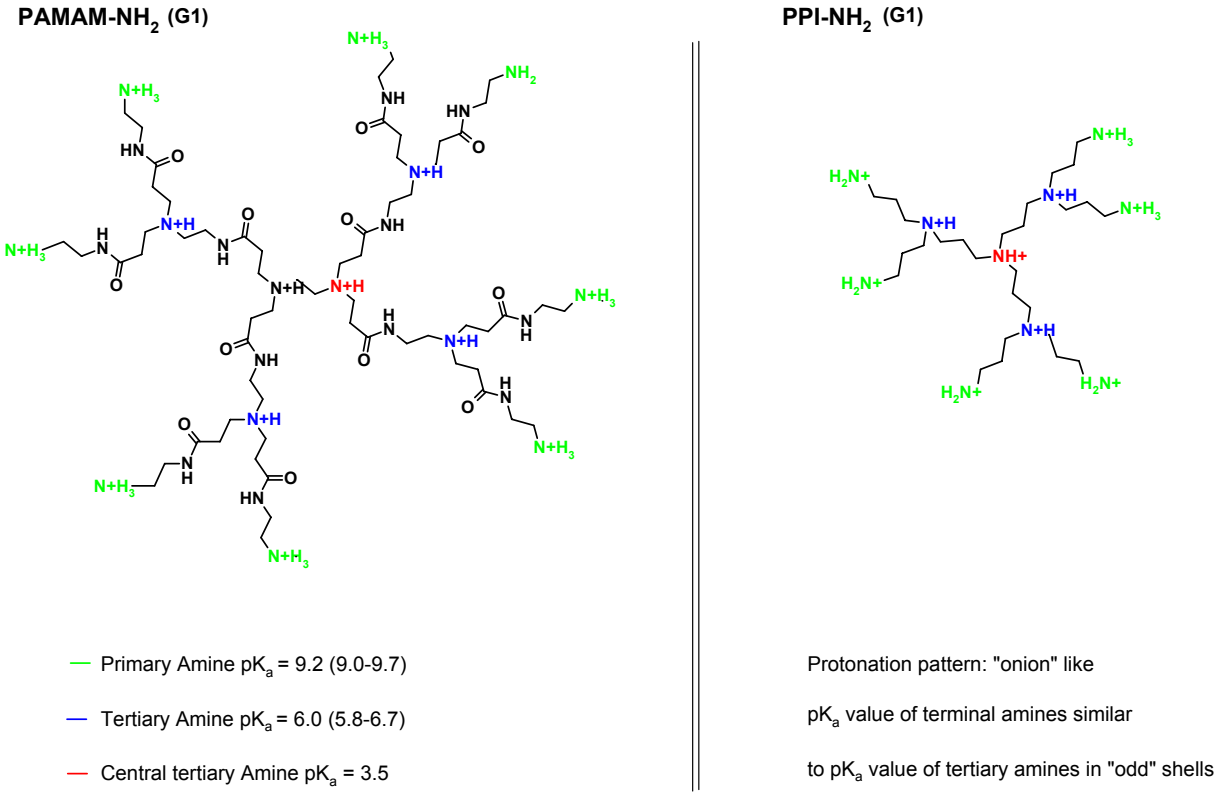

Figure 2.4: PAMAM-NH_2 dendrimer and PPI-NH_2 dendrimer in a protonated state

ionization constants of $pK_a = 9.2$ (9.0 - 9.7) (terminal amines) and $pK_a = 6.0$ (5.8 - 6.7) (tertiary amines), respectively [39][36][40]. Only one of the tertiary amines situated in the core is assumed to possess an intrinsic proton binding constant of round about 3.5 [36], but due to the numerous positive charges in large PAMAM-NH_2 dendrimers, this last protonation step contributes very little to the overall charge development and may not be distinguishable. In contrast to small dendrimers where this last step is clearly discriminable. Contrary to the protonation behaviour in PAMAM-NH_2, dendrimers protonation within the PPI-NH_2 dendrimer is suggested to occur in an "onion" like manner; meaning, the outermost primary amines and the tertiary amines of the odd shells protonate first (corresponding to 2/3 of the maximum charge) at a pH value of about 10. Thereafter, the even shells protonate at a lower pH - round about pH 5 [41][36]. This type of protonation pattern avoids strong repulsive

interactions between functionalities of likewise charge and is significantly different to the one observed for PAMAM-NH_2. The larger distance between charged sites in PAMAM-NH_2 [36] and the presence of amide bonds between branching points may be the reason for a different protonation pattern. Nearest-neighbour interactions are expected to be weaker in PAMAM-NH_2 and thus protonated sites influence each other to a lesser extent [36]. The pK_a value for the tertiary amines in PAMAM-NH_2 is about 1-2 units lower, than one is familiar with for a monomeric tertiary amine in a structurally related compound [39]. The reduced pK_a value is ascribed to a microenvironment within the dendrimer interior of higher hydrophobicity (reduced water accessibility), lowering the affinity towards protonation [39]. Additionally, electrostatic repulsion between already protonated sites causes the pK_a value to drop [39].

An ionic strength increase from I = 15 mM to I = 115 mM lifts the pK value of tertiary amines from 6.00 to 6.65, the pK value of the primary amines is merely affected by this jump in ionic strength (pK = 9.15 at I = 29 mM to 9.30 at I = 129 mM). The addition of salt decreases electrostatic repulsion between protonated binding sites because counter-ions screen the Coulomb charge of the positive sites by ion-pairing, this may even be more effective in an apolar environment. [39]

Charged groups do not only influence the protonation behaviour of sites in close vicinity, they also induce conformational changes in polymers because of repellent Coloumb interactions. This is especially pronounced in solutions of low ionic strength.

De Gennes and Hervet were the first researchers to report on the conformational behaviour of PAMAM in course of molecular growth using molecular simulations (1983). They concluded that the periphery becomes increasingly crowded upon generation growth, whereas the density of the interior remains low. Back-folding, as depicted on the right hand side in Figure 2.5 (i.e., dendrons bending into the dendrimer interior) was not taken into consideration by these researchers. [17]

Also, Lescanec and Muthukumar (1989) studied the conformational behaviour of PAMAM by computer simulation, but employed a different algorithm and model as De Gennes and Hervet [42]. They calculated intramolecular density profiles indicating a strong back-folding of the branches into the dendrimer interior instead of a restriction of the terminal groups to the surface, as proposed by De Gennes and Hervet.
Back-folding is an entropy driven processes to avoid the well ordered De Gennes dense periphery conformation and results in a uniform molecular density with a random distribution of the terminal groups throughout the molecule [33]. Back-folding can be prevented by introducing surface groups, which interact by hydrogen bonding or ion pairing with each other.

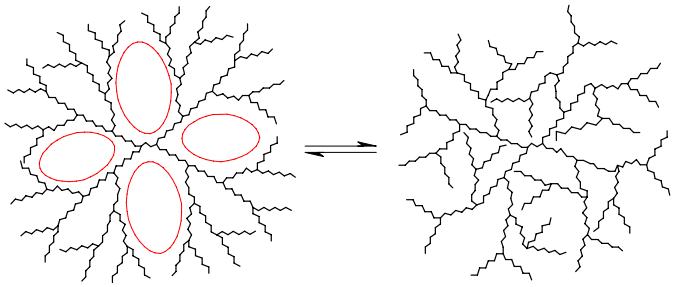

Figure 2.5: Left hand side: De Gennes and Hervet "dense shell" model [17]; red ovals represent the large voids within the dendrimer
Right hand side: schematic representation of back-folding in PAMAM-NH_2 dendrimers;

These forced "dense shell" dendrimers are termed "dendritic box" [17].

Not only computer based simulations but also experimental studies such as ^{2}H and ^{13}C NMR experiments and investigations with a negatively charged, polarity-responsive probe molecule (5-(dimethylamino)-1-naphtahlenesulfonic acid, DNS) confirmed back-folding in PAMAM-NH_2 [33].

Simulations and experiments focussing on the changes in PAMAM-NH_2 conformation and size as a consequence of pH differences led to the following model. PAMAM-NH_2 is expected to acquire a highly ordered, hollow, hydrated (increased polarity [33]) and expanded conformation at low pH values because of electrostatic repulsion between positively charged segments. As the pH increases, positive charges from the tertiary amines within the dendrimer disappear (resulting in a micro-environment of less hydrophilicity) and the dendrimer begins to shrink. At very high pH values, where no charged sites are present any longer, PAMAM-NH_2 is assumed to be of minimal size because of extended back-folding and the loss of repulsive forces. [17][33]

A very recent study carried out by Goddard and co-workers (2009) describes a slightly different picture. They performed refined computer simulations applying atomistic molecular dynamic simulations, including an explicit number of solvent molecules (water) and couterions (Cl^- ions) and a force field whose parameters were optimized by quantum mechanics. Their assumptions are based on solvent accessible surface area (SASA) and solvent excluded volume (SEV) calculations. They propose a "dense core" conformation due to extensive back-folding at high pH values, like proposed in the above model, but with uniform voids. At low pH values ion pairing within the dendrimer-water-counter-ion system is said to cause a "dense shell" with non-uniform voids. The internal surface area is predicted to decrease

by 63.5 % from high to low pH, just like the internal void volume by 21.0 %. This result is worth mentioning because it disagrees with intuitive expectations, but one often neglects the presence of counter-ions. Focussing on the schematic representation in Figure 2.5 one would rather expect uniform voids at conformations where less back-folding occurs, rather than at situations of intensive back-folding. Furthermore, Goddard and co-workers calculated a swelling of less than 5 % for PAMAM$-NH_2$ G4 upon pH decrease. This result is in excellent agreement with small angle neutron scattering experiments on PAMAM-NH_2 (G8 - G4) where no changes in the radius of gyration were observed by changes in pH or salt concentration but at variance to some other theoretical simulations and experiments [33]. They suggest that the insensitivity in size by means of pH changes derives from a competition between geometrical shrinking and mass redistribution. At low pH an outward mass redistribution is equaled by a reduced solvent accessible surface area. [43]

Well, the above findings show, that it is still not absolutely clear how PAMAM-NH_2 behaves upon pH changes. Anyhow, these calculations support the assumption that PAMAM-NH_2 dendrimers possess a high flexibility and perform conformational transitions as the pH varies. Especially, G5 - G7 dendrimers are strongly affected by changes in pH and ionic strength in comparison to higher generations, most probably because of the restricted motion of the outer segments in dendrimers of higher generation [17]. Dendrimers of higher generation resemble medium sized proteins in their molecular dimensions, e.g. haemoglobin (5.5 nm's in diameter). Just like proteins, dendrimers seem to change their conformation, even though not as sophisticated as the biomolecules due to changes in solvent, pH, ionic strength and temperature. Thus, dendrimers may be used as artificial mimics of proteins even though exposing a much higher multivalency than proteins of similar molecular size [17]. PAMAM-NH_2(G5) is also referred to as an "artificial protein" because of its size and the high number of peptide bonds within the molecule.

2.2 Dendrimer based Antimicrobials

Dendrimers became a matter of interest as potential antimicrobial agents because of the very tight arrangement of their multiple end groups. The high local concentration of the terminal functional groups was anticipated to support cooperative interactions or synergies. [30][6][21]
The effectiveness of multivalent interactions can be impressively demonstrated by the following example: Bacteria posses ligands that detect saccharide moieties on cell surfaces. Galabiose motifs were tethered to a carrier molecule generating dendritic galabiosides with either one, two, three or four galabiose motifs. The molecule possessing four saccharide

moieties was several hundred times more effective than the one with one motif in inhibiting haemagglutination by bacteria. Glycodendrimers have already been patented to fight bacterial and viral diseases. [30][6][21]

Whether dendrimers, possessing multiple positive charges, are more efficient in their antimicrobial properties in comparison to their mono-functional counterparts was assessed by Chen et al in the year 2000. They studied polypropylene imine dendrimers from G1 - G5, which got terminally functionalized by dimethyl alkyl (various lengths) ammonium groups in terms of their antimicrobial activity. In respect of killing gram negative bacteria (e.g. *Escherichia coli*) an increased efficiency of more than two orders was observed for dendrimer molecules in comparison to their mono-functional counterparts. This effect was also detected for gram-positive bacteria (e.g. *Staphylococcus aureus*), but they are commonly more prone to antimicrobials due to their less complex structure. The biocidal efficiency was shown to depend on the dendrimer size, the length of the hydrophobic chains in the quaternary ammonium groups and the counter-ion. Hydrophobic chains of 10 methylene units revealed the highest antimicrobial effect, but there is evidence that this may be depended on the structure of the biocide and the nature of the bacteria. Furthermore, bromine counter-ions seemed to support antimicrobial properties in comparison to chloride anions. The higher the dendrimer generation the higher their power in killing bacteria, implying that rather the functional group density is the decisive factor regarding the biocidal effect than the permeation through the cell membrane. Especially important, hyper-branched polymers carrying identical functional groups were less potent than the dendrimer counterparts. [30][6][21]

The above mentioned antimicrobial dendrimer carries well known antimicrobial agents at the periphery, but PAMAM-NH_2 was also determined to be biocidal without the tethering of quaternary ammonium functionalities. PAMAM-NH_2(G5) was reported to be highly toxic to the common gram-negative pathogen *Pseudomonas aeruginosa* and less toxic to gram-positive pathogen *Staphylococcus aureus*. Regarding eukaryotic cells PAMAM-NH_2 revealed low toxicity at low concentrations. PEGylating 43 % of the periphery of PAMAM-NH_2(G5) reduces cytotoxicity to epithelial cells. In spite of the PEG coating a high toxicity against *Pseudomonas aeruginosa* is retained, but a large decrease in toxicity to gram-positive strains was recorded. The toxcicity of PAMAM-NH_2 is ascribed to its poly-cationic nature, since the capping of the terminal groups by acetyl groups causes a loss of this property. [44]

Especially the observation that hyper-branched polymers with identical functional groups are less potent than their dendrimer counterparts supported the decision to investigate coatings based on dendrimers rather than on commonly used polymers for the application of antimicrobial coatings in biomaterial applications as aimed at in this thesis. It may be as-

sumed that this may be because dendrimers exceed polymers in respect to the accumulation of active groups. A further advantage of the poly-valency is that they posses the ability to displace bacterial membrane stabilizing ions, such as calcium and magnesium [30][6][21].

2.3 PAMAM Immobilization Strategies

Dendrimer coated surfaces have gained enormous interest, especially in the field of analytic biochip array technology [45][46]. The higher density of functional groups in dendrimer layers in comparison to linear alkyl-chain based SAMs was reported to enhance the sensitivity of analytical methods and thus reduce the limits of detection [46][45]. Also surface related phenomena like fluorination and adhesion are expected to be enhanced by this novel strategy [37].

PAMAM-NH_2 based surface coatings can either be achieved by electrostatic adsorption of the dendrimer onto the solid surface or by covalent fixation. Both deposition methods have been reported in literature. Observations made on dendrimers upon surfaces, explicitly PAMAM-NH_2, regarding these two ways of immobilization, will be summarized in this section.

Both, hydrophilic and hydrophobic surfaces effect the structure of PAMAM-NH_2 dendrimers (G4 - G9) upon adsorption [47][48]. Whereas on hydrophobic surfaces dendrimers retain their spherical shape [47][48], they are considerably flattened on negatively charged surfaces like mica [49] or indium tin oxide [50]. This reflects the strong contribution of electrostatics to the adsorption process [51]. On hydrophobic surfaces the interactions between the primary amines and the substratum are decreased [48]. The flattening on hydrophilic surfaces was observed to be dependent on the dendrimer generation. PAMAM$-NH_2$ of the generations 0 to 4 are strongly compressed, whereas generations higher than 5 resemble ellipsoids upon the surface [47][49]. Acidification of adsorbed PAMAM$-NH_2$ dendrimers (G6 - G9) caused a volume and height increase, as well as a decrease in diameter upon the surface [48]. This observation is attributed to maximum charge separation and the gathering of increased amounts of solvent [48]. Exposing dendrimer coated Au surfaces to solutions of hexadecanethiol solutions, the dendrimer conformation changes from oblate to prolate because stronger thiol-Au bonds displaced some of the amine-Au bonds leading to an increase in layer thickness [47]. The "multipoint attachment" is more pronounced for isolated dendrimers than for full monolayers, where intermolecular interactions between the dendrimers affect the conformation.

The first publication reporting covalent immobilization of PAMAM-NH_2 dendrimers onto surfaces was issued in 1996 and authored by Mona Wells and Richard M. Crooks [34][52].

They prepared monolayer dendrimer films on mercaptoundecanoic acid SAMs on gold and tested these films regarding their suitability for chemical sensing applications [34]. These films performed very well and were rated very high in fulfilling other application needs. Richard M. Crooks patented this invention in 1997 (Int. Pub. Number: WO 97/39041).

The confinement of PAMAM-NH_2 onto gold surfaces mediated by self assembled monolayers (SAMs) of ω-alkyl thiols is the fixation that is mostly applied [34][53][46]. This is an easy way of preparation but suffers stability in subsequent derivatization steps and is not a general method applicable for all kinds of surfaces. Fixation to hydroxide terminated surfaces via silane chemistry [54] is used to a lesser extend since the former preparation path is of higher ease. But also other layers, mediating between hydroxylated substrata and PAMAM-NH_2, have been used like plasma polymerized maleic acid anhydride [37]. Benters et al. prepared amino terminated surfaces by using (3-aminopropyl)trimethoxysilane and tethered PAMAM$-NH_2$ thereto, by either activating the amino groups using 1,4-phenylenediisothiocyanate or converting the amino groups into carboxylic acids by reaction with glutaric anhydride, linking PAMAM-NH_2using N-hydroxysuccinimide / N,N'-dicyclohexyl-carbodiimide coupling. Furthermore, they were also linked it to an epoxy-modified surface [54].

3 Surface Coatings based on Linear Alkyl Chains (SAM)

Molecular monolayers, only a few nano meters thick, are enough to completely change the properties of a solid surface (e.g. wettability) and introduce new characteristics like corrosive protection or biocompatibility [55]. Zisman and his co-workers reported in 1946 on the self-organization of long-chain hydrocarbons with polar head groups on polar surfaces [56]. The potential of this finding was long left unnoticed. It was only in 1978 that, Polymeropoulos and Sagiv propose first applications for this discovery. In 1980, Sagiv announced the formation of spontaneously formed, highly ordered organosilane monolayers on silicon dioxide surfaces adsorbed from solution [56][57]. In 1983, the term "self-assembling monolayer" (SAM) is firstly mentioned in a report on the work of Lucy Netzer and Jacob Sagiv [56].

There are a few self-assembling systems, like the self-organisation of sulfur (alkanthiols) containing molecules on gold, alkylsilanes on oxide surfaces, amines on platinum and fatty acids on aluminia [58][59]. But the two former adsorbate/substrate combinations are the ones most common. Whereas, comprehensive studies were preformed on alkylthiols on gold, less were carried out using alkylsilanes, but surface coatings based on siloxane chemistry were reported to be of higher stability in many cases (probably because of the cross linking among the molecules) [60], thus allowing a broader spectrum of post-modification steps.

The focus of this thesis is on self-assembled monolayers (SAMs) prepared from silane molecules on hydroxylated silicon based surfaces (Si-OH) and their further transformations to induce surface property changes. The following subsections will shortly introduce the nature of silane molecules, the preparation of SAMs by these molecules and the structural features of the resulting siloxane layers.

3.1 SAM Component: Organosilanes

ω-functionalized alkylsilanes ($Y-(CH_2)_n-SiX_3$) possess the ability to mediate between inorganic substrata and organic coatings. They are typically constituted of a terminal group (Y) (responsible for the exposed surface functionality), an alkyl chain linker ($-(CH_2)_n-$)

(promoting organization), a silicon atom and a hydrolyzable group [(X; alkoxides ($-OR$) or halides ($-Cl$)]. The high affinity of the hydrolyzable group to nucleophiles, especially of ω-alkyl-tri-chloro silanes, results in a reduced spectrum of possible terminal groups (Y). In other words, not all desired surface functionalities (Y) are compatible with the anchoring site in silane molecules [61]. Also, carboxylic acid- (-CH_2-COOH), amino- (-CH_2-NH_2) and hydroxy functionalities (-CH_2-OH) need to be created from non-polar precursors [59], if neatly formed SAMs are desired. This also applies for, positively charged terminal groups like trimethylammonium moieties. The head groups would compete with the silyls groups for surface occupation, where the head groups interact due to charge neutralization with the surface and the silyl groups to undergo hydrolysis. This causes coating disorders. They also need to be incorporated into the coating after silane fixation.

There are two popular ways to synthesise alkyltrichlorosilanes [59]:

$$\mathrm{R{-}Br + Mg \longrightarrow R{-}MgBr; R{-}MgBr + SiCl_4 \longrightarrow RSiCl_3} \qquad \textbf{Grignard based} \qquad (3.1)$$

$$\mathrm{R{-}CH{=}CH_2 + HSiCl_3 \longrightarrow R{-}CH_2{-}CH_2{-}SiCl_3;} \qquad \textbf{Hydrosilylation} \qquad (3.2)$$

Hydrosilylation of the olefine is performed by reaction with $HSiCl_3$ in CCl_4 using chloroplatinic acid catalyst [62]. Chlorosilanes are more reactive than alkoxysilanes [56] but alkoxysilanes are of higher stability in synthetic preparations. The may also be synthesized from the less reactive ω-alkyltrimethoxy silanes using trichloroacetyl chloride [56].

3.2 SAM Preparation and Transformation

Organic films prepared by organosilanes are known to be very sensitive in respect to the reaction conditions. The final structure is affected by numerous factors, like the reaction temperature, the nature of the silane (mono-, di-, or tri-alkoxy/chloro silane), the silane concentration, the incubation time, the type of solvent, the presence of a catalyst (base), post-curing and especially, the most crucial factor in the silanization process, the amount of water adsorbed to the surface or within the solution [56]. Furthermore, cleaning and oxidation procedure of the substrata (governing the concentration of surface hydroxyl groups), handling, preparation from vapour [63] or solvent phase additionally influence the morphology, thickness and conformation of the prepared monolayer coating [64][65]. It is out of scope of this thesis to review all these factors in detail, but a few will be emblazed in the next paragraph.

Layer formation is generally accomplished in more or less two hours, but incubation times of more than 12 hours have shown to generate surface coatings with less defects [58]. Well

defined coatings were obtained using silane concentrations of about 3 - 25 mM solutions. Recommended solvents for good quality monolayers of great reproducibility are toluene, hexadecane and carbon tetrachloride. Regarding chlorosilanes, ambient temperature leads to the formation of high-quality SAMs, whereas elevated temperatures cause coatings of poorer quality [56]. Because water is omnipresent in atmosphere reproducible coatings may only be achieved by careful handling procedures. Large amounts of water promote polymerization of the silanes in solution before deposition, these aggregates compete with single silane molecules to attach to the surface resulting in a heterogeneous, multilayer coat [66][65]. On the other hand, the absence of water generally leads to coatings of poor quality [56]. Long alkyl chains (e.g. eleven CH_2 units [67]) form highly ordered layers because van der Waals forces between the molecules stabilize the formation. Molecules constituted of shorter alkyl chains can not be arrayed in a perfect structure due to the reduced van der Waals interaction forces between adjacent chains [58][64]. Prior to silanisation surfaces need to be cleaned and treated to maximize the number of silanol groups. Usually strong acids (mixture of 30% H_2O_2 and concentrated H_2SO_4) or oxygen plasma are used to generate Si-OH groups upon substrata [56][46].

As mentioned in the previous subsection, some surface functionalities have to be introduced into SAMs after silane deposition. Then the terminal groups have to be converted quantitatively within a rigid and densely packed environment, and this is often a problem. Solution reactions with high yields are sometimes less successful when transferred to surfaces in regard of conversion yield and pace [60][61]. The reactivity of the participating functionality upon the surface may be decisively lowered because of steric constraints especially in reactions proceeding from backside (e.g., Sn2 reaction) or involving large transition states (e.g., esterification) [60][64]. Further limitations may be due to transport problems, solvation effects, dipole effects and charge [56]. Sometimes disordered SAMs are prepared on purpose, achievable with silanes composed of short hydrocarbon chains and bulky head groups (e.g. (3-glycidyloxypropyl)trimethoxysilane [66]), to increase conversion yields. Surface reactions should be reactions that proceed at quantitative conversion, under mild conditions (i.e., atmospheric pressure and room temperature), without catalytic activation or by-products because these may accumulate at the interface and retard or stop the reaction site [61] and at worst be impossible to remove. A further limiting factor in SAM transformation is the instability of SAMs in basic media. The hydrolysis of Si-O bonds causes delamination and coating loss [56]. Derivatization has to be accomplished in neutral to acidic media [56].

3.3 SAM Formation Mechanism and Siloxane Structure

The mechanism of self-assembled monolayers on silicon dioxide surfaces is still subject of debate [56]. SAMs are formed by immersing hydroxylated surfaces into silane solutions. Hydrolysis of the siloxy group forms silanol moieties which can condense with other silanol groups either provided by the substratum or other silane molecules. Condensation among organosilanes forms oligomers. Hydroxylated surfaces bearing high amounts of silanol groups, are hydrophilic and favour the adsorption of water molecules. Sagiv was the one to report on the necessity of water for silanization [56]. In anhydrous organic solvents traces of water assemble near the hydrophilic surface supporting silane hydrolysis in close vicinity to the surface hydroxyl groups promoting condensation with the surface [63][66]. It is assumed that silane molecules aggregate by attractive van der Waals forces between adjacent alkyl chains and hydrogen bond formation between the head groups before polymerization and Si-O-Si bond formation. The surface affine head groups guide the aggregate towards the surface. Sagiv hypothesised that subsequent to silane hydrolysis (Si-OH), condensation with hydroxyl moieties upon a surface (covalent anchorage) and among each other (polymerized network) (Si-O-Si bond formation) occurs [56]. But since SAMs of octadecyltrichlorosilane also form on gold, i.e. in the absence of hydroxyl groups, and the observation that the surface roughness of a pristine wafer decreases after SAM deposition, leads to the assumption that the siloxane layer forms on the adsorbed water film in a two-dimensional, carpet-like, network of Si-O-Si bonds with only a few molecules anchoring the network covalently onto the surface [56][68]. Therefore numerous silanol groups may be left free.

Depending on the alkyl chain length the SAM thickness may vary between 0.6 nm (three CH_2 units) and more or less 2.5 nm (seventeen CH_2 units) [59][69].

4 Electrokinetic Surface Charge

A charged interface is very often formed when a solid object is immersed into an electrolyte solution. Preferential ion/molecule adsorption, the ionisation of surface bound chemical groups (e.g. carboxylic acid groups), the presence of permanently ionic structures (e.g. tertiary amine groups), as well as isomorphic ion substitution (e.g. Si^{4+} ion replaced by an Al^{3+} ion) and partial desorption of ions from the solid surface are possible mechanisms for the generation of surface charge. The charged object surface and its adjacent solution phase, enriched with charge neutralizing ions, are referred to as the **E**lectrochemical **D**ouble **L**ayer (**EDL**, see Figure 4.1). [70]

The formation of an EDL enables a series of phenomena, when an electrolyte solution is tangentially moved along a charged surface. These phenomena are referred to as **E**lectro**K**inetic **P**henomena (**EKP**). EKP reveal information about the electrical properties of an interface. The relative movement of the solid phase against the liquid phase can be induced by an external electric field (e.g. electrophoresis, electro-osmosis) or by the application of a mechanical force (e.g. streaming potential/current, sedimentation potential). [71]

The **electrokinetic charge** (σ^{ek}) determined by EKP measurements reflects the properties of the outer parts of the EDL (i.e., at the slip plane, explained in detail in section 4.2) and not the **surface charge** (σ^0) as such. The surface charge (σ^0) can be determined by potentiometric titration of dispersed particles. "Surface charges and electrokinetic charges are very different double layer characteristics" as stressed by Lyklema et al, unfortunately this differentiation is often not made in literature. [72]
There are only a few analytical methods to determine the same electrical properties of a liquid/solid interphase [72], therefore results gained from EKP are mainly interpreted in terms of EDL models [71][73].

The following section will briefly introduce EDL models. Thereafter, the definition and determination of the well known ζ-potential obtained from electrophoresis and streaming current measurements will be presented, since the electrokinetic surface charge within this work was exclusively determined by these EKP. Also, the less popular value, surface conductivity, will be introduced there. The final section reports recent scientific developments

in the characterization of soft surface coatings.

4.1 Electrochemical Double Layer (EDL) Models

Even though EDL models describe the charge distribution and potentials in the vicinity of a solid surface in the static state, they have been successfully applied for the interpretation of dynamic EDL properties.

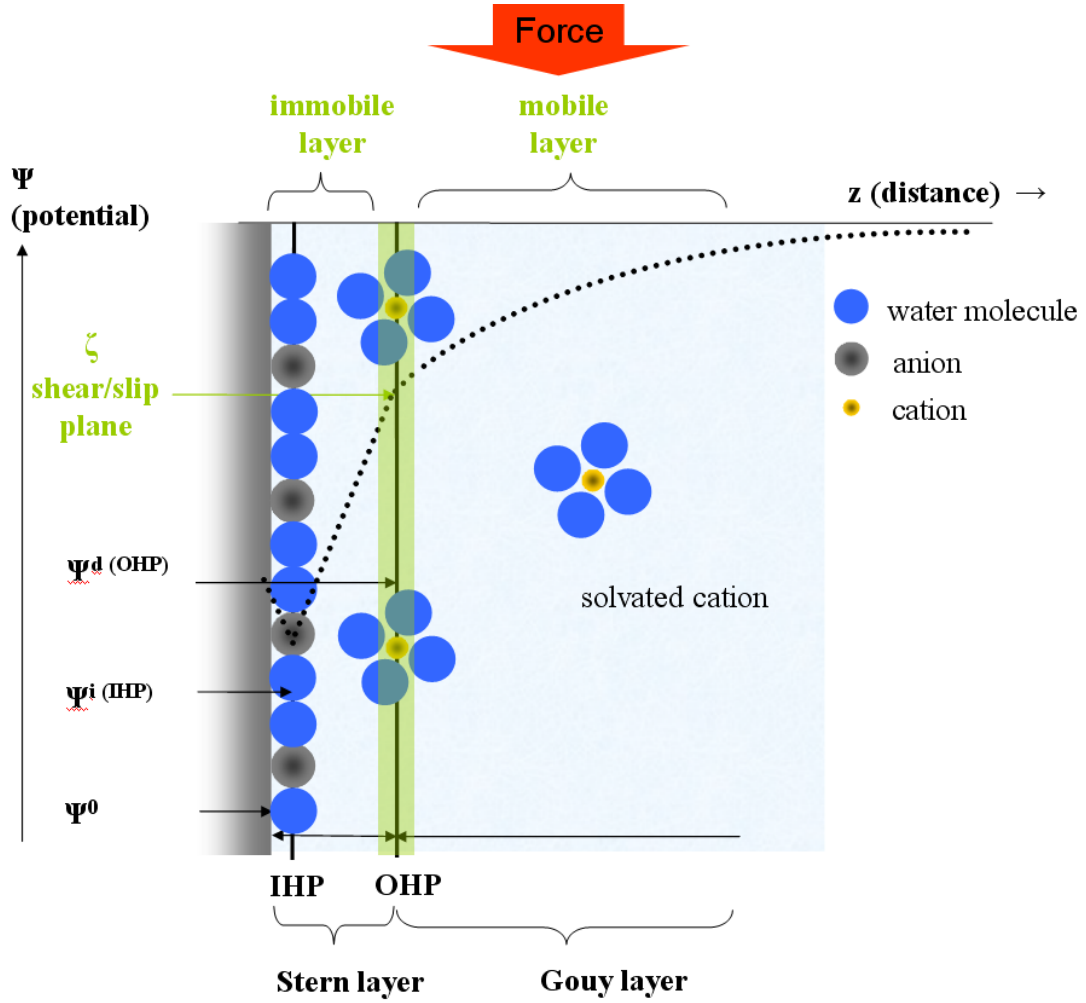

Figure 4.1: Schematic representation of the EDL according to the GCSG-model at a negatively charged surface. The potential (ψ) decreases with increasing distance (z) from the solid except for the gap close to the surface, as presented by the black dotted line. An example for specific adsorption is shown here, presented by partly dehydrated anions at the **i**nner **H**elmholtz **p**lane (IHP). This causes the initial potential drop near the surface. The **o**uter **H**elmholtz **p**lane (OHP) is the border separating the Stern layer from the diffuse Gouy layer. The zeta potential is defined as the potential at the shear plane, if an external force is applied (indicated by the red block arrow). This schematic representation is a combination of figures adapted from various publications: [74][72].

The very first EDL model was proposed by Helmholtz. In his model he aligned counter-ions along a charged surface for charge compensation. The parallel alignment of charges led to a linear potential drop with increasing distance from the surface. Thereafter, the model of Gouy-Chapman was proposed. In contrast to the Helmholtz model the compensating ions are not aligned in parallel to the surface but as a diffuse ion cloud. The diffuse ion cloud is formed because the model takes thermal movement into account. The Helmholtz and Gouy-Chapman models were extended and rarefied over the years leading to the model according to Gouy, Chapman, Stern and Grahame (GCSG-model). This is the model readers are most often referred to. A schematic representation of the GCSG-model is presented in Figure 4.1. As depicted in Figure 4.1 the liquid phase is composed of a Stern and a Gouy layer in the GCSG-model. The Stern layer is further subdivided into an **i**nner **H**elmholtz **p**lane (IHP) and an **o**uter **H**elmholtz **p**lane (OHP). Whereas partly dehydrated and immobile ions are situated at the IHP, the centres of hydrated counter-ions are located at the OHP or Stern plane. The potential drop between the IHP and the OHP is assumed to be rapid and linear. Dividing the Stern layer into an IHP and an OHP is necessary for the interpretation of experiments where specific ion adsorption takes place. One refers to specific ion adsorption, when ions have an increased affinity to a surface that does not result from coulomb interaction only. In contrast to ions that adsorb specifically, indifferent ions only adsorb because of attractive, electrostatic forces. They do not preferentially adsorb onto uncharged surfaces. Therefore, the IHP can be considered as the locus of specifically adsorbed ions. The Stern layer accommodates fixed and titrateable charges. Charge carriers within the Stern layer do not compensate the net surface charge completely, this is achieved by the adjacent Gouy layer. The Gouy layer is diffuse and contains an excess of counter ions and a deficit of co-ions to balance the remaining surface charge. The ion distribution within the Gouy layer is caused by the attraction and repulsion of ions by the surface (directed, electrostatic force) and the Brown's molecular (thermal) movement (non-directed force). Whereas the contribution of the Brown's movement (Boltzmann distribution) increases with increasing distance the directed, electrostatic forces diminish. The potential within the Gouy layer decreases exponentially with increasing distance from the surface. [74][72][71]

The effective thickness of the double layer is determined by the electrolyte solution and can be expressed by the Debye length κ^{-1}. The Debye length κ^{-1} is the distance from a charged surface, where the potential has dropped to an value of 1/e (about 37%) and can be calculated using equation 4.1. (The derivation of the equation for κ^{-1} is comprehensive and does not suit the cause. For detailed information and references, see [71]).

$$\kappa^{-1} = \lambda_D = \sqrt{\frac{k_B T \epsilon \epsilon_0}{2 N_A e^2 I}} \qquad \textbf{Debye length} \tag{4.1}$$

where I is the ionic strength [mole/m^3], ϵ_0 the permittivity of free space, ϵ the dielectric constant, k_B the Boltzmann constant, T the absolute temperature in Kelvin, N_A the Avogadro constant and e the elementary charge. The ionic strength can be expressed by the following equation 4.2

$$I = \frac{1}{2}\sum_i c_i {z_i}^2 \qquad \textbf{Ionic strength} \tag{4.2}$$

where, c is the concentration of the electrolyte and z the valency of the participating ions. In an aqueous solution ($\epsilon = 80$) containing a 1:1 electrolyte (e.g. NaCl) equation 4.1 reduces to

$$\kappa^{-1} = \frac{1}{F}\sqrt{\frac{RT\epsilon\epsilon_0}{2c}} \qquad \textbf{Debye length of a 1:1 electrolyte} \tag{4.3}$$

when using the following relations: $F = N_A \cdot e$ and $R = N_A \cdot k_B$ (R represents the gas constant, F the Faraday constant and c the molar concentration of the electrolyte). Thus, the Debye length in an aqueous 1:1 electrolyte solution (c = 1 mM) at a temperature of 25°C (298 K) is approximately:

$$\kappa^{-1} = \frac{1}{96480 C mol^{-1}}\sqrt{\frac{8.31 J mol^{-1} K^{-1} \cdot 298 K \cdot 80 \cdot 8.85 \cdot 10^{-12} C^2 (Jm)^{-1}}{2 \cdot 1 mol m^{-3}}} = 9.7 nm \tag{4.4}$$

This calculation comprises the condition that was present in all electrokinetic measurements performed within this thesis. Multivalent ions and electrolyte solutions of higher concentration cause the Debye length to shrink. Considering the situation in equation 4.4 an increase in electrolyte concentration would influence κ^{-1} as follows:

c(electrolyte) [mM]	κ^{-1} [nm]
1	9.6
10	3.0
100	1.0
1000	0.3

Table 4.1: The Debye length κ^{-1} depends on the concentration of an aqueous 1:1 electrolyte solution.

The ionic strength in physiological solutions is about 10 - 100 mM, therefore electrostatic forces are assumed to act only on very short length scales of about 3 - 1 nm's.

4.2 Electrokinetic Potential and Surface Conductivity

The liquid phase next to a solid is subdivided into the Stern and the Gouy layer in the GCSG model (view Figure 4.1), but the potential at the joint of these planes cannot be experimentally assessed [74]. A similar subdivision is made when studying electrokinetic experiments. The liquid phase is then subdivided into a hydrodynamically stagnant (immo-

bile) and a mobile layer. The mobile layer is pushed tangentially along the stagnant layer by an external force, either of mechanical or electrical origin. This force is represented by the red arrow in Figure 4.1. The slip plane or hydrodynamic shear plane separates the stagnant layer from the area beyond the slip plane where fluid flow occurs [72]. The exact position of the slip plane is uncertain, but is assumed to be very close to the OHP (see Figure 4.1) [71]. The gap between the slip plane and the OHP is the smallest, if the surface properties match the properties of an ideal surface (molecular smooth, chemically homogeneous and non-porous). The potential at this shear plane is referred to as the **electrokinetic** or **ζ-potential** according to Freundlich.

In terms of charged interfaces in electrolyte solution the ζ-potential is the most popular quantity. Despite its popularity its construction/interpretation in terms of the EDL composition is still not explicitly resolved [75], since in electrokinetic measurements the forces of ion adhesion are in equilibrium with the applied external force. Nevertheless, the ζ-potential provides information on the electrical properties of the interface between a solid surface and an adjacent electrolyte solution [75]. But the electrokinetic potential is not a surface property as such [71]. Changes in for e.g., ionic strength, pH value, additives in the liquid phase or upon the surface lead to changes in the EDL and cause a change in the electrokinetic potential. Both planes, the OHP and the slip plane, are abstractions from reality [71]. Neither of them, will be a sharp boundary in reality [71].

A further quantity, electrokinetically accessible and characterizing the electrical state of the interfacial region is the excess **surface conductivity** (K^σ). The surface conductivity provides information on the presence and mobility of charge carriers in the stagnant layer and the diffuse part of the EDL [72][76]. It was observed that the mobilities of monovalent coutner-ions in the stagnant layer are almost as high as in the bulk [72]. Molecules seem to pertain their mobility even though they are attracted to the surface. Similar as in gels, where large amounts of water may be immobilized although the diffusion of water molecules is hardly impeded [72]. Unlike the zeta potential, the surface conductivity does not depend on the hydrodynamic slipping plane and its possible position. The contribution of the surface conductivity (K^σ) to the bulk conductivity (K_B) is often expressed by the Dukhin number, Du [71]

$$Du = \frac{K^\sigma}{K_B a} \tag{4.5}$$

where, a represents the particle radius. These excess charges occurring additionally to the liquid bulk conductivity result from charge accumulation at the interface [76]. The K^σ is comprised of charge carriers located within the hydro-dynamically mobile part of the EDL

($K^{\sigma d}$) and charge carriers situated within the stagnant layer of the EDL ($K^{\sigma i}$).

$$K^{\sigma} = K^{\sigma,i} + K^{\sigma,d} \tag{4.6}$$

The contribution of K^{σ} to the overall conductivity is most pronounced in solutions of low electrolyte concentration and will be addressed in detail in subsection 4.2.2 [77]. The following two subsections describe, in the required extend, the two electrokinetic methods, electrophoresis and streaming current measurements, that were applied in this work.

4.2.1 Particle Surfaces: Electrophoresis

Electrophoresis is the translation of charged colloidal particles suspended in an electrolyte solution by an externally applied electric field [71]. Friction force hinders the particles on their movement to the electrode of opposite charge. When the electric force (F_{el}, presented by Equation 4.7) is in an equilibrium with the friction force (F_{fr}, presented by Equation 4.8), a particle with the radius (r) moves at a constant electrophoretic velocity (v_e [m/S]). The electrophoretic velocity can be determined either by measuring the particles way and the corresponding time or directly by laser Doppler anemometry (determination of the frequency change of the laser light after scattering) [71].

$$F_{el} = E \cdot Q = E \cdot \zeta \cdot C = E \cdot \zeta \cdot 4 \cdot \pi \cdot r \cdot \epsilon_0 \cdot \epsilon \qquad \textbf{Particle charge} \tag{4.7}$$

where, E represents the electric field strength, C the capacity and ζ the electrokinetic potential. The capacity of a sphere is given by $C = 4 \cdot \pi \cdot r \cdot \epsilon_0 \cdot \epsilon_r$, where r is the radius of the particle, ϵ_0 the permittivity of the free space and ϵ_r the dielectric number of the liquid.

$$F_{fr} = 6 \cdot \pi \cdot v_e \cdot r \cdot \eta \qquad \textbf{Stokes' law} \tag{4.8}$$

Dividing the electrophoretic velocity by the electric field strength E, in a given medium, results in the electrophoretic mobility u_e ($u_e = v_e/E$). Both equations (4.7, 4.8) are only valid for idealized conditions in infinity diluted electrolyte solutions. Equating equation 4.7 and 4.8 the following equation is obtained:

$$u_e = \frac{2}{3} \cdot \frac{\epsilon_0 \cdot \epsilon \cdot \zeta}{\eta} \cdot f(\kappa a) \qquad \textbf{Henry equation} \tag{4.9}$$

The additional complex function was introduced by Henry to take into consideration the ratio between the particles radius (a) and the effective thickness of the EDL (reciprocal Debye length). Electrophoretic potential determination by electrophoresis is usually performed in aqueous solutions of moderate electrolyte concentration. In such a case $f(\kappa a)$ becomes 1.5,

and the resulting equation is referred to as the Smoluchowski approximation:

$$u_e = \frac{\epsilon_0 \cdot \epsilon \cdot \zeta}{\eta} \qquad \textbf{Helmholtz-Smoluchowski equation; valid: } \kappa a >> 1 \tag{4.10}$$

The Smoluchowski equation is valid for systems of particles larger than 0.2 μm dispersed in electrolyte and at salt concentrations larger than 1 mM [71] (applicable in situations where the Debye length is short, in comparison to the particle diameter) [71]. For example, at c(KCl) = 1 mM and a = 500 nm ; κa = 52 allowing Smoluchowski approximation. This accounts for the conditions that were used within this thesis.
In the case of smaller particles in electrolyte solutions of low ionic strength $f(\kappa a)$ becomes 1.0 and the resulting equation is referred to as the Hückel approximation (strong contribution of Debye length) e.g. c(KCl) = 1 mM, a = 1 nm ; κa = 0.1.

$$u_e = \frac{2}{3} \cdot \frac{\epsilon_0 \cdot \epsilon \cdot \zeta}{\eta} \qquad \textbf{Hückel equation; valid: } \kappa a < 1 \tag{4.11}$$

The complex Henry function varies smoothly from 1.0, for low values of κa, to 1.5 as κa approaches infinity. A conversion of the electrophoretic mobility into ζ, as presented in the above equations, may only be performed at ideal surfaces of low zeta potentials and in the absence of surface conductivity (Du « 1). The fundamental knowledge on electrophoresis described up to here is sufficient for the qualitative interpretation of electrophoretic data. If zeta potential values determined by different electrokinetic phenomena want to be compared or other quantities like Gibbs free energy want to be calculated, the above approximations are not sufficient and more elaborate models need to be applied to convert measured electrophoretic mobilities into exact zeta potential values [71]. Theories that include surface conductivity have been developed by Overbeek. O'Brien and White provided a numerical solution for the electrokinetic equations to determine the electrophoretic mobility for systems of high zeta potentials that include surface conductivity, independent of κa and accounting for the presence of multivalent salts. Electrophoretic mobility is reduced when surface conduction and polarization (distortion of the double layer due to the applied electric field; accumulation of charge on one side of the particle and depletion on the other side results in the formation of a dipole) occur at the particle surface [71].

Particles need to be in the size range of 5 nm up to 30 μm to be suitable for electrophoresis measurements. The refractive index has to be different to the one of the surrounding medium. Furthermore, the suspension of the particles needs to be stable during the entire experiment without the occurrence of sedimentation. This last but significant obstacle is avoided by the electrokinetic examination of flat surfaces. Furthermore, streaming current and potential measurements permit the examination of uncharged surfaces and hydrophobic

surface coatings, impossible in electrophoresis.

4.2.2 Flat Surfaces: Streaming Current/Potential

The streaming current/potential originates from the displacement of mobile charges in the EDL, as the liquid phase is tangentially moved along the solid [77][71]. The tangential movement is achieved by the application of a pressure gradient across a channel. The conveyance of hydrodynamically mobile ions can be determined directly by measuring the electrical current between two electrodes, one upstream and one downstream of the channel [77][71]. The neglection of the back current through the channel is permitted since an amperemeter of sufficiently low internal resistance is used [77].

The liquid flow generated by the pressure gradient establishes the liquids velocity profile. The volume charge density can be expressed by the one dimensional Poisson equation correlating the potential ψ and the space charge density ρ with each other.

$$\rho = -\epsilon \cdot \epsilon_0 \frac{d^2\psi}{dz^2} \qquad \textbf{Poisson equation (1 DIM)} \tag{4.12}$$

Z is the distance from the surface, ϵ_0 the permittivity of the free space and ϵ_0 the dielectric number. After integration and selecting the appropriate boundaries one obtains the equation for the streaming current measurement (Details on the derivation can be looked-up in reference [78][71][79]):

$$\zeta = \frac{I_{str}}{\Delta p} \cdot \frac{\eta}{\epsilon_r \epsilon_0} \cdot \frac{L}{A} \qquad \textbf{Helmholtz-Smoluchowski; valid: } \kappa a >> 1 \tag{4.13}$$

where I_{str} [mA] is the measured current, Δp the pressure drop [A Pa^{-1}] across the channel, η the dynamic viscosity of the liquid [kg/(ms)], L the length of the channel and A its cross-section. The ζ-potential depends on the streaming current, the pressure drop and the channel dimensions. Just like in electrophoresis, a conversion of the $I_{str}/\Delta p$ into ζ using the above equation is only possible if $\kappa a >> 1$. In the case of κa being of intermediate value ($\kappa a \approx 1 - 10$), Helmholtz-Smoluchowski is invalid. Corrections can be performed by means of the Burgen and Nakache theory, but since this is not of interest in the measurements performed for this thesis one is referred to the manuscript of Delgado et al. for further details [71].

The electrokinetic potential can be measured with an electrometer of sufficiently high internal resistance between two connected electrodes positioned up and downstream of the channel [77][76]. Streaming potential results from the steady state of the charge separation by the liquid flow and a back current due to the electrical conductivity of the embedded liquid [77].

At high resistance, the ion transport results in the gathering of charges of opposite signs between the channel ends and results in a conduction current [77]. The conduction current, which is equal in magnitude to the streaming current at steady state is:

$$I = \frac{bhU_{str}K_B}{L} + \frac{2bU_sK_\sigma}{L} \tag{4.14}$$

where b, h and L are the channel dimensions (width, height and length), U_{str} the determined streaming potential, K_B and K_σ the conductivity of the bulk and the surface. Insertion of equation 4.14 in equation 4.13 yields the following expression:

$$\zeta = \frac{U_{str}}{\Delta p} \cdot \frac{\eta}{\epsilon_r \epsilon_0} \cdot (K_B + \frac{2K^\sigma}{h}) \qquad \textbf{Fairbrother-Mastin; valid: } \kappa a >> 1 \tag{4.15}$$

The ζ-potential depends on the streaming potential, the pressure drop across the channel, the total specific electrical conductance, and the distance between the samples. Surface conductivity is often neglected, which is only justified at large channel heights or electrolyte solutions of high ionic strength. The above equation is then reduced to:

$$\zeta = \frac{U_{str}}{\Delta p} \cdot \frac{\eta}{\epsilon_r \cdot \epsilon_0} \cdot K_B \tag{4.16}$$

Most frequently the surface conduction (K^σ) contributes significantly to the overall conductance (K_B) [71] and may not be neglected. In order to determine a value for the surface conductivity streaming potential and streaming current data need to be collected at a known cell geometry and inserted into an equation obtained by the combination of 4.13 with 4.15.

$$K^\sigma = \frac{1}{2}(\frac{(I_s/\Delta p)L}{(U_s/\Delta p)b} - K_B h) \qquad \textbf{Surface conductivity}[80] \tag{4.17}$$

Carsten Werner currently working at the Institute of Polymer Research in Dresden published numerous articles on the electrokinetic characterization of various surfaces by the streaming current/potential method [77][81].

For further details one is referred to the IUPAC report of Delgardo et al. who describe the main electrokinetic methods, explain the basic theory, state application ranges, aid the interpretation of electrokinetic phenomena and present the IUPAC codification for electrokinetics [71]. Actually, the above mentioned formula are strictly for hard and impermeable surfaces and their application in other systems may only be justified if changes in surface structure want to be observed. But for the correct determination of surface criteria more sophisticated models need to be applied. Soft and permeable surfaces gain increasing interest and

will briefly be addressed in the next section.

(Solutions $> 10^{-1}$ mol/L of 1:1 electrolytes are difficult to measure with the present techniques [71] since liquids with high concentrations of ions have nearly the same number of ions in the bulk phase as in the electrochemical double layer and a potential cannot be generated.)

4.3 Soft Interphases and Hard Interfaces

At ideal (i.e., smooth, chemically homogeneous, rigid, non-permeable, non-porous) surfaces streaming current data can be converted into ζ-potential values using the Smoluchowski relation, because of the rather discrete formation of a shear plane (sharp change in density occurs at the transition from the surface to the adjacent liquid) [71]. But usually surfaces are anything from smooth, chemically homogeneous, rigid and non-porous, especially in the fields with biological impact. Those surfaces are referred to as "soft" surfaces. They are patchy, permeable, thick and porous (Effects on the electrokinetics of bacteria have been addressed in section 1.1.2). Here, the interpretation of experimental results from electrokinetic measurements is dependent on the type and magnitude of the non-idealities and on the aim of the measurement [71]. Practically, the measurement of a quantity like u_e and I/dp, and their transformation by some equation will lead to an "effective" ζ-potential, but the interpretation is ambiguous [71]. It has to be kept in mind, that the obtained value has only a relative meaning and is not the actual electrostatic potential at the surface [71]. The effective electrokinetic potential can help to give a feeling for sign and magnitude of the part of the DL that controls the interaction with other particles. "Soft" surfaces are far more complex than hard surfaces and are rather referred to as an interphase instead of an interface towards the adjacent solution [23]. The formation of a discrete shear plane at soft surfaces is not achievable, because solvent and ions can penetrate the surface. The zeta potential looses its meaning at such an interphase [80]. Then the streaming current/potential versus pressure gradient is rather used to evaluate the charge formation process at the interface [76].

Duval et al. proposed an advanced theory for the evaluation of electrokinetic data (streaming current) obtained from heterogeneous soft thin films considering the influence of the lateral flow on the hydrodynamic and electrostatic field distributions (the penetration of the hydrodynamic flow into the polymer layer) [73]. This theory was extended by Zimmermann et al. including functional groups involved in dissociation and association processes [80]. Within the years 2010 - 2012 numerous publications on this topic were published by J. F. L. Duval and C. Werner and their co-workers. Comprehensive studies were performed on various polymer coatings. Based on streaming current and conductivity measurements they could quantify incorporated functional groups and unravel their degree of ionization [82][80].

Part III

Results and Discussion

5 Substrata

The all-embracing examination of the novel, as well as the established coatings, based on dendrimers and linear alkyl chains investigated in this study and intended for the use on biomaterials applied within the oral cavity at the trans-gingival passage required a pool of analytical methods. In order to determine the physico-chemical characteristics of these coatings, and to evaluate their impact on the biological response, it was necessary to use various substrata of different physical characteristics. Inorganic silicon based substrata were chosen since the applied silane chemistry is easily transferable onto other clinically relevant materials like titanium, ceramics or even plastics.

This chapter summarizes the substrata, that were chemically modified and their assignment within this cooperation project (the various strategies and handling concepts that were developed for each substratum are described in detail in the Experimental Part V of this thesis). Furthermore, the extent of the silanol groups upon the substrata surfaces, necessary for the preparation of the coatings via silanisation, is estimated. This knowledge is important to evaluate the amount of silanisation agents and to consider the influence of these groups on the electrokinetic data presented in chapter 8.
Four main categories of substrata were functionalized. They are presented in Figure 5.1.

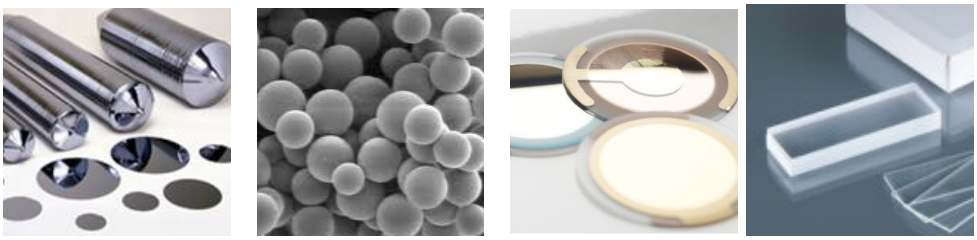

(a) silicon wafers (b) silica particles (c) QCM sensors (d) glass slides

Figure 5.1: Si-based substrata

Silicon wafers polished on a single side (1 cm x 1 cm) were used for surface characterization purposes and biological response testing. Surface characterization embraced wettability data gathered by static water contact angle goniometry (CA), information on the generation of charge at the surfaces in solution determined by streaming current measurements (SC), the chemical composition analysis examined by X-ray photoelectron

spectroscopy (XPS) and the ascertainment of the conversion rate upon modification by detecting free amino groups via a chemiluminescence based assay (CL). Single side polished wafers were further used for the determination of the surface free energy (SFE) and biological response testing under dynamic conditions at the University of Tübingen by Mirjam Eichler on behalf of her PhD thesis. At the University hospital of Regensburg biological response testing comprised bacterial adhesion and viability experiments, as well as cell adhesion tests under static conditions.
Silicon wafers polished on both sides were of rectangular geometry (1 cm x 2.5 cm) in order to evaluate the wettability and protein adherence to the surfaces under dynamic conditions. These experiments were carried out in Tübingen by means of the Wilhelmy technique (dynamic contact angle measurement) operated by Mirjam Eichler in the course of her PhD thesis.

Silica of different specific surface areas was used: silica beads (0.19 m^2/g; non-porous), silica spheres (2.99 m^2/g; non-porous), and silica particles (500 m^2/g; porous). Silica beads with the smallest specific surface area were used to study steady state protein adsorption by a colorimetric assay (bicinchoninic acid - BCA; explained in detail in section 14.1 and results presented in section 10.1). The very large area of silica particles (500 m^2/g) was initially used to monitor the success of the surface modification process by diffuse reflectance infra-red Fourier transformed spectroscopy (DRIFT) and electrophoresis. This worked well for linear alkyl chain based coatings, but was inappropriate for dendrimer based coatings since the area of these particles was too large to be rationally modified with the dendrimers. Therefore, silica particles were later replaced by silica spheres with a lower specific surface area (2.99 m^2/g) and a non-porous character, also applicable in electrophoresis experiments.

QCM resonators coated with silicon dioxide were modified for the project partner in Tübingen to study protein adsorption (from saliva and serum) and subsequent bacterial adhesion by means of quartz crystal micro-balance (QCM) measurements under dynamic conditions. Some of the obtained results are presented in the publication: "The impact of dendrimer-grafted modifications to model silicon surfaces on protein adsorption and bacterial adhesion" authored by M. Eichler [83].

Glass slides of pure molten quartz glass were used as an amorphous substratum for some introducing sum frequency generation spectroscopy (SFG) measurements summarized in chapter 9.

All substrata listed above were generally treated with nitric acid solution before silanisation, if not stated otherwise (see Experimental Part V for information). Nitric acid is an oxidizing agent removing organic surface contaminations. Furthermore, nitric acid generates

ultra-thin silicon dioxide layers on silicon [84]. Surfaces with Si-OH groups are decisive for the reaction with silanes as explained in chapter 3 and the basis of the selected coatings. Electrokinetic measurements allow a qualitative proposition of the surface hydroxyl groups on top of the substrata as shown below.
The surface charge on the freshly oxidized substrata is caused by the dissociation of the surface silanol groups (view equation 5.1 [85]).

$$\mathrm{Si{-}OH + H_2O \rightleftharpoons Si{-}O^- + H_3O^+} \qquad \textbf{Dissociation reaction} \tag{5.1}$$

Zeta-potential values gathered at the substrata surfaces in dependence on the pH of the adjacent solution, are presented in Figure 5.2. The electrokinetic techniques which were used to acquire these values were performed on two different instruments. Depending on the sample shape either streaming current experiments or electrophoresis experiments were performed (an assessment regarding the comparability of these two techniques is given in the introduction of chapter 8). Streaming current analysis was applied on flat silicon wafers, and the electrophoresis technique on silica particles and spheres.
The iso-electric points (IEPs) of the Si-substrata lie within the range of 2.1 - 3.0, correlating very well with data reported in literature [86][87].

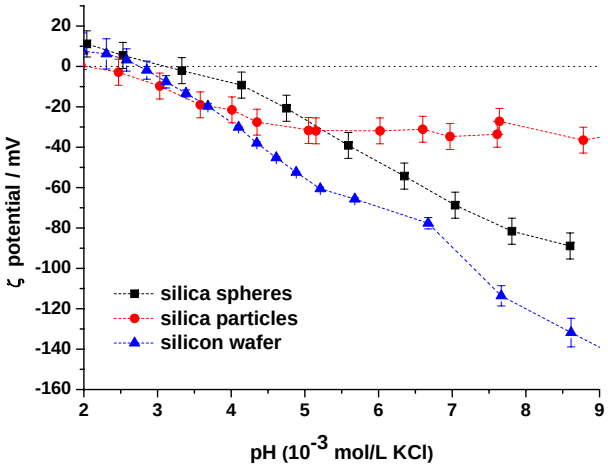

	$IEP\|_{\zeta=0}$	$\zeta\|_{pH=7}$
silica spheres	3.0	-68 mV
silica particles	2.1	-35 mV
silicon wafer	2.7	-90 mV

Figure 5.2: left: ζ-potential determination in 1 mM KCl solution performed by electrophoresis (particles and spheres) and streaming current measurements (wafer)
right: Iso-electric points (IEPs) and the zeta potential value at pH 7

An increase in negative ζ-potential value upon pH increase can be observed for all three types of substrata surfaces. Whereas the curve progression heads into saturation at high pH for silica particles (-40 mV) and silica spheres (-90 mV), a steep increase can be observed for the silicon wafer surface at pH values higher than 6.5. This strong increase in negative

zeta potential has been ascribed to preferential hydroxide ion adsorption in literature [78]. Whereas, preferential hydroxide ion adsorption is reasonable to be expected for the generation of charge at non-ionisable surface coatings [88], it seems rather questionable at a strong negatively charged surface, where a repulsion of hydroxide ions is rather assumed. Thus, it may be presumed that deprotonation on the silicon wafer surface occurs in more than one step, in order to accommodate charge at high concentration in a better way. In contrast, the concentration of silanols seems to be lower on spheres and particles enabling a steady deprotonation because the neighbouring sites do not strongly influence each other. Besides the fact that these data are gathered with two different instruments, it can be assumed that the silanol group arrangement and density on the three substrata differs. These results seem to reflect the different surface structures. Whereas the surface of the silica particles is porous (Kieselgel 60 was determined to have pores with a diameter of 6 nm [89]) and consequently rough, the one on wafers and spheres is non-porous. Therefore, the higher negative plateau potential detected on silica spheres and wafers suggests a higher amount of hydroxyl groups upon these surfaces in comparison to the silica particle surface.

The concentration of hydroxyl groups on fully hydroxylated silica was reported to be about 5.0 ± 0.5 OH groups per nm^2 [90][91], occupying about 20 $\mathring{A}^2$ per Si-OH group [87] (corresponding to $5 \cdot 10^{14}$ Si-OH groups per cm^2; 0.8 $nmol/cm^2$; 8.3 $\mu mol/m^2$). Whereas every silanol group occupies about 20 $\mathring{A}^2$, every linear alkyl chain, within a perfectly arrayed self assembled monolayer (SAM), occupies an area of about 21 - 25 $\mathring{A}^2$ [56]. The silane concentration (7.5 $\mu mol/m^2$) and consequently the terminal head groups at a wafer surface are thus slightly lower than the number of $Si-OH$ groups. This leads to the fact, that even at a complete coverage by silane molecules unreacted OH groups upon the surface are reasonable to be expected. There may even be more, since there are reasonable grounds to suspect that the SAM-carpet is only anchored to the substratum via a few Si-O-Si bridges [56][68] (see section 3.3 for information). This recognition is of importance for the analysis of the zeta-potential data presented in chapter 8.

The following chapter describes the characterization and preparation of coatings based on linear alkyl chains terminated by cationic, anionic and neutral head groups.

6 Coatings based on Linear Alkyl Chains (SAM)

Coatings, based on linear alkyl chains (SAM), were developed on silica and the steps of derivatisation, as well as the successful preparation were monitored by diffuse reflectance infra-red Fourier transformed spectroscopy (DRIFT) measurements. DRIFT allows the detection of introduced chemical functionalities into the coating. Whenever amino group functionalities were created, or converted on substrata modifications, the DRIFT measurements were supported by utilising the Kaiser test (see 13.7 for details). Promising concepts were transferred onto silicon wafers. X-ray photo-electron spectroscopy (XPS) was carried out to determine the elemental composition of the coating, and the chemical environment of some elements, revealing information on the conversion rate of derivatisation reactions, and whether the desired functionality had been introduced or not. Wettability determination by contact angle goniometry was employed as a control parameter for each batch of coated wafers. This chapter focuses on the preparation of the surface coatings only, their ability of generating a charged interface is summarized in chapter 8.

6.1 Cationic SAMs

6.1.1 SAM-C_3-NH_2

Among all silanisation agents, (3-**a**mino**p**ropyl)**t**ri**m**ethoxy**s**ilane (**APTMS**) and (3-**a**mino-**p**ropyl)**t**ri**e**thoxy**s**ilane (**APTES**) are the most popular. Both silanes are generally used to prepare amine terminated SAMs, which are readily created by these molecules and provide a favoured platform for the covalent immobilisation of biomolecules [65]. Furthermore, they are used in adhesive technology as adhesion promoters [56]. Despite the frequent application of amine functionalised surfaces, generated by APTMS or APTES molecules, fundamental aspects regarding structure and stability of the obtained coatings are often omitted, although referred to in literature. Surface modifications prepared by these silanes are commonly depicted as monolayers of uniformly organized molecules, i.e. all terminal groups point away from the surface and the alkyl chains are arrayed in a parallel manner. This scheme is an oversimplification that does not even approximate the true nature of the coating [92]. Generally, highly disordered coatings are created by APTMS and APTES molecules, as

depicted in Figure 6.1. One reason for this disorder is the negligible stabilizing effect by van der Waals interactions among the rather short hydrocarbon chains [66]. A further reason is the bi-functionality of the aminopropylsilanes. Both moieties, alkoxy and amino groups, may interact with the silanol groups of the substratum [56]. For example, the silane may either hydrolyse with the surface hydroxyl groups or interact with the silanol groups by hydrogen bond formation if the alkoxy group is not hydrolysed yet, and the amino head groups can also interact via hydrogen bond formation with the hydroxyl groups on the surface or by salt formation if the head group is protonated. Carbamide formation, due to the reaction of surface bound amines with atmospheric carbon dioxide may also take place [93].

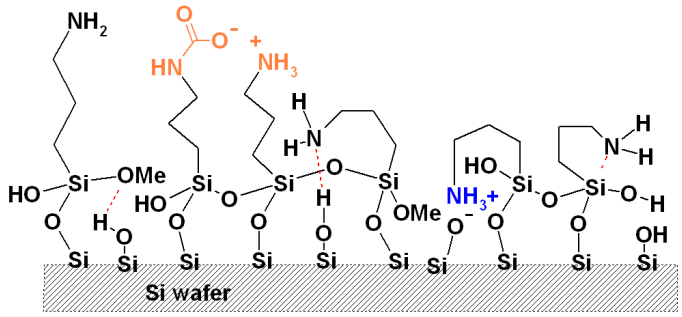

Figure 6.1: Schematic representation of the a coating generated by APTMS . This is only a small selection of adsorbed species, a few others are still imaginable, such as multilayer formation by vertical stacking. [65][63]

Furthermore, the structural constitution of aminopropylsilanes allows auto-catalyzed hydrolysis by forming a five membered ring as the amino group coordinates to the silicon centre [94]. Thus, aminoalkoxysilanes react more readily with nucleophiles than ω-alkylalkoxysilanes comprising other terminal functionalities [94]. Even in the presence of water traces aggregates form in solution with more ease. These polymerized structures may also settle on the surface and cause coating inhomogeneities. The above addressed properties of APTES/APTMS molecules cause imperfect coatings of reduced reproducibility, uncertain surface loading and uneven thickness (multilayer formation). Besides the structural problems, these coatings are also unstable. Aminopropylsilane coatings were detected to be of low stability in water [94] and saline solution [66], regardless of the preparation technique [94]. The deficiency of stabilizing van der Waals interactions [66], causing a loosely packed layer, makes the anchoring group vulnerable to hydroxyl ion attacks [94]. In contrast, aminosilanes composed of long alkyl chains ($>(CH_2)_{11}$) or ω-functionalized alkysilanes with terminal groups other than amine (regardless of the alkyl chain length) were examined to be of greater hydrolytic stability [94][66]. These observations confirm the presumptions and experiments made by Carsten Werner et al., who suggest, that the formation of hydroxyl ions near the surface

results from the basic character of the amine functionalities, inducing the stripping of the organic layer [95].
The irregular organic layer formed by APTMS/APTES makes this coating unsuitable for structure relation studies, as aimed for in our study. This surface coating is also infeasible as a basis for subsequent surface modifications, because of the inconsistency in structure which is conveyed into the following layers, making interpretations of analytical data collected from new modifications even more difficult. Furthermore, the instability of the coating in aqueous media makes it inappropriate for long term applications therein, as intended for biomedical devices [66]. Since it was the primary order of this study to generate several coatings on siliceous material on the basis of the APTMS coating, a few attempts were ventured before swapping to amino terminated SAMs with longer alkyl chains, as described in the next subsection (see 6.1.2). An improvement in terms of reproducibility was reached by optimizing the deposition conditions of silanes (details thereto are described in the Experimental Part in section 12.2). Furthermore, the influence of cleaning solvents after silanisation was evaluated. It was also observed, that surface characteristics changed upon storage and environmental contaminations were assumed to be the reason for that. This provoked to improve the storage conditions for all samples.

The SAM-C_3-NH_2 coating was carried out on silica particles at first and monitored by DRIFT spectroscopy. Therefore, the transmission spectrum of the APTMS was recorded at the beginning and is presented in Figure 6.2 (colour: black). Besides the classical alkyl bands within the regions 2800 - 3000 cm^{-1} (stretching vibrations [96]) and 1300 - 1450 cm^{-1} (deformation vibrations [96]) one can clearly observe signals representative for vibrations of the amine functionality (areas marked in grey). The N-H stretching vibrations occur within the range of 3150 - 3400 cm^{-1} [96]. Vibrations above 3300 cm^{-1} are assigned to the N-H stretch of free amine moieties, whereas signals at lower energy are attributed to protonated amine moieties [96]. The corresponding bands for the N-H deformation vibration can be observed in the region between 1500 cm^{-1} and 1700 cm^{-1} summarized in one peak [96]. The recorded vibrations document the presence of charged species as expected, since the silane molecule was not recorded in inert atmosphere, but in laboratory atmosphere between NaCl plates. The reaction with atmospheric moisture may have caused the formation of ammonium salts. Polymerization products are also present as indicated by the strong band at about 1100 cm^{-1} corresponding to the vibrations of the Si-O-Si network.

The DRIFT-spectrum of silica particles, covered by a 3-aminopropylsiloxane layer, is also presented in Figure 6.2 (colour: blue). The obligatory peak confirming silanisation is positioned at 3738 cm^{-1} [91]. It is a negative peak, resulting from the loss of isolated silanol Si-OH groups on the silica surface after silanisation in comparison to the uncoated refer-

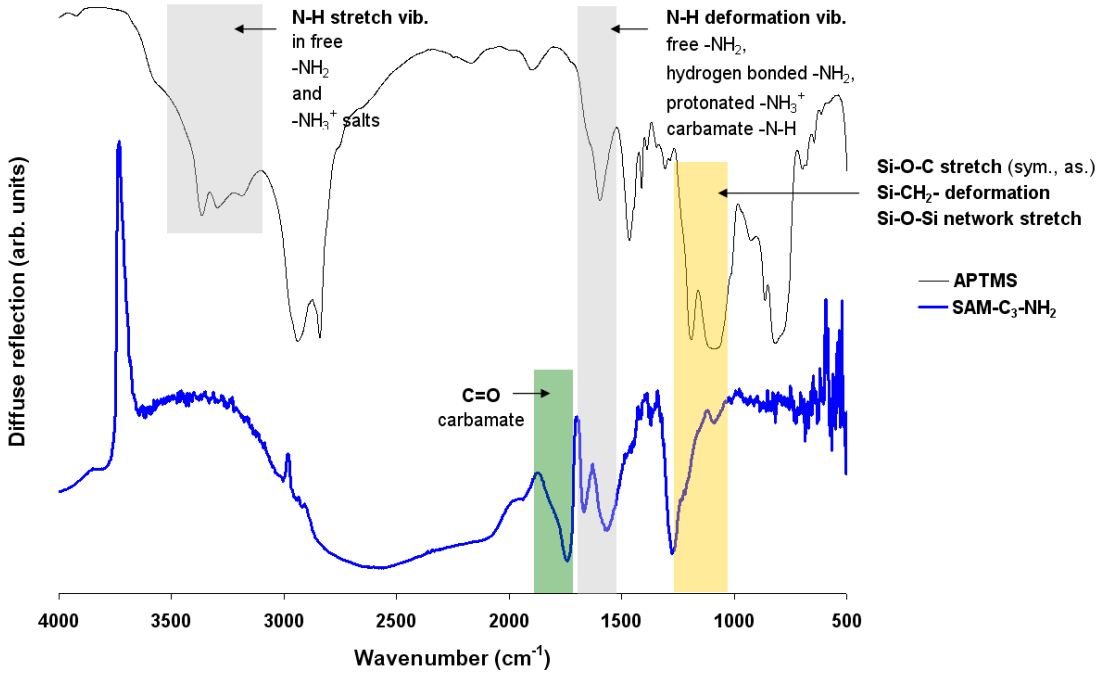

Figure 6.2: Transmission spectrum of APTMS and silica particles covered by an 3-aminopropylsiloxane layer. The particles are recorded in DRIFT mode using silica as a reference.

ence. The stretching vibrations of the alkyl chains are not clearly distinguishable and the peaks corresponding to the N-H stretching are undetectable, suggesting a very thin coating. Within the N-H deformation region two distinct peaks evolve. The sharp band at higher energy is attributed to the free amino group (1622 cm^{-1} [92]), whereas the broader peak at lower energy may be the result of hydrogen bonded amines, protonated amines and carbamate species. A very strong peak at 1750 cm^{-1} suggests the formation of a functional group containing a C=O vibration. Literature states, that amine terminated surfaces, readily react with carbon dioxide to form carbamates, according to the following stoichiometry [93]:

$$2\,R{-}NH_2 + CO_2 \longrightarrow R{-}NH_3^+ + R{-}NH{-}COO^- \qquad \textbf{ammonium carbamate formation}$$

The formation of such salts explains the additional peak in the N-H deformation region and the dominant peak at 1750 cm^{-1}. Even though the coated silica was stored in a snap vial after preparation, this reaction readily occurred, pointing out the susceptibility of the surface coating to react with carbon dioxide. At 1100 cm^{-1} the Si-O-Si vibration can be detected but an even stronger band occurs at 1250 cm^{-1}. This vibration is assumed to correspond to the ($Si{-}CH_2$) vibration. The increased intensity of this band emphasises the assumption that the terminal amino groups are not all pointing away from the surface but bending backwards exposing their inner moieties.

The silanisation procedure was transferred onto silicon wafers and characterized by static water contact angle measurements, since this was the only readily accessible analytical tool for wafer coated samples. Contact angle values were recorded 1 hour after preparation. In comparison to former works in our research group, the reaction condition for APTMS deposition was altered. The samples were originally heated in the silane solution for 3 hours at 110°C (the temperature value refers to the temperature of the silicone oil bath). This was reduced to 1 hour and a final curement step for 15 min at 130°C was introduced. The final temperature rise was believed to support condensation and a vertical orientation of the silane molecules due to the rupture of hydrogen bonds. This way of preparation in combination with the implementations in the silanisation apparatus, as explained in the Experimental Part of this thesis (12.2), did significantly unify the contact angle values, obtained from batch to batch.

The static and dynamic contact angle values, published in literature on 3-aminopropylsiloxane coated surfaces, are very heterogeneous. The reason for this might be the different preparation and storage conditions, as well as the different periods between preparation and characterization. Values of 19° up to 60° have been reported [94][97][98][99]. The surface coatings, prepared in this thesis with APTMS, showed a wettability of 47° (42° - 50°) which increased to 57° (56° - 58°) during a night stored in a desiccator under vacuum. An increase in hydrophobicity upon storage was also observed by other researchers [97]. Also samples sent to Tübingen for further measurements were routinely re-characterized by static water contact angle measurements, but the values obtained there, were always higher, than the ones recorded in Regensburg. The reaction with carbon dioxide to form carbamates, the adsorption of air impurities and a possible reorientation upon the surface to minimize surface energy (head groups orientating towards the surface) is most probably responsible for this wettability decrease. Therefore, from thereon coated wafers were always handled under argon atmosphere and stored in inert atmosphere thereafter. After preparation they were transferred into spectrometer tubes under inert atmosphere, sealed with parafilm® and placed into a plastic bag. This bag was filled with argon and sealed by using the melting function of a laminator. This bag was put into a further bag, which was again flooded with argon and sealed. This reduced the discrepancy in static water contact angle data.

It was also observed that the solvents, used for the removal of physisorbed silanes after silanisation, affected the wettability of the surfaces. The table below (Table 6.1) summarizes the applied solvents and recorded contact angle values. Even though the differences in contact angle values are not tremendous, it is clearly visible that the solvents toluene and chloroform provide surfaces with lower contact angle values and less scatter. Presumably, this is because of their lower polarity. Solvents of higher polarity may contain larger amounts of water that

Cleaning sequence	static contact angle (θ_w)
chloroform (2x), methanol (1x), water (1x)	51° (48° - 55°)
methanol (2x), acetone (1x), water (1x)	59° (56° - 59°)
toluene (1x), chloroform (1x), methanol (1x)	54° (52° - 56°)
toluene (3x)	45° (44° - 46°)
chloroform (3x)	45° (44° - 46°)
acetone (3x)	57° (55° - 59°)

Table 6.1: Wettability measurements after different rinsing procedures. Each set of data was obtained by analysing 5 wafers at four different positions (N=20).

may lead to protonation reactions, which induce structural changes upon the surface, like loop formation. Loops expose the alkyl chain towards the solvent and may thus cause an increase in contact angle value even though their terminal head groups may be of higher polarity due to charge formation.

In summary, the APTMS deposition was optimized in such a way that coatings of greater reproducibility were generated. Because of the sensitivity of the coating, storage conditions were upgraded. These storage conditions were then applied to all modified surfaces. Furthermore, the impact of rinsing solutions on wettability data was observed. Due to the negative aspects of the coating mentioned in this subsection, amine terminated SAMs were prepared from non-polar precursor layers from now on, as explained in the following subsection.

6.1.2 SAM-C_{11}-NH_2

Since amino group bearing surfaces generated by APTMS (view subsection 6.1.1) did not fulfil the structural requirements for the intended structure relationship studies, these coatings were generated from a well ordered non-polar pre-coating. This pre-coat was prepared by using 11-bromo-undecyltrichlorosilane to obtain surfaces covered by 11-bromoundecyl-siloxane (SAM-Br). The terminal bromine of this coating was then replaced by azide in a nucleophilic substitution reaction (this reaction is said to proceed quantitatively on surfaces, even at dense packing [61]). Thereafter, the peripheral azide was reduced by lithium aluminium hydride ($LiAlH_4$). This is a commonly used preparation pathway to achieve amine terminated surface coatings of high order [100]. The reaction sequence is illustrated in Figure 6.3. The suitability of stannous(II)chloride as an alternative reducing agent [101] was also evaluated for the SAM-C_{11}-NH_2 preparation. Amine terminated SAMs may also be prepared by converting cyanide [56] terminated coatings, but this way of preparation was not pursued.

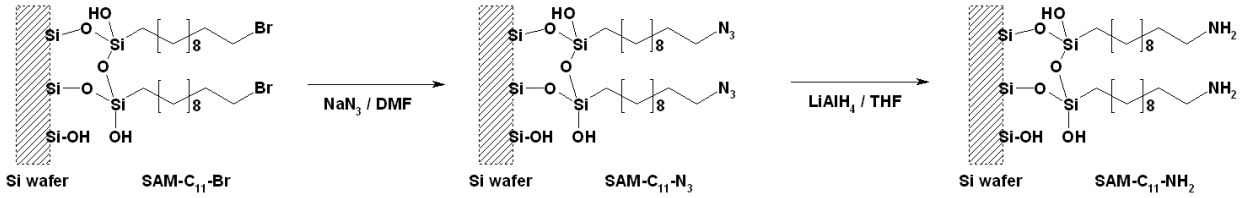

Figure 6.3: Schematic representation of the SAM-C_{11}-NH_2 preparation. Nucleophilic substitution of the bromine atom by azide and subsequent reduction by lithium aluminium hydride.

The SAM-C_{11}-NH_2 coating was carried out on silica particles at first and the derivatisation steps were monitored by DRIFT spectroscopy. Therefore, the transmission spectrum of 11-bromoundecyltrichlorosilane (BUTS) was recorded in advance and is presented in Figure 6.4 (colour: black, line-thickness: thin). Minor differences are observed comparing the transmission spectrum of BUTS with the DRIFT-spectrum of the SAM-Br coated particles (view Figure 6.3 (colour: black, line-thickness: thick)), supporting the assumption of a successful surface functionalization with terminal bromine atoms. Signals corresponding to the asymmetric and symmetric stretching vibrations of the methylene groups [96] within the alkyl chains, located at about 2929 cm^{-1} and 2855 cm^{-1}, respectively, are nearly identical with values reported for 11-bromoundecyl-siloxane monolayers on silicon detected by grazing angle FT-IR spectroscopy [64]. The position and structure of the peaks belonging to the alkyl stretching vibrations are indicative for the quality of the prepared monolayer [64]. Comparing the obtained peak positions with those reported for highly ordered n-octadecyl-siloxane monolayers (i.e., 2917 and 2850 cm^{-1}), a slight shift towards higher wavenumbers

is observable. This suggests a less densely packed coating [64], probably because of the shorter alkyl chain length and the relatively bulky character of the bromine function. Furthermore, the negative peak at 3740 cm^{-1} [91] confirms a successful surface functionalization. SAM-Br coated silica particles were then converted to 11-azido-undecylsiloxane (SAM$-N_3$) coated particles using sodium azide dissolved in dimethyl formamide (DMF). The successful introduction of the azide functionality was clearly detectable by DRIFT measurements (view Figure 6.4; colour: blue), because a very distinct peak arose at 2122 cm^{-1} (Literature: 2104 cm^{-1} [61]). Subsequent reduction by either $LiAlH_4$ (see Figure 6.4, colour: green) or $SnCl_2$ (see Figure 6.4, colour: yellow) caused the disappearance of this characteristic peak in the spectra. N-H bending vibrations of terminal amino groups can be observed in both spectra at a wavenumber of about 1590 cm^{-1} [96], verifying the successful transformation. But, whereas the spectrum obtained after $LiAlH_4$ treatment does not show any further changes within the siloxane layer, the spectrum recorded after $SnCl_2$ treatment indicates strong structural changes within the siloxane layer. The spectrum after $SnCl_2$ treatment resembles the spectrum recorded from APTMS coated silica (compare Figure 6.2) particles. Also the carbamate peak at about 1750 cm^{-1} is present. The observed difference does most probably originate from the two different reduction reagents and solvents involved in the preparation. $LiAlH_4$ reduction in DMF was thus chosen to prepare the amino group terminated surfaces.

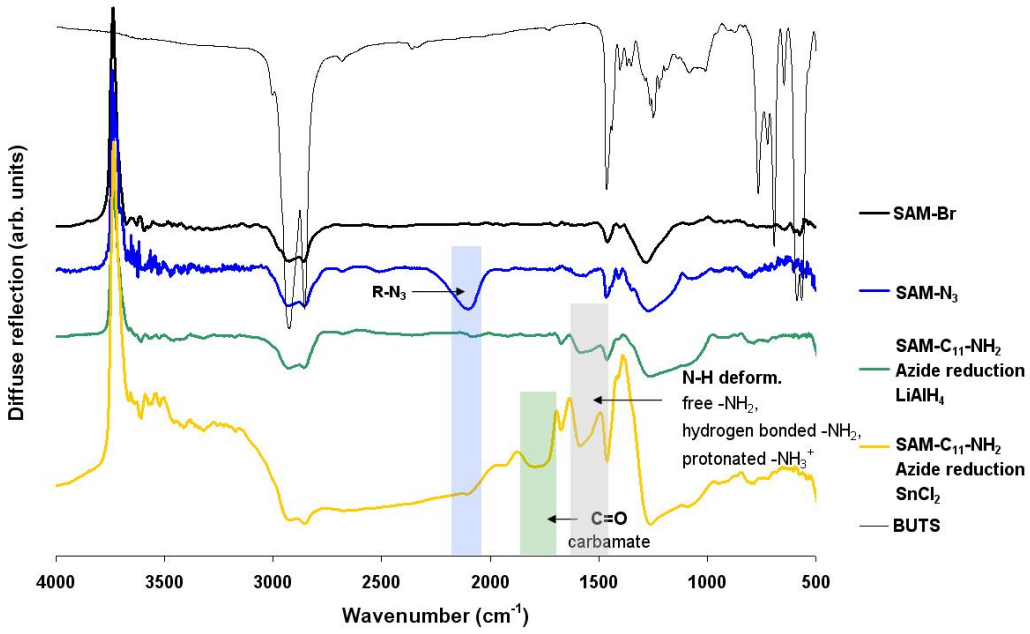

Figure 6.4: Transmission spectrum of BUTS (black, thin line). DRIFT spectra of silica particles covered by a 11-bromoundecylsiloxane layer (black, thick line), an 11-azidoundecylsiloxane layer (blue) and an 11-aminoundecylsiloxane layer prepared via two different methods (green and yellow). Reference: bare silica particles

It should be mentioned that after $LiAlH_4$ treatment the substrata were washed with diluted hydrochloric acid solution, whereas the ones reduced by $SnCl_2$ were rinsed with methanol and no acidic solution. This results in the protonation of the terminal head groups after $LiAlH_4$ treatment and unprotonated head groups after $SnCl_2$ exposure. Both preparation pathways were successful in amino group generation, but the unprotonated amino groups reacted readily with atmospheric components after preparation, as suggested by the additional peak at 1750 cm^{-1}, corresponding to the C=O carbamate vibration [93]. This observation suggests that the stability of the amino group functionality may be improved, if the final rinsing step is carried out with an acidic solution to convert the amino groups to NH_3^+, reducing the probability of transformations with air components. The presence of amino groups upon the silica surface was additionally confirmed by the Kaiser test (described in 13.7), colouring the substrata bluish.

The preparation sequence was transferred onto silicon wafers and characterized by static water contact angle and XPS measurements (data are presented in Table 6.2). SAM-Br coated wafers were of low wettability, as indicated by a high water contact angle. This wettability decrease in comparison to the uncoated wafers was expected, due to the introduction of hydrophobic moieties. After exchanging the bromide by the azide, the contact angle value changed impalpably. Only after reduction, a significant drop in the water contact angle value could be observed. The obtained value corresponds very well to literature data [100]. The successful surface functionalization was also supported by XPS analysis, where the carbon content rose after silanisation and the bromine peak appeared in the XPS spectrum. The nucleophilic substitution of the bromine by azide was confirmed by the disappearance of the Br peak and the appearance of the nitrogen peak. After the succeeding azide reduction the nitrogen content dropped slightly, as expected.

	XPS values [atomic %]					θ_{static} median
Surface coating	O(1s)	N(1s)	C(1s)	Si(2p)	Br(3d)	(25% - 75 %
sensitivity factors	[0.733]	[0.499]	[0.314]	[0.368]	[1.149]	interquartile range)
SiO_2	31	1	19	49	0	$< 10°$
$SAM{-}C_{11}{-}Br$	28	0	30	41	1	84° (83° - 85°)
$SAM{-}C_{11}{-}N_3$	29	3	30	38	0	81° (80° - 83°)
$SAM{-}C_{11}{-}NH_2$	28	2	32	38	0	65° (61° - 68°)

Table 6.2: XPS and static water contact angle data gathered on single-side polished wafers functionalized with SAM−Br, SAM−N_3, and SAM−C_{11}−NH_2. Static water contact angle (θ_{static}) values represent the median of four different areas on four different wafers with the corresponding 25 - 75% interquartile range. XPS data are the average values that were gathered on two independently prepared surface coatings at, at least, two places. (XPS spectra were acquired with the help of Dr. M. Soda, Physics, Regensburg)

The formation of the terminal amino group was further confirmed by streaming current measurements. These data are presented in chapter 8. The next subsection will describe the preparation and characterization of a further alkyl chain based coating terminated by a cationic functionality.

6.1.3 SAM-C_{11}-$N^+C_5H_5$ ($\widehat{=}$ SAM-Py)

Equipping a surface with functional groups, which provide a positive charge independent of the pH of the surrounding solution, was aimed at by preparing 11-pyridinio-undecyl-siloxane coated substrata (SAM-Py). The pyridinium functionality is an important structural element in anti-microbials, like cetyl-pyridinium bromide as mentioned in the Fundamental Part of this thesis (view subsection 1.2.3). To obtain pyridinium functionalized coatings, surfaces were facilitated with a 11-bromo-undecyl-siloxane precursor layer (SAM-Br), which was then treated with dry pyridine to substitute the terminal halogen atom by the heterocycle. A schematic drawing of the reaction is presented in Figure 6.5.

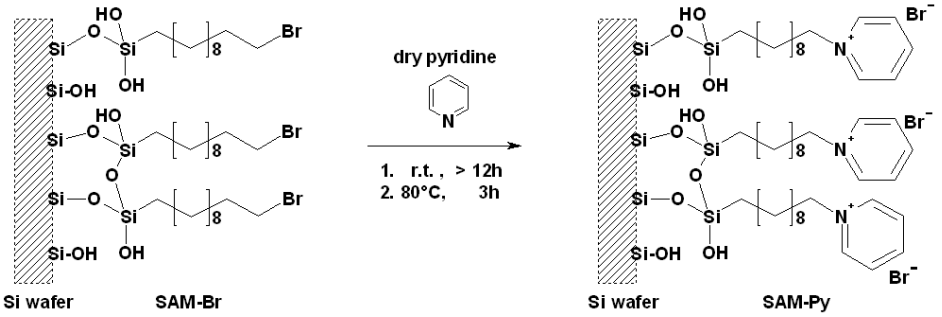

Figure 6.5: Schematic representation of the SAM-Py preparation. Nucleophilic substitution of the bromine atom by pyridine.

A prolonged reaction time and thermal endorsement was chosen for the nucleophilic substitution of the bromine atom by pyridine, because of various factors affecting the ease of this reaction negatively. These factors are, the bulkiness of the pyridine ring, the sterical hindrance of the S_N2-reaction and the introduction of a pH independent charge at the surface.

The preparation method for the SAM-Py coating was evaluated on silica particles at first and monitored by DRIFT spectroscopy using bare silica as a reference. Details regarding the precursor coating SAM-Br may be reviewed in the previous subsection 6.1.2.

In order to introduce the pyridinium function into the coating, experiments were conducted using a mixture of pyridine with different solvents, e.g. acetonitrile or dichloromethane, but none of the approaches were successful, as indicated by DRIFT measurements (results are not included, as they do not provide further information). Differences between the DRIFT spectrum of the precursor coating (SAM-Br) and SAM-Py were only observed as pyridine was used undiluted. The DRIFT spectra confirming the conversion are presented in Figure 6.6. After the reaction with pyridine no shift in peak position or intensity loss was observed for the signals belonging to the alkyl chains. Thus, suggesting neither an effect of

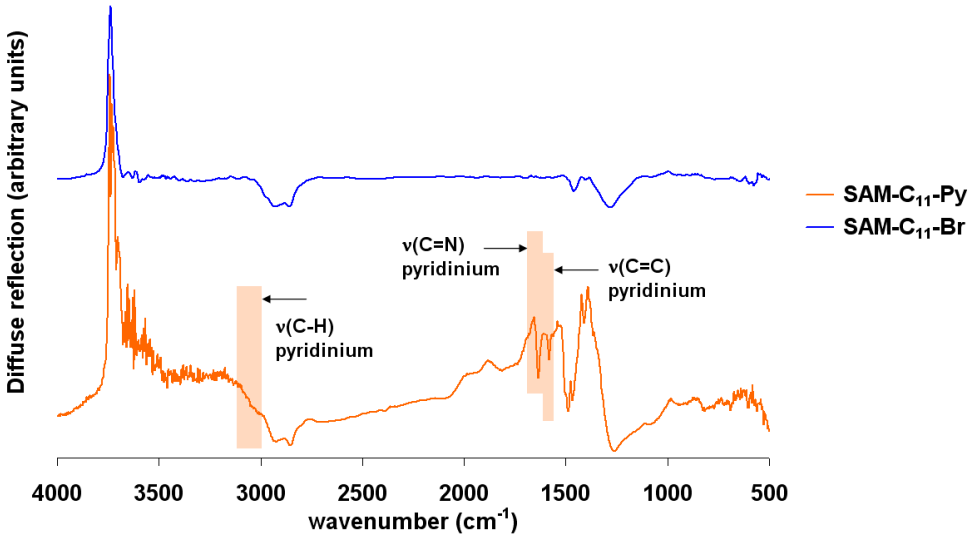

Figure 6.6: DRIFT spectra of 11-bromoundecyl-siloxane (SAM−C_{11}−Br; blue) and 11-pyridinio-undecyl-siloxane (SAM−C_{11}−Py; orange) coated silica particles. Reference: bare silica particles

the substitution on the coating structure nor an induced siloxane removal. New absorption bands at 1490 cm^{-1}, 1583 cm^{-1}, and 1637 cm^{-1} clearly indicate the presence of the pyridine ring upon the surface. Band assignments and data retreated from literature are listed in Table 6.3.

wavenumber [cm^{-1}] observed	wavenumber [cm^{-1}] Lit.[91]	assignment	comment
broad band 2977 - 3153	3070, 3090, 3135, 3190	ν(C-H) str.	pyridine ring
1583	1487/1523	ν(C=C)	pyridine ring
1637	1634/1599	ν(C=N)	pyridine ring
1490	1400, 1447	$\delta(C-H)_{aliphatic}$	pyridine ring

Table 6.3: Assignment of the absorptions detected by DRIFT on SAM-Py coated silica.

The transmission spectrum of 11-bromo-undecyl-trichlorosilane (presented in Figure 6.4) displays a pronounced profile in the fingerprint region, but no strong peaks are transferred into the DRIFT spectrum of SAM-Br. Because there is no distinguishable peak to track the substitution reaction of bromine by pyridine, DRIFT spectra were unsuitable to assess whether the reaction was accomplished quantitatively upon the surface or not. Therefore, the reaction sequence was transferred onto silicon wafers and investigated by XPS. Atomic concentrations obtained from a survey scan of the surface modifications are listed in Table 6.4. The successful formation of the SAM-Br coating is approved by the detection of a Br-signal and the typical atomic concentrations of Si and C generally obtained after SAM deposition. Subsequent substitution of the terminal functionality leads to a strong increase in C-signal

and a strong decrease in Si-signal supporting the assumption of a strong layer increase as expected for a large moiety such as the pyridinium. No nitrogen was detected on SAM-Br coated surfaces, but it was determined on the SAM-Py wafer hinting a successful introduction of the pyridinium functionality. As expected, bromine was detected on the SAM-Br surface, but none was found after bromide substitution even though one would assume the bromide anion to act as a counter ion on the pyridinium functionalized surface. Independent of the solvent used for pyridine removal, no bromide ion could be found. The only counter ion compatible with the XPS measurements is the presence of hydrogen carbonate (HCO_3^-), most probably attracted from the atmosphere. Imaginable is also a charge equalization of the head charge with $Si-O^-$ groups upon the silicon surface by loop formation. The decrease in water contact angle value from 84° (83° - 85°) to 59° (57° - 60°) after the bromide substitution, was expected due to the introduction of a charged moiety not directly exposed to the interface (data are listed in Table 6.4).

	XPS values [atomic %]					θ_{static} median
Surface coating	O(1s)	N(1s)	C(1s)	Si(2p)	Br(3d)	(25% - 75 %
sensitivity factors	[0.733]	[0.499]	[0.314]	[0.368]	[1.149]	interquartile range)
$SAM-C_{11}-Br$	28	0	30	41	1	84° (83° - 85°)
$SAM-C_{11}-Py$	26	2	48	24	0	59° (57° - 60°)

Table 6.4: XPS and static water contact angle data obtained from single-side polished wafers coated with SAM-Br and SAM-Py. Static water contact angle (θ_{static}) values represent the median of four different areas on four different wafers with the corresponding 25 - 75% interquartile range. XPS data are the average values that were gathered on two independently prepared surface coatings at, at least, two places. (XPS spectra were aquired by Helga Hildebrand, LKO, Erlangen)

The nature of the nitrogen atoms within the SAM-Py coating was further investigated by XPS at high resolution. The spectra are presented in Figure 6.7. Differently to what was expected, at least two distinct peaks were observed, indicating the presence of more than one nitrogen species upon the surface. Applying peak fitting, best results were obtained using three peaks to match the determined N-profile. The peak positions calculated by peak fitting were 399.8 eV (area = 198 units), 402.4 eV (area = 308 units) and 400.7 eV (area = 171 units). The signal at the highest energy can be assigned to protonated nitrogen species. The signals at lower energy seem to arise from species different than pyridine, not leading to a positively charged nitrogen atom. Comparing the peak areas representing the amount of nitrogen species on top of the surface one can conclude that 45% of the terminal atoms represent nitrogen species of charged character. This result is comparable to the findings of Kovalchuk et al. who prepared 3-chloropropylsiloxane coatings on silica and substituted the chlorine by pyridine to obtain weak anion-exchanging groups [91]. They could not achieve higher loadings than 50%. The reduced amount of pyridinium functionalities upon the sur-

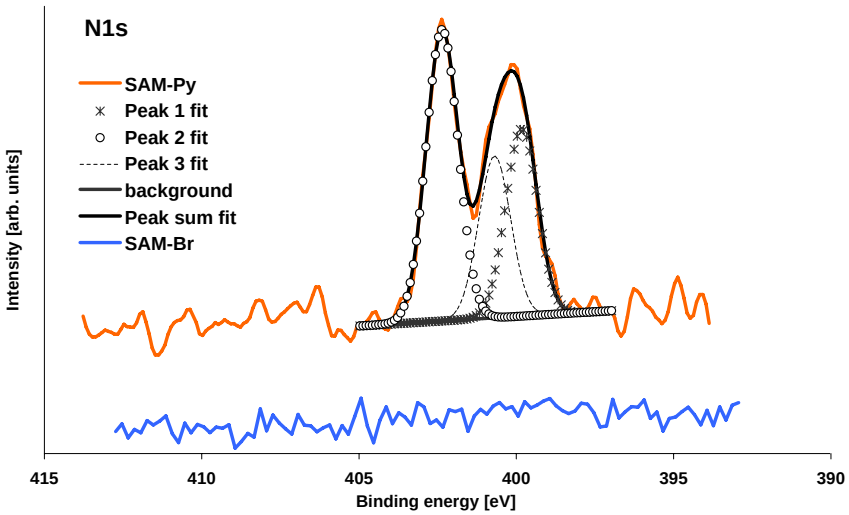

Figure 6.7: High resolution spectra of the nitrogen region in SAM-Py and SAM-Br; The N-peak of the SAM-Py coating was fitted best using 100% Gaussian function and three peaks of the same width at half maximum at the binding energies: 399.8, 402.4 and 400.7 eV.

face may be attributed to the charged character of the introduced pyridinium cations and their large dimensions. The origin of the additional nitrogen atoms, not stemming from the pyridinium, is very equivocal. Pyridinium was generally used as received, not paying attention to possible contaminations or by-products within the solution. It was only noticed later, that pyridine often contains contaminations of homologous pyridine (e.g. lutidine, picolines), aniline and phenole [102]. With a high degree of probability additional nucleophilic species within the solution, like aniline, are responsible for the observed peak. As it was done for a few preparations, pyridine should always be fractionally distilled before use. Although, it remains questionable, if a higher degree of charged pyridinium moieties is possible in this tightly organised alkyl chain coating.

The formation of the terminal pyridinium moiety and the presence of additional non-ionic functionalities upon the surface was further confirmed by streaming current measurements. These data are presented in chapter 8. The next subsections will describe the preparation and characterization of alkyl chain based coatings terminated by anionic functionalities.

6.2 Anionic SAMs

6.2.1 SAM-C_6-COOH

To the best of my knowledge the first report on the formation of carboxylic acid terminated SAMs (SAM-COOH) was published in 1995 [103]. In the following years various preparation methods were suggested, such as

1. ozonolysis (O_3) of vinyl terminated SAMs [104][105]
2. photo-oxidation of aldehyde terminated SAMs using UV light [106]
3. nucleophilic substitution of bromine terminated SAMs by cyanide and subsequent formation of SAM-COOH by using $NaHCO_3$ in water [86]
4. oxidation of vinyl terminated SAMs utilizing $NaIO_4/KMnO_4/K_2CO_3$ [59]
5. oxidation using $KMnO_4$ (5 w%, acidic solution) [107].

Ozonolysis of vinyl terminated SAMs seemed a very promising attempt in the preparation of SAM-COOH because the reagent is gaseous and unable to contaminate the surface, but both researching groups, J. Matijašević et al. [105] and T. M. McIntire et al. [104] observed a strong deterioration of the hydrocarbon chains after ozone exposure. Also, oxidation by UV light causes a complete photo-decomposition of the organic layer [106].
Nucleophilic substitution of bromine by cyanide in SAM-Br functionalized surfaces with subsequent formation of SAM-COOH by the use of sodium bicarbonate is an alternative way for the preparation of the desired SAM-COOH surface [86]. The imperative of a sealed pressure tube to provide ideal reaction conditions as described by Shyue et al. [86] and the lengthiness of the preparation process were discouraging in view of large quantities needed to prepare within this project.
A preparation method often mentioned in literature is the procedure reported by Wassermann et al.. They examined the oxidation of vinyl groups, forming carboxylic acid using a mixture of $KMnO_4$, $NaIO_4$ and K_2CO_3 [59]. Within this paper Wassermann et al. mention a method reported by Sagiv [108] using solely $KMnO_4$ either in aqueous or organic solution (supplement: [18]crown-6) and assume this way to be unsuccessful because the products obtained in solution are vicinal diols and alpha-hydroxy ketones, only [59]. Both ways of preparation seemed worth trying, not at last because the co-author of the Wassermann et al. paper was G. M. Whitesides, an expert in the field of siloxane based SAM preparation, just like J. Sagiv [108], pioneer in SAMs on Si.

Both preparation methods were performed on silica particles. At first, vinyl terminated SAMs were prepared using the 7-octenyltrichlorosilane (OeTS) to obtain 7-octenylsiloxane

functionalized (SAM−CH=CH_2) silica. The carbon-carbon double bond was then either oxidized by potassium permanganate (VII) ($KMnO_4$) in acidic solution (method A) or by an aqueous mixture of potassium permanganate ($KMnO_4$), sodium periodate ($NaIO_4$), and potassium carbonate (K_2CO_3) (method B) in order to obtain SAM-COOH. Figure 6.8 represents the reaction by method A converting the SAM−CH=CH_2 coating into SAM-COOH. The oxidation of terminal olefins by potassium permanganate leads to carboxylic acids of one less carbon due to the liberation of carbon dioxide [109].

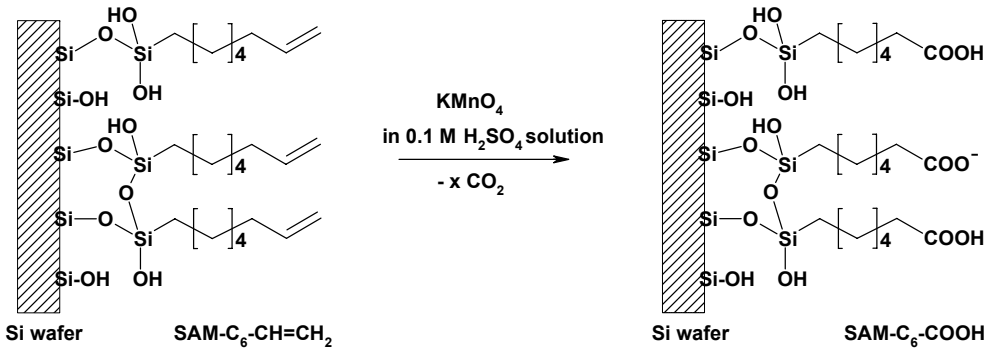

Figure 6.8: Schematic representation of the SAM−CH=CH_2 coating and its conversion into SAM−COOH.

Method B was carried out as described in literature [59]. The reaction solution turned brownish after the proposed reaction time. After separation of the particles from the reaction solution by means of a Büchner funnel the silica particles remained brown, most probably due to Braunstein precipitation. Rinsing with sodium bisulfite clearly lightened up the substratum but the colour did not vanish completely, suggesting strong contamination upon the surface. Contamination by manganese was later confirmed by XPS on wafer surfaces. Furthermore, the DRIFT spectrum of the obtained coating, presented in Figure 6.9 and labelled by the letter B, contains hardly any vibration in the carbonyl region (1700 - 1740 cm^{-1}) related to a carboxylic acid, ketone or aldehyde structure. The hump at wavenumbers larger than 3000 (hydrogen bonded -OH groups) rather suggests the formation of alcohols (C-O stretching vibration at 1200 cm^{-1} is within the vibration range of the Si-O-Si network). Preparation parameters favour the formation of carboxylate ions but even at 1610 - 1550 cm^{-1} ($\nu_{as}(COO^-)$) and 1420 - 1300 cm^{-1} ($\nu_s(COO^-)$) [110] no clearly identifiable vibrations occur. The alkyl chains are still detectable but resemble more the spectrum of the 7-octenyltrichlorosilane solution, suggesting a distortion of the alkyl chains. The prolonged exposure to the aqueous reaction solution seems to have a negative impact on the organic film structure. Results regarding method B were rather displeasing, and were thus no longer traced.

A method using solely $KMnO_4$ was evaluated. Liu et al. [107] performed this oxidation in hydrochloric acid solution which was avoided because of the possible formation of chlorine during the reaction. The oxidation here was performed in acidic solution prepared with sulphuric acid. $KMnO_4$ creates a terminal aldehyde and formaldehyde after reaction with the terminal alkene. Highly concentrated potassium permanganate $KMnO_4$ solutions were used to reduce the probability of aldehyde formation and achieve carboxylic acid terminated SAMs [111]. The liberated formaldehyde is oxidized by the oxidation reagent to water and carbon dioxide or formic acid [111]. Best results were obtained after an oxidation time of 10 min at room temperature as evaluated by DRIFT measurements. Excessive oxidation times resulted in a decrease of the alkyl chain. Assignment of the vibrations within the DRIFT spectra to structural elements is explained in detail in the next paragraph.

Figure 6.9 displays the transmission spectrum of the precursor molecule 7-octenyltrichlorosilane (OeTS), and the DRIFT spectra of the silica particles coated with a 6-carboxyhexylsiloxane (SAM-COOH) layer obtained via the preparation methods A and B, as well as the precursor coating octenylsiloxane (SAM−CH=CH_2).

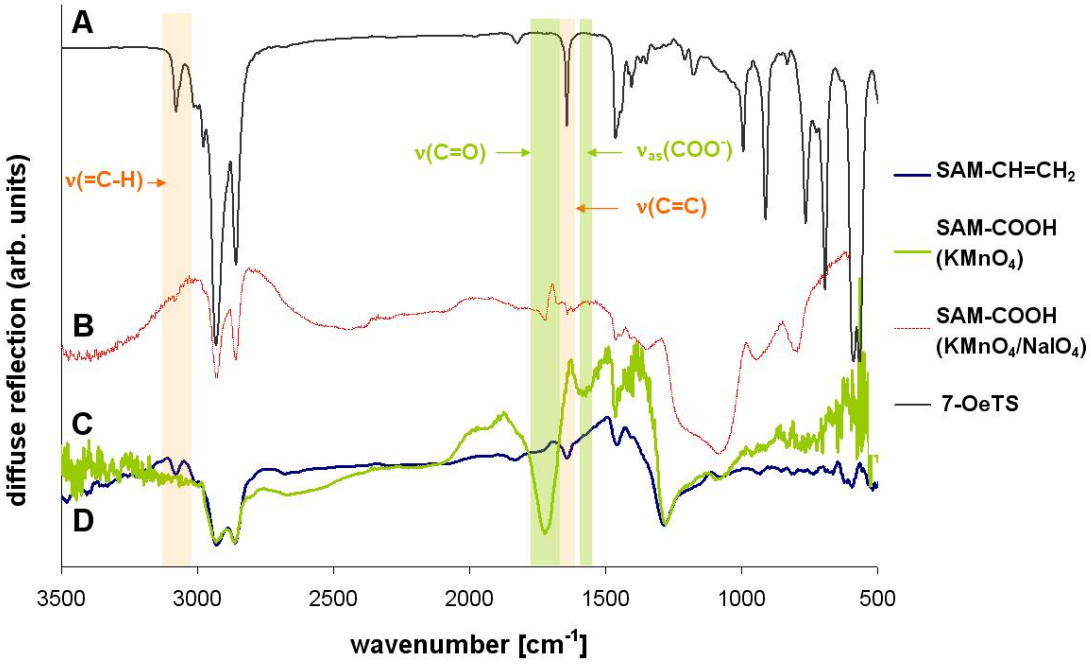

Figure 6.9: Transmission spectrum of 7-octenyltrichlorosilane (A); DRIFT spectra of surface-modified silica particles:
SAM−COOH ($KMnO_4$/$NaIO_4$)(B), SAM−COOH ($KMnO_4$)(C),
and SAM−CH=CH_2 (D).

The absorption bands at 1643 cm^{-1} (ν(C=C)) and 3081 cm^{-1} (ν(=C-H)) belong to the stretching modes of the double bond. They are clearly detectable in the transmission spectrum of OeTS, shown in Figure 6.9 and labelled with the capital letter A. Absorption bands at 2935 cm^{-1}, 2860 cm^{-1}, and 1465 cm^{-1} can be assigned to the vibrations of the alkyl chains $\nu_{as}(CH_2)$, $\nu_s(CH_2)$ and $\delta(CH_2)$, respectively. No broad and complex band is observed between 1250 - 975 cm^{-1} characteristic of ν(Si−O−Si) stretching modes of partially condensed polysiloxanols and ν(Si−OH) groups [105], in contrary very sharp peaks appear in this region. This tests and demonstrates that no polymerization within the reagent has occurred.

A comparison of the OeTS transmission spectrum with the DRIFT spectrum of the particles coated by SAM−CH=CH_2 confirms the preservation of the double bond functionality after silanisation, since the characteristic absorption peaks at 1643 cm^{-1}, and 3081 cm^{-1} are still observable. Between 1000 cm^{-1} and 1287 cm^{-1} a broad band is formed corresponding to the complex siloxane network (Si-O-Si) confirming polymerization of the silanol molecules upon the surface.

The successful functionalization of silica particles with carboxylic acid moieties is obvious as the DRIFT spectra of SAM−CH=CH_2 and SAM−COOH are compared. The disappearance of the vinyl absorptions and the formation of a new broad peak at 1734 cm^{-1}, as well as a broad peak of less intensity at 1599 cm^{-1} confirm a chemical conversion of the vinyl bond. The peak positions can be allocated to the ν(C=O) vibration, characteristic for acids, aldehydes and ketons. Aldehyde formation is ruled out because of the use of a highly concentrated potassium permanganate solution readily oxidizing aldehydes. Ketone formation can not be ruled out, since OeTS contains 10 - 30 % of isomers according to manufacturer's data.

Because of the broad shape of the two, newly formed peaks, carboxylic acid functionalities are presumed to be in multiple forms, i.e. either protonated $-COOH$ or carboxylated $-COO^-$ and/or within or without a hydrogen bond. IR absorption values of surface confined protonated carboxylic acids reported in literature fit very well to the obtained 1734 cm^{-1} ($-COOH$ surface 1734 cm^{-1} [112], $-COOH$ surface free 1744 cm^{-1} and $-COOH$ surface hydrogen bonded 1720 cm^{-1} [60]; corresponding -OH stretch at 3720 cm^{-1} is superimposed with Si-OH). The less intensive vibration band at 1599 cm^{-1} can be assigned to the asymmetric stretch of the carboxylate anion. The corresponding band of the symmetric stretch is superposed by the alkyl chain vibrations and can not be clearly identified. Literature data correlate very well with the recorded value for the carboxylate ($\nu_{as}(COO^-)$ at 1610 cm^{-1} - 1550 cm^{-1} and at 1420 cm^{-1} - 1300 cm^{-1} $\nu_s(COO^-)$) [110]. The alkyl vibrations are kept untouched, suggesting no delamination or deterioration of the organic layer at all.

DRIFT measurements confirm the successful introduction of the carboxylic acid group by oxidation with plain acidic $KMnO_4$ solution. The successful preparation method applied on silica particles was transferred onto silicon wafers. Wettability measurements were performed to detect changes in physico-chemical properties of the investigated surface. Table 6.5 summarizes wettability data for the vinyl- and carboxylic acid terminated monolayers obtained by experiments and collected from literature.

	XPS values [atomic %]				θ_{static} median
Surface coating	O(1s)	N(1s)	C(1s)	Si(2p)	(25% - 75 %
sensitivity factors	[0.733]	[0.499]	[0.314]	[0.368]	interquartile range)
SAM−C_6−CH=CH_2	29	0	28	43	94°(93° - 95°)
SAM−C_6−COOH	33	0	26	41	44° (41° - 47°)

Table 6.5: XPS and static water contact angle data obtained from single-side polished wafers coated with SAM−CH=CH_2 and SAM−COOH. Static water contact angle (θ_{static}) values represent the median of four different areas on four different wafers with the corresponding 25 - 75 % interquartile range. XPS data are the average values that were gathered on two independently prepared surface coatings at, at least, two places. (XPS spectra were aquired by Helga Hildebrand, LKO, Erlangen)

Immobilization of OeTS onto freshly oxidized silicon surfaces turned the surface from hydrophilic to hydrophobic as recorded by a static water contact angle increase from below 10° to 94° (93°- 95°) (Literature: 105°[107]; ∼ 97°[59]). This is due to the hydrophobic character of the terminal alkene moiety. After oxidation the water contact angle decreased to 44° (41°-47°) (Literature: 33°[106]; 48°[107]; ∼30°[59]). This increase in wettability was expected because of the polar character of the carboxylic acid and correlates well with literature data.

XPS analysis (data summarized in Table 6.5) confirmed an increase in oxygen content after oxidation supporting the introduction of acidic moieties. Furthermore, the slightly reduced carbon signal confirms the loss of carbon dioxide as expected. No residues were detected after oxidation by XPS in spite of the high sensitivity factor of manganese.

Even though stated differently in the publication of G. M. Whitesides, experiments performed here, provide clear evidence of the formation of SAM−COOH. The formation of the terminal carboxylic acid group was further confirmed by streaming current measurements. These data are presented in chapter 8. The next subsection will describe the preparation and characterization of a further alkyl chain based coating terminated by an anionic functionality.

6.2.2 SAM-C_{11}-SO_3H

Sulfonate-functionalized SAMs are negatively charged independent of the pH of the surrounding solution. Studies on polymers bearing sulfonate functionalities exhibit outstanding blood compatibility [113]. This is attributed to the heparin like structure, an anticoagulant, which possess numerous sulfonate functionalities.

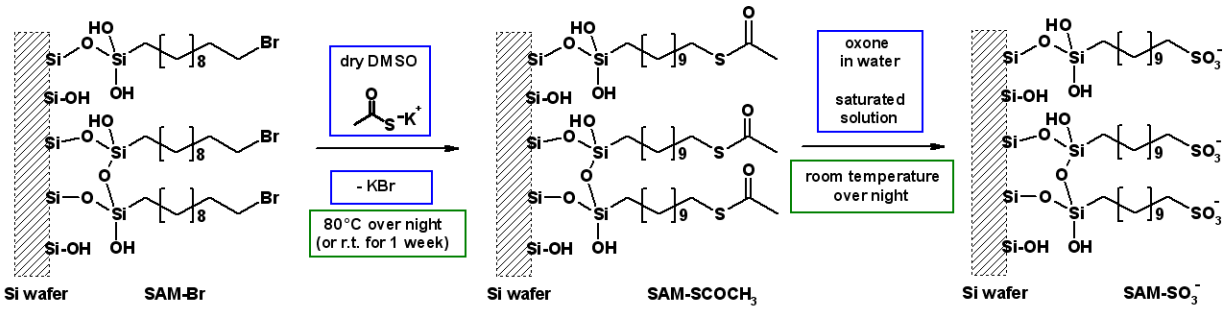

Figure 6.10: Schematic representation of the SAM−Br coating and its conversion into SAM−$SCOCH_3$ and SAM−SO_3^-, respectively.

The original idea to generate sulfonate terminated SAMs was to convert APTMS functionalized SAMs by the use of 1,3-propane sultone, but because of the disadvantages of APTMS films mentioned in section 6.1.1, this path was discarded. Literature on sulfonic acid terminated SAMs is not as comprehensive as on amine terminated SAMs. For example, surface coatings prepared by mercaptoalkyl-tri-methoxysilane were oxidized by a hydrogenperoxide solution to obtain sulfonic acid terminated SAMs, but oxidation in this reaction pathway was reported to be incomplete [62]. Sukenik et al. compared various oxidizing methods (peracetic acid, performic acid, photo-oxidation, oxone) to convert thioacetate terminated SAMs into sulfonic acid terminated SAMs [62][114]. The oxidation of thioacetate terminated SAMs by oxone was evaluated to convert in the highest yields. Oxone treatment is very convenient (no temperature control), gentle (does not cause delamination), non-toxic and eco-friendly [62][115]. A method described by Shyue et al. [86] was verified and adjusted in such a way that large amounts could be prepared in our laboratory.

At first, the preparation sequence (depicted in Figure 6.10) was performed on silica particles and monitored by DRIFT spectroscopy. The precursor coating, 11-bromoundecylsiloxane (SAM-Br) has been described in detail in the subsections 6.1.2 and 6.1.3. Subsequently, the terminal bromine functions were displaced by (potassium) thioacetate in anhydrous dimethyl sulfoxide (DMSO) via nucleophilic substitution. DMSO complexes cations very well and supports the nucleophilic substitution of the bromide by the thioacetate anion. Elevated

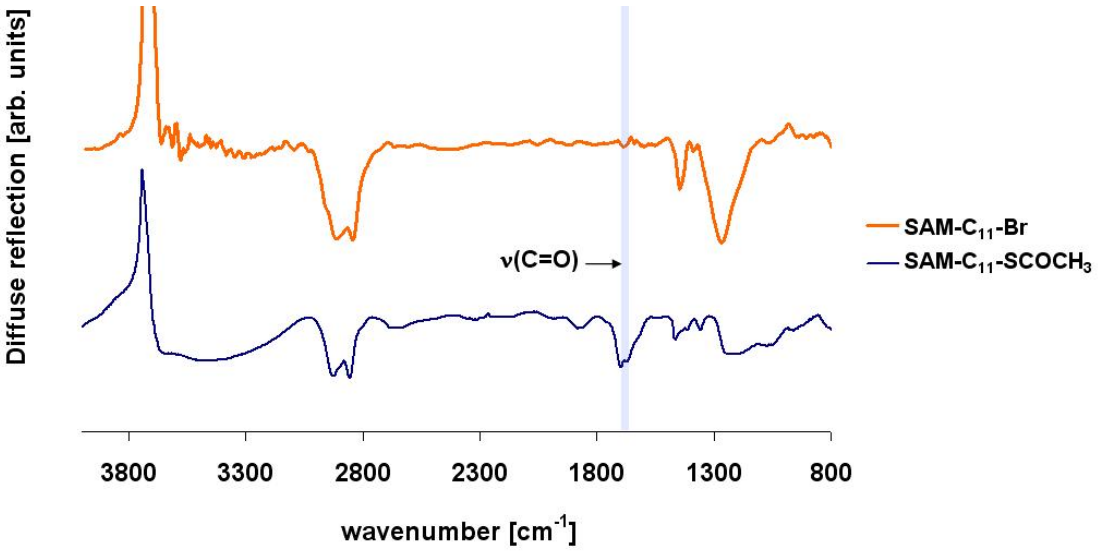

Figure 6.11: DRIFT spectra of surface-modified silica particles: SAM−C_{11}−Br and SAM−C_{11}−$SCOCH_3$

temperature is recommended for this step in literature [86]. Own experiments revealed that conversion at 80°C over night or at ambient temperature for one week led to comparable results. The sulfonate moiety was then achieved by oxidizing the terminal thioester functionality with an aqueous solution of oxone. Oxone is a 2:1:1 molar mixture of $KHSO_5$, $KHSO_4$ and K_2SO_4. The reactive species within this mixture is most probably $KHSO_5$. The incorporation of the thioester group could be clearly visualized by DRIFT measurements on functionalized silica due to the very strong ester vibration (C=O stretching) at about 1690 cm^{-1}. This value correlates well with the C=O vibration observed in non-surface confined thioacetate containing molecules, where the vibration occurs between 1688 cm^{-1} - 1700 cm^{-1} [116]. The rate of conversion can not be assessed because the C-Br band can not be observed on silica modified particles. After oxidation by oxone the disappearance of the C=O moiety is indicative for the successful reaction. But it was not possible to clearly distinguish a newly evolving peak for the sulfonate moiety within the range of 1000 - 1350 cm^{-1} belonging to S=O and S-O stretching vibrations [117], as the siloxane network and the alkyl deformation bands also occupy this area.

The reaction procedure was transferred onto silicon wafers and the success of each reaction step was monitored by XPS analysing the sulphur peak at high resolution. The high resolution spectra of the surface coatings are presented in Figure 6.12. No S-signal can be detected for the bromine terminated surfaces, but after introduction of the thioester moiety a pronounced signal appears at 163.8 eV. This signal disappears nearly completely after oxidation and a new peak arose at 168.4 eV. Both values correlate well with data reported

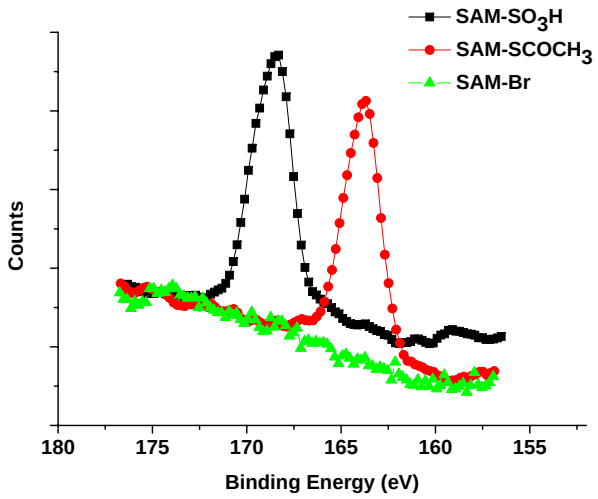

Figure 6.12: The high resolution XPS spectra of the S-region document the successful preparation of sulfonic acid terminated SAM. S(2p) spectra of SAMs terminated by sulfonic acid (squares), thioacetate (dots) and bromide (triangles) functionalities.

in literature [113][117][62]. Sulfur species generate two peaks of tiny separation due to spin orbital splitting with peak intensity ratios of 1:2 for S $2p^{1/2}$ and S $2p^{3/2}$. These two peaks were summarized and are presented by one peak in Figure 6.12.

The recorded elemental compositions of the coatings determined by XPS provide additional evidence for a successful incorporation of the thioester and sulfonate groups (data are presented in Table 6.6). The Br signal disappears completely after the reaction with potassium thioacetate and a signal reflecting a similar concentration upon the surface appears for sulfur. After oxidation the sulfur concentration remains more or less constant and an significant increase in oxygen content can be observed.

The wettability of the surfaces changed from 90° (86° - 92°) for the SAM-Br coating to 78° (74° - 79°) for the thioester functionalised surface (data summarized in Table 6.6). Advancing and receding contact angle values recorded on SAMs prepared by the direct deposition of thioacetate alkyltrichlorosilane onto silicon wafers were reported to be $72° \pm 1°$ and $65° \pm 2°$, respectively [62]. These values are slightly lower than the ones obtained by the own preparation path. This may be due to the different surface densities or head group arrangements induced by immobilizing alkyltrichlorosilanes with different terminal groups, such as bromide or thioacetate. A significant drop in static contact angle value from 78° (74° - 79°) to 51° (50°-53°) was observed after oxidation with oxone. Collins et al. [62] reported considerably lower values for sulfonate-functionalized surfaces. They determined advancing and receding contact angle values of $15° \pm 3°$ and $<4°$, respectively. Static contact angles recorded

on sulfonate bearing SAMs on gold revealed values of 34.0° ± 1.4° [113]. An increased hydrophilicity is expected due to the charged character of the sulfonate functionality. Probably unoxidised thioacetate, below the detection limit of XPS, contributed to a slightly increased water contact angle value. This might be because the formation of charge is hampered by electrostatic repulsion in respect to the substratum charge.

	XPS values [atomic %]						θ_{static} median
Surface coating	C(1s)	O(1s)	N(1s)	Si(2p)	Br(3d5)	S(2p)	(25% - 75 %
sensitivity factors	[0.314]	[0.733]	[0.499]	[0.368]	[1.149]	[0.717]	interquartile range)
SAM−C_{11}−Br	73	14	1	9	3	0	90° (86° - 92°)
SAM−C_{11}−$SCOCH_3$	74	15	0	8	0	4	78° (74° - 79°)
SAM−C_{11}−SO_3^-	61	25	1	5	0	5	51° (50°-53°)

Table 6.6: XPS values [at.%] and static water contact angles (θ_{static}) of SAM−C_{11}−Br, SAM−C_{11}−$SCOCH_3$, and SAM−C_{11}−SO_3^-; Static water contact angle (θ_{static}) values represent the median of four different areas on four different wafers with the corresponding 25 - 75 % interquartile range. XPS data are the average values that were gathered on two independently prepared surface coatings at, at least, two places. (XPS spectra were aquired by Helga Hildebrand, LKO, Erlangen)

In summary, a preparation pathway recorded in literature was verified and evaluated to be successful in preparing sulfonate terminated SAMs. For future preparations a direct deposition of the thioacetate terminated silane is advised to optimize the resulting concentration of sulfonate moieties. The next section describes the two reference coatings used within this thesis.

6.3 Non-ionizable SAMs

Both references mentioned below, SAM-PEG and SAM−C_7−CH_3, have been thoroughly studied in a former project at the department by R. Müller et al., and are published in the following literature: [118].

6.3.1 SAM-PEG

Surfaces coated by poly- or oligo(ethylene glycol) (PEG/OEG) units are well known to be strongly proteophobic as mentioned in the Fundamental part of this thesis (see subsection 1.2.1), but are susceptible to degradation via autoxidation [27]. They were employed as references. These surface coatings were achieved by immersing freshly oxidised surfaces into N-(triethoxysilylpropyl)-O-polyethylene oxide urethane
$((OEt)_3Si-(CH_2)_3-NH-CO-(OCH_2CH_2)_5-OH)$ (OEGTES) solutions.
Wafer surfaces coated by SAM-OEG are of hydrophilic character with a contact angle value of 39° (37°- 42°). Even though short chain ethylene glycol was used for the functionalization of the surfaces they are referred to as SAM-PEG because this is a more familiar denomination.

6.3.2 SAM-C_7-CH_3

Hydrophobic surface coatings were generated by using n-octyltrichlorosilane. These surfaces were employed as reference coatings. Hydrophobic coatings are less prone to the adsorption of contamination due to a lower surface free energy. The static contact angle determined for this coating was 95° (93°- 98°).

These surface coatings, terminated by non-ionizable functionalities, close the surface modifications based on linear alkyl chains arranged in self-assembled monolayers. The following chapter describes the dendrimer immobilization and the characterization and preparation of coatings based upon it. Dendrimer based coatings were terminated by cationic, anionic and neutral peripheral groups in analogy to the before mentioned alkyl chain based coatings.

7 Coatings based on Dendrimers (PAMAM)

This chapter describes in detail the establishment and characterization of the novel dendrimer based coatings. The tethering of the polyamidoamine (PAMAM-NH_2) dendrimer is specified in the first section of this chapter, thereafter, three sections address the transformation of the PAMAM-NH_2 coating into coatings terminated by anionic (carboxylic acid: PAMAM-COOH; sulfonic acid: PAMAM-SO_3H), cationic (amine: PAMAM-NH_2; pyridinium: PAMAM-Py) and neutral (acetamide: PAMAM-$COCH_3$) functionalities.

At the beginning of creating PAMAM-NH_2 based coatings the question was raised, whether it would be of greater success to perform the terminal modifications on PAMAM-NH_2 before or after tethering to the surface. Pre-modifying PAMAM-NH_2 in solution was considered beneficial at first glance because it would increase the spectrum of readily available and applicable analytical methods tremendously (e.g. $^{1}H/^{13}C$ nuclear magnetic resonance, isoelectric focusing, matrix-assisted laser desorption ionization time-of-flight mass spectrometry, potentiometric titration, polyacrylamide gel electrophoresis, size-exclusion chromatography, capillary electrophoresis [119], elemental analysis ...), compared to those available for surface analysis (e.g., X-ray photoelectron spectroscopy, ellipsometry, contact angle goniometry, atomic force microscopy). For the covalent attachment to the surface unreacted terminal amino groups were intended to be used. The reason this way was not went at the end, even though pilot tests were run (Preparation protocol for PAMAM-COOH is mentioned in subsection 12.5.2), is that the termini that are introduced in this work and the chosen substratum are of charged character. Dendrimers would influence each other in the way they approach the surface, creating different surface occupancy rates. Therefore, it had been decided to immobilize the dendrimer in advance and introduce the functional groups afterwards, providing a constant basis for all film preparations. The regularity of the coatings is indispensable when studying surface response relationships.

For the interpretation of the XPS data, mainly used to characterize the dendrimer based coatings, it is helpful to know the explicit structure of the dendrimer. The following table summarizes the atomic components of PAMAM-NH_2 (view Table 7.1) for the generations 0 up to 5.

	N_a	N_t	N_p	O	C_{al}	C_a	H_{al}	H_a	H_p
core	0	2	0	0	2	0	4	0	0
0	4	4	0	4	16	4	32	4	0
1	8	8	0	8	32	8	64	8	0
2	16	16	0	16	64	16	128	16	0
3	32	32	0	32	128	32	256	32	0
4	64	64	0	64	256	64	512	64	0
5	128	0	128	128	512	128	1024	128	256
Σ	252	126	128	252	1010	252	2020	252	256

Table 7.1: Atomic composition of PAMAM-NH_2; Abbreviations: N_a = amide nitrogen, N_t = tertiary amine nitrogen, N_p = primary amine nitrogen, O = oxygen belonging to the amide bond, C_{al} = carbon of the methylene groups, C_a = carbon of the amide bond, H_{al} = hydrogen atoms of the methylene groups, H_a = amide bond hydrogen, H_p = hydrogen at the primary amino groups.

7.1 Immobilization of PAMAM-NH_2

The most popular reaction to bind biomolecules onto surfaces is the reaction between the amino groups of biomolecules, present throughout proteins, and carboxylic acid or anhydride moieties on top of surfaces via amide bond formation. The tethering onto anhydride coatings is favoured over carboxylic acid terminated coatings because no additional reagents for carboxylic acid activation are needed. Activation spoils additional reagents, is time-consuming, and after all, the use of additional chemicals always carries the risk of residues remaining upon the surface.

Within the framework of this project diffuse reflectance infrared spectroscopy (DRIFT), ζ-potential determination by electrophoresis, wettability measurements by static contact angle measurements (CA) and X-ray photoelectron spectroscopy (XPS) analysis were prescribed for the analysis and establishment of the surface coatings. The two former techniques need to be performed on large surface areas and thus silica particles with a specific area of 500 m^2/g were proposed, the two later mentioned methods can be performed on tiny surface areas, such as wafers. Because of the large surface area of silica particles, a very high amount of PAMAM-NH_2 would be needed to cover the surface homogeneously, in line with modifications performed on silicon wafers. Due to the preciousness of dendrimers this method was thus inapplicable for trial and error experiments evaluating the best dendrimer immobilization pathway or derivatisation technique. Contact angle measurements were noted to be absolutely inadequate to evaluate trial and error experiments because of the minor differences detected among the derivatised PAMAM coatings. The examination of coatings based on linear alkyl chains was possible with this equipment, due to the low prices of these molecules.

Unfortunately, only towards the end of the project silica spheres (diameter = 1 μm) with non-porous character and a strongly reduced specific surface area of 3 m^2/g were tested to be excellent for the examination of PAMAM-NH_2 based coatings by DRIFT spectroscopy and electrophoresis. Whereas the analytical apparatuses for DRIFT, electrophoresis and static contact angle measurements were readily available, XPS measurements were hardly or not accessible. Therefore a frenetic search began to expand the pool of surface sensitive methods. Methods detecting surface bound amino groups were gathered. The covalent binding of a fluorescence pyrylium dye developed in Regensburg [120] led to puzzling results after analysing the surfaces under a fluorescence microscope or a fluorescence scanner (possible reasons could be, that the positive character and large dimensions of the dye gave rise to the strange results, not presented here), thus this method was shelved for good. It turned out, that the chemiluminescence based assay developed to detect protein adsorption on top of surfaces, invented by Rainer Müller et al. [118] was extremely valuable for the detection of covalently bound polyamidoamine by marking the terminal amino groups on top of the surfaces and their disappearance after conversion. Searching for further analytical methods a contact was established with the company Anton Paar in Austria. The excellent staff of this company provided a streaming potential/current apparatus for a very short time. Excellent measurements could be obtained directly on the wafer surfaces and derivatization of dendrimer coatings could be monitored. Thanks to Prof. Motschmann and his staff a few pilot tests were possible with sum frequency generation spectroscopy (SFG) and atomic force microscopy (AFM).

As the preparation of anhydride terminated SAMs was not successful at the beginning, binding of PAMAM to carboxylic acid terminated substrata was also investigated. The carboxylic acid bearing surfaces were prepared as described in section 6.2.1. Carboxylic acids were activated with a solution containing 1-(3-(dimethylamino)propyl)-3-ethylcarbodimide hydrochloride (EDC) and N-hydroxysuccinimide (NHS) in 2-morpholinoethane sulfonic acid (MES) buffer. Some of the results obtained by these experiments are included, because they were a valuable contribution to obtain a susceptibility for the preparation of the PAMAM-NH_2 based coatings.

7.1.1 "Diluted" Carboxylic Acid Terminated SAMs

PAMAM-NH_2 deposited onto surfaces, whether covalently or ionically, is flattened [47]. And it becomes even flatter the more terminal groups of the dendrimer are involved in anchorage [121]. Crooks at al. could reduce the flattening of PAMAM-NH_2 on gold by replacing PAMAM-amine-gold linkages by alkyl-thiol-gold linkages of added mercaptoalkanes [121].

Therefore, reducing the amount of anchoring groups for PAMAM-NH_2 by diluting the carboxylic acid moieties with aryl/alkyl terminated SAMs was an endeavour to maintain the globular shape of the dendrimer. It was intended by this approach to promote the accessibility of the terminal groups for subsequent functionalization and biological interactions.

The first attempt to reduce dendrimer linkages to the surface was to dilute the precursor of carboxylic acid terminated SAMs, the 7-octenyl trichlorosilane molecule, with phenyl trichlorosilane. It was expected that the bulky character of the phenyl group would support the lateral dilution of the alken terminated molecules. The lateral distribution of the alkene terminated silane could have been accessed by adding bromine to the double bond and determination by XPS, unfortunately no XPS contingent was available for confirmation. Contact angle measurements on the prepared surfaces revealed the surface to be very non-homogeneous. The deposited water droplets had a very irregular shape. Presumably the difference in chemical structure caused the formation of large islands of the one or other component and no homogeneous mixing occurred. Nevertheless, the surfaces were oxidized with potassium permanganate and PAMAM-NH_2 covalently bonded thereto by the EDC/NHS method. The inhomogeneity in contact angle values remained (21° (12° - 39°)), suggesting the dendrimer to be too small to cover the created hydrophobic islands.

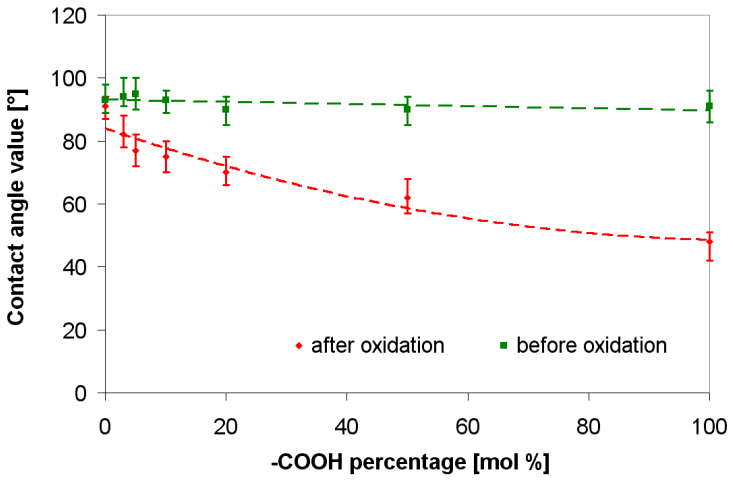

Figure 7.1: Contact angle value depending on the terminal group ratio: SAM-COOH/SAM$-CH_3$

Thus this idea was discarded and an alkyl-chain chosen to dilute the carboxylic acid moieties upon the surface. A similar approach was made by Tokuhisa et al. [53] who prepared mixed SAMs of mercaptoundecanoic acid and mercaptopentane on gold surfaces. Butyl trichlorosilane was selected because the shortness of the spacer would allow the terminal

carboxylic group to be exposed. In contrast to coatings diluted with phenyl trichlorosilane, the ones diluted with butyl trichlorosilane possessed a homogeneous surface character before and after oxidation. An even decrease in wettability could be observed as the amount of terminal carboxylic acid groups increased as presented in Figure 7.1. No PAMAM-NH_2 was bonded onto these surfaces (only to undiluted SAM-COOH coated surfaces; results are presented in subsection 7.1.3), since SAM coatings terminated by carboxylic acid anhydride groups were successfully generated at that time, and replaced the SAM-COOH coatings for dendrimer fixation. Nevertheless, these results demonstrate the possibility of diluting binding sites upon the surface using silane molecules. Controlling the surface concentration of dendrimers upon a surface via specific binding sites would provide a great platform for the design of standard surfaces applicable in streaming potential/current measurements, since there are none up to now.

7.1.2 Carboxylic Acid Anhydride Terminated Surfaces

3-(Triethoxysilyl) propyl succinic acid anhydride (TESPSA) seemed to be a convenient silanisation reagent to prepare anhydride bearing coatings on hydroxyl terminated surfaces. Besides the fact that covalent fixation of biomolecules is possible without additional reagents, the TESPSA coating creates an additional "carpet" of negative charges close to the silicon surface after the reaction with amines (see Figure 7.4). Negative charges within a siloxane coating were reported to increase the stability of the silane based film in aqueous media by shielding the anchoring Si-O-Si groups from hydroxyl ion attacks [95][122]. To the best of my knowledge, TESPSA has only been used for the generation of carboxylic acid functionalities [122][98] on surfaces but not for the straight forward tethering of biomolecules. The TESPSA silane molecule is illustrated in Figure 7.2.

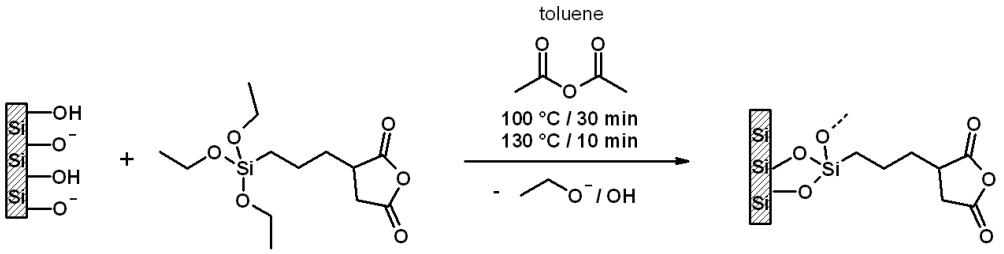

Figure 7.2: 3-(**T**rie**t**hoxy**s**ilyl) **p**ropyl **s**uccinic acid **a**nhydride (TESPSA); Schematic illustration of the coating applied for PAMAM immobilization. Oxidised silicon surfaces (OX) were modified with TESPSA to introduce anhydride groups.

DRIFT spectroscopy measurements on silica particles were used to monitor the achievements in developing anhydride terminated coatings. The final spectra are summarized in Figure

7.3. The transmission spectrum of TESPSA recorded between two NaCl plates was used as a reference (view spectrum A in Figure 7.3). The spectrum of TESPSA reveals the in-phase and out-of-phase C=O stretching modes of the two carbonyl groups located within the cyclic carboxylic acid anhydride functionality [123] at 1867 and 1795 cm^{-1}, respectively. According to literature, these vibration bands occur within the ranges of 1870 - 1820 cm^{-1} and 1800 - 1750 cm^{-1} at a distance of about 60 cm^{-1} [110][37]. Also the increased intensity of the band at lower frequency is consistent with bibliographical references [110]. An additional vibration at 1734 cm^{-1} could not be unambiguously assigned, but its location suggests a C=O stretch belonging to an ester (1720 cm^{-1} [69], 1733 cm^{-1} [122]) or acid moiety (-COOH surface 1734 cm^{-1} [112], -COOH surface free 1744 cm^{-1} and -COOH surface hydrogen bonded 1720 cm^{-1} [60]).

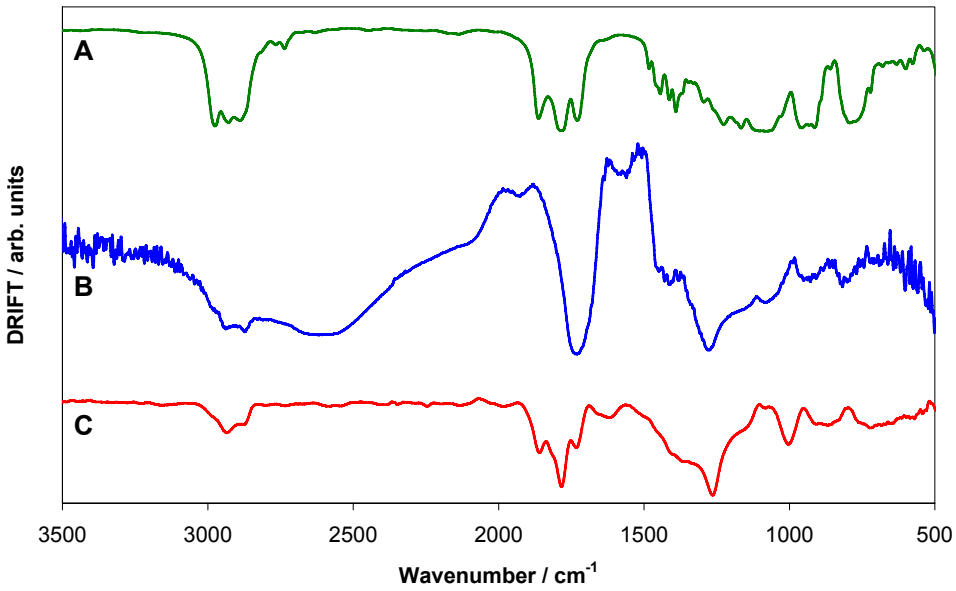

Figure 7.3: (A) Transmission spectrum of pure TESPSA recorded between two NaCl plates; (B) DRIFT spectrum of silica particles silanized with TESPSA from a 25 mM toluene solution; (C) DRIFT spectrum of silica particles silanised with a mixture of 1.6 mM TESPSA and 4.8 mM **a**cetic **a**cid **a**nhydride (AAA) from dry toluene.

After binding TESPSA from a 25 mM toluene solution to the silica particles by the standard silanisation procedure, as performed for silanes with ethoxy groups (e.g. APTMS (view Experimental section 12.3.1)) the IR spectrum presented an enhanced broad peak at 1740 cm^{-1} revealing the loss of the desired anhydride functionality (see spectrum B in Figure 7.3). The broad peak is most probably a superposition of the absorbances resulting from free carboxylic acid and ester moieties. The hump between 2300 cm^{-1} and 2800 cm^{-1} can be attributed to the O-H stretching vibration of carboxylic acids involved in hydrogen bonding [96]. While

PAMAM$-NH_2$ tethering to ester functionalized surfaces is still possible without activation reagents it is not in the case of acids. Furthermore, the negative charge generated by carboxylates influences the adherence of the dendrimer and makes it difficult to distinguish between electrostatic and covalent fixation to the surface. A method to maintain the original functionality of TESPSA was searched for. Adding acetic acid anhydride was believed to scavenge ethoxy- and hydroxyl- ions released during the silanisation process. And, adding acetic acid anhydride to the silanization solution led to a coating with a different terminal functionality as suggested by the recorded DRIFT spectrum (see spectrum C in Figure 7.3). A comparison of the TESPSA transmission IR with the DRIFT spectrum of TESPSA functionalized silica silanised with this specific mixture displays a high resemblance to that of unreacted TESPSA, indicating almost no structural changes after fixation to the substratum.

The silanisation procedure was transferred onto silicon wafers and characterized by static water contact angle measurements. The above findings were confirmed by static water contact angle measurements (summarized in Table 7.2), where higher values were recorded on surfaces coated with the additional acetic acid anhydride. Surfaces coatings without additional acetic acid anhydride exhibited lower water contact angles (32° (28°-34°)), correlating well with the water contact angle of 27.2 ± 5.1 determined by Lee et al [98].

	XPS values [atomic %]				θ_{static} median
Surface coating	N(1s)	O(1s)	C(1s)	Si(2p)	(25 % - 75 %
sensitivity factors	[0.499]	[0.733]	[0.314]	[0.368]	interquartile range)
Si / SiO_2	1	31	19	49	$< 10°$
TESPSA	0	39	53	8	32°(28° - 34°)
TESPSA/anhydride	0	35	42	22	62°(59° - 64°)

Table 7.2: XPS and wettability data of TESPSA and TESPSA/anhydride: Static water contact angle (θ_{static}) values are expressed as a median of four different areas on four different wafers with the corresponding 25 - 75 % interquartile range. XPS data are the average values that were gathered on two independently prepared surface coatings at, at least, two places. (XPS spectra were aquired by Helga Hildebrand, LKO, Erlangen)

Similar observations were made by Yan et al.. They converted carboxylic acid terminated SAMs into interchain carboxylic anhydrides by using trifluoroacetic acid and observed an increased hydrophobicity of the surface upon conversion [60]. Water contact angle values of about 72° were determined for the interchain anhydrides, whereas water contact angles of less than 15° were recorded for the carboxylic acid SAM [60]. This observation reflects

the lower polarity of the carboxylic anhydride moiety in comparison to the carboxylic acid / carboxylate anion functionalities [60]. The half-life time for hydrolysis of acetic anhydride in water was reported to be about 6 minutes [60]. Furthermore anhydride hydrolysis into the diacid is expected to be even slower on top of surfaces than in solution because the surface has a lower dielectric constant than water [60]. Therefore, water contact angle measurements determine the wettability of the anhydrides only [60]. After sonicating the anhydride terminated coatings in 1 mM NaOH solution water contact angle values smaller than 10° were achieved, either due to the formation of carboxylic acids by hydrolysis or delamination of the coating.

Using 25 mM TESPSA solutions for the preparation generates very thick siloxane layers. The increased layer thickness was confirmed by XPS data (listed in Table 7.2), where a diminished signal was obtained for the supporting substratum (Si-signal). The increased layer thickness was also observable with the naked eye, because iridescent circular figures formed on the silicon wafers after this kind of silanization. Even by dramatically reducing the silanization concentration down to 25/16 mM and adding acetic acid anhydride the layer thickness is still thicker as in conventional SAMs, where Si-signals of about 40% were generally obtained in comparison to the 22% recorded on TESPSA/acetic acid anhydride coatings prepared by 25/16 mM silane solutions. The increased thickness is most probably the result of the bifunctionality of the TESPSA molecule. Silanization with TESPSA does not seem to form neatly ordered anhydride terminated SAMs. Huang et al. presented a possible reaction scheme of TESPSA bonding to silicon dioxide surfaces [122]. They suggest that the anhydride group primarily reacts with the surface hydroxyl groups forming an ester bond and the carboxylic acid group. Water may be released by the condensation of the silanol groups with the remaining carboxylic acid. This water may hydrolyse the ethoxy groups from the silyl center. The hydroxyl group can either condensate with the silyl center of another TESPSA molecule or with the anhydride functionality of another molecule. In contrast to the observations made here, Huang et al. also preserved the anhydride moiety but without the addition of a scavenger molecule. Maybe the amount of water at the substratum is responsible for the different results, but with the addition of the scavenger one will always be on the save side to prevent anhydride functionality loss.

7.1.3 PAMAM-NH_2 Coupling

PAMAM-NH_2 was anchored to anhydride terminated SAMs via amide bond formation from an aprotic polar solution to prevent protonation of the amino groups and thus cooperative electrostatic interactions with the surface. The reaction is depicted in Figure 7.4.

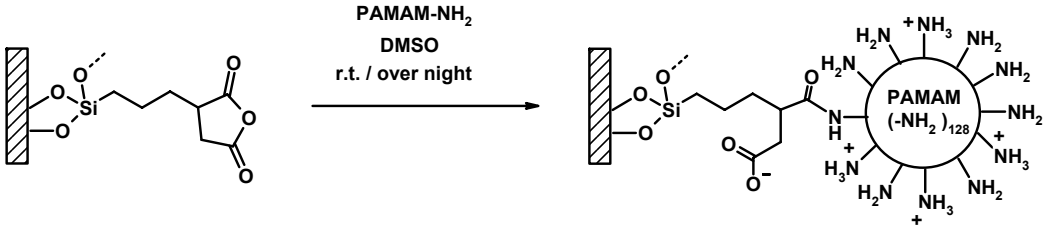

Figure 7.4: Schematic representation of TESPSA functionalized surfaces and the tethering of PAMAM-NH_2 thereto.

The PAMAM-NH_2 coating was carried out on silica spheres (1 μm in diameter) at first and was monitored by DRIFT spectroscopy. Thereto, the transmission spectrum of PAMAM was recorded in advance and is presented in Figure 7.5 (capital letter B). At 3276 cm^{-1} a large absorbance summarizes the N-H stretches of the amides and amino groups of the dendrimer involved in hydrogen bonds [124][125]. Peaks assigned to the amide I (C=O stretch) and amid II (N-H bend / C-N stretch) are positioned at 1643 cm^{-1} and 1553 cm^{-1}, respectively, and correlate well with data published in literature [121][60][126]. Stretching vibrations belonging to the methylene groups occur at 2940 cm^{-1} and 2836 cm^{-1}.

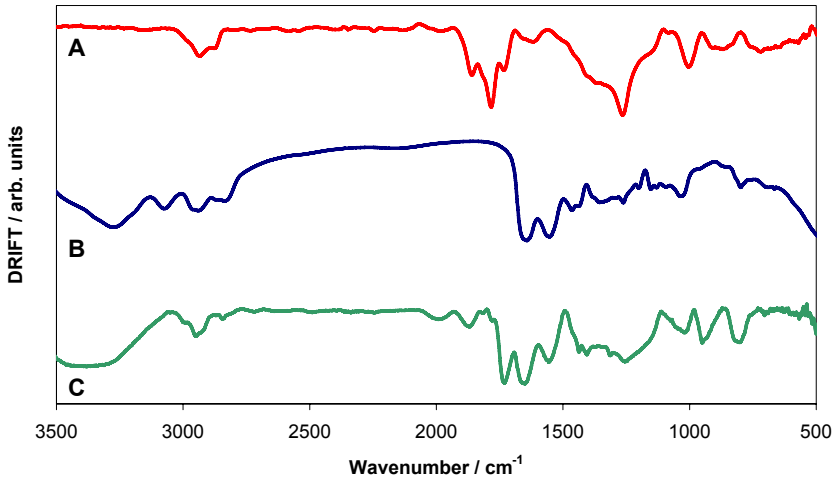

Figure 7.5: Transmission spectrum of pure PAMAM$-NH_2$ (B, blue), DRIFT spectra of surface-modified silica spheres: TESPSA coated spheres (A, red) and PAMAM immobilized to TESPSA activated silica spheres (C, green).

Furthermore, Figure 7.5 presents the DRIFT spectrum of TESPSA coated spheres (A) and the DRIFT spectrum of TESPSA coated spheres functionalized by PAMAM-NH_2 (C). The appearance of the amide I and amide II bands, characteristic of PAMAM$-NH_2$, substan-

tiates the immobilization of PAMAM to the TESPSA surface. The vibration occurring at 1737 cm^{-1} (C=O stretching vibration) may be ascribed to the mediating TESPSA coating [122].

The silanisation procedure was transferred onto silicon wafers and characterized by static water contact angle and XPS measurements (experimental values are summarized in Table 7.3). After the dendrimer immobilization the contact angle value dropped from 62°(59° - 64°) to 28° (23° - 29°). A drop in wettability was expected, resulting from the polar groups within and at the periphery of the dendrimer. The determined wettability correlates well with literature data, where hemispherical PAMAM-NH_2 (G4) on gold (bond via Au-S linkages; cystamine core hydrated by $NaBH_4$) was reported to provide a wettability of 37° [126]. Indium tin oxide surfaces incubated with a 20 mM Tris-HCl (pH = 7.4) solution of 28 μM PAMAM-NH_2 revealed a contact angle of 33° ± 2° [50]. Degenhart and co-workers immobilized PAMAM-NH_2 onto 11,11'-dithiobis(N-hydroxysuccinimidylundecanoate) SAMs on Au and determined an advancing contact angle of $\theta_{adv} = 30° \pm 3$ and a receding contact angle of $\theta_{rec} < 15°$ [46]. They attributed the large hysteresis to an increased disorder and mobility of the dendritic arms within the organic film.

	XPS values [atomic %]				θ_{static} median
Surface coating	N(1s)	O(1s)	C(1s)	Si(2p)	(25 % - 75 %
sensitivity factors	[0.499]	[0.733]	[0.314]	[0.368]	interquartile range)
Si / SiO_2	1	31	19	49	< 10°
TESPSA/anhydride	0	35	42	22	62°(59° - 64°)
PAMAM−NH_2	15	20	51	13	28° (23° - 29°)
Theoretical values PAMAM−NH_2	25	13	63	-	–

Table 7.3: XPS and wettability data of TESPSA/anhydride and PAMAM-NH_2: Static water contact angle values (θ) are expressed as a median value and its corresponding 25 - 75 % interquartile range determined at two different areas on four different wafers. XPS data (atomic concentrations) are the average values that were gathered from two independently prepared surface coatings at, at least, two places (XPS spectra were aquired by Helga Hildebrand, LKO, Erlangen). The theoretical values (theo.) are based on calculations assuming PAMAM to be free.

The immobilization step was also monitored by XPS analysis (data are summarised in Table 7.3). After the tethering of PAMAM-NH_2 to the TESPSA surface the Si-signal attenuated from 22% to 13%, ascertaining the covering of the surface by the dendrimer. The attenuation of the Si-signal is characteristic for a layer increase. But the layer is not thick

enough to exclude the substratum from probing depth, thus not being thicker than approximately 7 nm (see section 13.2 for details). Ellipsometric measurements of the PAMAM-NH_2 functionalized surface, conducted by M. Eichler, revealed a thickness of about 6.6 nm [83], corresponding well to the recorded XPS data. Physical adsorption of PAMAM-NH_2 on silica or gold created layers with a film thickness between 1.5 and 3.5 nm for G4, 3.1 nm for G6, and 4.4 nm for G8, all of which is indicative for a distinct deformation/flattening of the adsorbed dendrimer molecules [127][121]. Confining the free space for surface-adsorbed PAMAM-NH_2 molecules by co-adsorption of long-chain surface active compounds resulted in an increase of the dendrimer layer thickness varying between 5.3 - 6.4 and 9.5 nm for G4 and G8 [121], respectively, indicating that the molecules reorient to a prolate configuration. Thus, it is assumed that the newly developed anhydride-containing linker system reduces the flattening of the dendrimers and causes the formation of a compact dendrimer surface layer. This may be because of the high reactivity of the anhydride moieties and the chosen dendrimer concentration.

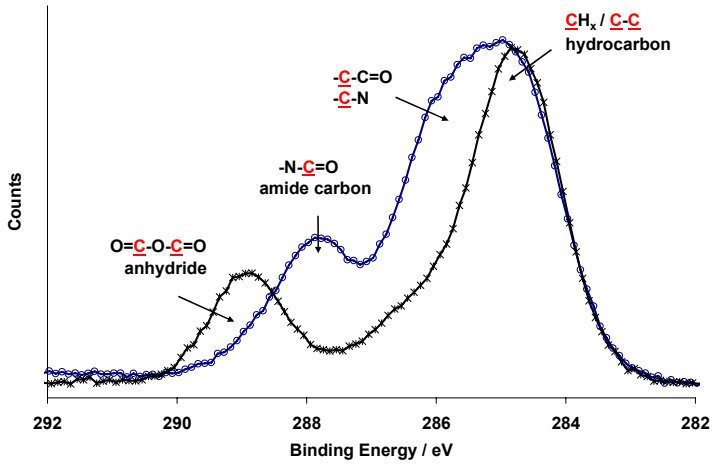

Figure 7.6: XPS high resolution carbon profile C(1s) of TESPSA (crosses) and TESPSA-PAMAM$-NH_2$ (circles) modified silicon surfaces.

The high resolution carbon profile recorded from the TESPSA and TESPSA-dendrimer coatings substantiate the successful immobilization. Two distinct peaks at 284.8 eV (C-C/C-H) and 289.0 eV (C=O) and a little hump at 286.6 eV (-C-O 286.6 eV [37]) can be observed in the high resolution carbon profile of the TESPSA coating belonging to the specific structural elements of TESPSA as depicted in Figure 7.6. After the reaction with the dendrimer the peak at 289.0 eV ((O=C-O-C=O) [37][60]) disappears and the amide bond at 287.8 eV (-N-

C=O [50]) and a very broad peak ranging from 286.2 eV - 284.2 eV (C-C/C-H [37]; carbon singly bonded to an amide carbon/amine nitrogen **C**-C-NHR(=O)/**C**-N at 285.7 eV [37][46]), mirroring the complex nature of the dendrimer upon the surface, emerge. Theoretically, if the XPS signals were solely from PAMAM$-NH_2$ one would expect 25% for N, 13% for O and 63% for C (as calculated from the dendrimer composition listed in Table 7.1). Since the subjacent TESPSA coating contributes to the values, no comment can be made on the atomic concentration of oxygen and carbon, but the lower atomic concentration of nitrogen may be attributed to the hiding of the amino groups within the dendrimer to reduce the surface free energy, when examined in air. An uneven distribution of the terminal amino groups of polyamidoamine orientating towards the substratum surface was also observed upon indium tin oxide [50].

The successful immobilization of the dendrimer upon the surface was also confirmed by streaming current measurements presented in Figure 7.7, clearly visualizing the charge reversal upon the surface after the immobilization of PAMAM-NH_2. An IEP of 9.4 is obtained and is in the range of the pK_a value of the primary amines for PAMAM-NH_2 found in literature [39]. Explicit explanations regarding the generation of charge will be given in chapter 8.

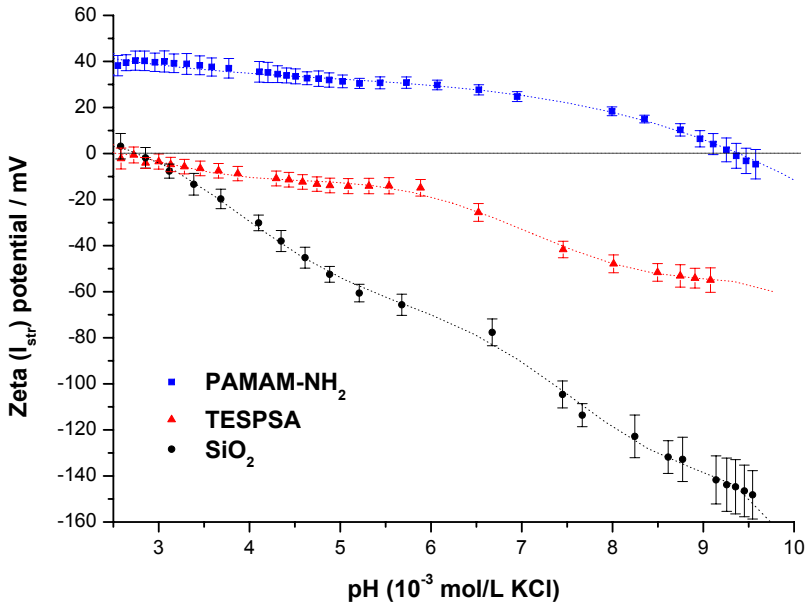

Figure 7.7: Dependence of the zeta potential on pH determined by streaming current measurements in 1 mM KCl. Experimental data are represented by symbols. Dashed lines are polynomial fittings of the third order. Interfacial system: SiO_2/TESPSA/PAMAM-NH_2/electrolyte solution

During the development of the TESPSA coating, covalent attachment of PAMAM-NH_2 to carboxylic acid terminated SAMs was also examined in case the preparation of the TESPSA coating failed. Despite the negative aspect of using activation reagents, i.e. using carbodiimide chemistry for the activation of carboxylic acids and the subsequent coupling to primary amines [128]. Fortunately, the preparation of anhydride terminated surfaces was successful and the circuitous route via SAM-COOH could be discarded. But some results will also be presented concerning the tethering to SAM-COOH coatings because they revealed some interesting aspects.

A comparison of both preparation methods by the chemiluminescence based amino group detecting assay revealed a far denser surface coating with PAMAM-NH_2 on the TESPSA coated surface in comparison to surfaces on the basis of SAM-COOH, presented in Figure 7.8. SAM-PEG coated surfaces were used as a reference bearing no amino groups.

(a) (b) (c)

Figure 7.8: Amino group detection assay (light exposure 30 s) comparing the amino group density upon the surface a) reference SAM-PEG b) PAMAM-NH_2 covalently bound to anhydride terminated coatings c) PAMAM-NH_2 covalently bound to carboxylic acid terminated coatings via EDC/NHS

Since both surfaces were coated with a dendrimer solution of the same concentration from anhydrous DMSO, the difference must arise from the different binding sites available at the surface or / and the yield of conversion of these sites due to the different reaction mechanisms. Streaming current measurements at the SAM-COOH and SAM-TESPSA surfaces revealed a slightly higher number of carboxylic acid functionalities at the SAM-TESPSA coating as visible in Figure 8.1. Furthermore, the active O-acylisourea intermediate formed by the reaction of the carboxylic acid groups upon the surface with EDC is quite space filling this intermediate may reduce the availability of some carboxylic acid groups for covalent attachment. This is presumably the reason for the lower concentration of PAMAM-NH_2 upon the surfaces of SAM-COOH.

AFM images were recorded from both immobilization paths, via SAM-COOH and TESPSA. The SAM-COOH coating with subsequent immobilization of PAMAM-NH_2 is presented below. The linear alkyl chain based SAM-COOH coating showed a significantly lower av-

Surface modification	SAM-COOH	PAMAM$-NH_2$ via COOH
RMS roughness [nm]	0.15 (± 0.03)	0.47 (± 0.08)
Average roughness [nm]	0.08 (± 0.02)	0.30 (± 0.08)
Average height [nm]	0.55 (± 0.20)	1.88 (± 0.60)
Heighest point [nm]	3.41	12.70

Table 7.4: Surface topography of a 1 μm x 1 μm sample area investigated by AFM. The alkyl chain based SAM-COOH coating shows lower root mean square and average roughness values in comparison to the dendrimer based coating.

erage roughness than the dendrimer modified surface (Table 7.4). A topographical image recorded by M. Haupt (Fraunhofer Institute for Interfacial Engineering and Biotechnology IGB, Stuttgart, Germany) on behalf of M. Eichler of a TESPSA surface covered by PAMAM-NH_2 revealed an average roughness of 1.55 nm (published in [83]). The increased roughness

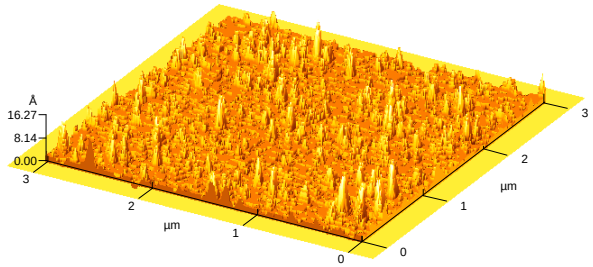

Figure 7.9: SAM-COOH

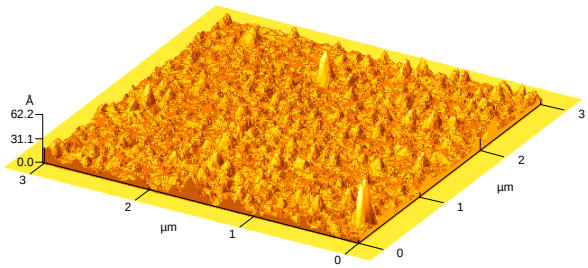

Figure 7.10: PAMAM$-NH_2$(EDC/NHS)

of the TESPSA-PAMAM-NH_2 system correlates with the results of the chemiluminescence based assay. Dendrimer flattening seems to be stronger and more even on SAM-COOH surfaces than on TESPSA surfaces upon drying. This may result from the lower dendrimer concentration upon SAM-COOH surfaces providing enough room for spreading. Dendrimer monolayers prepared by electrostatic deposition resulted in surfaces with a roughness of 0.3 - 0.6 nm [51], in line with the made observations.

The following sections will focus on the preparation of dendrimer based coatings terminated by cationic (pyridinium), anionic (sulfonic and carboxylic acid), as well as neutral (acetamide) functionalities.

7.2 PAMAM with Cationic Periphery: PAMAM-$N^+C_5H_5$ ($\widehat{=}$ PAMAM-Py) via PAMAM-Br

In order to prepare dendrimer based coatings terminated by a pyridinium functionality, PAMAM-NH_2 coatings were at first converted into PAMAM-Br using the acid chloride, 4-bromobutyrylchloride (BBC). A scheme of the chemistry to synthesize this coating is shown in Figure 7.11. In the course of the reaction between terminal amino groups and 4-BBC hydrogen chloride is liberated. Originally, immobilized PAMAM was considered to contain sufficient tertiary amines itself for the scavenging of hydrogen chloride. The amino group, chemiluminescence based, detection assay was utilized to determine the amino group conversion rate.

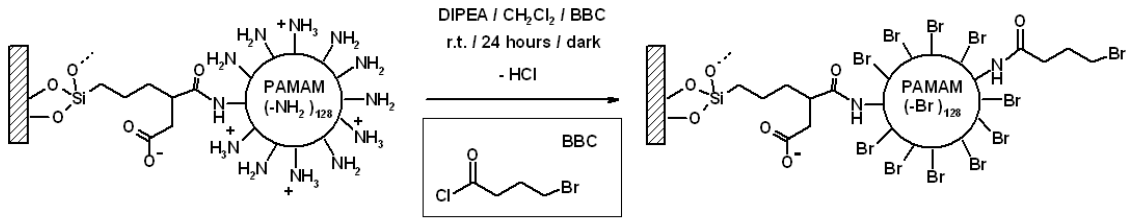

Figure 7.11: Scheme of the chemistry to synthesize PAMAM-Br. 4-Bromobutyrylchlorid (BBC) in dichloromethane (DCM) in presence of N,N-diisopropylamine (DIPEA) was used to obtain a bromo-functionalized dendrimer surface. All bromides are connected to the dendrimer via an amide anchored alkyl chain, but for a clearer representation only one is explicitly shown.

Both attempts using either dichloromethane or dimethylformamide without additional base were unsatisfactory. Only, after adding N,N-diisopropylethylamine (DIPEA) slightly better results were obtained. DIPEA is a sterically hindered base preventing the protonation of terminal amino groups by scavenging the developing hydrogen chloride during the reaction. Otherwise, protonated amino groups are lost for the conversion reaction with BBC. During the reaction the light impact was kept as low as possible to prevent the terminal bromine from separation by UV radiation [129].

Even though DIPEA and BBC were used in great excess, in respect to the reactive sites upon the surface, an adding of both substances at once led to an incomplete conversion of the amines. Therefore, experiments in which the reagent sequence was varied were conducted. The impact of the reagent addition order on the conversion rate was evaluated. The addition of BBC, DCM and DIPEA was varied. The highest reaction yield was achieved by adding the reagents in the following order: base, solvent, acid chloride (view Figure 7.12).

Mixtures containing 10 mmol/L, 100 mmol/L and 500 mmol/L BBC with the analogue

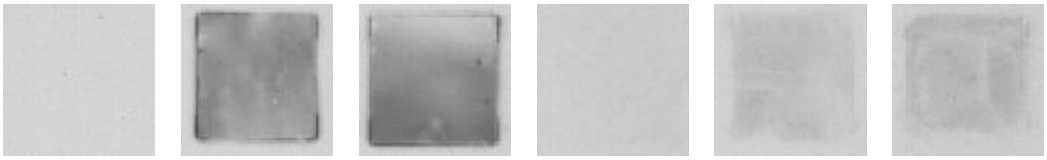

(a) (b) (c) (d) (e) (f)

Figure 7.12: Chemiluminescence tests detecting the yield in converting terminal amines into bromide a) Reference SAM-PEG b) PAMAM-NH_2 unmodified c) DCM, BSC and DIPEA were mixed in advance and the PAMAM-NH_2 wafer was placed into the ready solution d) DIPEA then DCM then BSC e) DCM then BSC then DIPEA f) BSC then DCM then DIPEA; 500 mmol BSC und 500 mmol DIPEA; solution volume 1 ml; light exposure time = 10s

amount of DIPEA were also tested to evaluate the concentration impact on the degree of amino group conversion. Most promising results were obtained by using the reagents at the highest concentration. Generally, concentrations of 100 mmol/L per reagent were sufficient for amino group conversion but concentrations of 500 mmol/L were necessary in this particular case. Traces of water in the solvent may have reduced the amount of active BBC. The chemiluminescence based assay clearly indicated the complete transformation of amino groups by BBC. A subsequent derivatisation of the PAMAM-Br coating by pyridine to achieve PAMAM-Py (Figure 7.13) could not be traced by the CL assay and had to be inspected by XPS analysis and contact angle determination (data are summarized in Table 7.5).

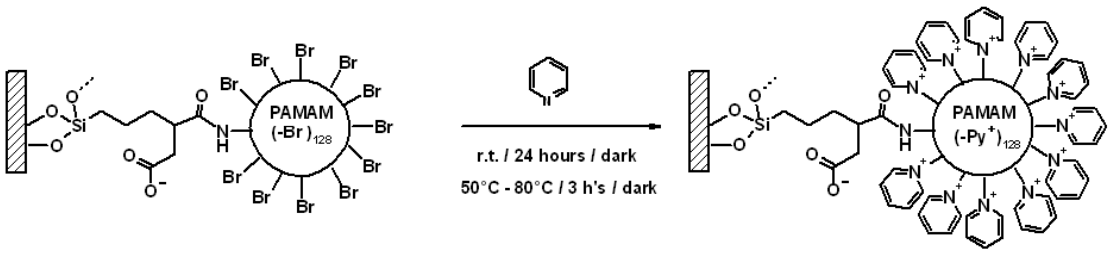

Figure 7.13: Schematic representation of the synthesis reaction to generate PAMAM−Py coated surfaces. Pyridine was used to obtain a pyridinium-functionalized dendrimer surface.

A significant attenuation of the Si-signal after the conversion of PAMAM-NH_2 into PAMAM-Br indicates that the coating thickness has increased. The rise in coating thickness goes hand in hand with an increase in the C-signal. Furthermore, the photo-electron peak for the bromine was detected to be nearly as high as expected from theoretical calculations. These observations suggest a successful covalent attachment of the acid chloride in line with the performed chemiluminescence assay. The tertiary amines within the dendrimer interior seem to be protonated by the liberated hydrogen chloride and gather chloride ions for charge com-

pensation. On PAMAM-Br coated surfaces a contact angle of 58° (57 - 59°) was recorded. The increase in contact angle value in comparison to the PAMAM−NH_2 coating was expected because of the uncharged, hydrophobic character of the newly introduced terminal moieties. After substituting the terminal bromine by pyridinium no change in contact angle value could be recorded. The bromine atom disappeared from the surface after the reaction with pyridine suggesting a complete transformation. Theoretically the carbon content should have increased from 64% to 68% upon conversion. This is no strong difference for XPS analysis and can not be consulted to varify the introduction of the new functionality. Also a closer look at the high resolution of the N peak could not help to determine the success of the reaction, because there are numerous nitrogen species of charged character within the dendrimer.

	XPS values [atomic %]						θ_{static} median
Surface coating	N(1s)	O(1s)	C(1s)	Si(2p)	Cl(2p)	Br(3d)	(25 % - 75 %
sensitivity factors	[0.499]	[0.733]	[0.314]	[0.368]	[0.954]	[1.149]	interquartile range)
PAMAM−NH_2	10	24	55	11	-	-	28° (23° - 29°)
PAMAM−Br	9	14	68	2	3	4	58° (57° - 59°)
PAMAM−Py	10	18	68	2	2	-	57° (55° - 58°)
Theo. values PAMAM−Br	18	14	64	-	-	5	–
Theo. values PAMAM−Py	18	11	68	-	-	4	–

Table 7.5: XPS and wettability data of PAMAM-Br and PAMAM-Py: Static water contact angle values (θ) are expressed as a median value and its corresponding 25 - 75 % interquartile range determined at two different areas on four different wafers. XPS data (atomic concentrations) are the average values that were gathered from two independently prepared surface coatings at, at least, two places (XPS spectra were aquired by Helga Hildebrand, LKO, Erlangen). The theoretical values (theo.) are based on calculations assuming PAMAM to be free and all terminal groups to be converted.

Neither XPS, nor wettability data could assist in determining whether pyridinium introduction was successful or not. Only, electrokinetic investigations at the PAMAM-Py coated surfaces, presented in chapter 8, provide evidence on the successful conversion.

Optimization proposal: Preparing PAMAM-Br using a bifunctional reagent like ω-bromoalkylisocyanate, OCN-R-Br to achieve -NH-CO-NH-R-Br would be an alternative to BBC without the liberation of hydrogen chloride. The protonation of the tertiary amines and their salt formation with chloride may cause the dendrimer to shrink and reduce its flexibility for further reactions.

Remark: S. A. Al-Baitaineh et al. published an article where brominated furanone coated surfaces were thoroughly analysed by XPS analysis and tested regarding their antimicrobial effect [129]. Halogenated furanones are often applied by marine organisms as a chemical weapon defending microbial colonization. These molecules seem to interfere in the signal chain (quorum sensing) of the biofilm formation of some bacteria. The exact mechanism of action is still unknown. It might be worthwhile to examine the PAMAM-Br coating in terms of its antimicrobial character.

7.3 PAMAM with Anionic Periphery

7.3.1 PAMAM-COOH

Terminal carboxylic acid functionalities were generated by the reaction of the primary amino groups of the PAMAM-NH_2 coating with succinic acid anhydride, elongating each dendrimer branch by two methylene groups (illustrated in Figure 7.14). These reaction conditions were used by X. Shi et al. in order to modify polyamidoamine in solution for characterization purposes [119].

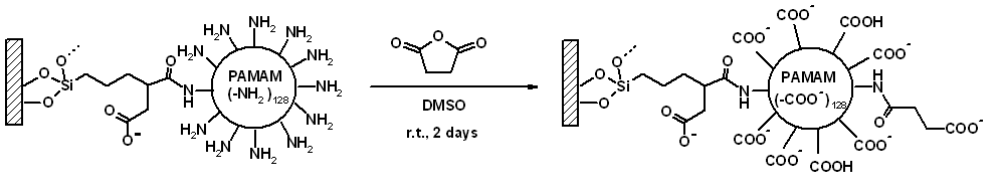

Figure 7.14: Scheme of the chemistry to synthesize PAMAM−COO^-. Succinic acid anhydride in dimethylsulfoxide (DMSO) was used to obtain a carboxylate-functionalized dendrimer surface. All carboxylic acid / carboxylate functionalities are connected to the dendrimer via an amide anchored alkyl chain, but for a clearer representation only one is explicitly shown.

The PAMAM-COOH coating was prepared on silica spheres and the derivatisation step, turning PAMAM-NH_2 into PAMAM-COOH, was monitored by DRIFT spectroscopy. Bare silica spheres were used as a reference. Both spectra belonging to the dendrimer coatings, PAMAM-NH_2 and PAMAM-COOH, are presented in Figure 7.15. The amide I and amide II bands at 1665 and 1565 cm^{-1}, respectively, are characteristic for PAMAM-NH_2, as well as the N-H stretching vibration between 3100 and 3500 cm^{-1}. After converting the terminal amino groups into carboxylic acid functionalities, the broad band between 3100 and 3500 cm^{-1} is attenuated. An intensity increase of the vibration at 1742 cm^{-1} in comparison with the amide bands suggests the presence of a larger amount of carboxylic acid groups upon the surface. Carboxylate functionalities are also present on the PAMAM-NH_2 coating belonging to the mediating TESPSA layer.

The successful preparation method applied on silica spheres was transferred onto silicon wafers. XPS and wettability measurements were performed on the wafer surfaces coated by PAMAM-COOH. The results are summarized in Table 7.6. An increase in the contact angle value from 28° (23° - 29°) on the PAMAM-NH_2 coated surface to 52° (45° - 54°) on PAMAM-COOH functionalized surfaces was recorded. Hardly any information can be found in literature on immobilised carboxylate terminated polyamidoamine regarding its wettability. The contact angle values obtained from the prepared surface coatings are contradictory

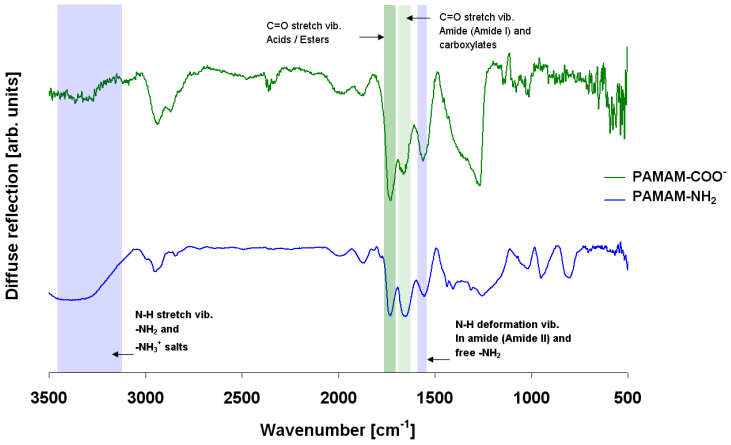

Figure 7.15: DRIFT spectra of surface-modified silica spheres: PAMAM-NH_2 (blue) and PAMAM-COOH (green). Reference: bare silica spheres.

to the one set of data found in literature. There hemispherical PAMAM-NH_2 (G4) on gold (bond via Au-S linkages - cystamine core hydrated by $NaBH_4$) was reported to provide a less wettable (36.8°) surface than hemispherical PAMAM-NH_2terminated by carboxylic acid moieties PAMAM-COOH (G4) (5.8°) [126]. No information is provided in this article on how this surface coating is obtained, therefore, a different preparation path maybe responsible for the different result. A charge neutralization of the internally protonated nitrogen atoms by the externally arranged carboxylate functionalities may lead to exposed methylene groups, this configuration is also indicted by SFG measurements (results presented in 9), and may be responsible for the increase in contact angle value.

	XPS values [atomic %]				θ_{static} median
Surface coating	N(1s)	O(1s)	C(1s)	Si(2p)	(25 % - 75 %
sensitivity factors	[0.499]	[0.733]	[0.314]	[0.368]	interquartile range)
Exp. value PAMAM−NH_2	10	24	55	11	28° (23° - 29°)
Exp. value PAMAM−COOH	16	23	60	1	52° (45° - 54°)
Theoretical values PAMAM−COOH	17	22	61	-	–

Table 7.6: XPS and wettability data of PAMAM-NH_2 and PAMAM-COOH: Static water contact angle values (θ) are expressed as a median value and its corresponding 25 - 75 % interquartile range determined at two different areas on four different wafers. XPS data are the average values that were gathered from two independently prepared surface coatings at, at least, two places (XPS spectra were aquired by Helga Hildebrand, LKO, Erlangen). The theoretical values (theo.) are based on calculations assuming PAMAM to be free and all terminal groups to be converted.

Changes in the elemental composition determined by XPS analysis after the post-modification were rather tiny but correlate well to the atomic concentration that was expected from theoretical point of view. The amino group detection assay verified the successful transformation of all easily accessible primary amino groups upon the surface. The area on the X-ray film in contact with the PAMAM-COOH coated surfaces remained light and not shaded as in the case of the PAMAM-NH_2 coated surface. Results are presented in Figure 7.16. Experiments evaluating the necessity of an additional base (DIPEA, NEM) for deprotonation purposes suggest the addition to be needless (Results are not included).

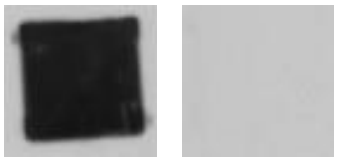

(a) (b)

Figure 7.16: Amino-group detecting chemiluminescence based assay
a) PAMAM−NH_2 b) PAMAM−COOH;
light exposure time = 30s; duplicates are not shown

The amino group detecting assay, as well as XPS analysis data, provide clear evidence of a successful surface modification. Data presenting the formation of charge at this surface in aqueous solution are presented in section 8.2.3. The next subsection will describe the preparation and characterization of a further PAMAM based coating terminated by an anionic functionality.

7.3.2 PAMAM-SO_3H

In order to prepare PAMAM−SO_3^- coated surfaces the terminal sulfonate functionalities were introduced by the reaction of the primary amino groups of the PAMAM-NH_2 coating with 1,3-propane sultone, elongating each dendrimer branch by three methylene groups. A scheme of the chemistry is shown in Figure 7.17.

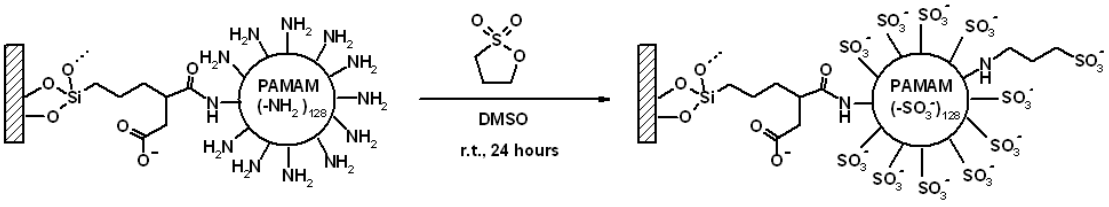

Figure 7.17: Scheme of the chemistry to synthesize PAMAM−SO_3^-. 1,3-Propane sultone in dimethylsulfoxide (DMSO) was used to obtain a sulfonate-functionalized dendrimer periphery. All sulfonic acid functionalities are connected to the dendrimer via an amine anchored alkyl chain, but for a clearer representation only one is explicitly shown.

The amino-group detecting chemiluminescence based assay was employed to confirm the successful conversion of the peripheral amino groups of the PAMAM-NH_2 coating. PAMAM-NH_2 functionalized wafers caused a dark shaded area on the X-ray film, whereas no darkening was observed in the areas of the X-ray film that were exposed to the PAMAM−SO_3^- coated surfaces (view Figure 7.18)

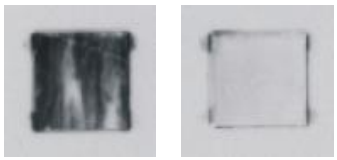

(a) (b)

Figure 7.18: Amino-group detecting chemiluminescence based assay
a) PAMAM−NH_2 b) PAMAM−SO_3^-;
light exposure time = 30 s; duplicates are not shown

A static water contact angle value of 33° (31° - 37°) was determined upon the PAMAM-SO_3^- coated surfaces. Because of the generation of a coating with zwitterionic character a good wettability of the surface was expected even though further alkyl groups were implemented.

The increase in layer thickness after alkylation was indicated by the reduced Si-signal in XPS analysis. In addition the atomic concentration of carbon rose and the introduced sulphur was detectable. The atomic concentration of oxygen upon the surface did not increase, but

this may be explained by the fact that the value is compensated by the oxygen that was originally a contribution of the substrate SiO_2. The position of the sulphur peak correlates well with the 167.3 eV peak detected for the sulphur within the SAM−SO_3^- functionalized coating. A comparison of the theoretical values mirroring the atomic concentration of an unbound, fully transformed dendrimer correspond quite well with the atomic concentration detected by XPS analysis. PAMAM−SO_3^- shows a pronounced peak at 401.5 eV, stronger as in all other modifications corresponding to positively charged nitrogen atoms. Assuming that after the reaction of the sultone with N-atoms at the periphery an inner salt has been formed PAMAM−N^+H_2−$(CH_2)_3$−SO_3^-.

	XPS values [atomic %]					θ_{static} median
Surface coating	N(1s)	O(1s)	C(1s)	Si(2p)	S(2p)	(25 % - 75 %
sensitivity factors	[0.499]	[0.733]	[0.314]	[0.368]	[0.717]	interquartile range)
Exp. value PAMAM−NH_2	10	24	55	11	0	28° (23° - 29°)
Exp. value PAMAM−SO_3^-	12	23	59	2	4	33° (31° - 37°)
Theoretical values PAMAM−SO_3^-	17	22	57	-	4	–

Table 7.7: XPS and wettability data of PAMAM−NH_2 and PAMAM−SO_3H: Static water contact angle values (θ) are expressed as a median value and its corresponding 25 - 75 % interquartile range determined at two different areas on four different wafers. XPS data (atomic concentrations) are the average values that were gathered from two independently prepared surface coatings at, at least, two places (XPS spectra were aquired by Helga Hildebrand, LKO, Erlangen). The theoretical values (theo.) are based on calculations assuming PAMAM to be free and all terminal groups to be converted.

The amino group detecting assay, as well as contact angle and XPS analysis, provide clear evidence of a successful modification of the surface. An additional alkylation of the tertiary N-atoms forming quaternary ammonium functionalities may not be ruled out, but is expected to be low due to the sterical hindrance of these sites. Data showing the formation of charge at this surface in aqueous solution are presented in section 8.2.3.
The next subsection will describe the preparation and characterization of a PAMAM coating with a non-ionizable periphery, i.e. terminated by acetamide functionalities.

7.4 PAMAM with Non-Ionizable Periphery: PAMAM-CH_3

PAMAM coatings terminated by acetamide groups were prepared because they do not possess charges at the peripheryPeripheral acetamide groups were generated by the reaction

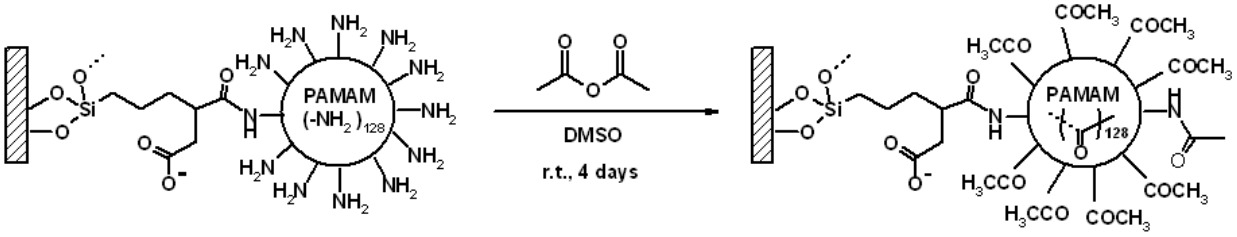

Figure 7.19: Scheme of the chemistry to synthesize PAMAM−CH_3. Acetic acid anhydride in dry DMSO was used to obtain an acetamide-functionalized dendrimer periphery. All methyl functionalities are connected to the dendrimer via an amide bond, but for a clearer representation only one is explicitly shown.

of the primary amino groups of the PAMAM-NH_2 coating with acetic acid anhydride and without additional base as illustrated in Figure 7.19. The chemiluminescence based assay for amino-group detection confirmed the successful conversion of, at least, all easily accessible amino groups. PAMAM-NH_2 functionalized wafers caused a dark shaded surface area on the X-ray film, whereas no darkening was observed in the areas of the X-ray film that were exposed to the PAMAM−CH_3 coated surfaces (view Figure 7.20).

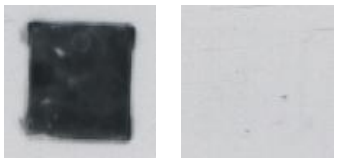

(a) (b)

Figure 7.20: Chemiluminescence based assay for amino-group detection
a) PAMAM−NH_2 b) PAMAM−CH_3;
light exposure time = 30 s; duplicates are not shown

An increase in the contact angle to a median value of 50° (48° - 54°) was observed after the conversion of the terminal amino groups into acetamide functionalities. This rise in wettability was expected due to the lower polarity of the acetamide functionality in comparison to the amino groups. Changes in the elemental composition, determined by XPS analysis, after the modification of the PAMAM-NH_2 coating correspond well to the atomic concentrations expected on behalf of the theoretical calculation. The lower atomic concentration for nitrogen is expected because it may be assumed that protonated tertiary amines within the dendrimer orientate towards the substratum surface. The increase in layer thickness is

	XPS values [atomic %]				θ_{static} median
Surface coating	N(1s)	O(1s)	C(1s)	Si(2p)	(25 % - 75 %
sensitivity factors	[0.499]	[0.733]	[0.314]	[0.368]	interquartile range)
Exp. value PAMAM−NH_2	10	24	55	11	28° (23° - 29°)
Exp. value PAMAM−CH_3	15	19	63	1	50° (48° - 54°)
Theoretical values PAMAM−CH_3	21	16	63	-	–

Table 7.8: XPS and wettability data of PAMAM−NH_2 and PAMAM−CH_3: Static water contact angle values (θ) are expressed as a median value and its corresponding 25 - 75 % interquartile range determined at two different areas on four different wafers. XPS data are the average values that were gathered from two independently prepared surface coatings at, at least, two places (XPS spectra were aquired by Helga Hildebrand, LKO, Erlangen). The theoretical values (theo.) are based on calculations assuming PAMAM to be free and all terminal groups to be converted.

reflected by the decreasing Si-signal of the wafer surface. These data are summarized in Table 7.8.

The amino group detecting assay, as well as contact angle and XPS analysis, provide clear evidence for a successful modification of the surface. Data showing the formation of charge at this surface in aqueous solution are presented in section 8.2.1.

These surface coatings, terminated by a non-ionizable periphery, close the surface modifications based upon dendrimers. The following chapter presents the surface charge formation in 1 mM KCl solution at all the created surface coatings.

8 Surface Charge Characteristics: Electrokinetic Potentials

Charge patterns on surfaces are known to influence molecular and cellular adhesiveness to biomaterial surfaces [130][76][131] and induce biological processes like coagulation. A comprehensive study of surface charge characteristics is indispensable in determining the impact of surface coatings on physiological fluids. Therefore, the surface charge formation on the dendrimer based coatings was studied as a function of pH in 1 mM KCl solution by streaming current measurements and compared to the charge development at linear alkyl chain based coatings.

The transformation of pressure-dependent streaming current data into electrokinetic zeta-potentials was achieved according to Smoluchowski relation (for details view the Experimental Part of this thesis 13.1.1). Streaming current measurements exclude the contribution from surface conduction [130] in contrast to streaming potential measurements. Even though the measurements were performed at solution pH values and an ionic strength beyond the physiological range they are necessary to gain insight on the structure-charge relationship at the biomaterial/aqueous solution interface/interphase. Within this chapter streaming current data obtained from SAM coatings will be addressed first, thereafter the electrokinetic charge development at PAMAM-based coatings will be presented. The chapter closes with the determination of charge at a bacterial surface by electrophoresis.

All streaming current measurements were performed with an apparatus kindly provided by the company Anton Paar, Austria. The modified silicon wafers were analysed in a hydrated state, similar to the conditions they are expected to be employed in. The investigation of hydrophobic surfaces was also possible, in contrast to electrokinetic measurements based on electrophoresis. Electrophoresis was additionally used to explore the solid/liquid interface on silica, as the apparatus was readily available. Originally, silica particles (500 m^2/g) were used to monitor the generation of charge upon modification. This worked well for linear alkyl chain based coatings, but was inappropriate for dendrimer based coatings as the area was far too large to be functionalized with the precious dendrimers. Therefore, they were substituted by 1 μm silica spheres with a lower specific surface area. It is often

discussed in literature whether streaming current data are comparable to data acquired from electrophoresis. It was out of scope of this thesis to evaluate this, but measurements performed on bare silica spheres, particles and wafers as presented in Figure 5.2 and on dendrimer functionalized wafers and spheres (results not shown), suggest great correlation, if the substrata are exposed to identical conditions and handled with diligence.

8.1 Zeta-Potentials of SAM Coated Surfaces

Because surfaces covered by SAMs are smooth and impermeable to solvent molecules the potential at the shear plane (ζ-potential) is in good approximation to the potential at the outer Helmholtz plane (OHP) in the GCSG-model of the double layer [132]. A conversion of the streaming current data into ζ-potential values using the Smoluchowski equation is valid at these conditions.

8.1.1 SAMs Terminated by Anionic Groups

Figure 8.1 illustrates the dependence of the ζ-potential on pH for the carboxylic acid terminated coatings, TESPSA and SAM-COOH, the sulfonate terminated coating, SAM$-SO_3H$, and the pure, uncoated SiO_2 surface. As expected, both coatings terminated by carboxylic acid functionalities show a similar pH dependence. They do not possess a true isoelectric point (IEP), but approach the zero zeta-potential round about a pH of 3. This was also determined by J.-J. Shyue et al. [86]. Within the pH range 3 to 6, both coatings behave alike. Upon further pH increase the TESPSA coated surface generates stronger zeta-potential values than the SAM-COOH coating.

Both, TESPSA and SAM-COOH, are protonated at low pH, revealing nearly no net charge. A significant increase in ζ-potential can be observed at pH values higher than 6, levelling off at a plateau at -60 mV for TESPSA and -40 mV for the SAM-COOH coating, corresponding to the deprotonation of the carboxylic acid groups upon the surface. Protonation/deprotonation processes at surface confined molecules are known to be affected by the polarity of the surface, interfacial electrostatic fields, and the local structure of the solvent [56][112]. They may differ significantly from the dissociation constants of the same molecules in solution [112]. Furthermore, especially the deprotonation of immobilized carboxylic acids is said to be influenced by intramolecular complexation to other carboxylic acid moieties, if the alkyl chains are within a well ordered SAM, because it strengthens the remaining hydrogen bond [112]. Additionally charge, generated by ionization, influences the approach of a further OH^- ion, which is necessary to dissociate the remaining carboxylic acid group [112]. Carboxylated SAMs were reported to be deprotonated to 0%, 10%, 30%, 85% and

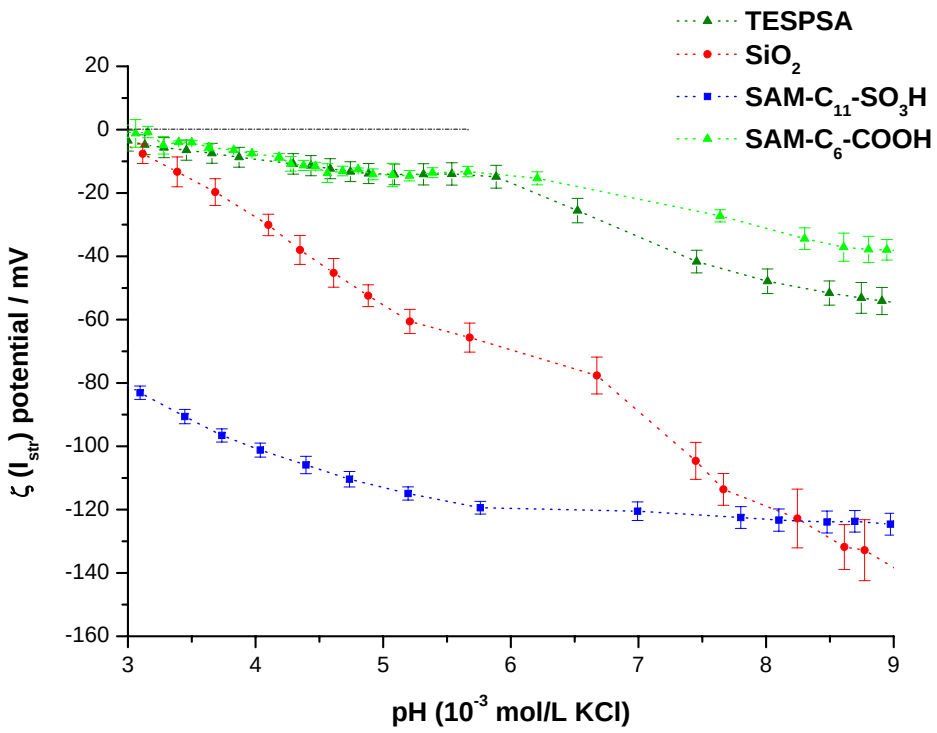

Figure 8.1: Electrokinetic ζ-potentials from streaming current measurements as a function of pH. Solution is 1 mM KCl, pH is adjusted with potassium hydroxide and hydrochloric acid. Surface coatings investigated: the carboxylic acid terminated coatings, TESPSA and SAM-COOH, the sulfonate terminated coating, SAM$-SO_3H$, and the pure, uncoated SiO_2 surface. Experimental data are represented by symbols. Dashed lines are polynomial fittings of the third order. Error bars in the graph show the deviation between two measurements performed on the same sample.

100% at pH values of 3, 5, 7, 9, and 11, respectively [86]. This correlates with the obtained data. The higher negative ζ-potential value for TESPSA in comparison to SAM-COOH at high pH, seems to reflect the rather imperfect structural organisation of TESPSA upon the surface, as mentioned in section 7.1.2, facilitating deprotonation.

An IEP of 2.6 was detected at the hydroxylated surface (SiO_2) (see Figure 8.1), corresponding very well with data recorded in literature [86]. The zeta-potential drops upon pH increase to about -70 mV, where some sort of plateau is reached, this may be due to the deprotonation of silanol moieties upon the surface. A further negative zeta-potential increase occurs beyond the pH of 7. This has been ascribed to preferential hydroxide ion adsorption in literature [78]. Whereas, preferential hydroxide ion adsorption is reasonable to be expected for the generation of charge at non-ionizable surface coatings [88], it seems rather questionable at a strong negatively charged surface. It may rather be presumed that deprotonation on the SiO_2 surface occurs in more then one step, in order to accommodate large concentrations of charge in a better way.

The coating terminated by sulfonate functionalities presents a very strong negative electrokinetic ζ-potential at pH 3 (-80 mV). With increasing pH the negative ζ-potential rises further to a plateau value of -120 mV. Experiments by Shyue et al. revealed a pK_a of 2 for surface confined sulfonic acid, much higher than the one for molecules in solution, which is about -7 [86]. At a pH value of 5.5 full deprotonation is expected which corresponds perfectly to the recorded zeta-potential [86]. Sulfonic acids are stronger than carboxylic acids because their conjugate base is of better resonance stabilization [133].

8.1.2 SAMs Terminated by Cationic Groups

Figure 8.2 illustrates the dependence of the ζ-potentials on pH for the amino group terminated coatings, $SAM{-}C_{11}{-}NH_2$ and $SAM{-}C_3{-}NH_2$, and the coating with pyridinium functionalities ($SAM{-}Py$).

Regarding the amino group terminated coatings, the monolayer $SAM{-}C_{11}{-}NH_2$ showed the lower IEP of 7.3. A slightly higher IEP of 8.6 was detected for the well-known $SAM{-}C_3{-}NH_2$ coating. The amino group terminated modifications caused the formation of positive charges upon the surfaces with a maximum in the zeta potential of 40 mV at low pH. Upon pH increase the zeta potentials steadily decrease, correlating with the degree of amino group deprotonation. Most probably remaining $Si{-}O^-$ groups upon the substratum surface contriubute to the decrease in surface charge. A zeta potential plateau at high pH values

corresponding to full deprotonation was nearly reached for the SAM−C_{11}−NH_2 coated surface (about -30 mV at pH 9). The shift of the IEP for the SAM−C_3−NH_2 coating towards higher values can be ascribed to the higher density and accessibility of amino groups at the SAM−C_3−NH_2 surface in comparison to the SAM−C_{11}−NH_2 layer. This confirms the observations of many studies that silanization with 3-aminopropyltrimethoxylsilane results in the formation of coatings of decreased order. A decreased order seems to facilitate the generation of charge upon a surface.

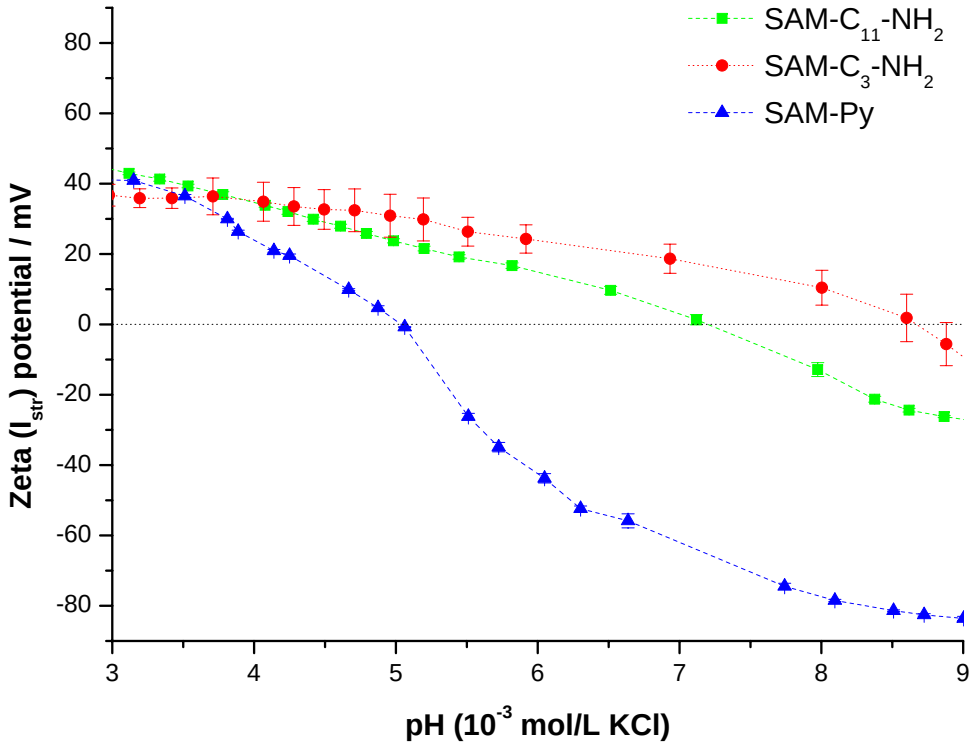

Figure 8.2: Electrokinetic ζ-potentials from streaming current measurements as a function of pH. Solution: 1 mM KCl, pH is adjusted with potassium hydroxide and hydrochloric acid. Surface coatings investigated: the amino group terminated coatings, SAM−C_{11}−NH_2 and SAM−C_3−NH_2, and the coating with the pyridinium functionality (SAM−Py). Experimental data are represented by symbols. Error bars in the graph show the deviation between two measurements performed on the same sample.

Pyridinium functionalized surfaces revealed an, at first glance, unforeseen dependence of the ζ-potential upon pH. Pyridinium groups were expected to generate a positive charge over the whole pH range. However, with increasing pH the charge at the surface decreases more rapidly as at the amino group terminated SAMs. An IEP of 5.1 was detected and the charge reaches a plateau value of -80 mV at a pH of 9. A similar dependence of the ζ-potential

upon pH can be observed for surfaces bearing coatings without ionizable groups, illustrated in the following subsection 8.1.3.

The presence of positive charges within the SAM-Py coating is confirmed by the strong positive ζ-potential at a pH value of 3, comparable with the one found on SAM$-C_{11}-NH_2$ and SAM$-C_3-NH_2$. At non-ionizable surface coatings this value is lower. Also, the increased IEP value (SAM-OEG = 3.2; SAM-Py = 5.1) in comparison to values detected on non-ionizable surface coatings supports the assumption of positive functionalities to be within the coating. There may be several reasons that are responsible for the detected charge development at the SAM-Py surface:
As explained in chapter 5; even at a complete coverage by silane molecules unreacted OH groups upon the surface are reasonable to be expected, this is because alkyl chains occupy areas of about 21-25 $\mathring{A}^2$ and silanol groups of about 20 $\mathring{A}^2$. Furthermore, only a few silanol groups are said to be involved in silane anchorage. The pyridinium bromide head-group was estimated to occupy an area of 34 $\mathring{A}^2$ [134]. Therefore, there are even fewer head groups of charged character within the coating to equalize deprotonated silanol groups at the surface, as if there would be if every head group, in a well organized SAM, would contribute to charge compensation. The reduced number of terminal pyridinium groups results in a shift of the IEP to lower values. Furthermore, XPS measurements on the SAM-Py coatings suggested the presence of surface confined amines other than pyridinium. This is a further reason for a surface coating of reduced cationic character. If large aryl moieties are additionally present upon the surface a preferential adsorption of hydroxide ions in alkaline medium is also reasonable to be expected. Taking all this into account, the determined electrokinetic measurement substantiates the assumptions already made, on behalf of the XPS, DRIFT and contact angle measurements, referred to in subsection 6.1.3.

8.1.3 SAMs terminated by Non-Ionizable Groups

Figure 8.3 displays the pH dependence of the ζ-potential on a hydrophilic surface coated with oligo(ethylene) units (SAM-PEG) and a hydrophobic surface modified by octyltrichlorosilane (SAM$-CH_3$). Both surfaces show a comparable zeta-potential dependence on the pH. Even though both do not possess dissociative groups they reveal a negative zeta-potential value at high pH values and low iso-electric points (IEP(SAM-PEG) = 3.2; IEP(SAM$-CH_3$) = 3.8). This corresponds well to literature data, where surfaces without ionizable surface groups typically exhibit IEPs of about 4 [24]. Because of the absence of ionizable groups within the coating the charge is most probably generated by the accumulation of negative charges (even though not fully understood yet, this phenomenon is believed to occur due to the adsorption of water ions, such as hydroxide (OH^-) [73][88]) and the contribution of the substratum to the charge development. Anions are known to be attracted stronger to a surface than cations because anions are less hydrated [70].

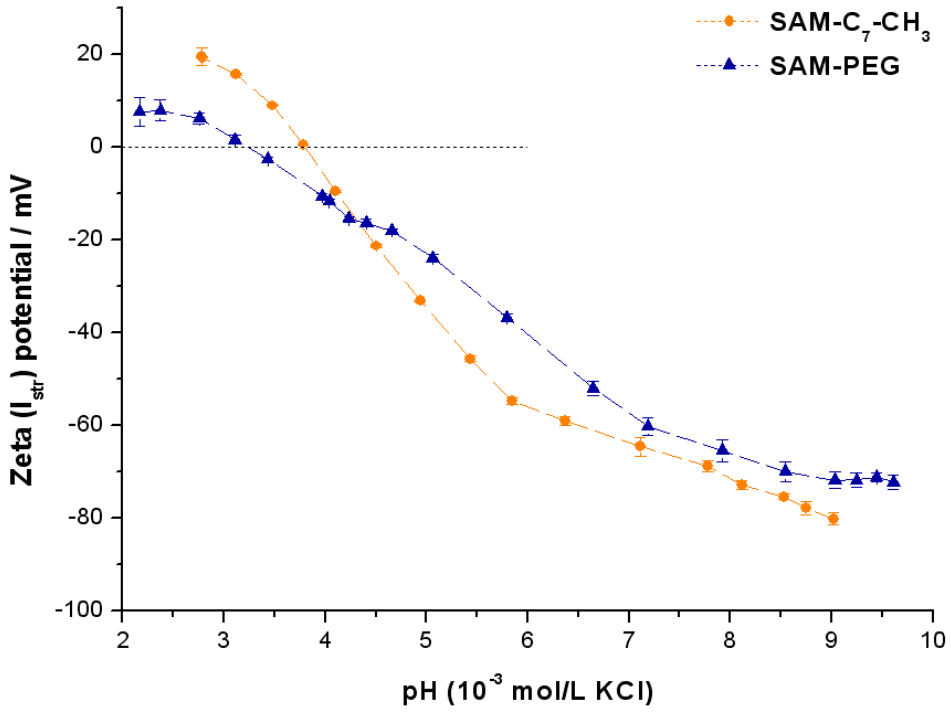

Figure 8.3: Electrokinetic ζ-potentials from streaming current measurements as a function of pH. Solution: 1 mM KCl, pH is adjusted with potassium hydroxide and hydrochloric acid. Surface coatings investigated: non-ionic coatings SAM$-$OEG (IEP = 3.2) and SAM$-C_7-CH_3$ (IEP = 3.8). Experimental data are represented by symbols. Error bars in the graph show the deviation between two measurements performed on the same sample.

8.2 Zeta-Potentials of PAMAM Coated Surfaces

Although streaming current data gathered at soft coatings are often converted into ζ-potentials, this is actually not correct since the layers are generally irregular on the length scale of the EDL [135], the penetration depth of the hydrodynamic flow into the soft layer and thus, the explicit position of the plane of shear is unknown. Since the conversion has no impact on the line progression and zeta potentials are more familiar than dI/dp values [nA/mbar], this conversion was performed even though the assumptions to do so are not justified. The pH dependent charging of dendrimer coated surfaces was analysed by streaming current experiments and will be addressed in this section.

The range of electrostatic interactions is characterized by the Debye screening length. The distance over which the electrostatic potential decays is about 9.7 nm in aqueous solution ($\epsilon = 80$) containing a 1:1 electrolyte (e.g. KCl) at 1 mM concentration. Electrostatic interactions are expected to be strong at low ionic strength. Although most biological fluids are characterized by a rather high ionic strength (e.g. PBS), overemphasized electrostatics in solution of lower ionic strength can help to accentuate the interactions responsible for structural arrangements [135]. For the dendrimer based coatings, which do not exceed a layer thickness of 10 nm's, as explained in subsection 7.1.3, an influence of the substratum and the sub-jacent TESPSA coating on the dendrimer may be taken into consideration.

At present, numerous attempts are undertaken by scientists like J. F. L. Duval [73], R. Zimmermann [80], C. Werner, Lyklema [72] to explore and develop advanced theories to describe the physico-chemical properties of fixed-diffuse charge layers as they are present throughout nature. An excellent review summarizing the current achievements in electrokinetics on charged diffuse layers was published by A. C. Barbati et al. [79].

8.2.1 Comparison: PAMAM-NH_2 and PAMAM-CH_3

The PAMAM−NH_2 coated surface is compared to the PAMAM−CH_3 coated surface because the charge in PAMAM−NH_2 depends on amino groups at the dendrimer exterior and tertiary amino groups within the dendrimer interior, whereas it is solely dependent on the charged moieties within the dendrimer interior in PAMAM−CH_3. Thus, reflecting the contribution of the internal tertiary amines on the charge development upon dendrimer functionalized surfaces.

As mentioned in the Fundamental Part of this thesis, PAMAM−NH_2 of the fifth generation is embraced by 128 primary amines. 126 tertiary amines are located within the dendrimer interior. Experiments by titration carried out in solution on PAMAM−NH_2 and PAMAM−OH

revealed pK_a values of 9.2 (9.1 - 9.3) for the primary amines and 6.0 (6.0 -6.6) for the tertiary amines [39]. The pK_a value reported for the tertiary amines of the central core is 3.5, only [36]. In a study performed by W. Chen et al. the authors state that only at a pH of 8.3 one can be certain that the charge formation depends on solely the primary amines [33].

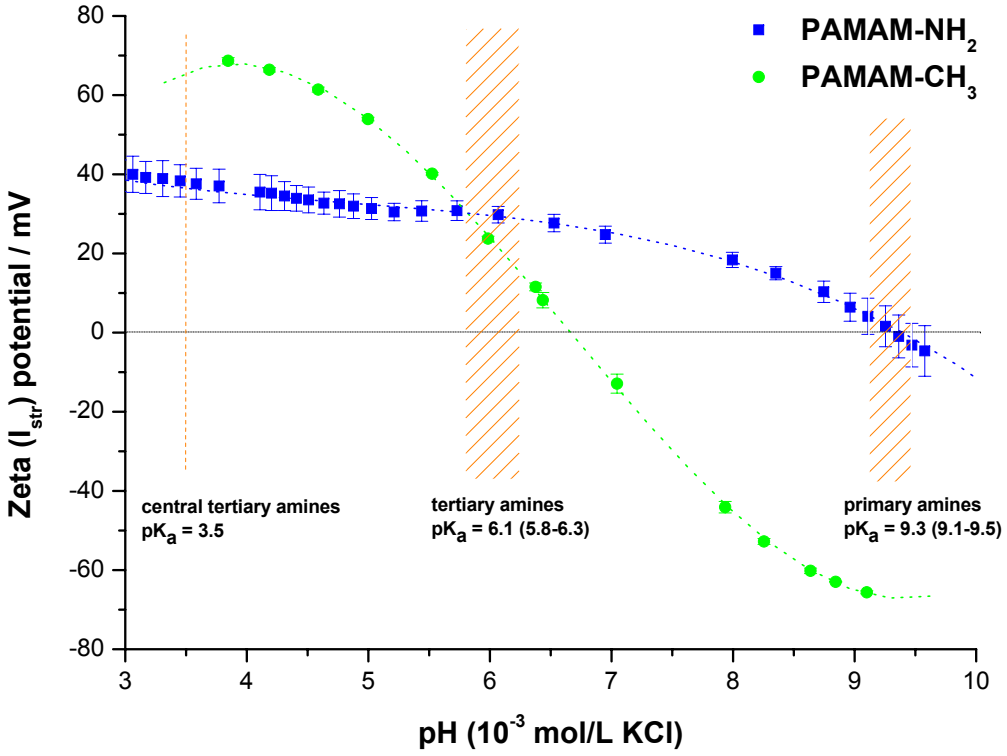

Figure 8.4: Electrokinetic ζ-potentials from streaming current measurements as a function of pH. Solution: 1 mM KCl, pH is adjusted with potassium hydroxide and hydrochloric acid. Surface coatings investigated: PAMAM−NH_2 and PAMAM−$COCH_3$. Experimental data are represented by symbols. Error bars in the graph show the deviation between two measurements performed on the same sample. Dashed lines are polynomial fittings of the third order.

Both surface coatings, PAMAM−NH_2 and PAMAM−CH_3, possess a positive charge at low pH, overcompensating the negative charge of the substratum. The "effective" ζ-potential value is lower for PAMAM−NH_2 than for PAMAM−CH_3 at a pH value of 3. This is not expected, because the PAMAM−NH_2 coating possess additional positive charges at the periphery due to protonated amino groups in comparison to PAMAM−CH_3. It is most likely, that this is a result of the increased swelling of the dendrimer due to ionic charge separation. All tertiary amines at the branching points and the primary amines at the periphery are protonated and there are only few ions within the electrolyte for charge compensation. Fur-

thermore, the chemistry of the amino groups facilitates interaction with water. Therefore, the structure of PAMAM−NH_2 is assumed to significantly influence the hydrodynamic flow of the adjacent liquid. Streaming current has been reported to strongly decrease in absolute value as the diffuseness of a film increases, since an increased friction is exerted on the fluid flow by the polymer tangling into solution [80]. No electrostatic repulsion among the terminal groups is present in the PAMAM−CH_3 coating, which probably reduces the film thickness. Additionally, the acetamide moieties at the periphery may interact with water molecules not as strongly as amino terminations. Hydrophobic moieties are also known to be prone to the preferential adsorption of hydroxide ions. Streaming current measurements at varying ionic strength and streaming potential measurements are advised to determine the contribution of surface charge to substantiate the above made speculations.

Upon pH increase the "effective" ζ-potential value at the PAMAM−NH_2 coating decreases gradually, but no plateau value could be reached in the area of measurement. The isoelectric point (IEP) is shifted from pH 6.7 of the PAMAM−CH_3 film to 9.4 for the PAMAM−NH_2 coating. This clearly confirms the presence of a higher amount of positive charges upon the surface in comparison to the PAMAM−CH_3 film. The IEP of the PAMAM−NH_2 functionalized surface is even higher than the one determined for the APTMS (IEP = 8.6) coated surface, presented in subsection 8.1.2. Therefore, PAMAM−NH_2 is the coating that bears the highest amount of amino groups upon the surface in comparison to SAM−C_{11}−NH_2 and SAM−C_3−NH_2. This supports the results obtained from the amino group detecting assay based on chemiluminescence upon the modified wafer surfaces (results may be viewed in the publication [136]). The gradual decrease in "effective" ζ-potential value upon pH increase at the PAMAM−NH_2 coating is attributed to the deprotonation of protonated primary and tertiary amino groups. Two distinct deprotonation steps (at pH 6.1 and 9.3) were expected for the tertiary and primary amines, but this is not witnessed. This may be the result of two superposed events. The film thickness decreases upon pH increase because the repulsive effect among the tertiary amino groups diminishes due to deprotonation, this causes the streaming current to increase on the one hand because less friction is exerted on the fluid flow, but on the other hand streaming current is decreased to the reduced amount of positive sites upon the surface. Furthermore, especially the tertiary amino groups within the dendrimer possess various environments, depending on their position within the film. This influences the protonation/deprotonation behaviour of these functionalities.

The "effective" ζ-potential value at the PAMAM−CH_3 coated surface reaches a plateau value at pH = 9 of -70 mV. This is the point were all tertiary amino groups are deprotonated and the film has, most probably, the lowest thickness. From the line progression (superimposed: swelling might effect the streaming current values, but this is expected to be low for this

coating;) one can determine a pK_a value of 6.7 for the tertiary amino groups upon the surface. This value is in absolute agreement with the one reported in literature for the tertiary amines within PAMAM−NH_2 in solution 6.0 (6.0 -6.6) [39], suggesting a rather undisturbed behaviour upon the surface.

8.2.2 PAMAMs Terminated by Cationic Groups

The line progression of the "effective" ζ-potential value in dependence on the pH is identical for the coatings PAMAM−CH_3 (as depicted in subsection 8.2.1) and PAMAM−Br. This is conceivable because they both possess non-ionizable peripheral groups, and the same molecular interior. After the conversion of PAMAM−Br into PAMAM−Py the $IEP|_{\zeta=0}$ is shifted from 7 to 8.3.

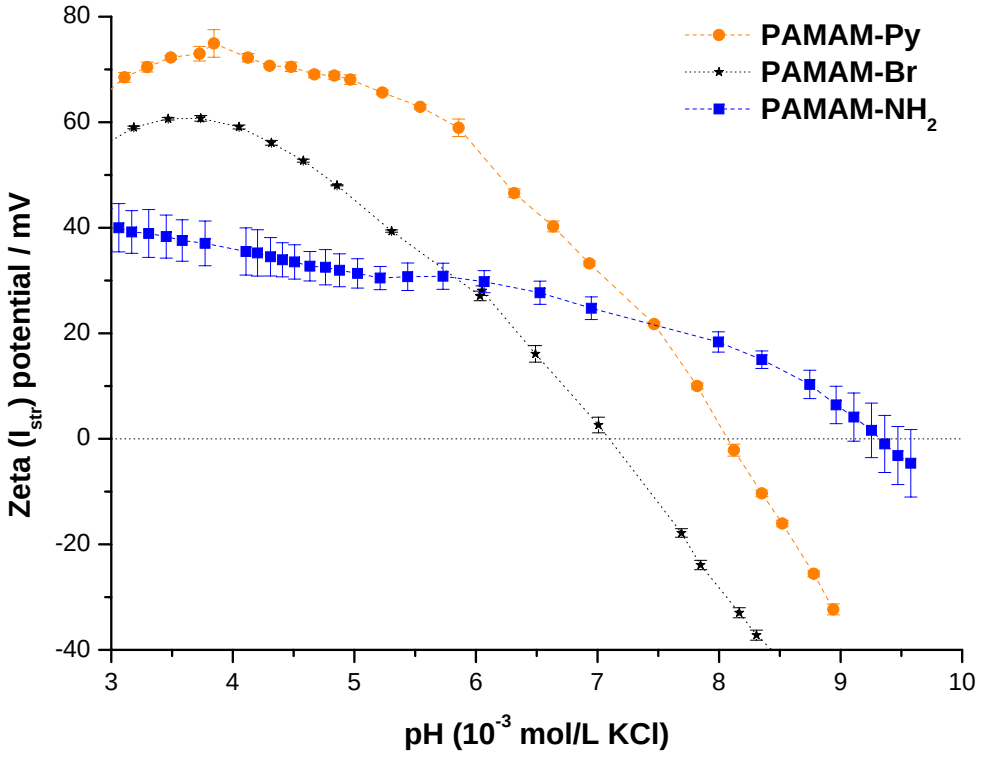

Figure 8.5: Electrokinetic zeta-potentials from streaming current measurements as a function of pH. Solution: 1 mM KCl, pH is adjusted with potassium hydroxide and hydrochloric acid. Surface coatings investigated: bromine terminated PAMAM coating PAMAM−Br, pyridinium terminated PAMAM-Py and amino group terminated PAMAM−NH_2. Experimental data are represented by symbols. Error bars in the graph show the deviation between two measurements performed on the same probe.

This shift, and the increased positive ζ-potential value at low pH in comparison to the

PAMAM−Br coating, confirms the incorporation of pyridinium functionalities. But the positive IEP-shift turns out smaller than expected. This observation is similar to the one made at SAM-Py coated surfaces (presented in subsection 8.1.2).

It may be founded on electrostatic repulsion, that not all terminal groups may have been converted. In experiments conducted by Crooks at al. terminal amino groups of polyamidoamine (G4 - G6) could not be functionalized to a higher degree than 50% with glycidyltrimethylammonium chloride [137]. This reduced reactivity is prescribed to electrostatic repulsion effects between the partially functionalized dendrimer and the positivley charged molecules in solution, because termination by tert-butyl glycidyl ether led to 100% conversion rate. Even though the pyridine is not positively charged in advance, electrostatic repulsion at the dendrimer periphery may reduce the reactivity of the remaining sites. Furthermore, pyridinium was generally used as recieved, not paying attention to possible contaminations or by-products (homologous pyridine, aniline, phenole) within the solution (mentioned in the subsection 12.3.2). It may be due to the electrostatical difficulties that contaminations contriubted stronger to the outcome of the conversion. The "effective" ζ-potential versus pH line progression of PAMAM-Py substantiates the assumption of the presence of further, rather non-ionic moities, since the pH dependence resembles the ones of PAMAM−Br and PAMAM−CH_3. Non-ionic functionalities preferentially adhere hydroxide ions, which may account for the rather steep decrease to negative ζ-potential values at high pH. The high "effective" ζ-potential value at pH = 3 for the PAMAM-Py coating, in comparison to PAMAM−NH_2, which should posses an equal amount of positive charges at this pH, implies a reduced effect on the hydrodynamic flow. This could be due to the increased amount of non-ionic moieties, like N-aryl functionalities. Furthermore, the prolate organisation of the dendrimers upon the surface might result in a reduced ratio between terminal groups exposed to the interphase and internal tertiary amines within the interior. These assumptions are advised to be substantiated by streaming potential determination and the variation of ionic strength.

8.2.3 PAMAMs Terminated by Anionic Groups

Even though, both coatings,PAMAM-COOH and PAMAM−SO_3H possess the same internal structure and a periphery of acidic nature they reveal a very different charge behaviour in solution upon pH as shown in Figure 8.6.

The surface functionalized with PAMAM−SO_3H possess the lowest "effective" ζ-potential (20 mV) of all PAMAM-based coatings at pH = 3. With increasing pH the "effective" ζ-potential decreases monotonously, passing the point of 0 "effective" ζ-potential at pH =

5.8. A plateau at high values is not reached in the area of examination. At low pH the coating is assumed to be very crumpled, as the measurements were performed at low ionic strength, expecting the functional groups (protonated tertiary amino groups and sulfonate functionalities) to approach each other for the sake of charge compensation. Because the "effective" ζ-potential is positive at pH 3 it is presumed that there are more positively charged functionalities upon the surface than anionic ones. This is attributed to the prolate organisation of the dendrimers upon the surface and the necessity of terminal groups to be involved in surface confinement, reducing the ratio of denderimer exterior to dendrimer interior moieties. After the deprotonation of the quaternary ammonium ions the charge of the surface is based on the sulfonate groups only. A repulsion among the functional groups may result in film swelling.

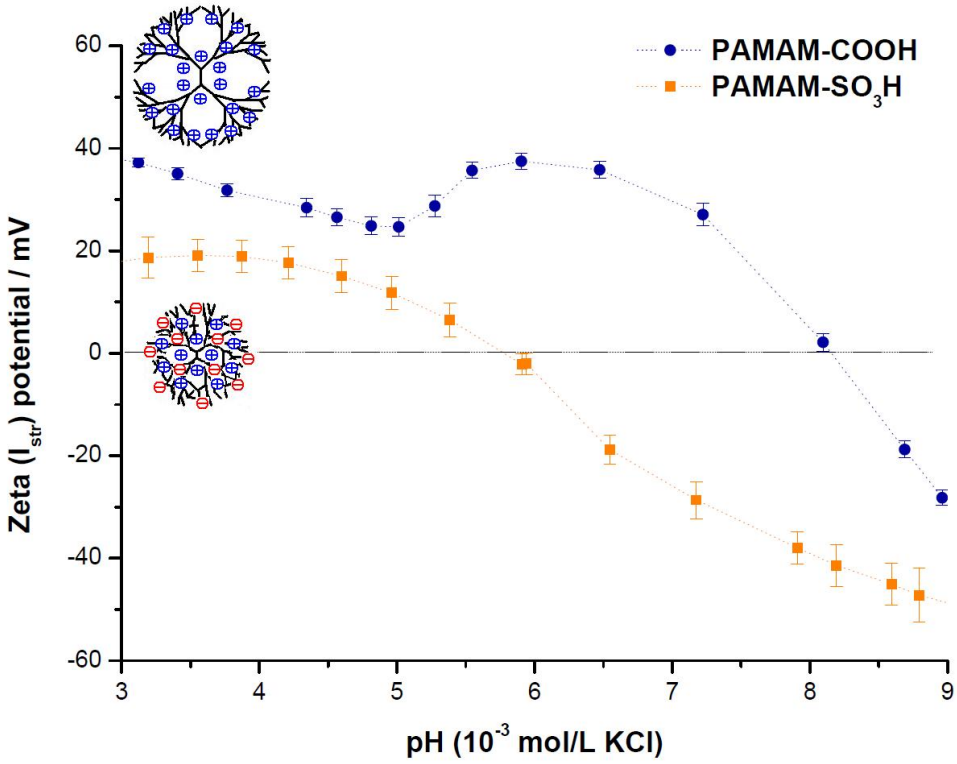

Figure 8.6: Electrokinetic zeta-potentials from streaming current measurements as a function of pH. Solution: 1 mM KCl, pH is adjusted with potassium hydroxide and hydrochloric acid. Surface coatings investigated: carboxylate terminated PAMAM coating PAMAM−COOH and sulfonate terminated PAMAM coating PAMAM−SO_3H. Experimental data are represented by symbols. Error bars in the graph show the deviation between two measurements performed on the same probe.

A non-monotonous charge development was observed upon the surfaces covered by carboxylated polyamidoamine. The carboxylated dendrimer surface shows an "effective" ζ-potential of $\tilde{4}0$ mV at pH = 3, which declines steadily up to the pH of 5. Thereafter, an unexpected

positive charge "regeneration" takes place before the curve drops to the IEP of 8.1 and further decreases to negative ζ-potential values.

It is assumed that at a pH of 3 all tertiary amines within the dendrimer interior and most of the carboxylic acids at the exterior are protonated (propionic acid $pK_a = 4.87$ [138]) resulting in a rather expanded dendrimer structure as depicted in Figure 8.6. Within the low pH range (2-5), a deprotonation of the tertiary amines takes place and the dendrimer interior shrinks due to the reduced positive charge repulsion, at the same time the carboxylic acid groups start to deprotonate. The dendrimer shrinkage might lead to a polarity decrease in the dendrimer interior forcing the further tertiary amines to deprotonate (a polarity decrease forces charged groups to deprotonate earlier as in the case of basic groups or later as in the case of acidic groups). As soon as there are enough deprotonated carboxylic acid groups on the dendrimer periphery to repel each other, the structure begins to expand, becomes more open and gains polarity (a similar behaviour has been observed on carboxylated PPI [17]). Maybe, previously deprotonated tertiary amines now become reprotonated because they experience an environment of increased polarity after the conformational change of the dendrimer. At high pH eventually all tertiary amines are deprotanated, and the surface charge relies on the negative carboxylic groups only. It was observed from titration experiments that tertiary amines may be protonated within PAMAM$-NH_2$ up to pH $\geq$ 8.3 [33]. Additionally, the dimensions of the coating may influence the hydrodynamic flow and thus the streaming current value. At low pH the film may be rather thick, reducing the streaming current signal. Upon pH increase the film shrinks and shows lower friction on the hydrodynamic flow causing a streaming current value to increase. But, only the strong changes in conformation may truly account for the large difference in IEP between the PAMAM$-$COOH and PAMAM$-SO_3H$ functionalized surface. It is possible that the PAMAM-COOH charge development is also dependent on the equilibration time upon pH increase, maybe different observations are made by choosing longer times for adjusting the pH.

8.3 Charge Characteristics of *S. gordonii* DL1 and *S. aureus*

Bacteria are "electrophoretically soft", i.e. they possess an ion-penetrable surface that permits electro-osmotic fluid flow. Mobile ions within this ion-penetrable layer give rise to surface conductivity. The slip plane is located somewhere inside this ion-penetrable layer, but its exact location is unknown. The ease with which the fluid can flow thorough this layer is characterized by the "electrophoretic softness" (λ^{-1}) of the bacteria and influences its electrophoretic mobility (determined by assessing the electrophoretic mobility in terms of the ionic strength). Double layer polarization and surface conductivity reduces the elec-

trophoretic mobility of a bacterium. The electrophoretic mobility is said to be higher if the bacterium is characterized by a "electrophoretically soft" exterior. [139]

The bacterial electrophoretic mobilities were only determined as a function of pH in 1 mM KCl by electrophoresis for *S. gordonii DL1* and *S. aureus*.

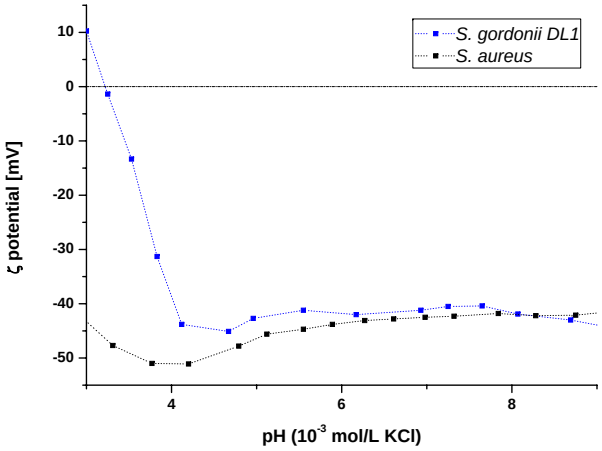

Figure 8.7: "Effective" ζ-potentials determined from electrophoresis experiments using the Helmholtz-Smoluchowski relation as a function of pH measured in 1 mM KCl solution for *S. gordonii DL1* and *S. aureus*. For the sake of clarity only one measurement is presented of each strain.

The bacterial electrophoretic mobilities were transferred to ζ-potentials by the Helmholtz - Smoluchowski equation, knowing this not to be fully correct (electrophoresis polarizes the surrounding double layer of a bacterium causing a dipole moment that opposes the electric field, especially in solutions of low ionic strength [139]. Surface conductivity increases the polarization effect [139].) Figure 8.7 shows the pH dependence of the "effective" ζ-potentials for *S. gordonii DL1* and *S. Aureus*. Whereas no IEP was determined for *S. aureus*, the one for *S. gordonii DL1* was 3.05 (2.99 - 3.15). Since the charge upon the bacterial surface is based upon the number of carboxyl, phosphate and amino groups (that is, if no preferential ion adsorption occurs), one could assume from the obtained data, that *S. gordonii DL1* possess more amino groups at the outer envelope than *S. aureus*. Furthermore, the charge of each bacterium was determined in PBS solution at physiological pH (pH = 7.4). *S. gordonii DL1* revealed a lower negative charge (-14 mV ± 2 mV) than *S. aureus* (-23 mV ± 2 mV) under these conditions. Since PBS is composed of numerous ionic species, preferential ion adsorption is likely and a more comprehensive study is necessary to determine the effect of PBS on the charge development. *S.aureus* is said to posses a rigid and less permeable exterior (low hydrodynamic softness) [23].

Both bacteria possess a comparable charge of ±-40 mV at pH 7 in 1 mM KCl solution. At physiological pH (pH = 7.4) *S. aureus* reveals a higher negative charge than *S. gordonii DL1*. A detailed examination regarding the electrokinetic properties of the microbial interphases applying the recently developed diffuse soft particle electrokinetic formalism (DSPE) is advised. This formalism is based on the full numerical integration of the governing electrohydrodynamic equations of soft particles and accounts for the chemical heterogeneities and the physical diffuse character of the interphase on the electrophoretic motion [23].

9 Coating Characterization by Sum Frequency Generation Spectroscopy (SFG): A Pilot Experiment

SFG spectroscopy is a second-order, non-linear optical technique to study interfaces. At interfaces the centro-symmetric structure of the adjacent bulk phases (random distribution of molecules) is broken. In SFG spectroscopy experiments two pulsed laser beams are focused onto an interface. One of the laser frequencies is fixed in the visible, whereas the other is tunable in the infra-red region. The spatial overlap and temporal synchronisation of both lasers induces SFG photons. SFG spectroscopy records vibrational spectra, unravels the identity of chemical functionalities at an interface and reveals information on the orientation of interfacial structures. Experiments can not only be performed at a liquid-gas interface but also at a liquid-liquid and a solid-liquid interface.

Pilot SFG spectroscopy experiments on substrata with covalently immobilized PAMAM molecules were performed to gather evidence on preferential orientations of the dendrimer moieties at the solid-air interface. SFG spectra were only recorded of the amino- and carboxylate-terminated PAMAM layers on glass. Two interfaces exist upon the sample, a glass-dendrimer and a dendrimer-air interface. Only the latter is changed after derivatization. Therefore, changes in the SFG spectrum are solely attributed to changes in the outer sphere of the PAMAM molecules.

The PAMAM backbone is based on 1010 methylene groups. After functionalization with succinic acid anhydride, further 256 methylene groups per molecule are theoretically gained. Changes in the C-H stretching region (2800 - 3000 cm^{-1}) were recorded upon terminal derivatization and are shown in Figure 9.1. Strong peaks are observed in the spectra indicating the loss of ideal symmetry of the dendrimer upon immobilization.

Within the PAMAM$-NH_2$ spectrum, two alkyl peaks at 2878 and 2944 cm^{-1} can be observed, which are assigned to the symmetric and antisymmetric stretches of the dendrimer's methylene groups [140]. A broad band emerging in the region between 3200 and 3300 cm^{-1}

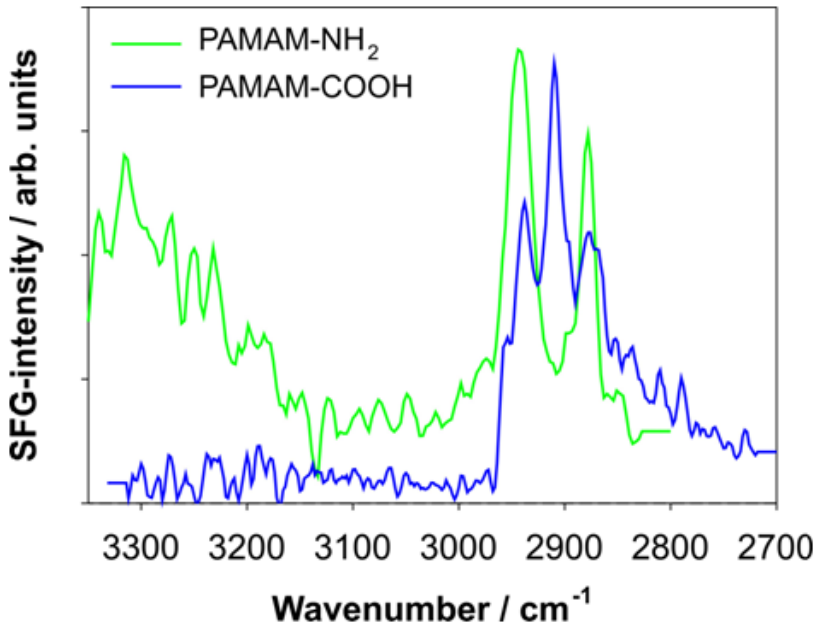

Figure 9.1: SFG spectra (ssp-polarization) of PAMAM−NH_2 and PAMAM-COOH immobilized on glass slides.

can be attributed to N-H stretching vibrations of the terminal amino groups [140]. Primary amines generally show two sharp absorption bands, symmetric and antisymmetric valence vibration, around 3335 cm^{-1} separated typically by 70 cm^{-1} [96]. The broad band in the PAMAM−NH_2 spectrum is most probably a result of the various amino groups associated in hydrogen bonds of varying distances and angles. Modes due to the presence of water can be ruled out due to the way the samples were prepared. Because of the complex structure of the dendrimer molecule, the orientation of the terminal amino groups could not be predicted by SFG.

Within the PAMAM−COOH spectrum the two distinct methylene signals that were also observed in the PAMAMA−NH_2 scan can be detected, but with a lower relative intensity. Furthermore, the disappearance of the broad N-H band at higher wavenumbers and the appearance of a signal at 2906 cm^{-1} [140] are alterations compared to the PAMAM−NH_2 scan. Because the broad N-H vibration is not replaced by a O-H vibration of the -COOH functionality, one must assume a complete deprotonation of the terminal groups. The additional peak at 2906 cm^{-1} can be assigned to the methylene groups next to the carboxylic acid moiety. The occurrence of this mode is most probably not due to Fermi resonance since the newly introduced moieties do not show peaks at a corresponding energy, and additionally an IR spectrum recorded of PAMAM-COOH does not show a mode at an eligible wavenumber. Since the transition strength stays the same (C-H transition), an increased signal of this

moiety at a rather low concentration upon the surface suggests a greater orientation of this specific group in comparison to all other methylene groups, as they were observed in the PAMAM$-NH_2$ scan. The signal supports the assumption of an increased order and number of cis-configurated, peripheral methylene groups. A trans-orientation cannot be suggested because one would expect a cancellation of peaks rather than a formation.

Even though the orientation of the terminal groups of PAMAM$-NH_2$ cannot be determined, the SFG spectroscopy scans indicate a burrowing of the terminal carboxylate moieties in PAMAM-COOH functionalized substrata exposing the outer methylene groups to the solid-air interface.

This pilot test demonstrates the potential of SFG to study PAMAM functionalized surfaces. Further details regarding the orientation of the methylene groups in the dry state may be obtained from spectra recorded in different polarization modes. However, it would be of considerable incentive to study the dendrimer functionalized surfaces in a hydrated state, that is under the same conditions as they are expected to be employed. The influence of pH, ionic strength and ion type on the dendrimer conformation is highly interesting. Furthermore, water is believed to significantly govern adsorption processes at surfaces. SFG spectroscopy is capable of unravelling the interfacial structure of water, also in phosphate buffered saline solution. Further studies on dendrimer functionalized surfaces by SFG would shed light into the surface structure - water relationsship and may help to understand subsequent biological processes occurring on these substrata.

10 Biological Response to Modified Surfaces

Protein adsorption at an interface between biomaterial and surrounding bodily fluid is an essential aspect in the cascade of subsequent biological reactions [131] and determines the biocompatibility of the artificial surface. Biological responses like adhesion, proliferation and differentiation of cells, as well as processes like inflammation and the foreign body response are believed to be mediated by the amount, type and conformation of the adsorbed proteins at the interphase [131].

Tooth implants face two different types of bodily fluids. Saliva surrounds the implant tip reaching into the oral cavity and serum surrounds the implant root anchoring within the gingiva. Protein adsorption from human whole saliva and foetal calf serum onto the modified surfaces is presented in the following section. Bacterial colonization at the designed surfaces, either exposed to bodily fluids in advance or not, by *Streptococcus gordonii* DL1 and *Staphylococcus aureus*, will be addressed in the section thereafter. The viability of the adhering bacteria on each surface modification was also determined. At the end of this chapter first results regarding the adhesion of eukaryotic cells onto the surfaces coatings will be presented.

10.1 Protein Adsorption from Saliva and Serum

With the focus of implantation within the oral cavity protein adsorption from serum and saliva was examined. Beforehand, the protein concentration within these two bodily fluids was determined by the conventional BCA assay, as described in section 14.1. 0.74 (0.69 - 0.78) mg/ml [Lit.: 0.72 - 2.45 mg/ml [141]] was found in human whole saliva and 32.21 (28.31 - 36.07) mg/ml [Lit.: 30 - 45 mg/ml as stated on the rmbio homepage; cited on the 07.01.2015] in foetal calf serum with reference to the BSA (bovine serum albumine) standard. Therefore, the protein concentration in serum is about 40 times higher than the one in saliva.

Silica beads were chosen to perform protein adsorption studies because they possess a significantly higher specific surface area than the wafer surfaces. A chemiluminescence-based assay invented by R. Müller and coworkers [118] to determine adsorbed proteins directly on wafer surfaces was infeasible because in the case of amino group bearing coatings their contribu-

tion to the final signal can not be differentiated. The amount of proteins adsorbed onto the functionalised silica beads (specified in 11.1) after exposure to either human whole saliva or foetal calf serum (1 hour) was therefore determined by the bicinchoninic acid (BCA) method (explained in detail in 14.1). The BCA assay is based on a non-specific reaction, where Cu^{2+} ions are reduced in the presence of proteins to Cu^{+}. Generated Cu^{+} ions form a complex with bicinchoninic acid. In contrast to other protein determining assays the protein is not bound to the colourant in the BCA assay. This fact provides the possibility to determine surface adsorbed proteins. Oxidised silica beads and beads coated by SAM−PEG served as references.

Figure 10.1 summarizes the values of the BCA assay which were obtained after protein adsorption from human whole saliva to chemically modified silica beads.

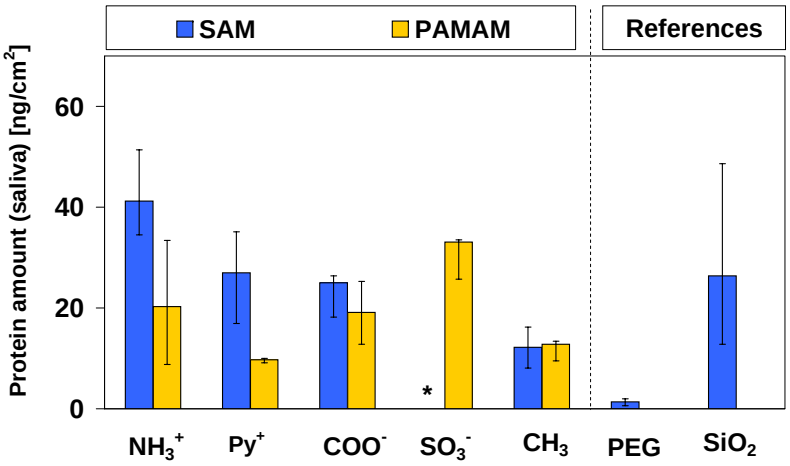

Figure 10.1: Protein amounts adsorbed to differently modified silica beads. Quantification by the BCA-assay. Silica beads were incubated for 1 hour in **human whole saliva**. Surface modifications terminated by the same functionality and based on either linear alkyl chains (SAM / blue) or dendrimers (PAMAM / yellow) are placed next to each other. Amounts are presented as medians including 25-75% quartiles. Data for SAM−SO_3^- have not been determined (*), yet.

Proteins from human whole saliva adhered the least to SAM based surface coatings bearing uncharged moieties (SAM−PEG and SAM−CH_3) and the most to amino group (SAM−NH_2) terminated surfaces. Protein adsorption on SAM−CH_3 beads may be underestimated because submersion was difficult due to their hydrophobic character. A medium protein content was detected on surfaces coated with SAM−COOH and SAM−Py, as well as on bare silicon dioxide (SiO_2). The adherence of protein onto SAM−SO_3H functionalized surfaces has not been determined, yet.

In case of the dendrimer based coatings PAMAM−SO_3H showed the highest affinity for saliva proteins. Medium amounts were detected on PAMAM−NH_2 and PAMAM−COOH, whereas the lowest protein amount was detected on PAMAM−Py and PAMAM−CH_3 functionalized substrata.

A replacement of the alkyl chain base by the dendrimer reduced the amount of protein adhering to the surface in comparison to their SAM based analogue (PAMAM−NH_2, PAMAM−Py) or kept it more or less the same (PAMAM−COOH, PAMAM−CH_3). Preliminary tests on surface coatings bearing N^+Me_3 (Me = CH_3) moieties support this observation. Upon SAM−N^+Me_3 coated surfaces 20.9 (19.8 - 21.5) ng/cm^2 was detected and upon the dendrimer analogue no protein at all. Thus, the PAMAM−N^+Me_3 coating would show an even stronger proteophobic character than the SAM-PEG surface. Since, the surface characterizations for N^+Me_3 coated surfaces were not comprehensive, these results are not included in the above graph and need to be proven by further experiments (preparation techniques and pilot results may be viewed in the annex).

M. Eichler investigated saliva adsorption to the surfaces SAM−PEG, SiO_2, SAM−COOH, SAM−NH_2, PAMAM−COOH, and PAMAM−NH_2 by quartz crystal microbalance [83] under dynamic conditions. She found the adsorbed pellicle on SAM−PEG, SiO_2, and SAM−NH_2 coated surfaces to be rather rigid, in contrast to the SAM−COOH coated surface where a more visco-elastic behaviour was observed. The PAMAM based coatings were embedded within these two states. Rinsing the saliva coated surfaces with PBS buffer did not reduce the amount of remaining protein significantly, with the exception of the PAMAM−COOH layer, where more than the half of the proteins could be deleted by rinsing. The amount of protein determined by QCM technology resulted in much higher numbers than the protein amount determined under non-flow conditions by the BCA assay. This is attributed to the fact that QCM data include surface bound water, whereas surface bound water is excluded in the BCA assay.

Figure 10.2 summarizes the values of the BCA assay which were obtained after protein adsorption from foetal calf serum to chemically modified silica beads.

Proteins from serum adhered the least on SAM based surface coatings bearing uncharged moieties (SAM−PEG, SAM−CH_3) and on SAM−COOH. Here again, as in the case of saliva, the amount on SAM−CH_3 coated surfaces may be underestimated because of the poor submersion due to the hydrophobic character of the beads. Carboxylic acid terminated surfaces were as proteophobic as SAM−PEG surfaces regarding protein adsorption from serum. SAM−Py and SAM−NH_2 coatings, as well as the bare SiO_2 surface favoured

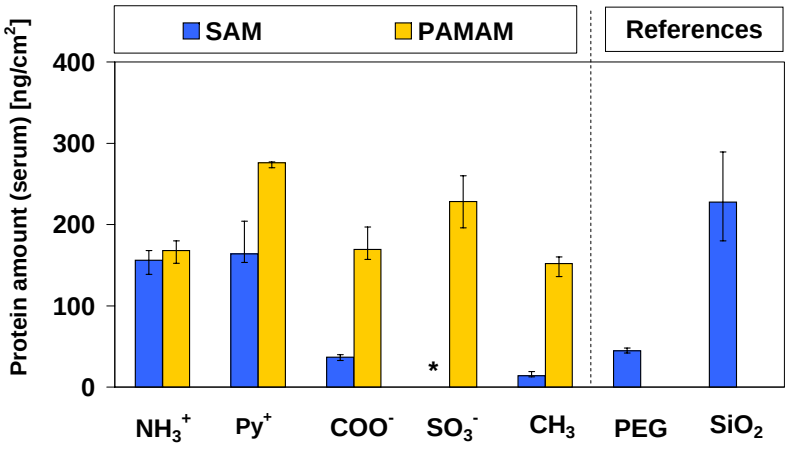

Figure 10.2: Protein amounts adsorbed to differently modified silica beads and quantified by the BCA-assay. Silica beads were incubated for 1 hour in **foetal calf serum**. Surface modifications terminated by the same functionality and based on either linear alkyl chains (SAM / blue) or dendrimers (PAMAM / yellow) are placed next to each other. Amounts are presented as medians including 25-75% quartiles. Data for SAM$-SO_3^-$ have not been determined (*), yet.

the adsorption of protein from serum. The increased adsorption of proteins from foetal serum albumin onto amino group terminated SAMs was also observed by other researchers [101]. However, on carboxyl terminated SAMs N. Faucheux et al. [101] determined similar amounts of protein as on amino group terminated SAMs, whereas in this study protein adsorption to SAM$-$COOH surfaces was reduced. It should be noted that their way of preparing SAM$-$COOH was evaluated to be less successful in generating carboxyl moieties. Details are explained in subsection 6.2.1. Unfortunately, no values have been determined for the SAM$-SO_3H$ functionalized surface, yet.

The dendrimer based coatings PAMAM$-CH_3$, PAMAM$-NH_2$, and PAMAM$-$COOH possess a equal affinity for serum proteins, whereas a proteophilic property was observed for the coatings PAMAM$-$Py and PAMAM$-SO_3H$.

Exchanging the alkyl chain basis of SAM coatings by the dendrimer led to a noticeable increase of adsorbed proteins (PAMAM$-$Py, PAMAM$-$COOH, PAMAM$-CH_3$) or a comparable protein amount (PAMAM$-NH_2$). A similar observation was made by examining N^+Me_3 (Me = CH_3) terminated coatings. Because the characterization has not been done comprehensively yet, these are preliminary results (preparation techniques and pilot results may be viewed in the annex). Protein adsorption was slightly higher after exchanging the alkyl chain by the dendrimer. 48.0 (43.8 - 55.2) ng/cm^2 was detected on SAM$-N^+Me_3$ and

56.0 (55.2 - 60.8) ng/cm^2 on PAMAM$-N^+Me_3$.

In summary, an exchange of the alkyl chain (SAM) anchorage by the dendrimer led largely to a decrease in protein adsorption in the case of saliva, but rather supported the adsorption of protein in the case of serum. PAMAM$-N^+Me_3$ revealed proteophobic properties comparable to SAM$-$PEG after saliva and serum exposure. SAM$-NH_2$ and SAM$-$Py favoured the adsorption of protein, whereas SAM$-$COOH, SAM$-CH_3$ and SAM$-$PEG showed a lower affinity for proteins. The amount of adsorbed protein is clearly affected by the functional groups and their way of confinement, but a clear categorisation into cationic, anionic and non-ionic termination can not be made.

The different amounts of protein on the various surfaces suggest that the composition of the proteinacous films varies on each surface modification. The impact of the surface modification on the protein pattern was determined by G. White (Department of Oral Biology, School of Dental Medicine, University of Buffalo, NY, USA). In pilot tests he observed significant differences in the amount and composition of adsorbed proteins from saliva on silica beads with variable functionalities determined by SDS-PAGE (sodium dodecyl sulphate polyacrylamide gel electrophoresis). For example, MG1 (saliva mucin - glycoprotein) was not found on bare SiO_2 but on SAM$-NH_2$ and SAM$-$Py, whereas MG2 (saliva mucin - smaller glycoprotein) was preferentially adsorbed to SiO_2 and SAM-PEG. He also found that the protein composition of the pellicle was rather similar in the case of dendrimer based coatings, but of significant difference on alkyl-chain based coatings.

10.2 Adhesion of *S. gordonii* DL1 and *S. aureus*

The adherence of bacteria and cells onto surfaces in the presence of a proteinaceous conditioning film complicates the mechanism of adhesion because specific ligand-receptor bonds may be involved [12]. On unconditioned surfaces adhesion is mainly governed by the properties of the surface and the micro-organism itself [12].

Examinations to study bacterial colonization of the modified surfaces was performed with the micro-organisms *Streptococcus gordonii* DL1 (Challis) and *Staphylococcus aureus* (ATCC 8325-4) (two of the at least 300 species of oral bacteria [142]). Their affinities towards the surfaces with and without protein pre-coat were evaluated. The surfaces were immersed into the appropriate physiological solution for 30 min at room temperature. Unbound protein was removed by rinsing with phosphate buffered saline (PBS). Incubation of the surfaces was performed with a bacterial suspension of 10^8 cells per ml in PBS for one hour. Adhering

bacteria were detected by a fluorescence based assay and quantified by means of standards with known cell numbers [143].

Figure 10.3 summarizes the attached numbers of *S. gordonii* DL1 with and without pre-treatment with saliva.

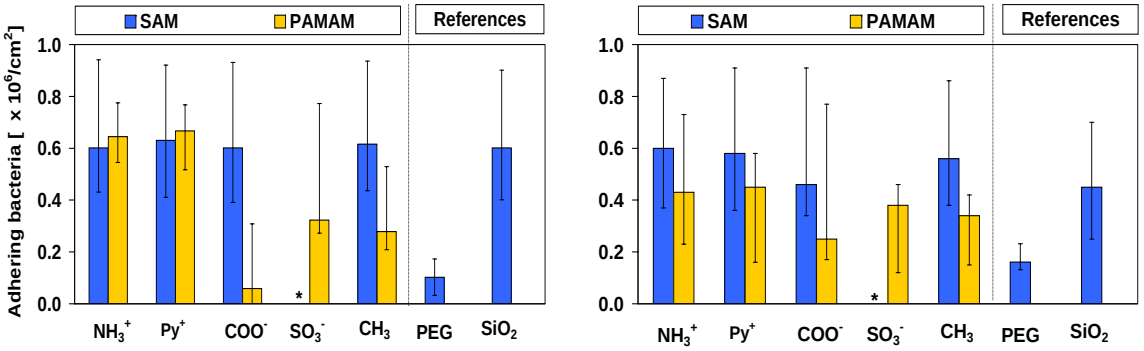

(a) *S. gordonii DL1* / PBS (b) *S. gordonii DL1* / human whole saliva

Figure 10.3: *S. gordonii DL1* attached to differently modified surfaces as determined by a fluorescence-based bacterial overlay method. Values obtained for the alkyl-chain and the corresponding dendrimer based modification are placed next to each other for each particular terminal functionality. Bars represent the medians including the 25-75% quartiles (N=8).
(a) adhesion to surfaces without protein pre-coat; PBS = phosphate buffered saline;
(b) adhesion to surfaces which were exposed to saliva in advance

Alkyl-chain based coatings were bacterially colonized irrespective of the head group, with the exception of the SAM−PEG coating where only a sixth of the cell numbers were found in comparison to all other coatings. Pre-conditioning of the surfaces with saliva did not change the number of adhering bacteria significantly.

In PBS solution *S. gordonii* DL1 showed the lowest affinity towards PAMAM−COOH coated surfaces, comparable to the SAM−PEG coated surface. Modest amounts were detected on PAMAM−CH_3 and PAMAM−SO_3H. The highest numbers of *S. gordonii* DL1 were detected on PAMAM−NH_2 and PAMAM−Py in PBS. Bacterial adhesion after conditioning with saliva caused an equalization of the adhering bacteria. Numbers on PAMAM−NH_2 and PAMAM−Py dropped slightly, whereas they rose on PAMAM−COOH. (Remark: Investigations under dynamic conditions by means of QCM technology performed by M. Eichler revealed low levels of bacteria on PAMAM−NH_2 surfaces [83].)

An exchange of the terminal group confinement from SAM to PAMAM caused, without saliva pre-coating, no changes in adhering cells for coatings terminated by -NH_2 and -Py, but a significant reduction was observed after binding the carboxy group to the dendrimer instead

of the alkyl chain. A similar but not so pronounced effect can be observed by the coatings terminated by the methyl moiety. Even though saliva caused equalization in bacterial numbers among the differently terminated dendrimer coatings it is remarkable that all dendrimer coatings showed reduced attachment of bacteria in comparison to their alkyl chain analogues.

Figure 10.4 summarizes the attached numbers of *S. aureus* with and without pre-treatment with serum.

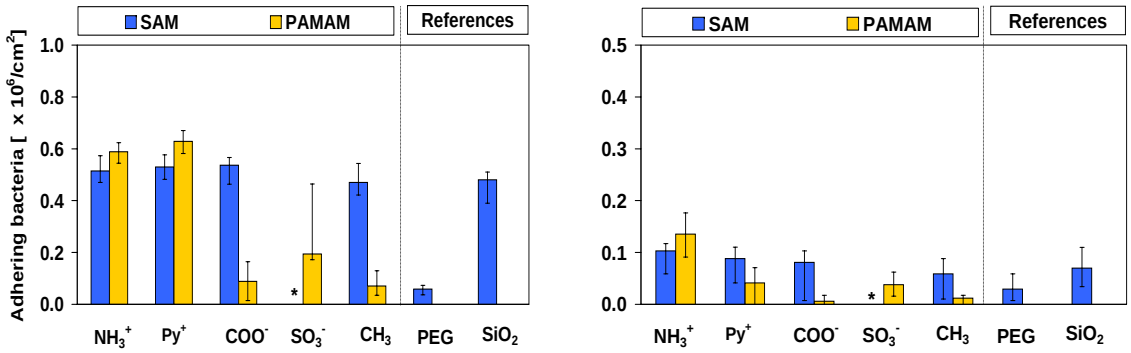

(a) *S. aureus* / PBS (b) *S. aureus* / foetal calf serum

Figure 10.4: *S. aureus* attached to differently modified surfaces as determined by a fluorescence based bacterial overlay method. Values obtained for the alkyl-chain and the corresponding dendrimer based modification are placed next to each other for each particular terminal functionality. Bars represent the medians including the 25-75% quartiles (N=8).
(a) adhesion to surfaces without protein pre-coat; PBS = phosphate buffered saline;
(b) adhesion to surfaces which were exposed to serum in advance

Comparable to *S. gordonii* DL1, alkyl chain based coatings were colonized by *S. aureus* irrespective of the functionality in PBS solution. Exchanging the backbone did not result in any changes in the PAMAM−NH_2/SAM−NH_2 and PAMAM−Py/SAM−Py system but led to a strong reduction of adhering bacteria on PAMAM−COOH and PAMAM−CH_3. Bacterial adhesion of the two latter coatings is even comparable with the bacteriophobic character of the SAM−PEG coating.

After conditioning the modified surfaces with serum a strong reduction in bacterial adhesion was observed. No clear assessment can be made for these data. It seems as the adhesion pattern stays the same, i.e. similar amounts adhere on alkyl chain based coatings and after confinement via the dendrimer basis a reduction is observed for PAMAM−COOH and PAMAM−CH_3.

In summary, the adhesion pattern for both bacteria is comparable when facing the surfaces

without any protein pre-coat. Whereas both bacteria adhere to all alkyl based coatings irrespective of the terminal functionality they prefer surfaces with dendrimers terminated by cationic functionalities and avoid the settlement on surfaces with dendrimers possessing anionic and neutral moieties.

10.3 Vitality of *S. gordonii* DL1 and *S. aureus*

Besides the quantification of the bacteria upon the surfaces their viability was also determined by a fluorescence stain kit. The fluorescence kit possesses two stains: SYTO9 and PI. SYTO9 marks all bacteria green because it passes the cell wall. PI can not pass an intact cell wall and can only replace the green dye if it may enter the cell when their membrane is damaged sufficiently to cause cell death (for further details see subsection 14.2.2).

Figure 10.5 shows that the number of viable bacteria of *S. gordonii* was reduced to about 60 % in comparison to the SiO_2 reference on the SAM−PEG coated surface with and without saliva conditioning. All alkyl-chain based coatings had no effect on the viability of the attached bacteria, with the exception of SAM−Py. The amount of viable *S. gordonii* cells was reduced to about 80 % on these surfaces. After exchanging the backbone from alkyl to dendrimer this detrimental effect increased, reducing the viable bacteria to 50 %. Unfortunately, both effects were abolished after coating the surfaces with saliva in advance.

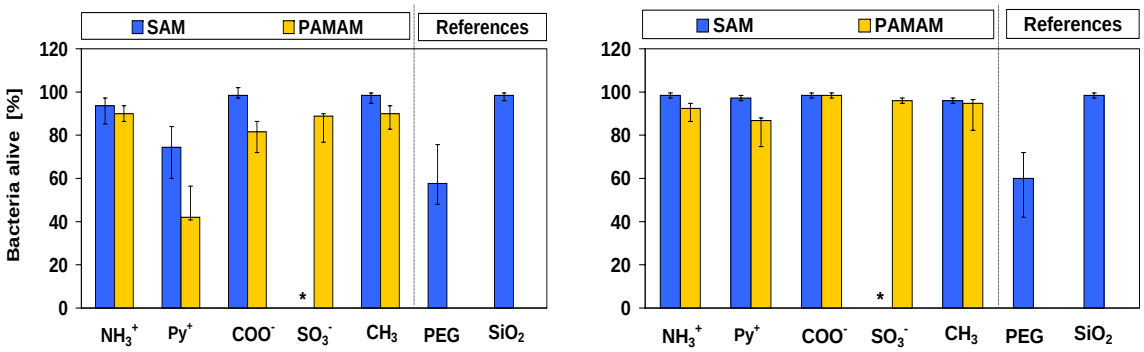

(a) *S. gordonii* DL1 / PBS

(b) *S. gordonii* DL1 / human whole saliva

Figure 10.5: Viability of *S. gordonii* DL1 attached to differently modified surfaces as determined by a fluorescent vital stain. Values obtained for the alkyl-chain and the corresponding dendrimer based modification are placed next to each other for each particular terminal functionality. Bars represent the medians including the 25-75 % quartiles (N=8).
(a) adhesion to surfaces without protein pre-coat; PBS = phosphate buffered saline;
(b) adhesion to surfaces which were exposed to saliva in advance

S. aureus was as viable as on the reference SiO_2 on all alkyl-based surfaces irrespective of the functionality with the exception of SAM−Py where a slight decrease in viability to about 80 % was detected.

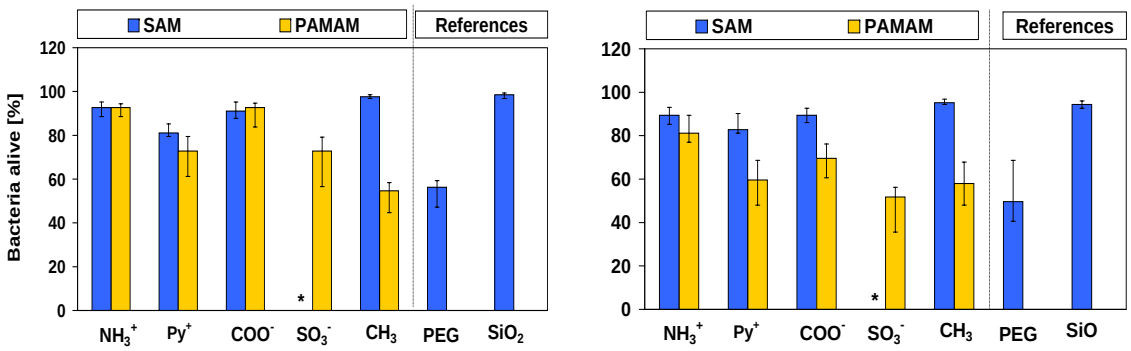

(a) *S. aureus* / PBS

(b) *S. aureus* / foetal calf serum

Figure 10.6: Viability of *S. aureus* attached to differently modified surfaces as determined by a fluorescent vital stain. Values obtained for the alkyl-chain and the corresponding dendrimer based modification are placed next to each other for each particular terminal functionality. Bars represent the medians including the 25-75 % quartiles (N=8).
(a) adhesion to surfaces without protein pre-coat; PBS = phosphate buffered saline;
(b) adhesion to surfaces which were exposed to serum in advance

No changes were observed after introducing a serum pre-coat. As in the case of *S. gordonii*, the detrimental effect of the SAM−PEG coating was also observed in this experiment. Only 50 % of the attached bacteria were viable on SAM−PEG before and after coating with serum. Swopping from the alkyl chain base to the dendrimer base reduced the vitality of bacteria on PAMAM−CH_3 modified surfaces to the same level as detected on SAM−PEG. This antimicrobial effect was also not compensated after pre-conditioning with serum. The vitality of *S. aureus* on the surfaces without protein conditioning was independent of the confinement for the functional groups NH_2 and COOH and as high as on the reference SiO_2. A tiny antimicrobial effect of the SAM−Py (about 20 % dead) coating was intensified by changing the anchorage to the dendrimer (about 30 % dead). After a conditioning with serum all surface coatings based on dendrimers possessed an antimicrobial character in comparison to their alkyl chain based analogoues.

10.4 Adhesion of Eukaryotic Cells

The surface of a biomaterial determines its biofunctionality. Initial cell attachment guides subsequent processes like cell spreading, morphology, migration, proliferation and differentiation [144]. Initial cell adhesion studies were carried out with human MG-63 osteoblasts (ATCC CRL-1427), representatives for cells derived from bone tissue and relevant in implantology. These experiments were carried out at the University Hospital in Regensburg by C. Waha under the supervision of Prof. Dr. Dr. H. Schweikl. Experimental details are described in [144]. The adhesion of cells was determined after pre-conditioning the surfaces in foetal calf serum (1 hour at room temperature) or without protein pre-adsorption. 100,000 cells were seeded on each wafer and the cell amount was detected 24 hours after routine culturing. The number of cells on each wafer was determined by using a crystal violet assay.

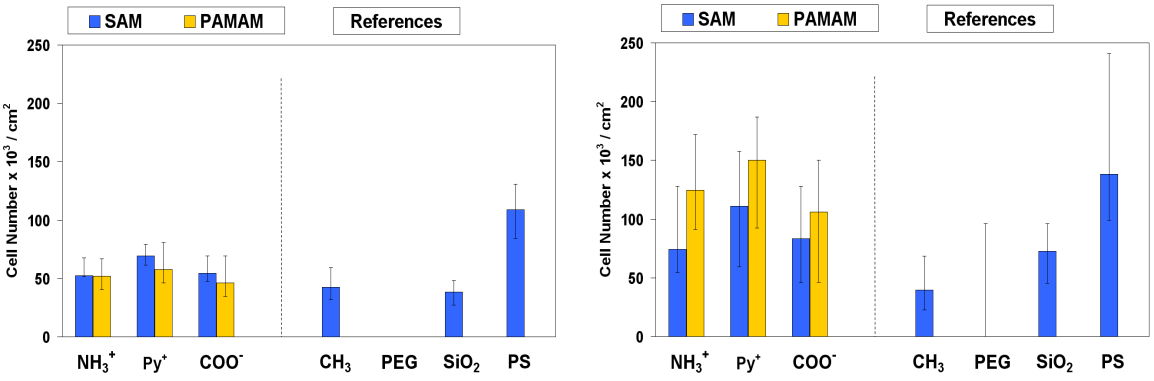

(a) without serum (b) precoated with serum

Figure 10.7: Adhesion of human MG-63 osteoblasts on modified wafer surfaces before and after serum exposure (PS = tissue culture polystyrene). The bars represent the medians including the 25 %-75 % qartiles (N=8).
(a) adhesion to surfaces without protein pre-coat
(b) adhesion to surfaces which were exposed to serum in advance

Experiments on all novel coatings has not been completed up to now. The data that have been obtained so far are presented in Figure 10.7.

In the absence of serum precoating the way of functional group confinement, either by linear alkyl chains or dendrimers, had no significant influence on the adherence of MG-63 osteoblasts. At least among the investigated functionalities -NH_3^+, -Py^+ and COO^-. However, significantly more cells adhered to polystyrene tissue culture plates (PS). Hardly any cells were detected on SAM-PEG coated wafers. In comparison to polystyrene culture surfaces about 50 % of the MG-63 cells adhered onto the SAM and PAMAM surfaces irrespective of the investigated terminal functionalities.

Pre-coating the surfaces with serum promoted cell adhesion on all surfaces with the exception of the SAM$-CH_3$ functionalised surface. Higher cell numbers were found on all dendrimer based coatings in comparison to their linear analogues, among the investigated terminal functionalities. Upon pyridinium terminated surfaces the adhesion was strongly supported. Cell numbers as high as on PS were determined on PAMAM-Py coated silicon wafers. Whereas the adherence was comparable on SAM-NH_2 and SAM-COOH, the confinement via dendrimers led to a higher amount of cells on the PAMAM-NH_2 surface in comparison to the PAMAM-COOH surface. Therefore, the dendrimer fixation emphasises the influence of the individual functional groups that is tethered to the surface.

Part IV

Conclusion and Perspective

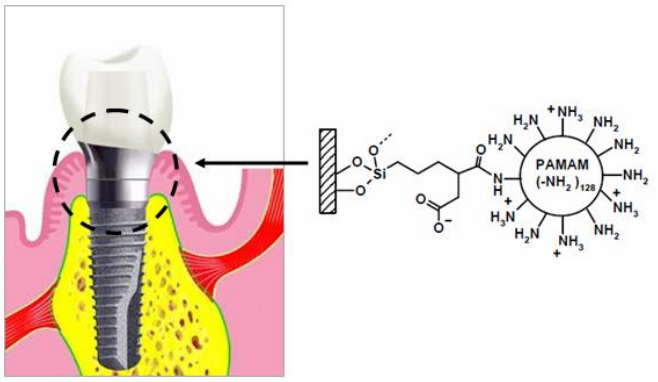

Figure 10.8: The centre of attention is marked by a black circle - transgingival area of a dental implant. ©Zahntechnik, Esslingen

According to a recent survey at least a third of all dental implants is affected by peri-implantitis 10 years after implantation. To date there are no bi-functional coatings that suppress the adhesion and growth of pathogenic organisms while simultaneously stimulating the integration of the implant into the surrounding tissue at the trans-gingival passage. A coating combining both properties is believed to reduce the incidence of peri-implantitis. The location of the trans-gingival passage is illustrated in the above Figure 10.8.

Unfortunately, the impact of surface properties such as charge, surface wettability and coating agility on protein adsorption and subsequent biological events is still not fully unravelled. Consequently, it is not possible to tailor surfaces that fulfil the above requirements by introducing certain properties or structural elements into a surface coating. To gain more insight into these processes, ionic functional groups of different structure and polarity (ammonium $-N^+H_3$, pyridinium $-N^+C_5H_5$, carboxylate $-COO^-$, and the sulfonate $-SO_3^-$) were tethered to model surfaces in terms of highly branched, dendrimeric structures (PAMAM), since multivalent motifs are efficient concepts in biology, and compared to the same functional groups immobilized via non-branched, alkyl chain based structures (SAM).

The dendrimer, polyamidoamine of the fifth generation, was anchored to carboxylate terminated SAMs using carbodiimide chemistry and to anhydride terminated coatings. Because the fixation to anhydride terminated coatings is possible without the necessity of further reagents, and since additional negative charges are formed close to the anchoring sites of the mediating molecules, this immobilization technique was favoured over fixation to the SAM-COOH coating. Straight forward silanization with silanes terminated by succinic acid anhydride moieties resulted in thick coatings, where the anhydride functionality was lost. A scavenger molecule was introduced to react with ethoxy and hydroxyl ions generated during the silanisation process. After adding the scavenger, acetic acid anhydride, to the silaniza-

tion reaction, the functionality was preserved.

Coatings based on PAMAM resulted in films of about 7 nm thickness. Since the hydrodynamic radius of PAMAM is about 5.4 nm, this suggests a prolate configuration of the dendrimers upon the surface.

An exchange of the alkyl chain (SAM - two dimensional distribution of charge) anchorage by the dendrimer (PAMAM - three dimensional distribution of charge) resulted in a higher allocation of terminal functionalities and thus a higher distribution of charge carriers as impressively presented by means of a chemiluminescence based amino group detection assay and by streaming current measurements in aqueous solution on surface coatings bearing amino group functionalities.

In terms of the surface wettability, surfaces modified on the basis of PAMAM were either of about the same hydrophilicity (-Py, -COOH) or of higher hydrophilicity (-N^+H_3, -SO_3^-, -CH_3) as their alkyl chain based counterparts (SAM). This is attributed to the polar structure of the dendrimer interior.

All coatings, based upon linear alkyl chains generated a mainly pronounced negative electrokinetic potential (-30 mV to -120 mV) in neutral aqueous solution, with the exception of the amino-group terminated SAM, where a value around zero was determined. The reason for the negative ζ-potential at pyridinium functionalized surfaces at neutral pH is believed to result from a lower concentration of terminal groups in comparison to surfaces terminated by amino groups. Only about 45 % of the terminal groups are of charged character in SAM-Py. This is attributed to the larger dimensions of -$N^+C_5H_5$ in comparison to -N^+H_3, their affinity to adsorb hydroxyide ions from solution and the presence of a pH independent charge. In contrast the novel coatings based upon dendrimers are rather moderately charged (-20 mV to +30 mV) at pH 7.

The streaming current values in dependence of the pH of the surrounding solution at the alkyl chain based coatings were observed to depend solely on the ionic properties of the surface confined functionalities, whereas the "effective" ζ-potential-pH profiles at the novel dendrimer coatings could only be explained considering film swelling, structural rearrangements and the interaction of the functionalities with the adjacent liquid phase influencing the tangential fluid flow. That the dendrimer maintained its flexibility upon immobilization was also supported by pilot sum frequency spectroscopy (SFG) measurements at the coating/air interface by comparing the coatings PAMAM$-NH_2$ and PAMAM-COOH. Methylene units next to the carboxyl group preferentially went into cis orientation in order to hide their ter-

minal groups. Therefore, the conformational behaviour of the attached dendrimer is affected by the chemistry of the peripheral groups.

An exchange of the alkyl chain anchorage by the dendrimer led mainly to a decrease in protein adsorption from human whole saliva, especially on coatings terminated by cationic functionalities. In contrast, protein adsorption from serum was mainly supported on dendrimer based coatings in comparison to their SAM analogues.

Bacterial electrophoretic mobilities of *S. gordonii* DL1 and *S. aureus* were recorded by electrophoresis and revealed the netto negative charge of *S. gordonii* to be weaker than the one of *S. aureus* in phosphate buffered saline.

Both bacterial strains, *S. gordonii* DL1 and *S. aureus*, adhered in high amounts to all alkyl chain based coatings irrespective of the terminal functionalities, if the surfaces were not exposed to physiological solutions in advance. An exchange of the functional group confinement by dendrimers led to a strong bacterial decline at the surfaces terminated by non-ionizable (-CH_3; no hydrogen bond acceptors at the periphery) and acidic (-SO_3^-, -COOH) moieties and left the numbers untouched at modifications terminated by basic functionalities. The PAMAM-COOH (zwitterionic nature) coating was even as effective as the gold-standard in anti-adhesive coatings (polyethylene glycol; SAM-PEG). This observation clearly shows that the concentration of terminal functionalities and their way of confinement within the SAM system is not capable of strongly influencing the amount of adhering bacteria. The attachment and supply of the terminal functionalities via the dendrimeric system is able to modulate the adhering bacterial cell numbers. Furthermore, pre-conditioning the surfaces with saliva resulted in less *S. gordonii* DL1 on all dendrimer based coatings in comparison to their linear analogues. Serum conditioning of the surfaces caused a strong decrease of *S. aureus* on all coatings with exceptional low numbers on PAMAM-CH_3 and PAMAM-COOH.

The vitality of *S. gordonii*, was only significantly influenced by pyridinium coated samples, where the bactericidal effect was stronger on PAMAM-Py (killing 50 % of bacteria) than at the SAM-Py (killing 20 % of bacteria) coated surfaces. This effect was lost after saliva preconditioning. Regarding *S. aureus* the pyridinium functionalized coatings also reduced the viability of adhering bacteria (SAM-Py: killing 20 % and PAMAM-Py killing 30 % of bacteria), but the most pronounced effect was achieved with methyl terminated polyamidoamine (killing 40 % of bacteria). After serum exposure this bactericidal property was maintained and the one of pyridinium functionalized dendrimers enforced. The antimicrobial property of PAMAM$-NH_2$, reported in literature, could not be maintained after tethering the molecule to the surface.

Cell adhesion studies were carried out with human MG-63 osteoblasts (ATCC CRL-1427), representatives for cells derived from bone tissue. In the absence of serum precoating the way of functional group confinement, either by linear alkyl chains or dendrimers, had no significant influence on the adherence of MG-63 osteoblasts. At least among the investigated functionalities -NH_3^+, -Py^+ and COO^-. However, significantly more cells adhered to polystyrene tissue culture plates (PS). Pre-coating the surfaces with serum promoted cell adhesion on all surfaces with the exception of the SAM$-CH_3$ functionalised surface. Higher cell numbers were found on all dendrimer based coatings in comparison to their linear analogues. Cell numbers as high as on PS were determined on PAMAM-Py coated silicon wafers.

This study demonstrates, that a dendrimeric amplification of terminal groups upon a surface capable of forming charges possesses the potential of modulating the oral biological response, in contrast to the supplement of the functional groups via linear alkyl chains. Both bacteria investigated preferred dendrimer based coatings terminated by cationic functionalities and avoided the settlement on surfaces functionalized by dendrimers with anionic or neutral periphery. PAMAM-COOH is as effective and PAMAM-CH_3 nearly as effective as the gold standard SAM-PEG in prohibiting bacterial attachment. This property was even slightly enforced after serum conditioning, whereas it was slightly reduced after saliva conditioning. In contrast all alkyl chain based coatings were colonized by both bacteria irrespective of the terminal functionality.

Since PAMAM-CH_3 revealed a gentle antimicrobial property towards *S. aureus* and reduced the settlement of bacteria, PAMAM-CH_3 might be promising in reducing peri-implantitis at the trans-gingival passage without minimizing the attachment of bone forming cells.

Proposals for further investigations will be mentioned on the next page.

Perspective

Unfortunately, no clear correlation could be drawn among the investigated factors wettability, charge and bacterial response. This may be due to several reasons:

- Dendrimer based coatings are structurally different in air than in a hydrated state. Wettability data recorded 15 s after water deposition do not characterize the surface in an equilibrium state. Furthermore, surface contaminations from air occur instantly and alter the surface properties. It is recommended to perform characterizations by the captive bubble method. Instead of forming a liquid drop on the surface, an air bubble can be formed beneath the sample, which is immersed in the testing liquid. The surface is than in a water saturated atmosphere and may not be exposed to air impurities. Investigations may even be performed in phosphate buffered saline.

- Electrokinetic (EK) data acquired in this thesis were performed in 1 mM potassium chloride, only. EK data conducted in this thesis should be supplemented by streaming potential measurements to obtain conductivity data of the stagnant layer. The generation of charge should also be investigated at various electrolyte concentrations (ionic strengths) and compositions (ions relevant in physiological fluids). This additional information would extend the knowledge on the ionization status of the functional groups, their positioning within the dendrimer coating, the swelling properties of the film and the influence of preferential ion adsorption [80]. These data are advised to be correlated and inspected by data obtained from potentiometric titration (surface charge density due to functional groups only, excluding preferential ion adsorption). The 1 μm silica spheres provide an excellent platform for these investigations, since they may also be employed in electrophoresis experiments. EK measurements with protein or bacterial solutions may even provide information on the kinetics of protein adsorption and bacterial adhesion. A combination of streaming current and streaming potential measurements would also allow an estimation of the hydrodynamic thickness of the adsorbed protein layer [77].
  Regarding bacteria, EK measurements should be performed by the aspects of the diffuse soft particle electrokinetic formalism (DSPE) to obtain further knowledge on the impact of the bacterial envelope and surrounding ions on the electrophoretic mobilities.

- The pilot test demonstrated the potential of SFG to study PAMAM functionalized surfaces, however, it would be of considerable incentive to study these surfaces in a hydrated state, that is under the same conditions, as they are expected to be employed

in. This method allows to study the influence of the ionic strength and ion type on the dendrimer conformation.

Regarding the bicinchoninic assay determining the protein amount upon the surfaces: Difficulties arise from the fact that the BCA solution does also react with the surface coatings as determined by blind testing. This complication may be avoided, if a specific amount of saliva is added to modified beads and the proteins remaining in solution characterized by a protein specific test in the absence of the beads. This is referred to the protein depletion method in literature. Thus, assays where the binding of the colourant to the protein occurs may also be considered. The 1 μm silica spheres seem to be appropriate for this study.

At present there is no standard with a specific surface charge for microslit electrokinetics. The defined size and structure of dendrimers, and their different generation levels in combination with SAMs of varying binding sites (diluting carboxylic acid moieties upon the surface by adding alkyl silanes, as explained in this thesis) may provide a powerful tool to vary the dendrimer density upon the surface and develop such a standard.

PAMAM-Br optimization proposal: adding pyridine to the PAMAM-Br preparation solution. The formation of hydrogen chloride within the reaction seems to affect the dendrimer structure, because charge neutralization within the dendrimer leads to a shrinkage and reduced reactivity of the outer groups. Using reactions without the formation of hydrogen chloride might increase the transformation yield. OCN$-$CH$_x-$halide substance are recommended.

Not only the nature of the dendrimer periphery may influence the biological response, but also the dendrimer generation level which controls the surface concentration of terminal groups. This seems to be worth to be investigated.

Part V

Experimental Part

11 Materials

11.1 Substrata

Inorganic, Si-based substrata of different physical characteristics were used to study the selected surface modifications. The substrata are listed below:

Single-side polished silicon wafers (n-type; phosphor-doped; 1 - 10 Ωcm resistivity) were purchased from Wafer World Inc. (West Palm Beach, FL, USA). The obtained wafer discs were cut into pieces of 10 mm x 10 mm x 575-675 μm by Disco Hi-Tec Europe GmbH (Kirchheim, Germany) using a wafer saw.

Double-side polished silicon wafers (n-type; phosphor-doped; 20 - 50 Ωcm resistivity) were purchased from Si-Mat Silicon Materials (Kaufering, Germany). The obtained discs (diameter = 100 mm; thickness = 1000 ± 25 μm) were cut into individual samples of 25 mm x 10 mm by Disco Hi-Tec Europe GmbH (Kirchheim, Germany) using a wafer saw.

Silica particles (diameter 63 - 200 μm, specific surface area 500 m^2/g, Kieselgel 60, amorphous silica, molecular weight = 60.09 g/mol) were purchased from Merck/VWR (Darmstadt, Germany).

Silica beads (non-porous, sintered 250 - 350 μm in diameter) were purchased from Brace GmbH (Alzenau, Germany). Measurements using a nitrogen adsorption apparatus (BET) revealed a specific surface area of 0.19 m^2/g.

Silica spheres (non-porous, diameter 1 μm, poly-dispersity index <0.2) were purchased from Micromod Partikeltechnologie GmbH (Rostock, Germany, Productnr.: 43-00-103, sicastar®).

1 mg contains $9.5 \cdot 10^8$ spheres. The surface charge density was stated by the supplier to be 7 μmol/g. Measurements using a nitrogen adsorption apparatus (BET) indicated that the specific surface area of the sample is 2.80 ± 0.04 m^2/g. According to the manufacturer' s data ($O = \pi \cdot d^2 = 3.1 \cdot 10^{-12}$ m^2 surface area per sphere) a theoretical value of 2.99 m^2/g can be calculated for the specific surface area. The convergence of the theoretical and the experimental (BET) value confirms the non-porous character of the spheres.

Quartz crystal resonators (silicon dioxide-coated QCM resonators, diameter = 14 mm; surface area ≈ 1.5 cm^2) were provided by the project partner from Tübingen (University Hospital Tübingen, Department of Prosthetic Dentistry, Section Medical Materials and Technology, Germany). They obtained the resonators from LOT Oriel GmbH (Darmstadt, Germany).

Glass slides (amorphous quartz) were used for infrared-visible sum frequency generation spectroscopy (SFG) measurements.

The surface area of the above listed substrata increases in the following order: wafer single-side polished (1.0 cm^2) < QCM resonators (1.5 cm^2) < glass slides (3.0 cm^2) < wafer double-side polished (5.0 cm^2) < silica beads (0.2 m^2/g) < silica spheres (2.8 m^2/g) < silica particles (500 m^2/g).

11.2 Chemicals and Solvents

Unless stated otherwise, chemicals and solvents were of analytical grade (p.A.) and either purchased at the company Merck/VWR (Darmstadt, Germany) or at Sigma-Aldrich Chemie GmbH (Deisenhofen, Germany). Chemicals needed in more than one reaction are listed below, whereas specific chemicals needed for only one reaction are listed in the particular section.

Sterile filtrated water was purified by an ultrafiltration apparatus of Millipore Corp. (Billerica, MA, USA) and afterwards poured through a bottle-top filter with a nylon membrane (MF75, Thermo Fisher Scientific, Nalgene). This water is referred to as **sf-water** (**s**terile **f**iltrated-water).

Half-concentrated nitric acid 32.5 % w/w was obtained by diluting concentrated nitric acid ($w(HNO_3)$ = 65 % w/w) with de-ionised water

Silanes were either purchased from ABCR GmbH & Co. KG (Karlsruhe, Germany) or Gelest (Morrisville, PA, USA). They were used without further purification. The silanes were stored within a glovebox under nitrogen atmosphere.

Anhydrous toluene was purchased from Sigma Aldrich. It was dried over a molecular sieve (4 $\AA$) in a five litre round bottom Schlenk flask flooded with argon. Additionally, toluene (dried over 4 $\AA$ molecular sieve) was deposited in the glovebox in a 50 ml round bottom Schlenk flask for the dilution of silanisation reagents.

Dimethylsulfoxide (DMSO), N,N-dimethylformamide (DMF) were purchased from Sigma Aldrich (anhydrous, ≥ 99.8 %) and dried by adding 4 $\AA$ molecular sieve into their stock solution flasks.

Acetic acid anhydride (AAA) was purchased from Sigma Aldrich ($\geq$ 99 %, CAS 108-24-7, molecular weight = 102.09 g/mol, δ = 1.08 g/ml) and dried over 4 $\AA$ molecular sieve. The solvent was stored inside the glovebox in a sealed 25 ml round bottom Schlenk flask. The Schlenk flask was dried in an oven before use and the solution was filled into the flask under argon atmosphere.

PAMAM$-NH_2$ dendrimer (G5) emanating from an ethylenediamine core and terminated by 128 amino groups was purchased from Sigma-Aldrich. It was delivered as a 5 wt. % solution in methanol.

PBS-buffer (**P**hosphate **B**uffered **S**aline solution, 10 mM, adjusted to pH 7.4) was composed as follows:

c(NaCl)	137.0 mM	(8 g, 58.44 g/mol)
c(KCl)	2.7 mM	(0.2 g, 74.55 g/mol)
$c(Na_2HPO_4 \cdot 2H_2O)$	10.0 mM	(1.78 g, 178.01 g/mol)
$c(KH_2PO_4)$	2.0 mM	(0.27 g, 136.09 g/mol)

A stock solution with 100 mM PBS-buffer was prepared in advance. This solution was diluted on demand. The solution was prepared using sf-water.

N,N-Diisopropylethylamine (DIPEA) was purchased from Sigma Aldrich (CAS 7087-68-5; molecular weight = 129.25 g/mol; ρ = 0.742 g/ml; Biotech grade, 99.5 %)

N-Ethylmorpholine (NEM) was purchased from ABCR GmbH & Co. KG (Karlsruhe, Germany) (CAS 100-74-3; molecular weight = 115.17 g/mol; ρ = 0.905 g/ml)

12 Surface Functionalizations

General remarks concerning handling and preparation:

- **Teflon forceps** were always used to handle wafers, glass slides and QCM resonators to prevent scratches upon their sensitive surfaces.
- **Surfaces are prone to contamination** from laboratory air, thus
  - they were handled in a large plastic basin flooded with argon
  - solvent exchanges, in vials containing wafers, were always performed using pipets; no tilting into a basin was performed, because the surfaces would be exposed to air. Therefore, as soon as one solvent was sucked out of a vial, it was immediately replaced by the next solvent.
  - Desiccators and round bottom flasks containing freshly oxidized or coated substrata were always opened in argon.

12.1 Substrata Cleaning and Oxidation

Substrata surfaces were cleaned from organic contaminations, and for the binding of the silane reagent, provided with a sufficient amount of hydroxyl groups by oxidation. This was achieved by exposing them to half-concentrated nitric acid solution at room temperature. Substrata dependent treatment peculiarities are addressed below:

Silicon wafers, single-side and double-side polished, were stored within diluted nitric acid solution for at least two weeks. Sonication in diluted nitric acid solution for 30 minutes, as it was performed in earlier works, was found to be insufficient. The silicon wafers were stored as follows:
Single-side polished wafers were placed into little snap vials (V = 5 ml) containing 1 ml of acid with the polished side facing the acid. Double-side polished wafers were deposited in a skew, upright position in larger snap vials (V = 10 ml) filled with 8 ml of acid. The snap vials were closed with the appropriate lids and stored at room temperature until needed. Yellow-brownish vapours developed in some snap vials, most probably in those, which contained wafers with a high amount of contamination.

Prior to silanisation neutralization was accomplished as follows:
The single-side polished wafers were transferred from the snap vials into a large petri-dish filled with sf-water. This step was found to be very economic and time-saving in neutralizing large quantities of wafers, since the major part of acid was removed at once. Then, new snap vials were filled with 1 ml of sf-water and the wafers were distributed into these. Rinsing was supported by an ultrasonic bath for 5 min. Sf-water exchange and ultrasonication (3 min per cycle) was continued until the pH of the rinsing solution was not lower than pH 6. The freshly oxidized and neutralized wafers were then retreated from the water under argon. Large amounts of water were removed by holding the wafer in a tilted position touching a filter paper with the bottom edge. They were then placed inside a petri-dish, facilitated with a filter paper. This petri-dish was deposited inside a desiccator provided with a drying agent (silica beads) and put under vacuum by a diaphragm pump.

The rectangular double-side polished wafers were transferred from the snap-vials filled with acid into new snap vials filled with sf-water, just as the single-side polished wafers. Sf-water exchange and ultrasonication (3 min per cycle) was carried out until the pH of the rinsing solution was not lower than pH 6. These wafers were then retreated from the vials under argon, and after contacting the bottom edge with a filter paper in order to remove most of the water, mounted to a teflon ring. The teflon ring, which was used for this purpose, is presented in Figure 12.1. It is designed to enable drying and silanisation in an upright position. Its diameter is 5 cm, it has 14 slits (each about 3 mm in depth) and the inner hole provides space for a magnetic stirrer. Two perforations, on opposing sides, were drilled into the ring for the fixation of two sticks to make transport easier. Unfortunately, the sticks did not last and became loose. Transfer was then performed by long forceps. The teflon ring was ordered and produced at the Department of Precision Mechanical Work at the University of Regensburg.

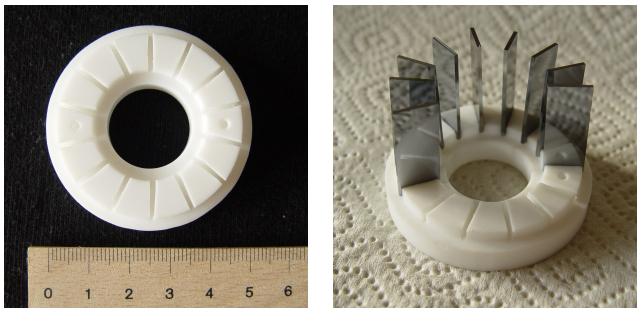

(a) (b)

Figure 12.1: a) top view of the teflon ring used for rectangular double side polished wafers
b) teflon ring with 8 rectangular wafers

The ring was placed into a desiccator. The desiccator (drying agent: silica beads) was closed, and by means of a diaphragm pump, a vacuum was generated.
The drying process was carried out until no water was observed on top of the surfaces with the naked eye. This procedure can take up to one hour depending on how many wafers need to be dried. The desiccator was opened under argon to prevent contaminations from the laboratory air and the substrata were directly introduced into the silanisation process as described in the next part.
Remark: Wafers were never stored in sf-water containing 0.1 w % of NaN_3. Prolonged storage in sf-water led to an increased hydrophobicity of the surfaces as determined by contact angle analysis, the most probable cause being the adsorption of contamination.

Glass slides were treated just like the silicon wafers.

QCM resonators were observed to loose their top SiO_2 layer when exposed to nitric acid solution for too long. Therefore, organic contaminations were removed by successive sonication in acetone, toluene, acetone again, ethanol, and sf-water. QCM resonators can not be sonicated in snap-cap vials because the multiple contacts with the glass bottom, caused by the vibrations, eliminate the electrodes on the resonator. Therefore, a teflon resonator holder, similar to the one available from Q-Sense (Västra Frölunda, Sweden) was made at the Department of Precision Mechanical Work at the University of Regensburg (presented in Figure 12.2).

Figure 12.2: QCM resonator holder, available from Q-Sense (Västra Frölunda, Sweden) Photo was taken by MSc. M. Eichler

This holder, capable of accommodating five resonators at once, was placed into a beaker filled with the appropriate solvent. After the cleaning procedure the resonators were sonicated in nitric acid for 30 minutes at room temperature, the solution being renewed after 15 minutes.

They were then immediately washed neutral by dipping the holder twice into two beakers filled with sf-water to remove large amounts of acid. Sf-water exchange and ultrasonication (3 min per cycle) was then carried out until the pH of the rinsing solution was not lower than 6. QCM resonators may not be dried in a desiccator since it was noticed by MSc. M. Eichler to influence the vibration characteristics negatively. Thus, as a first step, large amounts of water were removed by placing the holder onto a filter paper. Thereafter the holder was thoroughly dried in a nitrogen stream and four baths of dry toluene (plus ultrasonic bath) before placing it into the silanisation solution.

Silica spheres were obtained in bags filled with inert gas. The preparation technique of the spheres and the handling thereafter makes a cleaning procedure and oxidation unnecessary. They were silanised without prior oxidation or cleaning.

Silica particles need to be separated from washing or reagent solutions by centrifugation. Centrifugation was always performed for 5 minutes at 2300 U/min. Silica particles were dispersed in nitric acid solution and left therein over night. The next day they were washed neutral by numerous sf-water washing cycles utilizing the ultrasonic bath (5 min per cycle) and suspension by a glass rod. Depending on the amount of silica at least 8 washing cycles are advised. The final pH of the supernatant was aimed to be between pH 5 - 6.

Silica beads were cleaned and oxidized in the same way as silica particles with the exception that less water washing cycles were needed because of the lower specific surface area of the beads and their non-porous character.

After acid removal silica beads and particles were dried in vacuum using the membrane and thereafter the oil pump. Exposure to laboratory air was avoided at all times. Thus, the round bottom flasks were always opened in argon atmosphere.

12.2 Silanisation

- All glassware, which came in contact with silanes during the preparation process, was cleaned in a base bath (potassium hydroxide 20 g/L, 70 % 2-propanol and 30 % water; hydroxide removes adhering silanes) over night, neutralized by subsequent deposition in a hydrochloric acid bath, and rinsed with water. Then it was stored in an oven at 110 °C until use.
- All silanisation reactions were performed under inert argon atmosphere in absolute

toluene to prevent silane polymerization induced by air moisture.

- Storage - sensitive issue: Functionalized substrata were always placed in appropriate containers and then inside plastic bags filled with argon and sealed with a foil heat sealer to prevent contamination. Storage in a desiccator is not recommended since laboratory air may intrude and cause alternations of the surface characteristics by contamination.
  - single-side polished wafers were individually put into the wells of 24-well plates
  - rectangular double-side polished wafers were put upright into half-micro cuvettes for photometers, not touching the silanised surfaces
  - QCM resonators were put into the boxes they were delivered in
  - beads, spheres and particles were filled into snap vials

Prior to substratum silanisation the demanded amount of the corresponding silane (view table 12.1 for details) was pipetted into a dry snap vial (V = 5 ml) which had already been filled with 2 ml of dry toluene. This step was carried out in the glove box under N_2 atmosphere. The snap vial was sealed with a lid and remained there till needed.
(For the sake of convenience a stock of dry snap vials was deposited within the glove box. The stock was prepared by heating the snap vials and placing them into a bottle facilitated with a drying agent.)

Depending on the substrata and the type of silane different techniques were applied for the coating procedure. These treatment peculiarities are explained below. Regarding the silane type, silanisation with methoxy- and ethoxy silanes was performed at elevated temperatures, whereas silanisation with trichlorosilanes was conducted at room temperature.

Coating **silicon wafers** and **glass slides** at **room temperature** was performed as follows:

A large plastic basin was flooded with argon and filled with a desiccator, a glass rod, a beaker containing the amount of dry toluene needed, and a glass pipette.
When coating **single-side polished wafers** or **glass slides** an appropriate petri dish with lid had to be added to the basin. If rectangular **double-side polished wafers** were coated a glass beaker with a lid large enough to be facilitated with the teflon ring and its 14 upright wafers as shown in Figure 12.1 had to be added. The substrata were transferred from the desiccator (opened under argon), where they were dried in, into the petri dish or glass beaker, respectively, within the basin.
Subsequently the earlier prepared silane solution within the glove box was taken out and opened in the argon flooded basin. The silanising solution was extracted by a pipette and dispensed into the beaker filled with dry toluene. Thorough mixing was done by a glass rod. In order to prevent the wafers or glass slides from moving the mixture was then poured very gently into the petri dish or the beaker, respectively. The reaction vessel was closed with a glass lid, placed inside the desiccator (drying agent: silica beads) and left within the argon basin for the required time.
After silanisation the single-side polished wafers were put into snap vials priorly filled with the first rinsing solution to remove excess silane. This was also done for the rectangular wafers and glass slides.
Caution: In case of the rectangular wafers one has to take care not to invert them during the transfer!! The edge which was jammed in the teflon ring has an irregular coating and its position has always to be kept in mind, especially for later analytical characterization.
Rinsing was performed with different solutions, depending on the silanisation reagent. Each rinsing cycle was supported by ultrasonication for 5 minutes.

Coating **silicon wafers** and **glass slides** at **elevated temperature** was performed as follows:

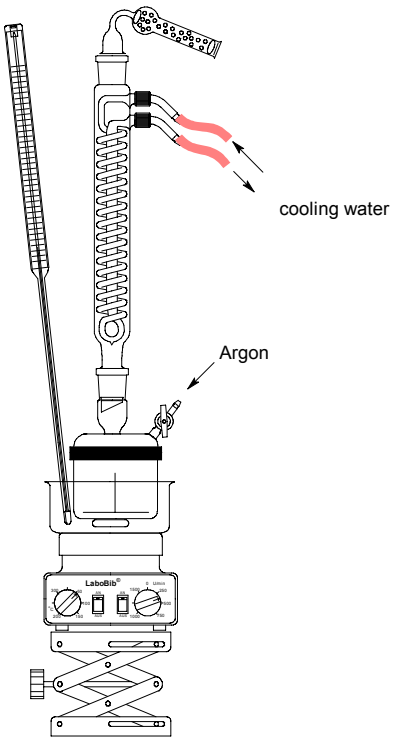

Figure 12.3: Silanisation apparatus: coating silicon wafers with methoxy- or ethoxy silanes at elevated temperature

Just like the coating at room temperature, coating at elevated temperature was started in a large basin flooded with argon. The basin was filled with the desiccator containing the substrata, a pipette and either a special coating pot for the **single-side polished wafers/glass slides** or a special coating beaker for the **double-side polished wafers**, both equipped with a magnetic stirring bar. Figure 12.3 shows the configuration of the silanisation apparatus as it was used for the coating of the single-side polished wafers/glass slides. Here the coating pot was a flat flange reaction vessel with a flat bottom. The corresponding lid had a side arm fitted with a PTFE stopcock (no ground glass stopcock because the toluene will remove the necessary vacuum grease and contaminate the coating solution!) to fill the pot with inert gas and a regular ground joint right at the top for the fixation of the reflux condenser. A glass insert was already designed for this pot in earlier works. The glass insert is a perforated plate with three little feet at the bottom to allow stirring by a magnetic stirring bar and a perpendicular glass rod in the middle pointing upwards, functioning as a handle. The area of the glass insert was large enough to provide space for about 35 wafers thereon. The glass beaker, which was designed especially for silanising **rectangular double-side polished wafers** had a ground glass joint instead of a normal rim at the top to connect the beaker to the reflux condenser and a Schlenk, on the side, very close to the top, fitted with a PTFE stopcock.

It was crucial to the silanisation process at elevated temperature that the reflux condenser was kept dry on the inside at all times. As it was found to influence the reproducibility of coating results tremendously. This was achieved by rinsing the condensers with ethanol and acetone, blowing them dry with a hair dryer and sealing them with two plugs. This arrangement protected the condenser from water deposition by atmospheric moisture inside the condenser. This implementation was observed to be indispensable to achieve uniform

coating results throughout the year (i.e., different humidities cause different water concentrations and induce differences in coating structure).

Single-side polished wafers/glass slides were transferred from the desiccator onto the glass insert of the coating pot. A magnetic stirring bar and the glass insert were placed inside the coating pot and filled with dry toluene (Volume = 150 ml) using a pipette. This was done very gently to prevent wafers to slide on top of each other. Subsequently the silane solution prepared in the glove box was taken out and opened in the argon flooded basin. The silanising solution was extracted by a pipette and dispensed into the coating pot. A gasket ring was placed on top of the flat flange and a clamping ring joined lid and pot tightly together. The coating pot was filled with argon and mounted to the reflux condenser using a teflon collar. A metal ring kept the pot in place. Heating was performed by a silicone oil bath. A gentle temperature rise is recommended to prevent a sudden vigorous behaviour of the solution leading to an overlapping of the wafers. The argon flooding was stopped at elevated temperature.

Double-side polished wafers were transferred within the teflon ring into the special beaker. The beaker was facilitated by a tiny magnetic stirrer. Dry toluene was poured gently into the beaker using a pipette. Thereafter, the silane solution was added. The beaker was then mounted to the appropriate reflux condenser using a teflon collar and heated by a silicone oil bath.
After the heating period the oil bath was removed. The apparature was left to cool until the coating solution turned lukewarm or cooler. In the meantime new vials were prepared with the appropriate rinsing solution. Wafers were retrieved form the coating solution and transferred directly into the rinsing solution. Rinsing was performed with different solutions, depending on the silanisation reagent. Each rinsing cycle was supported by ultrasonication for 5 minutes each.
After the removal of excess silanisation reagent, the wafers were blown dry in an argon or nitrogen stream.

QCM resonators were coated just like the double-side polished wafers but using the special teflon holder for QCM resonators as shown in Figure 12.2. At elevated temperatures a tiny magnetic stirring bar was added to the beaker. The magnetic stirrer was not positioned in the centre of the holder but next to it. After the removal of excess silanisation reagent, the sensor crystals were blown dry in an argon or nitrogen stream.

Silica particles, **spheres** and **beads** were coated in glass equipment of different size: 10 ml round bottom vessels for silica spheres, 50 ml round bottom Schlenk vessels for particles and

250 ml round bottom vessels for beads. The substrata, meant to be coated, a pipette for the dry toluene, a pipette for the silane, and a dry round bottom Schlenk flask equipped with a magnetic stirring bar were deposited in a basin flooded with argon. The desired substratum was scooped into the round bottom flask with the stirring bar and the appropriate amount of dry toluene was taken from the stock solution and added to the substratum. Thereafter, the silane from the glove box was poured to the substratum-toluene suspension. The round bottom flask was either sealed with a drying tube used for reactions performed at room temperature or mounted to one of the dry reflux condensers using a teflon collar. Stirring was minimized as much as possible. The stirrer was stopped and started in intervals since the particles and especially the beads start to grind each other eliminating the coating and changing the surface properties. In case of short reaction times a circulus magnetic stirring bar was used, but in the case of very long reaction times a laboratory shaker was used instead. Solvents were removed from the substrata by centrifugation or by using the Büchner funnel. The rotary evaporator was found to be impractical because of the grinding of the substrata.

The concentration of the silane, dependent on the substratum, is listed in Table 12.1. Linear alkyl chains in perfectly arranged SAMs were experimentally determined to occupy an area of about 21-25 $\AA^2$ [56] per each chain. Therefore, at least 3.3 - 4.2 mmol need to be used to cover an area of 500 m^2; It was not possible to use the same concentration/substratum area ratios for silica beads/spheres/particles as it was applied for wafers and QCM resonators because of the very enlarged surface areas. Wafers and QCM resonators were immersed into solutions containing silane molecules in 5000-fold excess, whereas beads, spheres and particles were treated with silane solutions of lower excess, such as a 100-fold, a 20-fold and a 0.5-fold, respectively (values are listed in Table 12.1). The area referred to for the wafers and QCM resonators includes the surfaces of the glassware which the silanisation reagent also comes into contact with. The value listed within the brackets in the fourth column of the Table 12.1 refers to the batch size used for the specific substratum.

Substratum	A	n(monolayer) [μmol]	c [mmol/L]	n-fold
Wafer/Glass slide	0.1 m^2	0.7	25 (150 ml)	5000
QCM resonator	0.05 m^2	0.4	25 (75 ml)	5000
Silica Beads	0.2 m^2/g	1.4	50 (35 g/100 ml)	100
Silica Spheres	2.8 m^2/g	20.2	25 (100 mg/2 ml)	20
Silica Particles	500 m^2/g	4000	200 (1 g/10 ml)	0.5

Table 12.1: Silane concentrations used for the specific substratum

12.3 Self-Assembled Monolayer (SAM-X) Preparation

- All snap vials used in combination with dry solvents were dried in an oven at 110°C before use.
- Substrata were always handled within a large plastic basin flooded with argon.
- The removal of physisorbed silanes and reagents was always supported by using the ultrasonic bath for 5 minutes in each step.

12.3.1 SAM-NH_2 including SAM-Br and SAM-N_3

Two types of SAM coatings bearing terminal amino groups were prepared. The difference between these two coatings is the hydrocarbon chain length connecting the terminal group with the anchoring unit.

SAM-C_3-NH_2

3-**A**mino**p**ropyl**t**ri**m**ethoxy**s**ilane (**APTMS**, 96 %, molecular weight = 179.29 g/mol, ρ = 1.01 g/ml, abcr AB110910, CAS 13822-56-5) was used as received to prepare the surface coating with a hydrocarbon chain comprising 3 methylene units.
Silanisation was performed from dry solvent without the addition of extra water, only with the thin water film left from neutralization, in order to obtain as thin organic films as possible. The substrata were heated in an anhydrous toluene solution containing the appropriate amount of silane for the particular substratum (listed in Table 12.1) at 110 °C for 1 h. Silanisation was completed after the temperature was raised up to 130°C (this temperature refers to the temperature regulation at the silicone oil bath!) for further 15 min. Excess silane was removed by sonicating the substrata twice in toluene and once in chloroform.

SAM-C_{11}-NH_2

11-Aminoundecylsiloxane monolayers comprising 11 methylene units between the head group and the silane anchor were prepared using a three step reaction protocol published by Balachander and Sukenik as a guideline [145]:

The *first step* in the reaction sequence is the preparation of a surface coating terminated by bromine (**SAM-Br**) groups. Substrata were exposed to a solution of dry toluene containing the appropriate amount of 11-bromoundecyltrichlorosilane (BUTS; 97 %, molecular weight = 368.64 g/mol, ρ = 1.26 g/ml, abcr AB110910, CAS 79769-48-5, amber in colour) (view Table 12.1). Silanisation was performed for at least 12 hours at room temperature and in the dark to prevent damage by photocatalytic degradation. Toluene was used twice and chloroform once to remove excess silane molecules. SAM-Br functionalized surfaces were stored in the dark (covered by aluminium foil).

The second step in the reaction sequence to obtain SAM-C_{11}-NH_2 coatings is the conversion of bromine into azide groups: SAM-Br precursor coated substrata were placed into a saturated solution of sodium azide (NaN_3; molecular weight = 65 g/mol) in dry DMF (0.2 g in 25 mL) for at least two days at room temperature. The preparation was carried out in a large basin filled with argon and the necessary pre-dried equipment. Afterwards, both, snap vials used for wafer and glass slide preparation, as well as round bottom flasks for the coating of particles, spheres and beads were sealed with a lid and extra parafilm and put on a laboratory shaker. Sodium azide was then removed by rinsing with water for four times. [Disposal of NaN_3 solution was achieved by adding iodine (molecular weight = 253.8 g/mol) and sulfide to the solution. The following reactions take place: $S_2^- + I_2 \longrightarrow S + 2\,I^-$ followed by the reaction of $S + 2\,N_3^- \longrightarrow S_2^- + 3\,N_2$. In summary iodine reacts with azide to iodide and nitrogen.]

The third step is the reduction of the azide into amino groups: SAM$-N_3$ coated substrata were treated with a saturated $LiAlH_4$ solution in pre-dried tetrahydrofuran (0.2 mol/L) for one day at room temperature. Only the clear supernatant was used for reducing the azide-terminated surface. The substrata were cleaned by washing once with 10 % HCl, twice with a diluted HCl solution (0.1 mol/L) and several times with water. No triethylamine was used to support the conversion of -NH_3^+ into -NH_2.

Complementary, reduction was also achieved using 100 mg of $SnCl_2$ in 20 ml methanol.

12.3.2 SAM-Py

The preparation of 11-(N-pyridinio)undecyl-siloxane coated surfaces is based upon the SAM-Br surface coating, replacing the terminal bromine by the pyridine ring via a nucleophilic substitution. SAM-Br (for preparation details see subsection 12.3.1) functionalized surfaces were covered by pure pyridine (95%, Sigma Aldrich). The pyridine was dried over potassium hydroxide (KOH, 30g/kg) and distilled (main fractions at 74 °C and 78-75 °C (n_{lit} = 1.510, n_{exp} = 1.508)). Thereafter, it was filled back into the stock solution bottle and facilitated with molecular sieve (4 $\AA$). Pyridine was left upon the substrata for at least 12 hours in the dark, afterwards, the temperature was raised up to 80 °C and left for additional 3 hours. Surface cleaning was performed using acetonitrile twice and dichloromethane once.

12.3.3 SAM-COOH including SAM-CH=CH_2

Carboxylic acid-bearing SAMs were prepared on the basis of a reaction protocol published by Liu et al. [107]. The protocol was optimized regarding the oxidation condition, as well as the cleaning procedure.
The substrata were exposed to a solution of dry toluene containing the appropriate amount of 7-oct-1-enyl-trichlorosilane (OeTS; 95 % with 10-30 % isomers, CAS 52217-52-4, molecular weight = 245.65 g/mol, ρ = 1.07 g/ml), listed in Table 12.1. Silanisation was performed for 3 hours at room temperature. Excess silane was removed by sonicating the substrata twice in toluene and once in chloroform. Oxidation of the terminal alkene bond was achieved with a 25 mmol/L potassium permanganate ($KMnO_4$, molecular weight = 158.03 g/mol) solution prepared with 0.1 mol/L diluted sulfuric acid (H_2SO_4, diluted from concentrated sulphuric acid 96 % 18 M). Oxidation was performed for 10 min at room temperature. After removing the oxidation solution, the substrata were sonicated twice in 0.1 mol/L H_2SO_4 solution, twice in 0.3 mol/L sodium bisulfite ($NaHSO_3$) solution for manganese dioxide (MnO_2) removal, once in 0.1 mol/L HCl solution, and several times in water until the cleaning solution was no longer acidic. Afterwards no basic solution was used to support the conversion of -COOH into COO^-.

12.3.4 SAM-SO_3H including SAM-$SCOCH_3$

This surface coating was prepared after the instruction published by J. J. Shyue et al. [86]. Surfaces coated with the precursor SAM-Br (for preparation details see subsection 12.3.1) were the starting point for this surface functionalisation. The terminal bromine was substituted by a thioacetate ion using potassium thioacetate salt. The conversion was performed in the dark using a saturated potassium thioacetate (molecular weight = 114.3 g/mol) solution in dry DMSO at 80 °C for 24 hours. Excess reagent was removed by rinsing twice with DMSO and triple times with sf-water. The subsequent oxidation of the terminal thioester

into the sulfonate group was achieved by immersing the samples into a saturated solution of oxone (2 $KHSO_5 \cdot KHSO_4 \cdot K_2SO_4$; supplier: Sigma Aldrich, potassium hydrogen monopersulfat) in water at room temperature. Excess reagent was removed by rinsing triple times with sf-water.

12.3.5 SAM-PEG (reference)

The substrata were heated in an anhydrous toluene solution containing the appropriate amount of N-(Triethoxysilylpropyl)-O-polyethylene oxide urethane
$((OEt)_3Si-(CH_2)_3-NH-CO-(OCH_2CH_2)_5-OH)$
(PEGTES, molecular weight = 485.64 g/mol, ρ = 1.09 g/ml, abcr AB111458, CAS 37251-86-8) listed in Table 12.1, at 125 - 135 °C for 2 hours. Toluene was used twice and chloroform once to remove excess silane molecules.

12.3.6 SAM-CH_3 (reference)

A surface coating bearing terminal methyl groups was prepared by exposing the substrata to a solution of dry toluene containing the appropriate amount of n-octyltrichlorosilane (OTS, molecular weight = 247.67 g/mol, ρ = 1.07 g/ml, abcr AB139887, CAS 5283-66-9) listed in Table 12.1. Silanisation was performed for at least 12 hours at room temperature. Toluene was used twice and chloroform once to remove excess silane molecules.

12.4 Immobilization of PAMAM-NH_2

PAMAM$-NH_2$ (G5) dendrimers were purchased from Sigma-Aldrich, manufactured by Dendritech®. Table 12.2 summarizes the characteristics of this particular dendrimer and its stock solution.
Methanol was removed from the dendrimer solution by vacuum. A pale yellow, hygroscopic syrup of dendrimer formed at the flask bottom. The dendrimers were redissolved, dependent on the reaction, either in dry DMSO or dry DMF supported by an ultrasonic bath for 10 min. Round bottom flasks containing dendrimers were always opened in argon atmosphere to avoid contact with air and room humidity.

PAMAM$-NH_2$ (G5), ethylene diamine core	
molecular weight	28824.81 g/mol
concentration	5.0 wt. % in methanol (MeOH)
density	0.797 g/ml (at 25°C)
number of surface groups	128
received solution mass	5.0 g (brown glass bottle)
CAS-Nr.	163442-68-0

Table 12.2: Characteristics of the dendrimer stock solution PAMAM$-NH_2$ (G5)

A reasonable PAMAM$-NH_2$ concentration for the preparation of the PAMAM functionalised surfaces was evaluated after thorough recherché, calculations and considerations:
one flask of methanolic PAMAM$-NH_2$ solution (V = 6.3 ml) contains 0.25 g of PAMAM$-NH_2$ equivalent to **8.7** μmol ($5.2 \cdot 10^{18}$ molecules). The hydrodynamic radius of PAMAM$-NH_2$ is about 5.4 nm [49]. Projecting a sphere with a radius of 5.4 nm [homepage manufacturer: Dendritech©, Midland, Michigan, USA]($r_{hydrodynamic}$ = 5.7 nm by light scattering; V = 776 nm^3, density = 1.22 g/cm^3 [48]) onto a flat surface would result in a circle occupying a surface area of 22.9 nm^2 ($A = \pi \cdot r^2$). Therefore, considering ideal arrangement of the dendrimer on a surface, a maximum surface area of approximately **120 m^2** could be theoretically covered with the contents of one bottle. Taking into account that the dendrimers may not arrange in a close packing of equal spheres, but rather interpenetrate each other, and that dendrimers may even adopt a more prolate shape instead of an oblate configuration upon the surface at coating solutions of high dendrimer concentration, led to the assumption that more than one dendrimer will occupy the area of 22.9 nm^2. Furthermore, the adherence to the used glassware needs to be taken into account even though protonation was avoided to its best, as cationic dendrimers (PAMAM$-N^+H_3$) are fond of glass surfaces (Si$-O^-$).

Substratum	A	n(monolayer) [μmol]	n-fold	c(PAMAM) [mM/L]
Wafer/Glass slide	0.1 m^2	0.007	250	0.04
QCM resonator	0.05 m^2	0.004	250	0.04
Silica Beads	0.2 m^2/g	0.01/g	5	0.04
Silica Spheres	2.8 m^2/g	0.20/g	5	0.04
Silica Particles	500 m^2/g	36/g	–	—

Table 12.3: Dendrimer amounts used.

Table 12.3 summarizes the PAMAM$-NH_2$ concentration used for the functionalization of the substrata. Regarding the area of the flat surfaces, this value is an approximation taking into account all the surfaces participating such as the vials and the pipette. This was not done for beads and spheres because the area of the particles is far larger than the glass surface of the round bottom flask. In case of the wafers and glass slides 50 ml were generally prepared. For resonators 25 ml of solution. For the beads 35 g in 50 ml and spheres 500 mg in 10 ml. Particle functionalization was not performed due to the very large surface area and the exclusiveness of the dendrimer.

Immobilization of PAMAM$-NH_2$ was always carried out under argon atmosphere to prevent the protonation of the terminal amino moieties by atmospheric moisture, the reaction of the terminal amino groups with atmospheric carbon dioxide and oxidation reactions of the terminal amino groups with atmospheric oxygen.
Sterically hindered bases like DIPEA or NEM were initially added to deprotonate primary amines, but it turned out to be unnecessary for the immobilization process.
PAMAM$-NH_2$ immobilization onto model surfaces was achieved conducting two different ways. One method was to covalently bind the terminal amino groups of the dendrimers to terminal carboxylic acids of SAMs via an activation mechanism. The second method used the high reactivity of a succinic acid anhydride coating as an anchor for the fixation of PAMAM$-NH_2$. Both methods are described in the next subsection.

12.4.1 via Carboxylic Acid Groups

Mixed SAMs terminated by methyl and carboxylic acid groups were prepared by adding a mixture of the silanes n-butyltrichlorosilane (BTS; 97 %, CAS 7521-80-4, abcr AB110926,

molecular weight = 191.56 g/mol, ρ = 1.16 g/ml) and 7-oct-1-enyl-trichlorosilane (OeTS; 95 % with 10-30 % isomers, CAS 52217-52-4, molecular weight = 245.65 g/mol, ρ = 1.07 g/ml) to the substrata. This particular experiment was only conducted on wafers. Oxidation of the terminal alkene moiety was achieved as described in section 12.3.3. The concentration ratios used for BTS/OeTs were as follows 25.0 mM/0 mM, 24.2 mM/0.8 mM, 23.8 mM/1.2 mM, 22.5 mM/2.5 mM, 20 mM/5 mM, 12.5 mM/12.5 mM and 0 mM/25 mM increasing the amount of carboxylic acids from 0 %, 3 %, 5 %, 10 %, 20 %, 50 % up to 100 %.
Activation of the carboxylic acid terminated SAMs was achieved by a solution containing 100 mM 1-(3-(dimethylamino)propyl)-3-ethylcarbodimide hydrochloride (EDC; molecular weight 191.70 g/mol) and 100 mM N-hydroxysuccinimide (NHS) (molecular weight = 115.09 g/mol) in 0.1 M 2-morpholinoethane sulfonic acid (MES) buffer (adjusted to pH 5.4; without additional NaCl) for 2 hours. They were then rinsed once with MES buffer and once with anhydrous DMSO, afterwards they were immediately covered by a solution of 0.04 mM PAMAM$-NH_2$ in anhydrous DMSO for 1 hour. Physically adsorbed PAMAM was removed by rinsing three times with methanol.

12.4.2 via Anhydride Groups

The functional groups upon the surface for dendrimer anchorage were introduced by silanisaton with 3-(triethoxysilyl)propyl succinic anhydride (TESPSA; 94 %, MW = 304.4 g/mol, ρ = 1.08 g/ml, CAS 93642-68-3). Two different silanisation techniques were applied: the standard silanisation was carried out using TESPSA solution in toluene at concentrations generally used for silanisation (listed in 12.1) at 125 °C for 2 hours. For the alternative silanisation method the concentration of TESPSA was reduced taking only 1/16 of the generally used amount plus 3 molar equivalents of acetic acid anhydride (AAA) solution (molar ratio TESPSA : AAA, 1:3) in dry toluene. The solution was heated up to a temperature of 100 - 105°C for 30 min. Afterwards the temperature was raised up to 130 °C for a further 10 min. After the reaction was cooled down, excess silanisation reagent was removed by ultrasonication (5 min per rinsing cylce) using dry toluene twice and chloroform once. Silanised wafers, facilitated with this highly reactive surface, were shortly dried under vacuum, until the dendrimer solution was prepared and used directly thereafter.
The volume of dendrimer solution needed (listed in Table 12.3) was pipetted into a dry round bottom flask under argon and the solvent methanol was evaporated in vacuum. The methanol-free dendrimer was re-dissolved in dry DMSO and ultrasonicated for 10 min. Then, the dendrimer solution was poured onto the TESPSA coated substrata. They were shaken at room temperature and in inert atmosphere for one day. Physically adsorbed, unbound dendrimer was removed by rinsing twice with dry DMSO and twice with methanol supported

by a ultrasonic bath (5 min per each cycle).

12.5 Post-Modifications of tethered Polyamidoamine (PAMAM-X)

All chemical transformations on wafer samples were performed in snap vials.

12.5.1 PAMAM-Py including PAMAM-Br

PAMAM-Br as a precursor for PAMAM-Py was prepared as follows:
The implementation of bromine into PAMAM$-NH_2$ modified coatings was conducted with 4-bromobutyrylchloride (BBC; 95 %, molecular weight = 185.45 g/mol, ρ = 1.6 g/ml at 25 °C, CAS 927-58-2) in dichloromethane. In the course of the reaction between terminal amino groups and BBC forming an amide linkage, hydrogen chloride is liberated. In order to prevent the protonation of amino groups that still need to be modified, DIPEA was added. The derivatization of the coated substrata and their storage was carried out in the dark to prevent the separation of the terminal group induced by UV radiation [129]. Due to the high reactivity of the acid chloride with air humidity all steps were carried out under argon, in a large bowl flooded with the gas. BBC and DIPEA were used at a concentration of 500 mmol/L in CH_2Cl_2. DIPEA was added first, then the solvent and finally the acid chloride. Best results were achieved using this sequence of reagent addition. The reaction time was 24 hours in the dark on a laboratory shaker. Rinsing was performed using dichloromethane twice.
The subsequent transformation from PAMAM-Br to PAMAM-Py was achieved using absolute, pure pyridinium as prepared for SAM-Py (for details see section 12.3.2) under argon for 24 hours at room temperature and in the dark. After this period the temperature of the pyridine was raised up to 50 °C (resonators)/ 80 °C (wafer and beads/spheres/particles). Rinsing of the substrata was done using acetonitrile twice and chloroform once (5 min US each).

12.5.2 PAMAM-COOH

Terminal primary amino groups, not involved in dendrimer fixation, were converted into terminal carboxylic acid groups by reacting with succinic acid anhydride (p.a. grade, Merck-Schuchardt, Munich, Germany). DIPEA generally used for primary amino group deprotonation was found to be unnecessary in this case, probably due to the tertiary amines already present in the dendrimer. PAMAM$-NH_2$ coated surfaces were immersed in 100 mmol/L succinic acid anhydride (molecular weight = 100.1 g/mol) solution in dry DMSO and shaken at room temperature and in inert atmosphere for two days. Thereafter, excess reagent was

removed by sonicating (5 min each) twice in methanol and twice in DMSO.

PAMAM-COOH dendrimers prepared in solution: PAMAM$-NH_2$ (50 mg, 1.7 μmol) was dissolved in dry DMSO (8 ml) and ultrasonicated for 5 min. Succinic acid anhydride (m = 0.08 g, n = 0.8 mmol, 1:4 equivalents per dendrimer amine : BSA) were added under argon atmosphere. The mixture was stirred for 4 days, then washed and filtered in Cenricon tubes (10000 MWCO; Amicon) alternatively the yellowish solution was purified by exhaustive dialysis against deionized water, using a 10000 MWCO membrane (Spectrum Medical Industries). The retentate was concentrated by rotary evaporation. A yellow-brownish, sticky substance remained.

12.5.3 PAMAM-SO_3H

Terminal amino groups of PAMAM$-NH_2$ were converted into terminal sulfonic acid (-SO_3H) groups by reaction with 1,3-propane sultone (Aldrich, 98 %, CAS 1120-71-4, MW = 122.14 g/mol, melting point = 30 - 33 °C, ρ = 1.392 g/ml), elongating each dendrimer branch by three methylene groups. PAMAM$-NH_2$ coated surfaces were immersed into a mixture of 100 mmol/L sultone in dry DMSO. They were placed on a laboratory shaker for at least 24 hours at room temperature. Excess reagent was removed by sonicating once in DMSO and twice in methanol each time for 5 min.

12.5.4 PAMAM-CH_3

Terminal primary amino groups of PAMAM$-NH_2$, not involved in dendrimer fixation, were converted into terminal methyl groups by reaction with acetic acid anhydride (AAA), elongating each dendrimer arm by a carbonyl group. All steps were carried out under argon atmosphere. PAMAM$-NH_2$ coated surfaces were immersed in 100 mmol/L AAA in dry DMSO and placed on a flat laboratory shaker for four days at room temperature. Excess reagent was removed by sonicating twice in methanol for 5 min each.

13 Surface Characterization Methods

13.1 Electrokinetic measurements

13.1.1 Streaming Current - Flat Surfaces

The interfacial charge formation on silicon wafers functionalized with different SAMs and tethered PAMAM was determined by streaming current measurements in electrolyte solution. Measurements were carried out with an **E**lectro **K**inetic **A**nalyser (EKA - SurPASS), facilitated with an adjustable gap cell, which was kindly provided by Anton Paar GmbH (Austria). The streaming current (I_S) is generated by applying various pressure differences across a gap, formed by two pistons facing each other at a constant distance of approximately h = 100 μm. Onto each piston a silicon wafer sample is fixed using double-sided adhesive tape, as presented in Figure 13.1b. The gap (length = 20 mm; width = 10 mm) is part of an adjustable gap cell presented in Figure 13.1a.

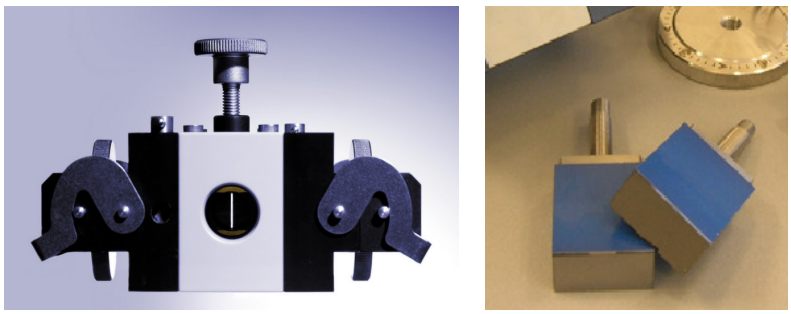

(a) Adjustable gap cell (b) Pistons of the gap cell

Figure 13.1: Adjustable gap cell used for the detection of the streaming current; Image was kindly provided by the company Anton Paar (Dr. C. Onitsch, Graz, Austria)

Transformation of the pressure-dependent streaming current data into ζ-potential data was achieved according to Smoluchowski equation

$$\zeta(I_S) = \frac{\eta}{\epsilon_0 \epsilon} \frac{L}{bh} \frac{dI_S}{dp} \tag{13.1}$$

where dI_S represents the change in streaming current, dp the pressure drop across the microchannel, η the dynamic viscosity of the electrolyte, ϵ_0 the permittivity of vacuum, and ϵ the

dielectric constant of the fluid. L, b, and h are the length, width and height of the gap cell.

The electrolyte solutions were prepared with vacuum degassed water and potassium chloride at a concentration of 1 mmol/L. Titration was performed with potassium hydroxide (0.1 mol/L) and hydrochloric acid solution (0.1 mol/L). Titrations were started at pH = 2, forcing the dendrimer to expand due to protonation. Usually measurements should be started from neutral pH to prohibit reactions supported by very low or high pH values.
A maximal pressure difference of 300 mbar was used for the zeta potential determination, and a pressure difference of 100 mbar for the rinsing procedure. The rinsing time was set to 900 s. During rinsing the new pH was adjusted and equilibrated by the machine. Generally, three independent measurements were performed from each surface modification. All measurements were conducted at room temperature and in both flow directions.

Exemplary pressure slopes at different pH values are shown in Figure 13.2 (left hand side). A linear dependence of the streaming current upon the pressure difference can be recorded ($R^2 = 0.99$). The slope is used to calculate the zeta potential. The corresponding volume flow versus pressure difference measurement is presented in Figure 13.2 (right hand side). These data are recorded first after each experimental set-up because they reveal whether the samples are properly in place or not. Furthermore, changes in streaming channel dimension can be observed by these measurements.

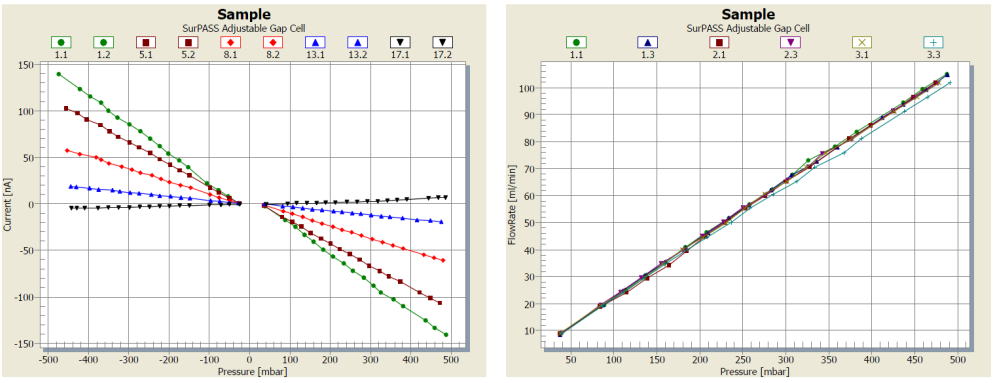

Figure 13.2: left hand side: pressure ramps (I_S versus p) at various pH values
right hand side: flow rate versus differential pressure

Remark: Streaming current measurements are performed on tiny surfaces and are easily affected by contamination, therefore a preparation in inert atmosphere is indispensable.

13.1.2 Electrophoresis - Particles

The interfacial charge of particles and spheres was determined by electrophoretic measurements performed with the Zetasizer 3000 (Malvern Inc., UK). The particle velocity v_e in dependence on the electric field strength E ($\frac{v_e}{E}$ = electrophoretic mobility) was determined by laser Doppler anemometry. The zeta potentials were calculated according to the Helmholtz-Smoluchowski equation

$$\zeta = \frac{\eta}{\epsilon_r \epsilon_0} \frac{v_e}{E} \tag{13.2}$$

where η represents the viscosity of the medium, E the electric field strength, ϵ_0 the permittivity of free space and ϵ_r the dielectric constant of the liquid. The electrophoretic measurements were conducted at 25 °C.

Silica particles and spheres were suspended in 1 mM KCl solution. Particles were measured at solid concentrations of about 0.05 % (w/w), and spheres at solid concentrations of about 0.01 % (w/w), dependening on the surface coating slight adjustments had to be made. The resulting solutions were slightly turbid after conditioning for 19 hours at room temperature, under continous stirring in a sealed vessel. Hydrochloric acid solution (0.1 M) was added to the suspension to adjust a pH value of about 2. Afterwards the pH was incrementally increased with potassium hydoxide solution (0.1 M) during zeta-potential measurement.

13.2 X-ray Photoelectron Spectroscopy (XPS)

The prepared films on silicon wafers were characterized by XPS, which provides quantitative information on the elemental composition of the coating and the electronic state (chemical environment) of each element within the coating. XPS measurements were carried out on a PHI 5600 (Physical Electronics) spectrometer equipped with a monochromatic AlK_α X-ray source ($h\nu$ = 1486.7 eV) operating at a power of 300 W. Spectra were referenced to the C(1s) peak of hydrocarbon ($\underline{C}H_x$) at 285.0 eV. Emitted photo-electrons were collected at a take-off angle of $\alpha = 45°$ from the substrate normal. Elements present on the sample were identified by a survey spectrum recoded over the energy range 0 - 1200 eV at a pass energy of 187.85 eV. High-resolution spectra were recorded at a pass energy of 23.5 eV, to identify the chemical environment of the elements. The resolution within the survey spectrum is about 1.4 eV and about 0.8 eV within the high resolution scan. Atomic concentrations were obtained by numerical integration of the peak areas using the following sensitivity factors: C(1s) = 0.314; N(1s) = 0.499; O(1s) = 0.733; Si(2p) = 0.368; S(2p) = 0.717; Cl(2p) = 0.954; Br(3d) = 1.149 (XPS is insensitive to hydrogen and helium).
The relationship between information depth and take-off angle in XPS analysis may be approximated by the following equation: information depth/nm $\approx$ 10 sin α. At an angle of

45° the information depth is about 7 nm.

Two samples from two different batches were analyzed at two different areas per each surface modification and the average was taken. Fittings were performed using XPS peak 41 (freeware). The line shape of the curves were assumed to be 100% Gaussian for SAM coatings.

Remark to be kept in mind: XPS is more sensitive to the organic groups close to the monolayer-air interface than to those near the substratum-coating interface [59].

13.3 IR-Spectroscopy

Infrared spectra of unreacted silanes and PAMAM solutions were recorded in the transmission mode using a FT/IR-610 instrument from Jasco Inc. (Japan). The spectra of these liquid samples were recorded after preparing thin films within two NaCl plates. Surface modifications on silica particles and spheres were monitored using a diffuse reflectance accessory (DRIFT; EasiDiff^{TM}) of Pike Technologies (Madison, WI, USA) in combination with the spectrometer. The spectrum of the unmodified silica particles was used as a background signal.

13.4 Contact Angle Measurement - Wettability

Static water contact angle (θ_{static}) measurements were performed on a P1 goniometer of Erna Inc. (Tokyo, Japan) by means of the *sessile drop* technique. The goniometer is equipped with an optical microscope system and back light. Water droplets (sf-water, pH = 6) with a volume of 2 μL were deposited on the wafer surface by an automatic dosing system. The measurements were performed at room temperature (298 K) in air. The angle was noted 15 s after the first surface contact. At least two silicon wafers of each batch were analysed at four different positions. Wettability measurements were routinely done to control the quality of each batch.

13.5 Atomic Force Microscopy (AFM)

Surface relief images were acquired using "Autoprobe CP" atomic force microscope (AFM) from Park Scientific Instruments Inc., equipped with a 100 μm scanner. Images were recorded in non-contact mode under ambient conditions. The surfaces were scanned with a silicon tip upon the cantilever with a spring constant of about 30 N/m. The obtained data were converted by the program ProScan (Vers. 1.1, ThermoMicroscopes, Park Scientific Instruments

& Topometrix) into the presented images. Images were taken with a size of 3 μm x 3 μm and second order flattening was applied.

13.6 Chemiluminescence Based Assay: Amino Group Detection on Flat Surfaces

A chemiluminescence based assay was conducted to detect amino groups present at wafer surfaces. This chemiluminescence assay was previously issued by Müller et al. [118]. Detailed information can be obtained from this publication and the test will only be addressed here in short notice.
Amino groups were biotinylated by immersion into a 0.1 mg/ml solution of biotin amido hexanoic acid 3-sulfo-N-hydroxysuccinimide ester (sulfoNHSLCbiotin) in borate buffer (pH = 9.0 - 9.3) for 1 h at room temperature. The biotinylating agent was removed by washing twice for 5 min in borate buffer and twice for 5 min in 50 mM Tris-buffered saline (TBS, pH 7.6) containing 0.1 % Tween 20. For detection of bound biotin, a solution containing 4.5 $\mu g/ml$ of unlabled avidin-D and 0.5 $\mu g/ml$ of horseradishperoxidaseconjugated avidinD (from Vector laboratories, in 0.05 M $NaHCO_3$, pH 8.3) was prepared in TBS-Tween 20. Incubation was performed for 30 min at room temperature, thereafter the wafer specimen were washed four times in TBS-Tween 20, and twice in TBS for 5 min each. Each wafer surface was covered with 125 μl luminol-containing ECL Western blotting detection reagent and got immediately exposed to a BioMax Light-1 X-ray film of Eastman Kodak (USA) for a specific time interval. These experiments were carried out by Andreas Eidt at the Department of Operative Dentistry and Periodontology at the University of Regensburg.

13.7 Kaiser Test: Amino Group Detection on Silica

Terminal amino groups tethered to silica particles were qualitatively analysed by performing the *Kaiser-Test* [146]:

Solution 1 (S1) 6.5 mg of potassium cyanide (KCN, molecular weight = 65.116 g/mol) was dissolved in 100 ml of water. 2 ml of this solution was transferred into a graduated flask (100 ml), which was then fully filled with pyridine.

Solution 2 (S2) 2.5 g of ninhydrin was dissolved in 5 ml ethanol and stored in the dark under inert atmosphere.

Solution 3 (S3) 40 g of phenol (molecular weight = 94.11 g/mol) was dissolved in 10 ml of ethanol.

Testing for primary amines was performed as follows: 2 - 5 mg of silica particles were placed into a snap vial. Thereafter, 4 drops of each solution was added. The snap vial was placed on a warm heating plate in the hood. The colour development is said to be complete after about 10 min. A dark blue colour formation is indicative for the presence of primary amino groups on the surface, otherwise will the mixture stay yellow. A reference test was always performed with uncoated particles.

13.8 Sum Frequency Generation (SFG) Spectroscopy

Experiments presented within this thesis were recorded by Dr. Christiane Stage using the following SFG setup:

Sum frequency generation measurements were performed using a high power Nd:YAG laser (Ekspla) with a pulse duration of ∼27 ps and a repetition rate of 10 Hz. The tunable IR is generated from a $AgGaS_2$ crystal by a difference frequency generation (DFG) process using part of 1.064 μm laser and tunable near-IR radiation (idler beam) from the optical parametric generator (BBO crystal) as inputs. Experiments were carried out in reflection geometry using the visible laser (532 nm) and the tunable infrared beam at incidence angles of ∼60° and ∼55°, respectively. These beams overlap spatially and temporally at the sample surface and generate coherent sum frequency resonance [147]. Measurements were performed in ssp-polarization configuration (s-polarized sum-frequency, s-polarized visible and p-polarized IR). The SFG signal for PAMAM-COOH and PAMAM$-NH_2$, was obtained by averaging 300 shots per point for every 2 cm^{-1}. The sum frequency spectra were normalized with respect to the incident IR and visible intensities. The SF signal was collected by a photomultiplier tube. Smoothing of data was performed using the Savitzky-Golay fit. Coatings had to be prepared on glass slides in order to perform SFG measurements, the crystalline structure of the silicon wafer is inappropriate for such measurements.

14 Testing Biological Response

14.1 Protein Adsorption - Bicinchoninic Acid (BCA)

Protein adsorption onto the surfaces was examined after their exposure to either human whole saliva or fetal bovine serum. The chemiluminescence based assay as it was performed to visualize the amino groups on top of the surfaces, explained in detail in section 13.6, could not be used, as initially planed, to determine the adsorbed amount of proteins because it is not possible to distinguish between the amino groups of the coating and the amino groups of the covering proteins. Therefore, protein adsorption was examined on modified silica beads after they were exposed to either saliva or serum using the BCA assay as described by Müller et al. in reference [118].

Solutions are greenish in colour at the beginning and turn violet in the presence of proteins. No photometric end point is reached in this reaction, therefore a standard does always need to be run along. There is no linear correlation between optical density and concentration.

Stimulated whole saliva was collected from, at minimum, three individuals in sterile 50 ml polypropylene falcon tubes (BD Falcon, USA). Informed consent was obtained from the participating people. The saliva was sterile-filtrated using low-protein binding syringe filters (Acrodisc Syringe Filters with Supor PES membrane, Pall) with decreasing pore diameter (5 μm, 1.2 μm, 0.45 μm, 0.2 μm). The obtained filtrates were pooled, portioned, and frozen. Before use and after thawing the saliva was sonicated for homogenisation.

The protein content in saliva and serum was determined by a bicinchoninic acid (BCA, Sigma Aldrich, Germany) protein assay (Sigma-Aldrich, Absorption measured at 562 nm). Calibration curves were recorded with bovine serum albumin (BSA). Two calibration curves were prepared and recorded independently. Three differently diluted solutions of each physiological solution were used to determine the protein content.

Serum and saliva proteins were adsorbed to silicon beads, characterized in section 11.1, from undiluted solutions. 5 g of modified beads were placed into seal-able glass tubes (30 ml, Schott, Germany) and incubated in 20 ml of the particular physiological solution by shaking

for 60 min at room temperature in an overhead mixer. After the adsorption process the beads were separated from the physiological solution by means of a Büchner funnel. The beads were washed to remove unbound protein three times with 20 ml of PBS solution and once with water (each time in the seal-able glass tube, with the overhead mixer for 5 min). The beads were dried in vacuum and stored in the fridge.

The protein amount on each surface was determined in three individual measurements. Thereto, 500 mg (record correct value) of vacuum-dried protein-coated beads were filled into reaction cups (Eppendorf, Germany). 1.4 ml of BCA working solution, prepared according to the manufacturer's instruction, and 100 μl of water were added after placing the cups on ice. All cups were placed at once into a water bath at 40°C for 30 min to support the reaction. They were turned up side down by hand every 5 min and cooled on ice after 30 min to stop the colour development. Extinction was measured at 562 nm.

Standard curves were prepared by adding 100 μl of the respective protein solution of known concentration to 500 mg of beads (only oxidized) and 1.4 ml of BCA working solution. The beads were added to account for a possible reduction of sensitivity of the BCA assay by adsorbed proteins to surfaces. Extinction was measured at 562 nm with a Lambda-18 UV/VIS spectrophotometer (Perkin Elmer, USA).
Blanks, 500 mg per modification but without protein, were also treated with BCA solution in order to take into consideration the contribution of the surface coating to the colour development. Instead of protein solution 100 μl of water were added to the test.

14.2 Bacterial Response

These experiments were carried out by Andreas Eidt at the Department of Operative Dentistry and Periodontology at the University of Regensburg.

14.2.1 Bacterial Adhesion

Bacterial adhesion and viability experiments were conducted on single-side modified silicon wafers, which were pre-incubated in PBS or physiological solution (saliva or serum).

Staphylococcus aureus 8325-4 was grown under constant motion and aerobic conditions in caso-bouillon for 24 h at 37 °C, whereas *Streptococcus gordonii* DL1 was grown as a stationary suspension culture in brain-heart infusion in a micro-aerophilic atmosphere (5% CO_2) at 37 °C.

Bacteria, used for the adhesion and viability assays, were washed in PBS, suspended therein at a concentration of 10^8 organisms per ml (optical density at 600 nm: $1.0 \cdot 10^8$ Cfu/ml; Cfu = colony forming units; *S. gordonii* DL1 at OD 1.19 and *S. aureus* ATCC 25923 at OD 0.90), and labelled with sulfo-NHS-LC-biotin before they were used to perform the bacterial overlay assay. [148]

Wafers were placed individually into the wells of 24-well plates. There they were incubated with 2 ml of bacterial suspension for 1 h at 4 °C. After the incubation time unattached bacteria were removed by washing with PBS. The remaining bacteria were detected by incubating the samples for 30 min in the dark with a solution of 0.5 mg/ml fluorescein isothiocyanate (FITC)- conjugated avidin-D in 50 mmol/l Tris-buffered saline (TBS, 150 mmol/l NaCl, pH 7.6) containing 0.1 % Tween 20, 1 mmol/l $CaCl_2$, and 1 mmol/l $MgCl_2$. Excess avidin-D-FITC was removed by mulitple washing cycles using TBS-Tween 20.

The fluorescence of adherent bacteria was detected by a Typhoon 9200 imaging system of Amersham Biosciences and recorded as a TIFF-file. Densitometric analysis of signals was performed using the Optimas software. Standard curves were generated by serial two-fold dilutions of the same bacterial suspensions, prepared for use in the overlay, were applied to a Minifold I dot-blot-system SRC96 of Whatman Schleicher & Schuell (Dassel, Germany) as previously described to immobilize biotinylated bacteria on nitrocellulose membranes with 0.2 mm pore size (Whatman Schleicher & Schuell). Incubation with FITC-conjugated avidin-D, washing, detection of fluorescence signals and densitometric analysis were performed analogous to the wafers as described above.

14.2.2 Bacterial Viability

Bacterial viability was tested on modified silicon wafers which were either exposed to PBS buffer, serum or saliva in advance. Conditioning in saliva/serum was carried out for 30 min. Thereafter, the silicon wafers were immersed three times into PBS for 5 min. Wafers from PBS or pre-coated by physiological solutions were then incubated for 1 hour with a bacterial suspension (identical with the ones used for the adhesion experiments mentioned at subsection 14.2.1). The samples were then rinsed once with PBS, twice in TBS (polyoxyethylen(20)-sorbitan-monolaurat; BioRad) with 0.1 % Tween (Tris Buffered Saline, 2-amino--2-hydroxymethyl-propane-1,3-diol) and twice in 0.9 % NaCl (each time for 5 min on the laboratory orbital shaker).

The viability of attached bacteria was examined by means of the BacLight bacterial viability kit L 7007 of Molecular Probes Europe (Leiden, The Netherlands). Within this kit the green

fluorescence dye (Syto 9) marks viable bacterial cells, while a red fluorescence dye (propidium iodide) detects dead bacteria. Both dyes stain nucleic acid. Syto 9 marks all cells, those with intact membranes and those with damaged ones. Propidium iodide stains only bacteria with damaged membranes. If both dyes are present fluorescence of Syto 9 is reduced.

Colonized wafers were individually incubated in 24-well plates with 0.5 ml of dye solution for 15 min in the dark at room temperature. After washing with 150 mmol/l NaCl solution for 1 min, wafers were placed on microscopy slides supplied with a thin film of immersion oil. Epifluorescence microscopy was performed utilizing an Axiovert 200M of Carl Zeiss Microimaging GmbH (Göttingen, Germany) equipped with a 20 x Plan Apochromat objective and an Axiocam MRm digital camera. Fluorescence signals on digital photographs derived from either living or dead bacteria were individually analysed by planimetry using the Optimas software. Areas exhibiting fluorescence signals of a defined threshold have been integrated and standardised to the total surface area. Viability is expressed as percent of viable cells in relation to the total number of bacteria attached. [148]

Part VI

Annex

Preparation & Characterization:

SAM-$N^{+}Me_3$

The preparation of alkyl chain based surface coatings terminated by trimethylammonium chloride moieties is based upon the SAM-Br surface coating, replacing the terminal bromide by trimethylamine via a nucleophilic substitution (preparation path **A**). Trimethylamine in ethanol (33%, 4.2 M, Sigma Aldrich) was used as received and added to the SAM-Br substrata suspended (particles) in or covered (wafer) by acetonitrile. This was performed under inert atmosphere and the substrata were stored for 7 days on a laboratory shaker (The ultamative transformation was achieved by performing the conversion in a tiny autoclave facilitated with a teflon insert at 65°C for 24 h. Unfortunately this setup is inadequate to functionalize large amounts of wafer samples). All vessels were sealed with additional parafilm to prevent trimethylamine from escaping. In summer, at very high temperatures, they were stored in the fridge. Trimethylamine solutions are strongly hygroscopic and careless preparation instantly leads to delamination of the coating due to hydroxyl ion formation. This was varified by DRIFT measurements not presented in this thesis.
A test was performed to confirm the presence of quaternary ammonium cations, which, however, was only possible on silica particles since the area is large enough and the white substratum enables the detection by the eye. Analytical method for detection: 1 g Co(II)thiocyanate $Co(SCN)_2$ in 100 ml water. In the presence of quaternary ammonium cations the solution turns turquoise, if there are no quaternary ammonium cations present the solution remains faintly pink. Sadly, I can not recall were I found that test, I clearly state that I am not the inventor of this test.
Additionally, terminal trimethylamine groups were also generated on surfaces by using the silane 3-(trimethoxysilyl)propyl-N,N,N-trimethyl-ammoniumchloride (CAS 35141-36-7, MW = 257.83 g/mol, density = 0.93 g/ml, silane 50 % in methanol); (preparation path **B**). Silanisation was performed at elevated temperature (110 °C) for 2 hours and excess silane was removed by dimethyl formamide and methanol. A wettability of 40° (37°- 45°) was recorded on wafer surfaces. No characterisitc absorption bands can be observed in DRIFT spectra from $SAM{-}N^{+}Me_3$ coated silica. DRIFT measurements are inadequate for the confirmation of this terminal group upon the surface as ammonium salt does not posses characteristic absorption bands.

Electrophoresis measurements were conducted with silica particles modified by both above mentioned methods to confirm the presence of cationic functionalities. Quaternary ammonium salts are presenting a positive charge independent of the pH of the surrounding solution.

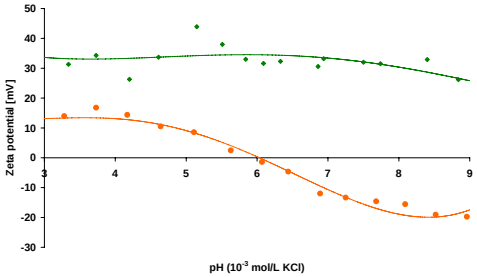

	$IEP\|_{\zeta=0}$
A $SAM{-}N^{+}Me_3$	-*
B $SAM{-}N^{+}Me_3$	6

Figure 14.1: left: ζ-potential determination in 1 mM KCl solution performed by electrophoresis on $SAM{-}N^{+}Me_3$-silica coated in two different ways. Method A: diamonds, green, Method B: dots, orange. right: Table contains iso-electric points (IEP); *out of detection limit

Figure 14.1 illustrates nicely, the problem of silanising silicous material by silanes with a positively charged component. The positively charged head group competes with the silyl moieties for the $Si{-}OH$ / $Si{-}O^{-}$ groups and reduces the amount of silane upon the surface because the positively charged head group occupies some surface sites. Loops form upon the surface and cause a deceased wettability by exposing the alkyl chains. This effect is especially strong when silanisation is performed with short chain silanes, because the van der Waals interactions among the alkyl chains are too tiny to support a parallel alignment.

PAMAM-$N^{+}Me_3$

Terminal amino groups of $PAMAM{-}NH_2$ were converted into terminal quaternary ammonium groups (-$N^{+}Me_3$ Cl^{-}) groups by reaction with
N-Chloro-betainylchloride ($Cl{-}CO{-}CH_2{-}N^{+}(Me)_3Cl^{-}$)(molecular weight: 172.1 g/mol) elongating each dendrimer branch by a -CO-CH_2- unit. $PAMAM{-}NH_2$ coated surfaces were immersed into a mixture of 100 mmol/L N-Chloro-betainylchloride and 200 mmol/L DIPEA in CH_2Cl_2 and placed on a flat laboratory shaker for three days at room temperature. Excess reagent was removed by sonicating (5 min each) twice in dichloromethane. Performing this reaction in dimethyl formamide and using N-ethyl morpholine instead of DIPEA was not successful because a bright yellow precipitate was generated.

Additionally, terminal amino groups of $PAMAM{-}NH_2$ were converted into terminal quaternary ammonium groups (-$N^{+}Me_3$ Cl^{-}) by reaction with
glycidyltrimethylammonium chloride ($OCH_2CHCH_2N^{+}Me_3Cl^{-}$; Sigma Aldich)
elongating each dendrimer branch by a -CH(OH)-CH_2- unit. $PAMAM{-}NH_2$ coated surfaces were immersed into a mixture of 100 mmol/L glycidyltrimethylammonium chloride in methanol and placed on a flat laboratory shaker for three days at room temperature. Excess

reagent was removed by sonicating twice in methanol (5 min). This conversion protocol is similar to the one reported by R.M. Crooks et al. [137]. This reaction protocol is preferred since no hydrogen chloride is liberated during the reaction.

List of Figures

List of Tables

Bibliography

[1] W. Siswomihardjo H.C. van der Mei H.-J. Busscher, M. Rinastiti. Biofilm formation on dental restorative and implant materials. *Journal of Dental Research*, 89(7):657–665, 2010.

[2] A. Herrmann H. C. van der Mei W. Norde A. K. Muszanska, H. J. Busscher. Pluronic-lysozyme conjugates as anti-adhesive and antibacterial bifunctional polymers for surface coating. *Biomaterials*, 32:6333–6341, 2011.

[3] G. Subbiahdoss P. C. Jutte J. J. A. M. van den Dungen S. A. J. Zaat M. J. Schultz D. W. Grainger H. J. Busscher, H. C. van der Mei. Biomaterial-associated infection: Locating the finish line in the race for the surface (review). *Science Translational Medicine*, 4(153):1–11, 2012.

[4] A. G. Gristina. Biomaterial-centered infection: Microbial adhesion versus tissue integration. *Science*, 237 (4822):1588–1595, 1987.

[5] S. A. M. Tofail. *Biological Interactions with Surface Charge Biomaterials*. RSC Publishing, 2012.

[6] P. Dhurjati T. K. van Dyk R. A. LaRossa S. L. Cooper C. Z. Chen, N. C. Beck-Tan. Quaternary ammonium functionalized poly(propylene imine) dendrimers as effective antimicrobials: Structure-activity studies. *Biomacromolecules*, 1:473–480, 2000.

[7] J. Dewald M. Hall G. Kallos S. Martin J. Roeck J. Ryder P. Smith D. A. Tomalia, H. Baker. A new class of polymers: Starbust-dendritic macromolecules. *Polymer Journal*, 17:117–132, 1985.

[8] N. K. Jain D. A. Tomalia A. s. Chauhan, P. V. Diwan. Unexpected in vivo anti-inflammatory activity observed for simple, surface functionalized poly(amidoamine) dendrimers. *Biomacromolecules*, 10:1195–1202, 2009.

[9] I. Sliepen M. Quirynen W. Teughels, N. van Assche. Effect of material characteristics and/or surface topography on biofilm development. *Clin. Oral Imp. Res.*, 17 (Suppl. 2):68–81, 2006.

[10] H. J. Busscher B. P. Krom A. E. J. van Merode, H. C. van der Mei. Influence of culture heterogeneity in cell surface charge on adhesion and biofilm formation by enterococcus faecalis. *Journal of Bacteriology*, 188 (7):24212426, 2006.

[11] Marion Martienssen. *Habilitationsschrift: Leistungen immobilisierter Mikroorganismen bei der Eliminierung von Schadstoffen.* PhD thesis, Martub-Luther Universität Halle, 2001.

[12] P. K. Sharma H. C. van der Mei H. J. Busscher, W. Norde. Interfacial re-arrangement in initial microbial adhesion to surfaces. *Current Opinion in Collioid and Interface Science*, 15:510–517, 2010.

[13] M. Hawton H. Schraft L. Power, S. Itier. Time lapse confocal microscopy studies of bacterial adhesion to self-assembled monolayers and confirmation of a novel approach to the thermodynamic model. *Langmuir*, 23:5622–5629, 2007.

[14] H. C. van der Mei H. J. Busscher. Physico-chemical interactions in initial microbial adhesion and relevance for biofilm formation. *Adv. Dent Res.*, 11(1):24–32, 1997.

[15] W. Norde H. C. van der Mei A. Roosjen, H. J. Busscher. Bacterial strains influencing adhesion of pseudomonas aeruginosa strains to poly(ethylene oxide) brush. *Microbiology*, 152:2673–2682, 2006.

[16] W. Norde. My voyage of discovery to proteins in flatland...and beyond. *Colloids and Surfaces B: Biointerfaces*, 61:1–9, 2008.

[17] P. M. H. Heegaard U. Boas, J. B. Christensen. Dendrimers in medicine and biotechnology - new molecular tools. *J. Mater. Chem.*, 16:3785–3798, 2006.

[18] A. Sellborn M. Andersson M. Hulander H. Elwing M. Berglin, E. Pinori. Fibrinogen adsorption and conformational change on model polymers: Novel aspects of mutual molecular rearrangement. *Langmuir*, 25(10):5602–5608, 2009.

[19] E. M. Benetti R. Konradi E. Rakhmatullina A. Mühlebach R. Zimmermann C. Werner V. Vogel M. Textor B. Pidhatika, J. Möller. The role of the interplay between polymer architecture and bacterial surfacce properties on the microbial adhesion tools polyoxazoline-based ultrathin films. *Biomaterials*, 31:9462–9472, 2010.

[20] S. C. Holman F. R. Champlin W-W-Wilson, M. M. Wade. Status of methods for assessing bacterial cell surface charge properites based on zeta-potential measurements. *Journal of Microbiological Methods*, 43:153–164, 2001.

[21] S. L. Cooper C. Z. Chen. Interaction between dendrimer biocides and bacterial membranes. *Biomaterials*, 23:3359–3368, 2002.

[22] Y. Shai. Mechanism of the binding, insertion and destabilization of phospholipid bilayer membranes by alpha-helical antimicrobial and cell non-selective membrane-lytic peptides. *Biochimica et Biophysica Acta*, 1462:55–70, 1999.

[23] F. Gaboriaud J. F. L. Duval. Progress in electrohydrodynamics of soft microbial particle interphases. *Current Opinion in Collioid and Interface Science*, 15:184–195, 2010.

[24] C. Werner M. Grunze Y.-H. M. Chan, R. Schweiss. Electrokinetic characterization of oligo- and poly(ethylene glycol) - terminated self-assembled monolayers on gold and glass surfaces. *Langmuir*, 19:7380–7385, 2003.

[25] R. Dahint G.M. Whitesides P.E. Laibinis P. Harder, M. Grunze. Molecular conformation in oligo(ethylene glycol)-terminated self-assembled monolayers on gold and silver surfaces determines their ability to resist protein adsorption. *J. Phys. Chem. B*, 102:426–436, 1998.

[26] S. Takayama R. E. Holmlin L. Yan G. M. Whitesides R. G. Chapman, E. Ostuni. Surveying for surfaces that resist the adsorption of proteins. *J. Am. Chem. Soc.*, 122:8303–8304, 2000.

[27] C. Cai G. Qin. Oxidative degradation of oligo(ethylene glycol)-terminated monolayers. *Chem. Communication*, pages 5112–5114, 2009.

[28] D. A. Tomalia G. L. Hagnauer A. T. McManus L. Balogh, D. R. Swanson. Dendrimer-silver complexes and nanocomposites as antimicrobial agents. *Nano Letters*, 1 (No. 1):18–21, 2001.

[29] H. Murata W. Wu S. B. Lee T. Kowalewski A. J. Russell K. Matyjaszewski J. Huang, R. R. Koepsel. Nonleaching antibacterial glass surfaces via 'grafting onto': The effect of the number of quaternary ammonium groups on biocidal activity. *Langmuir*, 24(13):6795–6795, 2008.

[30] S. L. Cooper C. Z. Chen. Recent advances in antimicrobial dendrimers. *Advanced Materials*, 12 (No.11):843–846, 2000.

[31] J. F. McCabe S. Imazato, R. R. B. Russell. Antibacterial activity of mdpb polymer incorporated in dental resin. *Journal of Dentistry*, 23 (3):177–181, 1995.

[32] M. A. Nordhaus J.-B. D. Green, T. Fulghum. *Science against microbial pathogens: communicating current research and technological advances*. Formatex Research Center (ISBN 978-84-939843-1-1), 2011.

[33] J. L. Thomas W. Chen, D. A. Tomalia. Unusual ph-dependent polarity changes in pamam dendrimers: Evidence for ph-responsive conformational changes. *Macromolecules*, 33:9169–9172, 2000.

[34] R. M. Crooks M. Wells. Interactions between organized, surface-confined monolayers and vapor-phase probe molecules. 10. preparation and properties of chemically sensitive dendrimer surfaces. *J. Am. Chem. Soc.*, 118:3988–3989, 1996.

[35] R. L. Juliano H. Yoo T. H. Dung, J. S. Kim. Preparation and evaluation of cholesteryl pamam dendrimers as nano delivery agents for antisense oligonucleotides. *Colloids and Surfaces A: Physicochemical and Engineering Aspects*, 313-314:273–277, 2008.

[36] M. Borkovec D. Cakara, J. Kleimann. Microscopic protonation equilibria of poly(amidoamine) dendrimers from macroscopic titrations. *Macromolecules*, 36:4201–4207, 2003.

[37] L. J. Ward W. C. E. Schofield J. P. S. Badyal C. A. Fail, S. A. Evenson. Controlled attachment of pamam dendrimers to solid surfaces. *Langmuir*, 18:264–268, 2002.

[38] L. Piehler I. Lee A. Myc I. Majoros A. K. Patri T. Thomas J. Mulé J. R. Baker Jr. A. Quintana, E. Raczka. Design and function of a dendrimer-based therapeutic nanodevice targeted to tumor cells through the folate receptor. *Pharmaceutical Research*, 19:1310–1316, 2002.

[39] R. M. Crooks Y. Niu, L. Sun. Determination of the intrinsic proton binding constants for poly(amidoamine) dendrimers via potentiometric ph titration. *Macromolecules*, 36:5725–5731, 2003.

[40] M. Miki D. Wang, T. Imae. Fluorescence emission from pamam and ppi dendrimers. *J. Colloid Interface Science*, 306:222–227, 2007.

[41] G. J. M. Koper M. Borkovec. Proton binding characteristics of branched polyelectrolytes. *Macromolecules*, 30:2151–2158, 1997.

[42] M. Muthukumar R. L. Lescanec. Configurational characteristics and scaling behavior of starbust molecules: A computational study. *Macromolecules*, 23:2280–2288, 1990.

[43] M. S. Diallo W. A. Goddard Y. Liu, V. S. Bryantsev. Pamam dendrimers undergo ph responsive conformational changes without swelling. *J. Am. Chem. Soc.*, 131:2798–2799, 2009.

[44] A. M. McDermott C. Cai M. K. Calabretta, A. Kumar. Antibacterial activities of poly(amdioamine) dendrimers terminated with amino and poly(ethylene glycol) groups. *Biomacromolecules*, 8:1807–1811, 2007.

[45] J. R. McElhanon P. M. Dentinger S. Pathak, A. K. Singh. Dendrimer-activated surfaces for high density and high activity protein chip applications. *Langmuir*, 20(5):6075–6079, 2004.

[46] H. Schönherr G. J. Vancso G. H. Degenhart, B. Dordi. Micro- and nanofabrication of robust reactive arrays based on the covalent coupling of dendrimers to activated monolayers. *Langmuir*, 20:6216–6224, 2004.

[47] L. A. Baker R. M. Crooks A. J. Ricco A. Hierlemann, J. K. Campbell. Structural distortion of dendrimers on gold surfaces: A tapping-mode afm investigation. *J. Am. Chem. Soc.*, 120:5323–5324, 1998.

[48] B. G. Orr D. R. Swanson D. A. Tomalia J. R. Baker Jr. T. A. Betley, M. M. Banaszak Holl. Tapping-mode atomic force microscopy investigation of poly(amidoamine) dendrimers: Effects of substrate and ph on dendrimer deformation. *Langmuir*, 17:2768–2773, 2001.

[49] D. Qin J. R. Baker D. A. Tomalia D. J. Meier J.Li, L. T. Piehler. Visualization and characterization of poly(amidoamine) dendrimers by atomic force microscopy. *Langmuir*, 16:5613–5616, 2000.

[50] N. Saucedo-Zeni G. Latini H. J. Gruber P. Mesquida Y. Samotskaya M. Hohage F. Cacialli S. Howorka R. Schlapak, D. Armitage. Preparation and characterization of dense films of poly(amidoamine) dendrimers on indium tin oxide. *Langmuir*, 23:8916–8924, 2007.

[51] V. V. Tsukruk. Dendritic macromolecules at interfaces. *Advanced Materials*, 10(3):253–257, 1998.

[52] J. M. J. Frechet D. C. Tully. Dendrimers at surfaces and interfaces: chemsitry and applications. *Chem. Communications*, pages 1229–1239, 2001.

[53] R. M. Crooks H. Tokuhisa. Interactions between organized, surface-confined monolayers and vapor-phase probe molecules. 12. two new methods for surface immobilization and functionalization of chemically sensitive dendrimer surfaces. *Langmuir*, 13:5608–5612, 1997.

[54] D. Drutschmann D. Blohm D. Wöhrle R. Benters, C. M. Niemeyer. Dna microarrays with pamam dendritic linker systems. *Nucleic Acids Research*, 30(2):1–7, 2002.

[55] W. T. S. Huck T. P. Sullivan. Microreview: Reactions on monolayers: Organic synthesis in two dimensions. *Eur. J. Org. Chem.*, pages 17–29, 2003.

[56] D. N. Reinhoudt S. Onclin, B. J. Ravoo. Review: Engineering silicon oxide surfaces using self-assembled monolayers. *Angewandte Chemie*, 44:6282–6304, 2005.

[57] J. Sagiv. Organized monolayers by adsorption - formation and structure of olephobic mixed monolayers on solid surfaces. *Journal of the American Chemical Society*, 102:92–98, 1980.

[58] A. Ulman. Self-assembled monolayers of alkyltrichlorosilanes: Building blocks for future organic materials. *Advanced Materials*, 2 (No. 12):573–582, 1990.

[59] George Whitesides Stephen R. Wassermann, Yu-Tai Tao. Structure and reactivity of alkylsiloxane monolayers formed by reaction of alkyltrchlorosilanes on silicon substrates. *Langmuir*, 5:1074–1087, 1989.

[60] A. Terfort G. M. Whitesides L. Yan, C. Marzolin. Formation and reaction of interchain carboxylic anhydride groups on self-assembled monolayers on gold. *Langmuir*, 13:6704–6712, 1997.

[61] H. Hoffmann T. Lummerstorfer. Click chemistry on surfaces: 1,3-dipolar cycloaddition reactions of azide-terminated monolayers on silica. *J. Phys. Chem. B*, 108:3963–3966, 2004.

[62] C. N. Sukenik R. J. Collins. Sulfonate-functionalized, siloxane-anchored, self-assembled monolayers. *Langmuir*, 11:2322–2324, 1995.

[63] B. Liedberg K. Uvdal R. Erlandsson H. Elwing I. Lundström E. T. Vandenberg, L. Bertilsson. Structure of 3-aminopropyl triethoxy silane on silicon oxide. *Journal of Colloid and Interface Science*, 147:103–118, 1991.

[64] U. S. Schubert C. Haensch, S. Hoeppener. Chemical surface reactions by click chemistry: coumarin dye modification of 11-bromoundecyltrichlorosilane monolayers. *Nanotechnology*, 19:035703, 2008.

[65] C. P. Tripp L. D. White. Reaction of (3-aminopropyl)dimethylethoxysilane with amine catalysts on silica surfaces. *Journal of Colloid and Interface Science*, 232:400–407, 2000.

[66] T. Cao S. O. Salley K. Y. S. Ng A. Wang, H. Tang. In vitro stability of organosilane self-assemble monolayers and multilayers. *Journal of Colloid and Interface Science*, 291:438–447, 2005.

[67] M. Sekar C. N. Sukenik Y. Barness, O. Gershevitz. Functionalized silanes for the preparation of siloxane-anchored monolayers. *Langmuir*, 16:247–251, 2000.

[68] K. Uosaki S. Ye, S. Nihonyanagi. Sum frequency generation (sfg) study of the ph-dependent water structure on a fused quartz surface modified by an octadecyltrichlorosilane (ots) monolayer. *Phys. Chem. Chem. Phys.*, 3:3463–3469, 2001.

[69] S. Prakash P.J. Majewski, T. M. Fuchs. Synthesis and properties of silane-based self-assembled-monolayers onto silica particles. *Materials Forum*, 29:489–493, 2005.

[70] C. Werner C. Bellmann H.-J. Jacobasch, F. Simon. Elektrokinetische meßmethoden: Grundlagen und anwendungen. *Technisches Messen*, 63:439–446, 1996.

[71] R. J. Hunter L. K. Koopal J. Lyklema ©IUPAC A. V. Delgado, F. González-Caballero. Measurement and interpretation of electrokinetic phenomena. *Pure Applied Chemistry*, 77 (10):1753–1805, 2005.

[72] J. Lyklema. Surface charges and electrokinetic charges: Distinctions and juxtapositions. *Colloids and Surfaces A: Physicochemical and Engineering Aspects*, 376:2–8, 2011.

[73] A. L. Cordeiro N. Rein C. Werner J. F. L. Duval, R. Zimmermann. Electrokinetics of diffuse soft interfaces. iv. analysis of streaming current measurements at thermoresponsive thin films. *Langmuir*, 25(18):10691–10703, 2009.

[74] G. Kellner K. Stana-Kleinschek V. Ribitsch M. Reischl, S. Köstler. Oscillating streaming potential measurement system for macroscopic surfaces. *Review of Scientific Instruments*, 79:113902(1–6), 2008.

[75] J. Lyklema. Molecular interpretation of electrokinetic potentials. *Current Opinion in Collioid and Interface Science*, 15:125–130, 2010.

[76] G. Gauglitz C. Werner R. Zimmermann, T. Osaki. Combined microslit electrokinetic measurements and reflectometric interference spectroscopy to study protein adsorption processes. *Biointerphases*, 2(4):159–164, 2007.

[77] R. Zimmermann S. Dukhin-H.-J. Jacobasch C. Werner, H. Körber. Extended electrokinetic characterization of flat solid surfaces. *Journal of Colloid and Interface Science*, 208:329–346, 1998.

[78] D. Li Y. Gu. The zeta-potential of glass surface in contact with aqueous solutions. *Journal of Colloid and Interface Science*, 226:328–339, 2000.

[79] B. J. Kirby A. C. Barbati. Soft diffuse interfaces in electrokinetics - theory and experiment for transport in charged diffuse layers. *Soft Matter*, 8:10598–10613, 2012.

[80] M. Kaufmann C. Werner-J. F. L. Duval R. Zimmermann, D. Kuckling. Electrokinetics of a poly(n-isopropylacrylamid-co-carboxyacrylamid) soft thin film: Evidence of diffuse segment distribution in the swollen state. *Langmuir*, 26(23):18169–18181, 2010.

[81] T. Kratzmüller C. Werner, R. Zimmermann. Streaming potential and streaming current measurements at planar solid/liquid interfaces for simultaneous determination of zeta potential and surface conductivity. *Colloids and Surfaces A: Physicochemical and Engineering Aspects*, 192:205–213, 2001.

[82] U. Freudenberg C. Werner R. Zimmermann, S. Bartsch. Electrokinetic analysis to reveal composition and structure of biohybrid hydrogels. *Analytical Chemistry*, 84:9592–9595, 2012.

[83] L. Scheideler M. Haupt-J. Geis-Gerstorfer G. Schmalz S. Ruhl R. Müller F. Rupp M. Eichler, V. Katzur. The impact of dendrimer-grafted modifications to model silicon surfaces on protein adsorption and bacterial adhesion. *Biomaterials*, 32:9168–9179, 2011.

[84] M. Takahashi H. Iwasa H. K. Asuha, O. Maida. Nitric acid oxidation of si to form ultrathin silicon dioxide layers wiht a low leakage current density. *J. Applied Phys.*, 94:7328, 2003.

[85] G. J. M. Koper M. Borkovec B. P. Cahill, G. Papastavrou. Adsorption of poly(amido amine) (pamam) dendrimers on silica: Importance of electrostatic three-body attraction. *Langmuir*, 24:465–473, 2008.

[86] T. Nakanishi Y. Masuada K. Koumoto C. N. Sukenik J-J. Shyue, M. R. De Guire. Acid-base properties and zeta potentials of self-assembled monolayers obtained via in situ transformations. *Langmuir*, 20:8693–8698, 2004.

[87] P. J. Scales P. G. Hartley, I. Larson. Electrokinetic and direct force measurements between silica and mica surfaces in dilute electrolyte solutions. *Langmuir*, 13:2207–2214, 1997.

[88] Carsten Werner Ralf Zimmermann, Nelly Rein. Water ion adsorption dominates charging at nonpolar polymer surfaces in multivalent electrolytes. *Physical Chemistry Chemical Physics*, 11:4360–4364, 2009.

[89] S. Barany. The role of interfaces in environmental protection (isbn 1-4020-1478-3). *Springer*, 24, 2002.

[90] L. T. Zhuravlev. Concentration of hydroxyl groups on the surface of amorphous silicas. *Langmuir*, 3:316–318, 1987.

[91] L. Kostenko V. Zaitsev J. Fraissard T. Kovalchuk, H. Sfihi. Preparation, structure and thermal stability of onium- and amino-functionalized silicas for the use as catalysts supports. *Journal of Colloid and Interface Science*, 302:214–229, 2006.

[92] C. P. Tripp S. M. Kanan, W. T. Y. Tze. Method to double the surface concentration and control the orientation of adsorbed (3-aminopropyl)dimethylethoxysilane on silica powders and glass slides. *Langmuir*, 18:6623–6627, 2002.

[93] T. J. Ritter D. E. Penny. Kinetic study of the reaction between carbon dioxide and primary amines. *J. Chem. Soc., Faraday Trans. 1*, 79:2103–2109, 1983.

[94] W. Chen E. A. Smith. How to prevent the loss of surface functionality derived from aminosilanes. *Langmuir*, 24:12405–12409, 2008.

[95] T. Kratzmüller R. Schweiss C. Werner T. Osaki, R. Zimmermann. Polyanion protection of silane bonds to silicon oxide revealed by electrokinetic measurements. *Langmuir*, 20:524–527, 2004.

[96] George Socrates. *Infrared and Raman Characteristic group frequencies (Tables and Charts)*. John Wiley & Sons, LTD ISBN 0-471-85298-8, 2001, 3rd Edition.

[97] P. Schunk T. Schimmel D. F. S. Petri, G. Wenz. An improved method for the assembly of amino-terminated monolayers on sio2 and the vapor deposition of gold layers. *Langmuir*, 15:4520–4523, 1999.

[98] R. Morris R. J. Composto P. Ducheyne M. H. Lee, D. A. Brass. The effect of non-specific interactions on cellular adhesion using model surfaces. *Biomaterials*, 26:1721–1730, 2005.

[99] H. Höcker D. Klee, J. Böing. Surface modification of titanium for improvement of the interfacial biocompatibility. *Mat.-wiss. u. Werkstofftech.*, 35 (No. 4):186–191, 2004.

[100] H. Yim M. D. Foster R. H. Wieringa A. J. Schouten V. Erb M. Stamm A. Heise, H. Menzel. Grafting of polypeptides on solid substrates by initiation of n-carboxyanhydride polymerization by amino-terminated self-assembled monolayers. *Langmuir*, 13:723–728, 1997.

[101] K. Lützow C. Werner T. Groth N. Faucheux, R. Schweiss. Self-assembled monolayers with different terminating groups as model substrates for cell adhesion studies. *Biomaterials*, 25:2721–2730, 2004.

[102] Einführung in die apparativen methoden in der organischen chemie von p. kreitmeier (uni regensburg 2001).

[103] D. Degenhardt H. Möhwald P. Quint R. Maoz, J. Sagiv. Hydrogen-bonded multilayers of self-assembling silanes: structure elucidation by combinded fourier transform infrared spectroscopy and x-ray scattering techniques. *Supramolecular Science*, 2:9–24, 1995.

[104] D. J. Gaspar N. Jaitly Y. Dubowski Q. Li B. J. Finlayson-Pitts T. M. McIntire, A. Scott Lea. Unusual aggregates from the oxidation of alkene self-assembled monolayers: a previously unrecognized mechanismfor sam ozonolysis. *Phys. Chem. Chem. Phys.*, 7:3605–3609, 2005.

[105] G. Reiter U.P. Fringeli J. Matijašević, N. Hassler. In situ atr ftir monitoring of the formation of functionalized mono-and multilayers on germanium substrate: from 7-octenyltrichlorosilane to 7-carboxylsilane. *Langmuir*, 24:2588–2596, 2008.

[106] T. Saito N. Shirahata A. Hozumi, H. Taoda. Formation of aldehyde- and carboxy-terminated self-assembled monolayers on sio2 surfaces. *Surf. Interface Anal.*, 40:408–411, 2008.

[107] F.K. Mante S.L. Wunder G.R. Baran Q. Liu, J. Ding. The role of surface functional groups in calcium phosphate nucleation on titanium foil: a self-assembled monolayer technique. *Biomaterials*, 23:3103, 2002.

[108] J. Sagiv R. Maoz. Penetration-controlled reactions in organized monolayer assemblied. 1. aqueous permanganate interaction with monolayer and multilayer films of long-chain surfactants. *Langmuir*, 3:1034–1044, 1987.

[109] Joyce M. Eldridge A. Paul Krapcho, James R. Larson. Potassium permanganate oxidations of terminal olefins and acetylenes to carboxylic acids of one less carbon. *J. Org. Chem.*, 42 (23):3749–3753, 1977.

[110] Bernd Zeeh Manfred Hesse, Herbert Meier. *Spektroskopische Methoden in der organischen Chemie*. Thieme, 2002.

[111] V. S. Chang D. G. Lee, S. E. Lamb. Carboxylic acids from the oxidation of terminal alkenes by permanganate: nonadecanoic acid. *Org. Synth.*, 7:397, 1990.

[112] Chaim N. Sukenik Olga Gershevitz. In situ ftir-atr analysis and titration of carboxylic acid-terminated sams. *Journal of American Chemists Society (JACS)*, 126:482–483, 2004.

[113] W.-H.Chuang J.-C. Lin. Synthesis, surface characterization, and platelet reactivity evaluation for the self-assembled monolayer of alkanethiol with sulfonic acid functionality. *J. Biomed Mater Res*, 51:413–423, 2000.

[114] C. N. Sukenik I. Aped, Y. Mazuz. Variations in the structure and reactivity of thioester functionalized self-assembled monolayers and their use for controlled surface modification. *Beilstein Journal of Nanotechnology*, 3:213–220, 2012.

[115] T. K. Vinod R. Gandhari, P. . Maddukuri. Oxidation of aromatic aldehydes using oxone. *Journal of Chemical Education*, 84:852–854, 2007.

[116] P. Moormann K. Görlitzer. Thioacetate aus canrenon und 2-methylencanrenon. *Arch. Pharm. (Weinheim)*, 328:165–167, 1995.

[117] S. P. Mirajkar A. P. Singh S. Shylesh, S. Sharma. Silica functionalised sulphonic acid groups: synthesis, characterization and catalytic activity in acetalization and acetylation reactions. *Journal of Molecular Catalysis A: Chemical*, 212:219–228, 2004.

[118] G. Schmalz S. Ruhl R. Müller, K.-A. Hiller. Chemiluminescence-based detection and comparison of protein amounts adsorbed on differently modified silica surfaces. *Analytical Biochemistry*, 359:194–202, 2006.

[119] M. T. Islam M. C. MuNiz L. P. Balogh J. R. Baker Jr. X. Shi, W. Lesniak. Comprehensive characterization of surface-functionalized poly(amdioamine) dendrimers with acetamide, hydroxyl, and carboxyl groups. *Colloids and Surfaces A: Physicochemical and Engineering Aspects*, 272:139–150, 2006.

[120] O. S. Wolfbeis B. K. Hoefelschweiger, A. Duerkop. Novel type of general protein assay using a chromogenic and fluorogenic amine-reactive probe. *Analytical Biochemistry*, 344:122–129, 2005.

[121] L. A. Baker V. T. Phan D. L. Dermody M. E. Gareia R. F. Peez R. M. Crooks T. M. Mayer H. Tokuhisa, M. Zhao. Preparation and characterization of dendrimer monolayers and dendrimer-alkanethiol mixed monolayers adsorbed to gold. *J. Am. Chem. Soc.*, 120:4492–4501, 1998.

[122] J. Dyke S. M. Hall J. Retrum B. Stein N. Remmes D. V. Baxter B. Dragnea L. M. Bronstein X. Huang, A. Schmucker. Magnetic nanoparticles with functional silanes: evolution of well-defined shells from anhydride containing silane. *J. Mater. Chem.*, 19 (24):4231–4239, 2009.

[123] B. Rinderer C. Schramm. Investigation of the hydrolysis of (3-triethoxysilylpropyl)succinic acid anhydride by means of ft-ir. *Journal Material Science*, 43:4215–4219, 2008.

[124] V. N. Uversky. *Vibrational Spectroscopy: Methods in Protein Structure and Stability Analysis*. Nova Science Publishers (ISBN 978-1600217036), 2007.

[125] J. F. G. A. Jansen D. A. F. J. van Boxtel E. M. M. de Brabander-van den Berg E. W. Meijer S. Stevelmans, J. C. M. van Hest. Synthesis, characterization, and guest-host properties of inverted unimolecular dendritic micells. *J. Am. Chem. Soc.*, 118:7398–7399, 1996.

[126] N. Yui Y. Miura T. Fukuda, E. Matsumoto. Peculiar wettability based on orientational change of self-assembled hemispherical pamam dendrimer layer. *Chem. Lett.*, 39:923–925, 2010.

[127] T. Nylander M.-L. Ainalem, R. A. Campbell. Interactions between dna and poly(amdioamine) dendrimers on silica surfaces. *Langmuir*, 26(11):8625–8635, 2010.

[128] V. Falque C. A. G. N. Montalbetti. Amide bond formation and peptide coupling. *Tetrahedron*, 61:10827–10852, 2005.

[129] Hans J. Griesser Sameer A. Al-Bataineh, Leanne G. Britcher. Rapid radiation degradation in the xps analysis of antibacterial coatings of brominated furanones. *Surface and interface analysis*, 38:1512–1518, 2006.

[130] S. Lauckner G. Neumann R. Becker L. Richter A. Voigt, H. Wolf. Electrokinetic properties of polymer and glass surfaces in aqueous solutions: Experimental evidence for swollen surface layers. *Biomaterials*, 4:299–304, 1983.

[131] M. Rezwan J. Vöros M. Textor K. Rezwan, L. P. Meier and L. J. Gauckler. Bovine serum albumin adsorption onto colloidal al2o3 particles: A new model based on zeta potential and uv-vis measurements. *Langmuir*, 20:10055–10061, 2004.

[132] F. Simon A. Janke P. B. Welzel B. Voit W. Knoll C. Werner R. Schweiss, D. Pleul. Electrokinetic potentials of binary self-assembled monolayers on gold: Acid-base reactions and double layer structure. *J. Phys. Chem. B*, 108:2910–2917, 2004.

[133] Naka Kensuke. *Biomineralization II.* Springer; ISBN 978-3-540-46378-8, 2007.

[134] C.-C. Wang R. Nagarajan. Theory of surfactant aggregation in water/ethylene glycol mixed solvents. *Langmuir*, 16:5242–5251, 2000.

[135] P. B. Welzel M. Müller M. Grimmer K. Salchert T. Taeger K. Schmidt W. Pompe C. Werner U. Freudenberg, S. H. Behrens. Electrostatic interactions modulate the conformation of collagen i. *Biophysical Journal*, 92:2108–2119, 2007.

[136] E. Deigele C. Stage P. Karageorgiev J. Geis-Gerstdorfer G. Schmalz S. Ruhl F. Rupp R. Müller V. Katzur, M. Eichler. Surface-immobilized pamam-dendrimers modified with cationic and anionic terminal functions: Physicochemical surface properties and conformational chages after application of liquid interface stress. *Journal of Colloid and Interface Science*, 366:179–190, 2012.

[137] H. Ye R. M. Crooks S.-K. Oh, Y.-G. Kim. Synthesis, characterization, and surface immobilization of metal nanoparticles encapsulated with bifunctional dendrimers. *Langmuir*, 19:10420–10425, 2003.

[138] A. O. Gamer U. Keuser U.-R. Samel, W. Kohler. *Ullmann's Encyclopedia of Industrial Chemistry (Propionic Acid and Derivatives).* Wiley Online Library, 2011.

[139] W. Norde H. J. Busscher A. T. Poortinga, R. Bos. Electric double layer interactions in bacterial adhesion to surfaces. *Surface Science Report*, 47:1–32, 2002.

[140] H. C. Allen A. P. Davis, G. Ma. Surface vibrational sum frequency and raman studies of pamam g0, g1 and acylated pamam g0 dendrimers. *Analytica Chimica Acta*, 496:117–131, 2003.

[141] C. C. Chang L. Y. Lin. Determination of protein concentration in human saliva. *PubMed*, 5(7):389–97, 1989.

[142] H. F. Jenkinson P. S. Handley, R. McNab. *Dental Plaque Revisited (oral biofilms in health and disease)*. Eastman Dental Institute - University College London.

[143] K.-A. Hiller G. Schmalz S. Ruhl R. Müller, G. Gröger. Fluorescence-based bacterial overlay method for simultaneous in situ quantification of surface-attached bacteria. *Applied and Environmental Microbiology*, 73 (8):2653–2660, 2007.

[144] K.-A. Hiller G. Schmalz H. Schweikl R. Müller, S. Ruhl. Adhesion of eukaryotic cells and staphylococcus aureus to silicon model surfaces. *J. Biomed. Mater. Res.*, 84A:817–827, 2008.

[145] C. N. Sukenik N. Balachander. Monolayer transformation by nucleophilic substitution: Applications to the creation of new monolayer assemblies. *Langmuir*, 6 (11):1621–1637, 1990.

[146] C. D. Bossinger P. I. Cook E. Kaiser, R. L. Colescott. Color test for detection of free terminal amino groups in the solid-phase synthesis of peptides. *Short Communications*, pages 595–598, 1969.

[147] H. Motschmann P. Viswanath. *J. Phys. Chem. C*, 112:2099, 2008.

[148] K.-A. Hiller V. Katzur M. Subat H. Schweikl S. Imazato S. Ruhl G. Schmalz R. Müller, A. Eidt. Influences of protein films on antibacterial or bacteria-repellent surface coatings in a model system using silicon wafers. *Biomaterials*, 30:4921–4929, 2009.

Declaration/Eidesstattliche Erklärung

Herewith I declare that I have made this existing work on my own. I have only used the quoted references, stated utilities and the support of the mentioned people.

Ich erkläre hiermit an Eides statt, dass ich die vorliegende Arbeit ohne unzulässige Hilfe Dritter und ohne Benutzung anderer als der angegebenen Hilfsmittel angefertigt habe; die aus anderen Quellen direkt oder indirekt übernommenen Daten und Konzepte sind unter Angabe des Literaturzitats gekennzeichnet.

Bei der Auswahl und Auswertung folgenden Materials haben mir die nachstehenden aufgeführten Personen in der jeweils beschriebenen Weise entgeltlich/unentgeltlich geholfen:

1. Dr. C. Onitsch, Dr. T. Luxbacher und A. Ewers der Firma Anton Paar GmbH (Graz, Österreich und Ostfildern, Deutschland) ermöglichten mir Messungen am Electro Kinetic Analyser (SurPASS) und führten zusätzlich Referenzmessungen durch. Zusätzlich unterstützten sie mich bei der Auswertung meiner Daten durch ihre langjährige Erfahrung mit diesem Gerät.

2. H. Hildebrand, angestellt am Lehrstuhl für Korrosion und Oberflächentechnik (LKO) in Erlangen, vermaß die meisten modifizierten Oberflächen mittels Röntgenphotoelektronenspektroskopie (XPS) und sandte mir die erhaltenen Daten zu. Zusätzlich wurden ein paar XPS Datensätze am Institut für Polymerforschung (IPF) in Leipzig generiert. Zu diesen Daten verhalf mir Dr. F. Weichelt.

3. Die Rasterkraftmikroskopischen Aufnahmen wurden von Dr. P. Karageorgiev aufgenommen und mit ihm ausgewertet.

4. A. Eidt, angestellt am Uni-Klinikum Regensburg, untersützte mich in der Durchführung der Aminogruppennachweise auf den Oberflächen. Er führte alle Versuche im Zusammenhang mit Bakterien durch.

Weitere Personen waren an der inhaltlich-materiellen Herstellung der vorliegenden Arbeit nicht beteiligt. Insbesondere habe ich hierfür nicht die entgeltliche Hilfe eines Promotionsberaters oder anderer Personen in Anspruch genommen. Niemand hat von mir weder unmittelbar geldwerte Leitungen für Arbeiten erhalten, die im Zusammenhang mit dem Inhalt der vorgelegten Dissertation stehen.

Die Arbeit wurde bisher weder im In- noch Ausland in gleicher oder ähnlicher Form einer anderen Prüfungsbehörde vorgelegt.

Geretsried, den July 6, 2015 ..... (Verena Katzur)